INTEGRATION OF LONG-TERM SHM DATA INTO BRIDGE CONDITION ASSESSMENT

XIA YUNXIA

Ph.D

The Hong Kong Polytechnic University

2017

THE HONG KONG POLYTECHNIC UNIVERSITY

DEPARTMENT OF CIVIL AND ENVIRONMENTAL ENGINEERING

INTEGRATION OF LONG-TERM SHM DATA INTO BRIDGE CONDITION ASSESSMENT

XIA Yunxia

A Thesis Submitted in Partial Fulfillment of the Requirements for the Degree of Doctor of Philosophy

February 2017

CERTIFICATE OF ORIGINALITY

I hereby declare that this dissertation entitled "***Integration of Long-Term SHM Data into Bridge Condition Assessment***" is my own work and that, to the best of my knowledge and belief, it reproduces no material previously published or written, nor material that has been accepted for the award of any other degree or diploma, except where due acknowledgement has been made in the text.

(Signed)

XIA Yunxia (Name of student)

To my family

for their love and support

ABSTRACT

The past two decades have witnessed a mushrooming of multidisciplinary research and applications of the structural health monitoring (SHM) technology to civil structures. Much attention was paid to long-span bridges because of their complexity, huge investment, and significance to the society. A great expectation has been placed on the long-term SHM to lead to the next significant evolution of design, assessment, and management of bridges. However, the gap between SHM and bridge condition assessment, that exists currently, impedes the bridge managers benefiting from the costly SHM systems. In connection with fifteen years of SHM data collected from the instrumented Tsing Ma Bridge, this thesis aims to develop a methodology to integrate SHM data into bridge condition assessment.

A reliability-based framework for evolutionary bridge condition assessment is proposed in the context of statistical inference. With elaborately configured strain gauge arrays, the structural reliability is evaluated at two levels: (i) individual chord level, and (ii) deck cross-section level. For long-term monitoring data, extreme value statistics is advantageous because it not only avoids the cumbersome modelling of multiple load effects but also provides a time reference in terms of a return period. Hence, extreme value distributions of the live load demands are inferred to evaluate the structural reliability indices.

The bridge is not equipped with sensors everywhere, and sensor fault may occur

sometimes in the SHM system. Thus, inspection results and finite element model (FEM) of the bridge are also essential. To obtain the evaluation results more reliable, a three-dimensional bridge condition rating system, comprising criticality rating, vulnerability rating and inspection rating, is proposed subsequently. This system comprehensively considers the data-driven and FEM-driven condition assessment results, inspection results, and exposure of structural components to adverse effects such as corrosion and ship collision, as well as other relevant information such as as-built report and maintenance record of the bridge.

Prior to the above studies, an effective and computationally efficient wavelet-based signal pre-processing scheme is first developed to automatically remove the noises, spikes, and trends embedded in the signals, and to separate the signals into different ingredients such as stress components due to the highway traffic, railway traffic and temperature. In addition, site-specific load models for the highway and railway traffic are developed, so that the full 3D FEM of the bridge can be employed to complement SHM data in the bridge condition rating.

LIST OF PUBLICATIONS

Journal Articles:

Xia, Y.X., and Ni, Y.Q. (2016), "A comparative study of different signal re-processing schemes for denoising, despiking and decomposing structural health monitoring data", *Mechanical Systems and Signal Processing*, in review.

Xia, Y.X., and Ni, Y.Q. (2016), "Extrapolation of extreme traffic load effects on bridges based on long-term SHM data", *Smart Structures and Systems*, Vol. 17, No. 6, 995-1015.

Ni, Y.Q., and **Xia, Y.X.** (2016), "Strain-based condition assessment of a suspension bridge instrumented with structural health monitoring system", *International Journal of Structural Stability and Dynamics*, Vol. 16, No. 4, 1-23.

Ni, Y.Q., Zhang, F.L., **Xia, Y.X.**, and Au, S.K. (2015), "Operational modal analysis of a long-span suspension bridge under different earthquake events", *Earthquakes and Structures*, Vol. 8, No. 4, 859-887.

Xia, Y.X., Ni, Y.Q., and Zhang, C. (2014), "Evaluation of torsional response of a long-span suspension bridge under railway traffic and typhoons based on SHM data", *Structural Monitoring and Maintenance*, Vol. 1, No. 4, 371-392.

Ni, Y.Q., **Xia, Y.X.**, and Ye, X.W. (2013), "Structural health monitoring of a tall building with huge floating platform", *Advances in Science and Technology*, Vol. 83, 177-187.

Ye, X.W., Ni, Y.Q., and **Xia, Y.X.** (2012), "Distributed strain sensor networks for in-construction monitoring and safety evaluation of a high-rise building", *International Journal of Distributed Sensor Networks*, Vol. 2012, Article ID 685054 (13 pages)**.**

Conference Papers:

Xia, Y.X., and Ni, Y.Q. (2016), "Development of site-specific live load models for bridge condition assessment based on long-term SHM data", *Proceedings of the 8th European Workshop on Structural Health Monitoring*, 5-8 July 2016, Bilbao, Spain.

Ni, Y.Q., Zhang, F.L., **Xia, Y.X.**, and Au, S.K. (2014), "Modal identification of a long-span suspension bridge under different earthquake events", *Proceedings of the 6th World Conference on Structural Control and Monitoring*, 15-17 July 2014, Barcelona, Spain, 303-317.

Xia, Y.X., Ni, Y.Q., and Zhang, C. (2014), "Monitoring-based evaluation of unsymmetrical dynamic response of a suspension bridge due to railway traffic and wind loading", *Proceedings of the 6th World Conference on Structural Control and Monitoring*, 15-17 July 2014, Barcelona, Spain, 331-343.

Xia, Y.X., Ni, Y.Q., and Wong K.Y. (2013), "Development of a 3D bridge rating system incorporating structural health monitoring data", *Proceedings of the 6th International Conference on Structural Health Monitoring of Intelligent Infrastructure*, 9-11 December 2013, Hong Kong.

ACKNOWLEDGEMENTS

I wish to express my deepest gratitude to my chief supervisor, Prof. Y. Q. Ni, for his unceasing support and guidance throughout the whole period of my study at The Hong Kong Polytechnic University. His conscientious and meticulous attitude to work will benefit me inexhaustibly in my future career.

Sincere thanks go to Dr. K. Y. Wong, the formerly senior engineer at the Highways Department of HKSAR Government, for providing me the valuable structural health monitoring data. I have also benefited a lot from his professional knowledge and practical experience. I am also grateful to other engineers at the Highways Department as well as the Tsing Ma Management Limited, for the help and guidance they provided when I collected the long-term monitoring data.

The financial support provided by The Hong Kong Polytechnic University, including the Ph.D. studentship, the payment for attendance of international conferences and research-associated equipment, is sincerely acknowledged. I am also grateful to the kind help from the staff members at the university library, research office, and general office of the Department of Civil and Environmental Engineering.

I also want to express my sincere thanks to all my friends, for their comfort and encouragement when I was depressed and lost in my research.

Last but not least, special thanks are given to all my family members, for their love, support, and encouragement.

CONTENTS

LIST OF FIGURES

LIST OF TABLES

LIST OF SYMBOLS

The main symbols used in this thesis are listed below:

Chapter 2

P_f	Probability of failure
β	Reliability index
R	Structural resistance
L	Load effect
μ_g	Mean value of performance function
σ_g	Standard deviation of performance function
$M(t)$	Safety margin
$R(t)$	Time dependent resistance
$S(t)$	Time dependent load effects
$f'(\theta)$	Prior density function
ε	Observed experimental outcome
$P(\varepsilon/\theta)$	Conditional probability of ε
$L(\theta)$	Likelihood of θ
$f''(\theta)$	Posterior distribution
RF	Rating factor
C	Capacity
R_n	Nominal member resistance
DC	Load effects due to weight of structural components and attachments
DW	Load effects due to weight of wearing surface and utilities
P	Load effects due to other permanent loads
LL	Load effects due to live load
IM	Load effects due to dynamic allowance

γ_{DC}	Load factor for weight of structural components and attachments
γ_{DW}	Load factor for weight of wearing surface and utilities
γ_P	Load factor for other permanent loads
γ_{LL}	Load factor for live load
φ_c	Condition factor
φ_s	System factor
φ	Resistance factor

Chapter 3

$f(t)$	Signal
$\psi(t)$	Mother wavelet function
a	Scale parameter
b	Translation parameter
$F_\psi(\cdot)$	Fourier transform
Z	Sets of positive integers
$\{\psi_{j,k}\}$	Discretized wavelets
$a_{j,k}$	Approximation coefficients
$d_{j,k}$	Detail coefficients
m	Number of wavelet coefficients
A_J	Approximation at level J
D_j	Detail at level j
$s(t)$	Real signal
$\varepsilon(t)$	Standard white noise $N(0,1)$
δ	Intensity of the noise
λ	Threshold
n	Signal size
α	Thermal expansion coefficient for structural steel
L	Length of the deck
T_0	Reference temperature
ΔT	Difference between effective temperature and reference temperature

Chapter 4

M_n	Maximum of the observed process over n time units
μ	Location of GEV distribution
σ	Scale of GEV distribution
ξ	Shape parameter of GEV distribution
u	Threshold level
z_p	Return level associated with the return period l/p

Chapter 5

σ_{total}	Maximum daily-total stress induced by traffic
σ_{railway}	Maximum daily-railway-induced stress
σ_{highway}	Maximum daily-highway-induced stress
α	Reduction factor

Chapter 6

$R(t)$	Structural resistance under the live loads
$Q_M(t)$	Live load demand derived from the measured strain
e	Uncertainties associated with the sensors
R_n	Nominal resistance
M	Variation in the strength of the material
F	Uncertainties in fabrication
P	Professional factor
$C(t)$	Average penetration in micrometers
t	Time in years
A	Site-specific parameter
B	Site-specific parameter
N	Axial force
M	Vertical bending moment
A	Area of the cross section
σ_a	Average stress in the cross section
σ_T	Stresses derived from strains measured at the top side of the chord

σ_B	Stresses derived from strains measured at the bottom side of the chord
Z_T	Section moduli corresponding to the positions of the top strain gauges
Z_B	Section moduli corresponding to positions of the bottom strain gauges
σ_{bB}	Bending stress at the bottom of the cross section
$A(t)$	Cross-section area of individual chords
f_N	Maximum allowable stress induced by live loads
$h(t)$	Effective height of the cross-section
$M_M(t)$	Bending moment derived based on the strain data
$V_M(t)$	Shear force calculated using monitored strain

LIST OF ABBREVIATIONS

AASHTO	American association of state highway and transportation officials
ADC	Analogue-to-digital converter
ASCE	American Society of Civil Engineers
ASR	Allowable stress rating
BCA	Bridge condition assessment
BCI	Bridge condition index
BCR	Bridge condition rating
BM	Block maxima
BMS	Bridge management system
CCTV	Close-circuit television video
CDF	Cumulative distribution function
CI	Confidence interval
COV	Coefficient of variation
CR	Criticality rating
CWT	Continuous wavelet transform
DWT	Discrete wavelet transform
EVD	Extreme value distribution
EVT	Extreme value theory
FDG	Foundation group
FLS	Fatigue limit state
FOSM	First-order second-moment
FT	Fourier transform
GEV	Generalized extreme value
GP	Generalized Pareto
GTW	Gross train weight

GVW	Gross vehicle weight
HGV	Heavy goods vehicle
HKRTR	Hong Kong road traffic regulations
IDWT	Inverse DWT
IR	Inspection-based rating
LCL	Lower control limit
LFR	Load factor rating
LGV	Light goods vehicle
LRFD	Load and resistance factor design
LRFR	Load and resistance factor rating
MC	Monte Carlo
MCMC	Markov Chain Monte Carlo
MGV	Median goods vehicle
MLE	Maximum likelihood estimation
MODWT	Maximal overlap discrete wavelet transform
MPN	Maintenance priority number
MSE	Mean square error
NBIS	National bridge inspection standards
PDF	Probability density function
PL	Profile likelihood
POT	Peaks-over-threshold
STFT	Short time Fourier transform
SHM	Structural health monitoring
SLS	Serviceability limit state
SSG	Suspension system group
SURE	Stein’s unbiased risk estimate
TI	Translation invariant
TLEs	Traffic load effects
TMB	Tsing Ma Bridge

UCL	Upper control limit
UDL	Uniformly distributed load
ULS	Ultimate limit state
VR	Vulnerability rating
VSG	Vertical structure group
WASHMS	Wind and structural health monitoring system
WIM	Weigh-in-motion
WT	Wavelet transform

CHAPTER 1

INTRODUCTION

1.1 Research Motivation

Bridges are critical transportation nodes that link highway networks and provide river or sea crossings. They deserve special concern not only because of their vast investment, but also because of the cost of the traffic disruptions and even the catastrophic casualties due to their failure. However, by their very nature, bridges are consistently subjected to traffic volumes and heavy truck loads as well as environmental stressors such as temperature, humidity, scour and chemical attack. In addition, they might suffer extreme events such as typhoon, earthquake or ship-collision occasionally. Therefore, they are deteriorating under the combined actions of the above factors as well as the material ageing. Bridge failure is not a problem of only the past; the recent failure of highway bridges, such as the Laval Overpass in Canada (2005), the I-35W Bridge in Minneapolis, USA (2007), the I-5 Skagit River Bridge in Washington (2013), and the Belo Horizonte overpass in Brazil (2014), reminds us that it is also a problem of today. There has been an increasing awareness of the condition of existing bridges.

To manage bridges effectively and economically, a management system is usually established. A typical bridge management system (BMS) includes modules of

inventory, inspection, condition assessment, deterioration model, performance prediction, management planning and optimization, etc. The most significant challenge for the existing BMS is perhaps the acquisition and interpretation of the field inspection data (Enright and Frangopol 1999a). Almost all the BMS worldwide are based on visual inspections. However, the limitations of the visual inspection have long been recognized. For example, many early signs of deterioration or damage may be missed because of the ability of human eyes; the inspection results are subjective; and long time, high manpower and cost are required. Another way is the structural analysis in terms of bridge capacity rating, which includes three methods: allowable stress rating (ASR), load factor rating (LFR), and load and resistance factor rating (LRFR). Among the three methods, the LRFR is the most advanced. In the LRFR, the ratio of live load capacity to the live load demand is calculated. However, a code-defined live load model representing bridges nationwide is employed to calculate the required live load capacity. This defined model may not be applicable to the concerned bridge. Inaccurate condition assessment has been recognized as the most critical barrier to the effective management of bridges (Aktan *et al*. 1996).

Since the late 1990s continuously operating structural health monitoring (SHM) systems have been deployed on bridges worldwide such as Korea, Japan, Hong Kong, China, North America and Europe (Pines and Aktan 2002; Wong 2004; Ko and Ni 2005; Abe and Fujino 2009; Ou and Li 2009; Chen 2010). SHM systems achieve site-specific data including loads and structural responses, through a variety of sensors and sophisticated data acquisition and transmission systems. The SHM data can reduce the uncertainty in the loadings and structural response, which increases the reliability of structural evaluation and management activities. As a result, the SHM technology has

a potential to decrease the life-cycle cost of civil infrastructures. Furthermore, it is expected to lead to the next significant evolution of design, assessment and management of civil infrastructures, just like what computers and structural analysis software did. The reason is that it provides the capability to implement some concepts, methods and ideas that have existed for a time but have not matured in practice yet. These include but not limited to: performance and durability based design, life-cycle design, and reliability-based structural assessment (Messervey 2008).

To realize the targets of SHM, the researchers in the civil SHM community worldwide have done a large amount of research. A number of literature review papers are available (Pines and Aktan 2002; Chang *et al.* 2003; Sohn *et al*. 2004; Ko and Ni 2005; Brownjohn 2007; Farrar and Worden 2007). Though a large amount of research has been dedicated to SHM-based damage detection (Doebling *et al*. 1996; Carden and Fanning 2004; Sohn *et al*. 2004; Friswell 2007; Worden and Manson 2007), success is demonstrated only in laboratory studies, simulations, and well-controlled tests (Maeck *et al*. 2001). Their effectiveness still needs to be proven for real civil structures, and in the near future, developments of SHM for civil engineering may not be expected to have an inherent capability for damage location and quantification in real time by system identification (Brownjohn 2007). Many bridge owners or relevant government departments are questioning the benefit-cost ratio of an SHM system, because it seems that it is difficult to convert the SHM data to useful information about the performance and safety of the bridges, and to assist in the inspection, maintenance and management activities. Therefore, at present the greatest and most urgent challenge in fulfilling the promise of SHM technology is how to integrate the monitored data into the bridge condition assessment.

A permanent SHM system was installed on the Tsing Ma Bridge (TMB) in Hong Kong from 1997 to 1999, after the completion of its construction. Data of the load and environmental conditions (highway and railway traffic, wind, and temperature), and structural responses of the bridge (acceleration, displacement and strain), are continuously measured. A wealth of high-quality SHM data has been collected and stored. This rich database provides a unique opportunity to address the urgent problems stated above. Stimulated by the challenging problems stated above and the valuable opportunity provided by the TMB, this thesis aims to develop a methodology to integrate the long-term SHM data into the bridge condition assessment, taking the most advantage of data collected from the TMB.

1.2 Research Objectives

This thesis focuses on the integration of long-term SHM data into bridge condition assessment, taking the TMB as a testbed. The emphasis is given on developing a framework to take the best advantage of the data, and combining them with other information, such as structural analysis results from FEM and inspection results. The specific objectives are:

1. To propose a signal pre-processing scheme to remove noises, spikes and trends embedded in the signals, and separate different signal sources. The long-term SHM data is non-stationary, and requires special techniques that go beyond the traditional time-domain approach and the classical Fourier approach. The volume of the data is so massive that except effectiveness, the signal processing paradigm should be automatic and computationally efficient.

2. To establish site-specific models for the highway and railway loads. Recognizing the limitation of an SHM system in the number of sensors, an FEM is often applied to complement the SHM system. To employ the FEM for structural analysis, live load models should be given. With the long-term WIM data, strain data, and the traffic situations recorded by the close-circuit television video (CCTV), the live load models can be developed.

3. To evaluate the bridge condition in terms of structural reliability based on extreme value distributions of the long-term strain data in the context of statistical inference. Reliability theory is an ideal tool to make full use of the measured data which are random variables in conducting bridge condition assessment. For long-term data, extreme value statistics are advantageous. The reason is that they do not only prevent the cumbersome modeling of multiple load effects, but also provide a time metric in terms of return period. The probability distributions of load effects are always varying, and the survival of the bridge continuously proves the structural resistance. As a result, the structural reliability should be updated gradually. To get a knowledge of the future performance of the bridge, the lifetime reliability profile should be outlined taking into account the structural deterioration.

4. To develop a comprehensive and reliable bridge condition rating system based on SHM data. In practice, the results of bridge condition assessment are often transformed into indices easy to understand by bridge managers, so that they can schedule the bridge management activities such as inspection and maintenance. These straightforward indices are often called bridge condition rating (BCR). A BCR system integrating the SHM data is required.

1.3 Outline of the Thesis

This dissertation is composed of eight chapters. It is organized as follows.

Chapter 1 introduces the motivation of the thesis, expounds its objectives, and states the outline.

Chapter 2 reviews the literature on relevant topics. The general concept and overview of long-term SHM, bridge management systems, structural reliability, and Bayesian statistics, is stated first. And then, the traditional bridge condition assessment techniques, including the inspection-based and the structural-analysis-based methods, are reviewed. What is introduced next is the existing studies on SHM-based bridge condition assessments. Subsequently, the potential effects of SHM data on the bridge evaluation, and the feasibility of integrating long-term SHM data into bridge condition assessment, are discussed. Finally, issues critical to bridge condition assessment based on long-term SHM data are recognized.

Chapter 3 describes a wavelet-based signal pre-processing methodology, in terms of de-nosing, despiking, and decomposing. It is inevitable that there are noises, spikes, and trends in the SHM data. Furthermore, different signal sources are required to be separated in some specific applications. Besides being non-stationary, long-term SHM data have an extremely large amount. An effective, automatic, and efficient signal pre-processing method is a great necessity. With the merit of multi-resolution and time-frequency analysis, the wavelet transform (WT) is a promising tool to process the long-term SHM data. An optimal denoising approach is selected among different

approaches in the two wavelet denoising methods: the classical method and the Bayesian method. A novel despiking method, which detects the spikes first, and then removes them by the wavelet despiking algorithm focusing on their neighboring time-domain information, is developed. The spike detection technique is based on continuous WT, and can identify the occurrence instants of the spike fast and automatically. Based on the characteristics of frequency and magnitude, the long-term SHM data can generally be divided into two categories: (i) the signal sources can be discriminated by frequencies; and (ii) the signal sources overlap in frequency but can be discriminated by magnitudes. Different wavelet decomposing methods are proposed accordingly.

Chapter 4 studies the extreme value distributions (EVD) and extrapolates characteristic values of load effects based on long-term strain data. Both the two widely accepted approaches in the extreme value theory, the block maxima (BM) and peaks-over-threshold (POT) approach, are employed. The likelihood-based methods including the maximum likelihood estimation (MLE) and profile likelihood estimation, and the Bayesian estimation method, are used to estimate the parameters of the extreme value distributions and the corresponding return levels. To provide a target stress for the development of site-specific live load models, the characteristic values of extreme stresses (stress with a certain return period) induced by highway and railway traffic respectively are also extrapolated.

Chapter 5 develops site-specific models for highway and railway loads, based on the continuously measured data, especially the WIM, strain data, and the CCTV record of the traffic. The highway load is modelled as a uniformly distributed load (UDL) with an additional knife edge load (KEL). The UDL is determined by the WIM data and the

traffic recorded by the CCTV. The KEL is calculated inversely by the full 3D FEM of the bridge, targeting an extreme stress level with a certain return period, which is derived in Chapter 4. The railway load is modelled by a series of concentrated forces simulating the wheel loads of an 8-car train. Similar to the KEL, the gross train weight (GTW) is also calculated inversely by the FEM of the bridge, targeting a certain extreme stress level. Live load models for both serviceability limit state (SLS) and ultimate limit state (ULS) evaluations of the bridge are developed.

Chapter 6 establishes a reliability-based framework in the context of statistical inference to assess the evolutionary bridge condition, based on nine years of strain data. The point-in-time reliabilities of the instrumented structural components are first estimated based on annual EVD of the load effects obtained from the strain data. Then the annual reliabilities are updated recognizing the fact that the structural resistance is proved continuously by load history and the EVD of the load effects is always changing. Benefiting from the elaborately designed strain gauge arrays, structural reliability at two levels: (i) individual chord level, and (ii) deck cross-section level, is evaluated respectively. To predict the future reliability, the lifetime reliability profile is obtained considering the structural deterioration.

Chapter 7 proposes an SHM-based BCR system, including criticality rating, vulnerability rating, and inspection-based rating. The criticality rating is to evaluate the strength surplus of structural components. It is determined in terms of four criticality factors, namely, structural reliability, fatigue life, imperfections of the as-built bridge, and failure consequence. These factors are based on the SHM data or the FEM of the bridge. The vulnerability rating mainly evaluates the fragility of the structural components to the adverse effects, including deterioration, damage, and

wear. The as-built report, and maintenance records of the bridge are needed in the rating. The inspection-based rating assesses the condition of the structural components in light of inspection results. This BCR system incorporates the SHM data, FEM, inspection results, as-built report and maintenance records of the bridge, so it is comprehensive and can provide more objective and accurate bridge condition assessment for bridge management.

Chapter 8 gives the conclusions achieved from the studies in this thesis. Recommendations for future work are also presented.

CHAPTER 2

LITERATURE REVIEW

2.1 Fundamental Concepts and Overview

2.1.1 Long-Term Structural Health Monitoring

2.1.1.1 General introduction

Long-term SHM can be defined as a long-term observation of the loadings and responses of a structure through instrumentation techniques, to assess the current structural condition and predict its future performance (Liu *et al*. 2009). The specific objectives of the SHM include (Wong 2004; Liu et al. 2009): (i) to detect potential structural damage; (ii) to predict a structure's remaining service life; (iii) to provide a database for optimal and economic maintenance decision; and (iv) to help the transition of structural design methodology from current semi-probabilistic design to future probabilistic performance-based design. A large amount of multidisciplinary research has sprung up, and a number of review papers and books are available (Mufti 2002; Pines and Aktan 2002; Chang *et al.* 2003; Ko and Ni 2005; Brownjohn 2007; Wenzel 2008; Boller *et al.* 2009; Catbas and Aktan 2009; Fujino *et al*. 2009; Ni *et al.* 2009; Xu and Xia 2011; Yun *et al.* 2011).

The application of SHM techniques to guiding bridge inspection, maintenance and management is still in its infancy (Hua 2006). It is likely to be difficult to convert SHM data to useful information about the performance and safety of the bridges, on target to assist in the inspection, maintenance and management activities. Many bridge owners or government agencies are questioning the benefit-cost ratio of SHM systems. Thus, one of the most urgent challenges in fulfilling the promise of SHM technology is how to integrate the monitored data into bridge management systems (BMS), and how to make it mature through codes, policy, and education.

2.1.1.2 Specific problems

Bridges often operate under intricate and varying loadings, including traffic and wind, and environmental conditions such as temperature and humidity. Furthermore, there might be errors in SHM systems. Thus, it is inevitable that the monitored SHM data are non-stationary and inter-fused with noises, spikes and trends. Moreover, in some applications signals are required to be separated to different components. For example, to study the respective effects of different loadings, the measured strain should be decomposed accordingly. Therefore, a signal pre-processing technique is desired.

The Fourier transform (FT) is a traditional but extremely useful tool in signal processing. However, the FT cannot capture the time information of the events, so it cannot present the evolutionary characteristics of the signals (Gurley and Kareem 1999). Moreover, ringing effects and spurious oscillations may be induced by the FT method (Kantz and Schreiber 2004). The short time Fourier transform (STFT) as a

time-frequency method, which localizes the analysis by a sliding time window with fixed length, attempts to overcome the drawback of the FT. However, the accuracy and flexibility of the STFT is significantly limited by the fixed size and shape of the window (Robertson *et al.* 1996). Among various time-frequency methods (Neild *et al.* 2003), the most promising one seems to be the wavelet transform (WT) (Stojanovic *et al*. 2013). Being a time-frequency method, the WT is not only able to keep the time information of the signal, but also possesses the merit of multi-resolution, which means having the capability to characterize concerned event coefficients in multiple frequency bands. Apart from the contamination of useless information and the heterogeneous data structure, the extraordinary volume of long-term SHM data is also of great concern. Therefore, in addition to effectiveness, the signal pre-processing technique for long-term SHM data should be both automatic and computationally efficient.

To manage the long-term data efficiently, selecting and keeping the extreme values is a good solution. Actually, the design and assessment of civil structures often considers the extreme values of random variables. For example, buildings, dams and bridges must withstand maximum wind loads, flood levels, and traffic loads respectively for a given time period (Messervey *et al*. 2011). Another advantage of the extreme value statistics is that it can prevent the miscellaneous modeling of variables, which is engendered by a variety of effects, including traffic, wind, and temperature that occur at different and varying frequencies. Furthermore, the extreme value distributions

provide a mechanism to incorporate time effects, which refers to the return period (Messervey 2008).

2.1.2 Bridge Management Systems

Bridge management is a process of making decision to select and prioritize the necessary activities, such as inspection, maintenance, and traffic control, to maintain the reliability of a bridge within acceptable limits. To maintain the acceptable performance of deteriorating bridges reasonably, most countries have developed and employed BMS. The BMS in North America, Europe, and South Africa can be found in Hearn *et al.* (2005), and that in the UK can be found in Rafiq (2005). For example, the BMS in UK includes the HiSMIS (Highways Structures Management Information System) developed by High-Point Randle (HPR), BridgeMan developed by TRL in association with Oxfordshire County Council, NATS owned by the Department of Transport, and COSMOS developed by Surrey County Council (Rafiq 2005). In the USA, there are two main BMS: the PONTIS developed by the FHWA and State Department of Transportation, and the BRIDGIT developed by the National Cooperative Highways research program (Ryall 2001).

The background of the historical development and evolution of BMS across different countries is similar. The BMS is usually constituted by modules performing different functions as shown in Figure 2.1 (Maraki 2003; Messervey 2008). Most BMS divide the bridges into elements to collect, store and analyze the relevant information. The

inventory module is used to store the general and historical data of elements and structures. The inspection module collects condition information of the structural elements through visual inspections. The condition assessment module evaluates the condition of elements on the basis of the information obtained in the inspection module and rates them using a predefined condition rating system. Deterioration rates for the bridges are provided by the deterioration module based on the historical and current condition of the bridge components. The maintenance module aims to make decisions regarding the activities like repair and replacement. The optimization module arranges management activities with a target of cost saving.

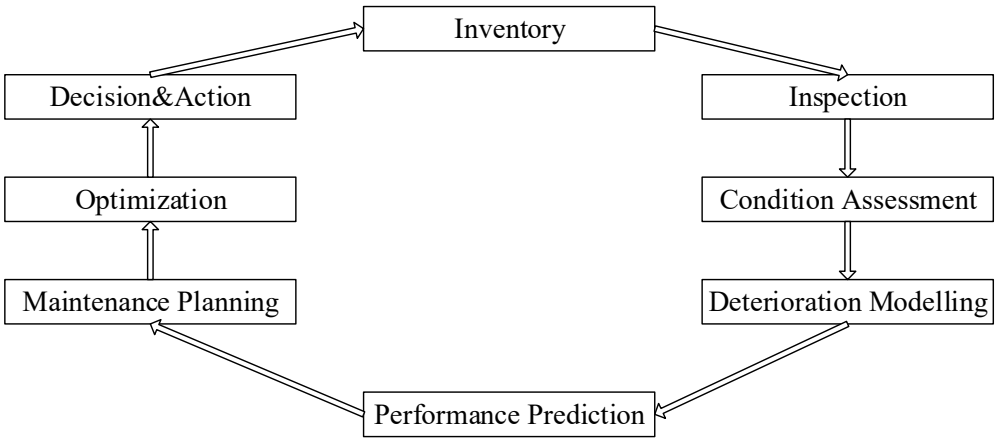

Figure 2.1 Main modules of bridge management system

Among the modules of the BMS, the inventory, inspection, and inspection-based assessment are relatively easy and nearly maturing. For instance, in the USA, national attention has been paid to the deterioration of existing bridges after several bridge failures in the 1960s, including the tragic collapse of the Silver Bridge (Small and Cooper 1998). The Federal Highway Act of 1968 required regular bridge inspections.

This act was soon followed by the American Association of State Highway and Transportation Officials (AASHTO) “grey book” Manual for Maintenance Inspection of Bridges (1970). The National Bridge Inventory (NBI) established by the Federal Highway Administration (FHWA) is a rich database classifying the state of USA bridges based primarily on biannual visual inspections (FHWA 2014). The FHWA revises national bridge inspection standards (NBIS) almost yearly following the improvement of methods and the knowledge gained in the field. Similar effort has been made by the American Society of Civil Engineers (ASCE). The ASCE began publishing a Report Card on the Nation’s Infrastructure in 1998, which has been updated biennially since then. This report currently consists of 15 categories of civil infrastructure, and the bridge is one of the categories (ASCE 2013).

Almost without exception, the BMS worldwide are based on visual inspection. Bridge inspections began in the 1960s and 1970s. The visual inspection, including what type of information is gathered, at what frequency, by which authority and with what level of certification, is regulated by a standard; for example, the NBIS was stipulated by the FHWA in the USA. According to the NBIS, more than 600,000 bridges in the USA should be inspected at least once every two years. Different countries have different standards, and the differences are listed in the FHWA international technology exchange program report (Hearn *et al.* 2005). Though the inspection types, intervals, and personnel carrying out the inspections are different, almost all programs follow

the UK defined inspection types (BA63/94 1994; BD63/94 1994; Rafiq 2005; Messervey 2008).

The drawbacks of visual inspection have long been recognized. The ability of the human eyes is the first limitation. The visual inspections might miss many of the early signs of deterioration or damage because some critical areas are not accessible during the inspections. Even when these signs are visible, it is difficult for persons to find them among hundreds of structural members and connections that have large dimensions. Secondly, some critical areas are not accessible during the inspections. Besides, the inspection results are subjective because they are based on the experience, intuition and personal judgment of the bridge inspectors. An investigation conducted by the FHWA, which aims to study the reliability of visual inspections, reveals that there is significant variability in the structural condition assignments by inspectors (Phares *et al.* 2004). In 2006, a highway overpass collapsed during routine usage in Laval, Canada, killing six people. The cause was the de-bonding of the internal steel reinforcement due to corrosion at the deck-column interface. Important facts are that the bridge had passed its periodic visual inspection just before the collapse, that hours before the event transportation officials were alerted to and cleaned up spalling material that had dropped onto the motorway below the overpass, and that immediately prior to the event, motorists reported a noticeable drop as they began crossing the bridge (Messervey 2008). This tragedy highlighted the question of the effectiveness of visual inspections. Furthermore, the genuine in-service loading and environment of

the bridges cannot be evaluated by visual inspections. Another drawback of visual inspections is the high manpower demand, so they cannot be performed frequently. For example, the biennial visual inspection of the Brooklyn Bridge in New York was reported to last for over three months at a cost of 1 million US dollars (Dubin and Yanev 2001).

The performance metric utilized in the condition assessment and prediction is the defining difference between different BMS. The most common one in practice is the condition index. The bridge condition rating systems around the world are summarized in section 2.2. In many BMS, the future state of the bridge components is obtained using a Markovian process. This process assumes that the future state depends only on the current state. The performance profiles are decreasing step functions over time. The two prevailing BMS in the USA, Pontis (Thompson *et al.* 1998) and BRIDGIT (Hawk and Small 1998), apply this approach. However, the Markovian process is not able to capture the propagation of uncertainties during the entire service life; and its accuracy may be largely reduced due to a number of discrete condition states (Das 1998a; Ng and Moses 1996; Frangopol and Liu 2007). Reliability analysis has been proposed to solve the limitations of the Markovian process (Das 1998b; Frangopol and Estes 1997; Frangopol *et al.* 2001). Anyhow, the primary concerns of condition state models are the drawbacks of visual inspection.

To complement visual inspection techniques, bridge owners and operators have embraced traditional non-destructive testing (NDT) techniques, including acoustic

emission, ultrasonic guided waves, X-ray diffraction, surveying, interferometry, magnetic flux, and corrosion potential measurements (Pines and Aktan 2002). Non-destructive evaluation methods are also called local health monitoring. They are often time-consuming and expensive, and the access is not always possible (Chang *et al.* 2003). Finite element analysis is another complement to visual inspection. The finite element model must be based on the actual structural properties, and operational environment and loading of the evaluated bridge. The two complementary methods have not been integrated into the condition assessment module of the BMS by formal standard.

The concept of life-cycle is usually employed in the BMS. An ideal structural performance curve is obtained based on reliability analysis. It is quite probable that actual reliability profiles are below the ideal curve (Rafiq 2005) because of structural deterioration. Recognizing that the budget for bridge management is in general very limited, to design an optimal maintenance strategy, initiation time and rates of deterioration, maintenance types, and effects of maintenance on bridges, must be modelled. The deterioration is difficult to model. Studies on deterioration of steel can be found in Estes (1997), and those on concrete can be found in Rafiq (2005).

Maintenance works can be categorized into routine maintenance, essential maintenance, and preventative maintenance (Das 1999). The routine maintenance is carried out at regular intervals to ensure minimal deterioration. The essential maintenance is to maintain safety of bridges, for example, to repair structures which

are assessed to be inadequate. It improves the bridge performance and decreases the deterioration rate. The preventative maintenance refers to work preventing or slowing down the deterioration rate. The management strategy is expected to be determined targeting the lowest life-cycle cost. It is a multi-objective optimization problem, in which the multiple but conflicting objectives (e.g. condition, safety, cost, etc.) need to be incorporated to approach a well-balanced solution (Neves *et al*. 2006b).

2.1.3 Structural Reliability

Uncertainty is inevitable in bridge design and evaluation. Factors such as the operational loadings, structural responses, geometries, material resistances, equipment or sensor errors, structural models, and deterioration mechanisms, might be highly uncertain. Probability distributions are usually utilized to characterize the uncertainty.

To provide an adequate level of structural safety, it is necessary to quantify and evaluate the significance of uncertainty. Historically, this was accomplished by a safety factor, which is usually based on past experience and expert opinion. Though simple to use, it cannot offer consistent levels of safety across various structures and may result in significant over- or under-design. To address this limitation, structural reliability theory was developed to provide a rational approach to account for the uncertainties inherent in engineering problems. The application of reliability theory has improved the structural design in terms of safety, serviceability and durability.

The reliability concept was introduced into the design code of civil infrastructures in the late 1970s, such as the building design code in the USA (Ravindra and Galambos 1978; Ellingwood 1980; Ellingwood *et al.* 1982) and the Ontario highway bridge design code in Canada (Nowak and Lind 1979). Since then reliability theory has been gradually used in the design and assessment specifications for civil structures. There are many classics on structural reliability theory (Ang and Tang 1975, 1984, 2007; Thoft-Christensen and Baker 1982; Melchers 1999; Madsen *et al*. 2006; Ayyub and McCuen 2011; Nowak and Collins 2012; Thoft-Christensen and Murotsu 2012). The structural reliability theory stated below is from these books.

2.1.3.1 Concept of reliability

As defined by Leemis (1995), the reliability of an item is the probability that it will adequately perform its specified purpose for a specified period of time under specified environmental conditions. That is to say, reliability is the probabilistic measure of performance. The random inputs for reliability analysis are defined as follows: X, represents the supply capacity, and Y is the demand requirement (Guo 2001). For continuous X and Y, the probability of failure P_f is expressed by

$$P_f = \int_0^{\infty} [\int_0^{y} f_{X,Y}(x, y)dx]\, dy \tag{2.1}$$

and the reliability P_s is

$$P_s = \int_0^{\infty} [\int_0^{x} f_{X,Y}(x, y)dy]\, dx \tag{2.2}$$

Mostly, X and Y might respectively be functions of several variables. Then, the performance function is

$$g(\mathbf{X}) = g(X_1, X_2, ..., X_n) \tag{2.3}$$

where $\mathbf{X}=(X_1,X_2,\ldots,X_n)$ is a vector of variables. Geometrically, $g(\mathbf{X})=0$ is an n-dimensional surface that may be called "failure surface" (Ang and Tang 1984). The corresponding reliability P_s is

$$P_s = \int_{\{g(\mathbf{X})>0\}} \ldots \int f_{X_1,\ldots,X_n}(x_1,\ldots,x_n)\, dx_1 \ldots dx_n = \int_{g(\mathbf{X})>0} f_{\mathbf{X}}(\mathbf{X})\, d\mathbf{x} \tag{2.4}$$

and the probability of failure is

$$P_f = \int_{g(\mathbf{X})<0} f_{\mathbf{X}}(\mathbf{X})\, d\mathbf{x} \tag{2.5}$$

2.1.3.2 Reliability index

The calculation of reliability P_s by Eqs. (2.2) and (2.4) requires the knowledge of the joint probability distribution functions (PDF) $f_{\mathbf{X}}(\mathbf{X})$. However, in practice this information is often unavailable because of insufficient data. Even when the required PDF is known, the exact calculation of p_s may still be impractical for the difficulty in numerical integration of the PDF. In applications, indirect evaluation of this probability, which is the reliability index, is adopted. Two methods are usually used to calculate the reliability index: (1) numerical approximation method, and (2) simulation method.

When variables are uncorrelated and normally distributed, the reduced variables can be introduced (Freudenthal 1956):

$$X_i' = \frac{X_i - \mu_{X_i}}{\sigma_{X_i}}; \qquad i = 1,2,...,n \tag{2.6}$$

The critical state equation $g(\mathbf{X})=0$ would be

$$g(\sigma_{X_1} X_1' + \mu_{X_1}, ..., \sigma_{X_n} X_n' + \mu_{X_n}) = 0 \tag{2.7}$$

Shinozuka (1983) has shown that the point $(x_1'^*, x_2'^*, ..., x_n'^*)$ on the failure surface with minimum distance to the origin is the most probable failure point. The point $(x_1'^*, x_2'^*, ..., x_n'^*)$ is usually called the "design point" (Hasofer *et al*. 1973). Therefore, this minimum distance can be used as the measure of reliability, which is called reliability index and denoted by β (Ang and Tang 1984):

$$\beta = D_{\min} = \frac{-\sum_i x_i'^* \left(\frac{\partial g}{\partial X_i'}\right)_*}{\sqrt{\sum_i \left(\frac{\partial g}{\partial X_i'}\right)_*^2}} \tag{2.8}$$

where the derivatives $\partial g / \partial X_i'$ are evaluated at $(x_1'^*, x_2'^*, ..., x_n'^*)$. In scalar form,

$$x_i'^* = -\alpha_i^* \beta; \qquad i = 1,2,...,n \tag{2.9}$$

where

$$\alpha_i^* = \frac{\left(\frac{\partial g}{\partial X_i'}\right)_*}{\sqrt{\sum_i \left(\frac{\partial g}{\partial X_i'}\right)_*^2}} \tag{2.10}$$

are the direction cosines along the axes X_i'. The pioneering application of reliability index was performed by Cornell (1967), who estimated the limit state function using a linearized limit state function at the point corresponding to the mean values of the reduced variables, not the design point as defined above. The method using the design point proposed by Hasofer *et al.* (1973) is a limestone in the evolvement of procedures to calculate the reliability index.

For calculation of reliability index based on non-linear limit state functions, the solution is to expand the performance function $g(\mathbf{X})$ in a Taylor series at a point $\mathbf{x}^*$ in the first order, that is

$$\begin{aligned} g(X_1, X_2, ..., X_n) &\simeq g(x_1^*, x_2^*, ..., x_n^*) + \sum_{i=1}^{n} (X_i - x_i^*) \left(\frac{\partial g}{\partial X_i}\right)_* \\ &= \sum_{i=1}^{n} (X_i - x_i^*) \left(\frac{\partial g}{\partial X_i}\right)_* \\ &= \sum_{i=1}^{n} (X_i' - x_i'^*) \left(\frac{\partial g}{\partial X_i'}\right)_* \end{aligned} \tag{2.11}$$

Consequently, the approximation of the mean value of $g(\mathbf{X})$, μ_g, is

$$\mu_g \simeq -\sum_{i=1}^{n} x_i'^* \left(\frac{\partial g}{\partial X_i'}\right)_* \tag{2.12}$$

and the corresponding variance is

$$\sigma_g \simeq \sum_{i=1}^{n} \sigma_{X_i'}^2 \left(\frac{\partial g}{\partial X_i'} \right)_*^2 = \sum_{i=1}^{n} \left(\frac{\partial g}{\partial X_i'} \right)_*^2 \tag{2.13}$$

Therefore, the reliability index β is

$$\beta = \mu_g / \sigma_g \tag{2.14}$$

Rackwitz and Flessler (1978) extended the approach of Hasofer *et al*. (1973), and transformed uncorrelated random variables of various probability distributions into standardized normal distributions. If X_1, X_2,…, X_n are non-normal random variables, the equivalent normal distribution can be used (Paloheimo and Hannus 1974; Ang and Tang 1984). This procedure is called Rackwitz-Flessler procedure. For correlated random variables, Hohenbichler and Rackwitz (1988) used the transformation procedure proposed by Rosenblatt (1952) to transform them into the uncorrelated standardized form. In the methods introduced above, only the first-order Taylor derivative and the second moment of the variables, are used to calculate the reliability index. It is consequently called the first-order second-moment (FOSM) method in application. This method has been extensively used in engineering applications (Tabsh and Nowak 1991; Micic *et al*. 1995; Enright and Frangopol 1998; Estes and Frangopol 1999; Akgül and Frangopol 2004a, b; Czarnecki and Nowak 2008; Frangopol *et al*. 2008; Nowak and Eamon 2008). The second-order method (SORM) is also employed sometimes. The probability of failure, P_f, in Eq. (2.5) can be approximated by

$$P_f = \Phi(-\beta) \tag{2.15}$$

where $\Phi(\cdot)$ is inversion of standard normal distribution function, and β is reliability index. For well-behaved limit states, Eq. (2.15) is an excellent approximation for the failure probability.

It is sometimes difficult to apply the numerical approximation methods for the involvement of complex mathematical functions. In such cases, the simulation methods are often employed. Among the simulation methods, the most popular one is the Monte Carlo (MC) method (Thoft-Christensen and Baker 1982). The Monte Carlo simulation is to sample at random to simulate artificially a large amount of experiments and to observe the results (Melchers 1999). When complex mathematical functions, e.g. inverse error function in the predictive models, and conditional probabilities which contain intersection functions, are involved in the reliability analysis, it is extremely difficult to apply the numerical approximation method. In this case, the MC method is more applicable. To use the MC method in structural reliability analysis, samples of each random variable, X_i, are generated randomly first. And then the performance function, $g(\mathbf{X})$, is evaluated for each set of generated random variables. The failure probability can be given approximately by (Melchers 1999; Nowak and Collins 2012)

$$p_f \approx \frac{n(\mathrm{g}(\mathbf{X}_i) \le 0)}{N} \tag{2.16}$$

where N is the total number of simulations, $n(g(\mathbf{X}_i)\leq 0)$ is the number of times for $g(\mathbf{X}_i)\leq 0$. What is described above is the direct sampling method, which is the simplest MC method.

For engineering problems, the failure probability, p_f, is very small, which implies that the number of samples to achieve a reasonable estimate of the p_f is required to be extraordinarily large. The direct sampling method is apparently not efficient. Many variance reduction methods have been proposed to increase the efficiency of the MC method, including Latin hypercube sampling, importance sampling, stratified sampling, adaptive sampling, directional simulation method, antithetic variates method, conditional and generalized conditional expectation method, etc. Among these methods, the Latin hypercube sampling method and the conditional and generalized conditional expectation method are more advantageous than others because they do not require information regarding the important regions or variables in advance, and are applicable to both time invariant and time variant problems (Sundararajan 2012).

2.1.3.3 Structural reliability

The measure of structural performance in civil engineering is usually termed by limit states. Typical limit states for civil structures include but not limited to ultimate (safety), serviceability, and fatigue. The ultimate limit state means the loss of structural capacity, i.e. failure or other deficiency in structural resistance, or collapse of a structure. The serviceability limit state refers to the unfulfilled service demand, such

as excessive deformations and vibrations, etc. The fatigue limit state represents the loss of strength under repeated loadings. Structures usually have a number of possible failure modes; for example, in strength-based analysis, compressive or tensile, flexural, shear, and torsional failures are usually concerned. All the failure modes should be treated separately in reliability analysis. Therefore, structural reliability in civil engineering refers to the probability that a structure will not violate a specified failure mode corresponding to a specified limit state during a specified period of time (Rafiq 2005).

2.1.3.4 Time-dependent reliability

Actually, the structural resistance decreases as its deterioration over time because of the ageing of materials, operational loadings and environment, etc.; on the other hand, the loadings and environment effects may change a lot during the service time of a structure. Therefore, the reliability of a structure is not constant but time dependent. The deterioration of different materials has been widely studied. In the late 1970s, deterioration was discovered in concrete bridges. Since then extensive studies on concrete's deterioration have been carried out (Brown 1987; Wallbank 1989; Basheer *et al.* 1996) and several mechanisms have been revealed. Corrosion models predicting where and when corrosion will cause section loss of steel components was developed for steel girders by Albrecht and Naeemi (1984) first and later improved by Thoft-Christensen *et al.* (1996).

The performance function of structures in civil engineering is also called limit state function or safety margin, and is often written as

$$M(t) = R(t) - S(t) \tag{2.17}$$

where $M(t)$ is the safety margin corresponding to a specified failure mode; $R(t)$ and $S(t)$ represent the time dependent resistance and load effects, respectively. All uncertainties in resistance such as the mechanical properties of materials and the geometry of structures, are incorporated into $R(t)$; and those in load effects, including axle forces, bending moments, shear forces, torsion angles, etc. are incorporated into $S(t)$.

Though in most cases the resistance and load effects are time dependent, in engineering applications they are often simplified to time independent quantities. For example, for a given time period, T, the resistance can be considered as time invariant, and only the load effects depend on time. The failure probability is defined as that the resistance cannot provide capacity for the maximum load effect during this time interval T. That is,

$$p_f(T) = p\left[\min_{0<t<T} M(t) \le 0\right] = p\left[R \le \max_{0<t<T} S(t)\right] \tag{2.18}$$

When both the resistance and load effects are time variant, but independent of each other, an upper bound approximation can be applied to reduce the problem to time independent reliability analysis (Li 2004):

$$M(T) = \min_{0<t<T} R(t) - \max_{0<t<T} S(t) \tag{2.19}$$

2.1.4 Bayesian Inference

Similar to other problems in engineering, in bridge condition assessment decisions are often made under uncontrolled conditions, where traditional statistics are impractical. Sometimes there is even no population from which the samples can be drawn (Lapin 1983). In this case, the Bayesian approach becomes promising. Bayesian updating techniques use both the prior information and new inspection information, to account for the relative uncertainty associated with each to obtain a balanced estimation (Estes and Frangopol 2003). There have been many classical works on Bayesian statistical inference (Zacks 1971; Ang and Tang 1975; Iversen 1984; Bernardo and Smith 2009; Box and Tiao 2011; Gelman *et al*. 2014). The concepts and theories stated below mainly refer to these literatures.

2.1.4.1 Theory and concept

The Bayesian statistical inference is based on the Bayes' theorem, which provides the possibility for inferring uncertain models based on their measurements. According to

this theorem, if event A occurred, the probability for the occurrence of a particular event E_i is

$$P(E_i / A) = \frac{P(A / \mathrm{E}_i)P(\mathrm{E}_i)}{P(A)} = \frac{P(A / \mathrm{E}_i)P(\mathrm{E}_i)}{\sum_{j=1}^{n} P(A / \mathrm{E}_j)P(\mathrm{E}_j)} \tag{2.20}$$

where the probability of event A, which is the average probability weighted by those of E_i, is called total probability. If the parameter of a distribution, θ, is a random variable with a prior density function $f'(\theta)$, and ε is an observed experimental outcome, $f'(\theta)$ can be revised using Bayes' theorem. That is, the posterior probability of θ is

$$f''(\theta) = \frac{f(\varepsilon / \theta) f'(\theta)}{\int_{-\infty}^{+\infty} f(\varepsilon / \theta) f'(\theta)\, d\theta} \tag{2.21}$$

where $f(\varepsilon/\theta)$ is the conditional probability density of the experimental outcome ε assuming a given θ. Thus, $f(\varepsilon/\theta)$ is a function of θ and is usually referred to as the likelihood of θ, which is denoted by $L(\theta)$. The dominator is independent of θ and is simply a normalizing constant, making $f''(\theta)$ a proper density function. Then, Eq. (2.21) can be expressed as

$$f''(\theta) = kL(\theta) f'(\theta) \tag{2.22}$$

where $k = [\int_{-\infty}^{+\infty} L(\theta) f'(\theta)\, d\theta]^{-1}$ and $L(\theta)=f(\varepsilon \mid \theta)$.

The posterior distribution $f''(\theta)$ can be set to a new prior distribution, so this process can be repeated with the evolution of data (Wang *et al.* 2009). In complicated models, analytically deriving $L(\theta)$ and k is generally a nuisance and even impossible. For many years, the difficulty prevented the application of Bayesian modeling techniques to real-world problems. This situation changed with the advent of Markov Chain Monte Carlo (MCMC) algorithms (Hastings 1970; Congdon 2002; Gilks 2005; Gamerman and Lopes 2006; Carlin and Louis 2008; Hamada *et al*. 2008; Robert and Casella 2013; Gelman *et al*. 2014).

2.1.4.2 MCMC algorithms

The MCMC method provides an algorithm to draw samples from the Bayesian posterior uncertainty distribution of model parameters based on the given likelihood function and the prior distribution. There are many MCMC techniques such as the Gibbs sampling and the Metropolis-Hastings sampling.

The Gibbs sampling can simulate from multivariate distributions by simulating only from the conditional distributions. Denoting the distribution of interest as $\pi(\boldsymbol{\theta})$, $\boldsymbol{\theta}=(\theta_1,\ldots,\theta_n)'$, and the full conditionals as

$$\pi(\theta_i|\theta_1,...,\theta_{i-1},\theta_{i+1},...,\theta_n) = \pi(\theta_i|\theta_{-i}), \qquad i = 1,...,n \tag{2.23}$$

the Gibbs sampling can be applied flowing the below procedure if it is possible to simulate from the full conditionals (Geman and Geman 1984).

(1) To initialize the counter to j=1 and the state of the chain to $\boldsymbol{\theta}^{(0)}=(\theta_1^{(0)},\ldots,\theta_n^{(0)})'$.

(2) Obtain a new value $\boldsymbol{\theta}^{(j)}$ from $\boldsymbol{\theta}^{(j-1)}$ by successive simulation from the full conditionals

$$\begin{aligned}
&\theta_1^{(j)} \sim \pi(\theta_1 \mid \theta_2^{(j-1)},\ldots,\theta_n^{(j-1)}) \\
&\theta_2^{(j)} \sim \pi(\theta_2 \mid \theta_1^{(j)},\theta_3^{(j-1)},\ldots,\theta_n^{(j-1)}) \\
&\vdots \\
&\theta_d^{(j)} \sim \pi(\theta_d \mid \theta_1^{(j)},\ldots,\theta_{n-1}^{(j)})
\end{aligned} \tag{2.24}$$

(3) Increase counter from j to j+1 and return to step 2.

After an initial "burn-in" period, the resulting chain will converge to the posterior distribution.

The Gibbs sampling simulates from full conditional distributions, nonetheless, it may not be straightforward to simulate from the full conditionals. Metropolis-Hastings schemes provide a way to improve this problem.

A reversible Markov chain, which has the distribution of interest, $\pi(\boldsymbol{\theta})$, as its stationary distribution, can be constructed. Simulating from such a Markov chain will obtain values from $\pi(\boldsymbol{\theta})$. The procedure is to construct a transition kernel $p(\boldsymbol{\theta},\boldsymbol{\varphi})$ to ensure that the equilibrium distribution of the chain is $\pi(\boldsymbol{\theta})$. This transition kernel is made up of two elements: an arbitrary transition kernel $q(\boldsymbol{\theta},\boldsymbol{\varphi})$, which is also known as the

proposal distribution, and an acceptance probability $a(\boldsymbol{\theta},\boldsymbol{\varphi})$. The acceptance probability is (Hastings 1970)

$$a(\boldsymbol{\theta},\boldsymbol{\varphi}) = \min\left\{1, \frac{\pi(\boldsymbol{\varphi})q(\boldsymbol{\varphi},\boldsymbol{\theta})}{\pi(\boldsymbol{\theta})q(\boldsymbol{\theta},\boldsymbol{\varphi})}\right\} \tag{2.25}$$

A chain with limiting distribution $\pi(\boldsymbol{\theta})$ can be obtained by the following procedure.

(1) To initialize the counter to j=1 and the chain to $\boldsymbol{\theta}^{(0)}$.

(2) To simulate a proposed value $\boldsymbol{\varphi}$ using the kernel $q(\boldsymbol{\theta}^{(j-1)},\boldsymbol{\varphi})$.

(3) To find the acceptance probability of the proposed value $a(\boldsymbol{\theta}^{(j-1)},\boldsymbol{\varphi})$.

(4) To accept $\boldsymbol{\theta}^{(j)}=\boldsymbol{\varphi}$ with probability $a(\boldsymbol{\theta}^{(j-1)},\boldsymbol{\varphi})$ and take $\boldsymbol{\theta}^{(j)}=\boldsymbol{\theta}^{(j-1)}$ otherwise.

(5) To increase the counter from j to j+1 and return to step 2.

2.2 Traditional Bridge Condition Assessment Techniques

2.2.1 Inspection-Based Condition Assessment

The results of the bridge condition assessment are preferred to be represented by indices corresponding to different terms, which is usually called bridge condition

rating (BCR). It facilitates the bridge engineers and decision makers to determine the maintenance priority and strategy.

2.2.1.1 BCR in the USA

FHWA guidelines

According to the FHWA guidelines (FHWA 2014), three structural items are rated: Deck (Item58), Superstructure (Item59) and Substructure (Item60). Five levels of bridge inspection are defined. Bridge inspectors consider the overall condition characterization of the entire item, not an indication of localized conditions. Most of the States in the USA have established their own BCR manuals. In some of these manuals, each of the three structural items is not evaluated as a whole but is further divided into different individual elements or sections.

Rating in the range of 0-9 is provided for each rated component. The overall bridge condition, which is presented by a deterministic sufficiency rating, is then derived by the condition rating results of the three items. The sufficiency rating combines serviceability and condition evaluations according to the weighted average formula: Sufficiency Rating=S_1+S_2+S_3-S_4. S_1 is 0-55% structural adequacy and safety; S_2 is 0-30% serviceability and functional obsolescence; S_3 is 0-15% essentiality for public use; and S_4 is 0-13% special reduction. S_1, S_2, S_3 and S_4 are defined using condition ratings generated from inspections, and geometric and traffic data from the inventory, and resistance of the bridge. The sufficiency rating is used to classify the necessity of

maintenance, and eligibility for funding. If the sufficiency rating for a bridge is less than 80, then the bridge is qualified for replacement.

New York guidelines

The New York system (Yanev and Testa 1997) reduces the rating scale into 7 instead of 9 used in the FHWA system: 7, new; 5, functioning well; 3, not functioning as designed; 1, failed; the even numbers 6, 4, and 2 denote intermediate conditions. Separated condition ratings for each span are introduced for better estimation. A typical bridge span is divided into 13 essential components, and all inspected elements over the span are grouped into these 13 components. Different from the FHWA, a simple weighting system is used to highlight the importance of some principal structural elements. Each essential component type has been assigned a higher weighting. The overall evaluation result, BCR, is derived using the lowest rating of the 13 essential components in any bridge span, multiplied by the prescribed weight:

$$BCR = \sum(\text{Component rating} \times \text{Weight}) / \sum \text{Weightings} \tag{2.26}$$

The calculated *BCR* helps the inspection team assign a general recommendation to the bridge.

2.2.1.2 BCR in Europe

In Europe, countries such as the UK, France, Germany, Slovenia, and Denmark all have their own BCR guidelines. The guidelines of the UK and Germany are taken as representatives here.

UK guidelines

Two BCR systems are adopted in UK: Bridge Condition Index (BCI) at the nation level, and Maintenance Priority Number (MPN) used by a local authority. The BCI is developed by the London Underground Limited, which began inspecting bridges since 1936. At that time, no reference manuals were provided, and the inspector was ordered to write his own comment of the structure in an exercise book. Since 1966, a 26-page inspection manual gave inspectors guidance on observing possible problematic area in bridge structures and introduced a standard report format. Nowadays, the development of the BCI is still kept on. Another system is adopted at Surrey County located in the south east of England. Surrey County Council's Infrastructure Group is in charge of the maintenance of over 2,000 structures on the county road and rights of way network. The MPN is used as an important parameter in the rehabilitation process.

There are four levels of inspection in the BCI guidelines of the UK. In each level of inspection, experienced engineers are required to record two aspects of the inspected elements: element type and severity (1-5). The bridges are divided into 33 element types. The BCI system integrates the inspected data into a numerical and normalized value, BCI, to evaluate the condition of the whole bridge (Blakelock *et al.* 1999). The BCI is based on two major factors: the element factor E_F, and the extent/severity factor S_F. Both factors were given a value between 1 and 10. The BCI is calculated by

$$BCI = 100 - F_1\left[F_2\left(E_{FP} \times S_F\right)/N_P + F_3\left(E_{FS} \times S_F\right)/N_S\right] \tag{2.27}$$

where E_{FP} is the element factor for primary elements; E_{FS} is the element factor for secondary elements; S_F is the extent/severity factor; N_P is the number of primary elements in the bridge; N_S is the number of secondary elements in the bridge; and F_1, F_2 and F_3 are a series of factors. The concept of primary and secondary elements is introduced to weight the elements in the index. The failure of primary elements (such as foundations, main beams, etc.) would either bring about collapse of the structure or at least render it unusable. As a result, higher weighting is given to the primary elements to highlight their importance. The BCI is 100 if all elements of a bridge have a severity factor of 1. If any primary element of a bridge has a severity factor of 5, the BCI for the bridge should be set to 0, which means that the bridge should be considered as non-functional.

In the MPN system (Brooman and Wootton 2000; Ryall 2001), each bridge is broken down into individual elements. Each element is assigned a condition value from 1 to 5, where condition 1 is good, and 5 is critical. The condition value (CV) is then converted to a condition factor (CF) to calculate the MPN. Depending upon the importance to the bridge, the location of each element in the structure is given a location factor (LF) in the range of 5-10. Moreover, a road factor (RF) between 9 and 14 is assigned to each type of road depending upon its importance. The MPN is the calculated by: MPN=CF×LF×RF/14. Therefore, each element in the bridge can have an MPN. The rehabilitation process would give priority to structural elements with an MPN of less than 20.

German guidelines

In Germany, the BCR presently follows a set of guidelines (Krieger and Haardt 2000), among which the DIN 1076 is taken as an example here. An inspected structure is divided into 14 component groups. The condition rating of the inspected structural members is based on the detailed evaluation of individual occurrences of damage. The condition rating of the overall structure is based on the highest condition rating of the component groups. It is a function of three damage evaluation sets (traffic safety, stability and durability), the total extent of damage, and the number of individual occurrence of damage, taking a defined evaluation key into account.

2.2.1.3 BCR in Japan

In Japan, the Public Works Research Institute (PWRI) of Ministry of Construction (MOC) is in charge of developing the bridge management system. There are five scales of deficiency rating to describe the damage level of an inspected element. Deficiency rating I (d_I) means serious damage, which may cause traffic problems, and deficiency rating IV (d_{IV}) represents slight damage (Yokoyama *et al*. 1996). A reducing factor α_i is introduced for each degree of deficiency rating to calculate the corresponding demerit rating. The demerit ratings are calculated by $D_i=d_i\times\alpha_i$. By a process of reduction, the overall BCR is obtained.

To make the condition assessment based on visual inspections more accurate and reliable, several approaches, such as fuzzy logic method (Liang *et al*. 2001; Sasmal and Ramanjaneyulu 2008) and neural network method (Cattan and Mohammadi 1997;

Kawamura *et al*. 2003), were attempted. Nevertheless, the basis of these methods is still the visual inspection results, so the improvement might be limited.

2.2.2 Structural-Analysis-Based Condition Assessment

Several countries use bridge capacity rating as a condition assessment tool. Two examples are the Load and Resistance Factor Rating (LRFR) method in the AASHTO Manual for Bridge Evaluation (AASHTO 2008), and a similar method in section 14 of Canadian Highway Bridge Design Code (CSA 2006). They provide guidelines and methods to determine if an existing bridge is competent to carry a particular set of loads. These methods are semi-probabilistic in nature, and partial factors are used for load effects and structural resistances. Strength limit states are calibrated to achieve a uniform reliability. The reliability index is used, but in an inverted sense. Rather than determining the probability of load demand exceeding capacity as is the case in structural reliability, the reliability index in condition assessment is a calibrated factor to ensure an adequate level of structural safety. The LRFR method is introduced as follows.

The LRFR method was first introduced in the AASHTO guide manual for bridge evaluation in 2003 (AASHTO 2003). The manual further evolved into the Manual for Bridge Evaluation (MBE). The MBE includes three analytical load rating methods: allowable stress rating (ASR), load factor rating (LFR) and LRFR. In the overall

approach, bridge design and condition assessment are similar, but they are different in the consideration of variables.

Overly conservative condition assessment will increase the load restriction, rehabilitation, and replacement, and therefore it should be prohibited. Load tests were conducted to evaluate in-situ bridge capacity (Moses *et al*. 1994; Chajes *et al*. 1997; Faber *et al*. 2000), and it was found that the safe load-carrying capacities of some bridges calculated based on design codes were underestimated (Bakht and Jaeger 1990). LRFR method adopted two levels of reliability for different rating vehicles with different length of exposure duration: design life for design load rating, and inspection interval for legal load rating.

Although detailed structural analysis is done in this condition assessment method, a defined live load model representing bridges nationwide, is adopted to calculate the live load capacity. This generalized model may not be applicable to the evaluated bridge. Moreover, the condition factor to determine the structural capacity is subjective.

2.3 SHM-Based Bridge Condition Assessment

A large proportion of the previous research on utilization of SHM data was dedicated to vibration-based damage detection, including parameter identification and pattern

recognition (Doebling *et al*. 1996; Carden and Fanning 2004; Sohn *et al*. 2004; Friswell 2007; Worden and Manson 2007). However, success is limited to simulations, laboratory studies and well-controlled experiments such as the Z24 bridge (Maeck *et al.* 2001). Their effectiveness still remains to be proven for operational civil structures (Brownjohn 2007). Actually, because of the interference of environment and operational loadings and large scale of long-span bridges, it is a significant challenge to detect damage through the SHM data. In the short term, maybe we cannot expect too much on SHM to be able to localize and quantify damage in real time by system identification.

SHM data can also be considered as proofed events, so the structural reliability can be updated continuously by the Bayesian statistical inference. This concept has been applied in NDT-based fatigue reliability updating (Zheng and Ellingwood 1998; Zhang and Mahadevan 2000). A methodology for effectively incorporating the data collected through in-service health monitoring to update the performance prediction is developed by Rafiq (2005).

Strain is one of the most important structural responses for SHM-based condition assessment. The reasons are listed as follows (Ko and Ni 2005; Catbas *et al*. 2008; Frangopol *et al*. 2008). Firstly, the stress of structural components induced by in-service loadings can be derived by strain data. As a result, reliability of structural components can be evaluated. Besides, inner forces of the monitored structural components can be derived by the data acquired from elaborately designed arrays of

strain gauges. Strain is a typical local structural response, so it would be better suitable to characterize local damage than global responses. DeWolf *et al.* (2002) introduced three examples of structural health condition evaluation based on short-term strain data. Bhattacharya *et al.* (2005) used peak strain measured in 11 days to conduct live-load ratings. However, the long-term characteristics of strain might be ignored in the short-term data. Xia (2012) developed a systematic framework for bridge condition assessment making use of strain data based on structural reliability. Cardini and DeWolf (2008) developed a long-term strain-based bridge evaluation framework. However, the robustness and capability of this framework have not been validated by long-term SHM data collected from real structures.

2.4 Potential Effects of Long-Term SHM on Bridge Evaluation

The assessment of bridges can be conducted at multiple levels. Take the guidelines for the management of sub-standard highway bridges in Britain (BD79/13 2013) as an example, the followings are such possible levels of assessment.

- Level 1: With the material properties and characteristic strengths, and partial factors for load and resistance from the relevant assessment standards (e.g., BD 44 for the assessment of concrete structures, BD 56 for steel structures, and BD 61 for composite structures), the conservative load capacity is estimated. It is the simplest form of assessment.

- Level 2: Analysis techniques including grillage analysis, finite element analysis or non-linear and plastic analysis, are employed to do more refined analysis. Characteristic strength is also determined based on the available data, e.g., mill tests on steel reinforcement, etc.
- Level 3: Bridge specific live loading and material tests are carried out for condition assessment based on code implicit safety levels.
- Level 4: Safety characteristic and bridge specific minimum safety/reliability levels are taken into consideration to assess safety of the bridge.
- Level 5: Using probability data for all variables involved in the limit states, full reliability analysis of particular structures or type of structures is carried out.

Level 1 to 3 assessments are based on code-implicit levels of safety, and are sometimes referred to as deterministic methods. However, uncertainties associated with the load effects, the actual performance of structures, and the nature and rate of deterioration, are inevitable and subject to change during the service life of bridges. As an extension to these levels of assessment, reliability-based methods can be used. Guidance for carrying out the assessment of Level 1 to 3 is available in the design manuals for bridges. Nevertheless, guidance for Level 4 and 5 assessments (reliability-based) is still in developing stage.

The reliability-based bridge condition assessment is attracting the attention of the bridge engineering community. The structural reliability profile is obtained based on

the deterioration and structural performance at each time point. It can be applied to schedule the bridge management activities. Reliability-based assessment of civil structures was initially applied to evaluate offshore structures (Benjamin and Cornell 1970; Ang and Tang 1975; Thoft-Christensen and Baker 1982). Since the research supported by the European Union (Thoft-Christensen 1993), it has been an active research area throughout the world (Mori and Ellingwood 1993; Micic *et al*. 1995; Ellingwood 1996; Estes 1997; Das 1998b; Thoft-Christensen 1998; Val *et al*. 1997, 1998, 2000; Enright and Frangopol 1999b; Chryssanthopoulos and Sterritt 2002; Neves and Frangopol 2005; Rafiq 2005; Neves *et al*. 2006a, b; Messervey 2008). These researches justify that the reliability index can be used as an alternative to the condition index, if the information about the loadings and structural responses is available. Furthermore, the lifetime assessment can be achieved based on reliability methods as well (Frangopol and Estes 1997; Thoft-Christensen 1997; Enright and Frangopol 1998; Czarnecki and Nowak 2008).

Usually, four categories of physical parameters are continuously collected by the long-term SHM system, including environment, operational loads, bridge features, and bridge responses (Ni and Wong 2012). They can be a great help to alarm abnormal loading and response, and to assess structural serviceability during extreme events and structural integrity after disasters. Apparently, SHM can effectively complement inspection with a wealth of high-quality data collected in-situ. There are compelling advantages by employing SHM technologies to improve bridge condition assessment.

The advantages can be summarized as follows: (1) updating existing models for the structural resistance and load effect; (2) performance updating over time; (3) warning against threshold levels; (4) bridge specific consideration; and (5) simplicity and efficiency (Messervey 2008). Therefore, SHM technologies can revolutionize the traditional way of bridge inspection in a timely, objective, and quantitative way. The SHM-based bridge condition assessment has a great potential to save cost in bridge management, such as repair, rehabilitation and inspection. Some structurally deficient bridges under the load rating with the specified truck models may be re-categorized as structurally safe bridges by using the actual live loads obtained from SHM data (Liu *et al.* 2009). With the structural specific SHM data, inspections can be scheduled on a demand basis.

Because of the limited knowledge of relevant random variables, integrating SHM into bridge condition assessment is still in development, and will take many years to implement ideas from research to practice. The reliability index has only been used to calibrate the partial load and resistance factors in the codes and manuals for bridge design and evaluation (Akgül and Frangopol 2004). Despite a large amount of SHM data have been collected, there has been very little research on efficiently integrating the valuable long-term SHM data into the bridge condition assessment.

2.5 Conclusions and Research Needs

This chapter reviewed the important concepts and methodologies relevant to this thesis. The fundamental concepts involved in this thesis, including long-term SHM, bridge management system, structural reliability, and Bayesian statistics, were introduced first. And then, the traditional methods for bridge condition assessment, including the inspection-based method and the structural-analysis-based method, were reviewed. The bridge condition rating systems in different countries were summarized. The LRFR method, which is applied to evaluate the bridge load carrying capacity, was illustrated. Next, the existing SHM-based methods for bridge condition assessment were introduced. Finally, the potential effects of long-term SHM data on bridge condition assessment were discussed.

Although the traditional bridge condition assessment methods have been devoted to evaluating the safety or serviceability of bridges, there are still many challenges. Most of the existing methods for bridge condition assessment are based on visual inspections. The drawbacks of visual inspections have been widely recognized. The methods based on structural analysis calculate the load carrying capacity of bridges using generalized live load models which represent the bridges nationwide, and some partial factors are relatively subjective. Inaccurate condition assessment is the most critical barrier to effective and cost-saving management of bridges.

Long-term SHM captures the loads and structural responses of bridges continuously. Thus, it has a potential to provide valuable information, including but not limited to live load models, live load demands, structural deterioration and detection of damage, to the reliability-based bridge evaluation. Because of the insufficiency of long-term SHM data in the previous studies, the interpretation of SHM data to useful information about the bridge performance and safety is still in its infancy. It has hindered the bridge engineers from benefiting from the SHM systems to arrange the bridge management activities. Therefore, to fulfill the promise of SHM technology, one of the most urgent challenges is to integrate the long-term SHM data into bridge condition assessment. To achieve this aim, the following issues should be primarily solved.

1. An effective signal preprocessing methodology. Noises, spikes, and trends are inevitable in the SHM signals. In addition, the measured data are generated by a mixture of different effects, such as traffic, wind, and temperature, hence the signals may need to be separated into different sources in a specific research. Recognizing the characteristics of long-term SHM data and their extraordinarily large volume, the signal processing methodology should have a capability of multi-resolution and multi-domain. Furthermore, it should be able to remove the noises, spikes and trends, and separate different signal sources automatically and computationally efficiently.

2. Site-specific live load models. It is nearly unrealistic that sensors are installed on all components of a bridge. Thus, an elaborate FEM of the bridge is usually

employed to complement the SHM through conducting structural analysis. To obtain more accurate results from the FEM-based structural analysis, site-specific live load models should be available.

3. A reliability-based framework for bridge condition assessment in the context of Bayesian inference. To make full use of the valuable SHM data, which are random variables, the reliability theory is a promising tool. It provides a structural reliability with respect to a limit state, such as SLS and ULS, to assess the bridge condition more accurately. Bayesian updating techniques are very useful in this framework. They have the capability to consider the uncertainty associated with both the prior information and new measured data to obtain a balanced estimation.

4. BCR system integrating SHM data. A BCR system provides explicit indices, which are understandable by and favorable for the bridge managers to determine the maintenance strategy. SHM data can make the rating results more objective and accurate, hence an SHM-based BCR system should be developed.

CHAPTER 3

WAVELET-BASED DENOISING, DESPIKING AND DECOMPOSING OF LONG-TERM SHM DATA

3.1 Introduction

The physical sizes of civil structures are grand, and the loadings and environmental factors are diverse and complex. Moreover, there are intricate interactions between the structures and operational loadings. In addition, even though the manufacturers and industries have attempted to improve the long-term stability of the SHM systems, it is still inevitable that there are errors occasionally in the sensors, signal conditioning unit, analog-to-digital converter (ADC), or digital communication network. Consequently, the signals are non-stationary and usually contaminated by noises, spikes, trends, which hinder us from taping the potential of long-term SHM data.

Signal pre-processing, which is to remove noises, spikes, and trends in the data, is the fundamental and vital step to extract useful information from the SHM data. In some specific studies, different signal sources, such as strain or displacement due to the respective effect of railway and highway traffic, are desired to be separated. Especially,

for long-term SHM data, which imply an extremely huge amount, automation and efficiency of a signal processing technique deserve particular concern in addition to effectiveness. Special signal pre-processing techniques enabling denoising, despiking and decomposing are essential.

Except keeping information in time-frequency domain, the wavelet transform (WT) has the merit of multi-resolution. That is, this technique can characterize concerned event coefficients in multiple frequency bands. Thus, it has exhibited its notable capabilities in processing non-stationary signals of many fields, such as mechanical engineering (Staszewski and Tomlinson 1994; Lin and McFadden 1997; Lin and Qu 2000; Peng and Chu 2004; Zhu *et al*. 2009; Yan *et al*. 2014), biomedical engineering (Li *et al.* 1995; Khadra *et al*. 1997; Addison 2005; Brechet *et al.* 2007; Rafiee *et al.* 2011; Martis *et al*. 2013), chemistry (Walczak *et al*. 1996; Walczak 2000; Ehrentreich 2002; Koo *et al*. 2011; Mahalakshmi *et al*. 2013), and astronomy (Starck and Murtagh 1994; Foster 1996; De Moortel and Hood 2000; Mészárosová *et al*. 2009; Hafez *et al*. 2010).

In the civil SHM field, the application of WT has mainly focused on damage detection by checking anomalies in the wavelet coefficients or their derivatives, such as wavelet energy, and the mathematical models of wavelet coefficients (Brownjohn 2002; Hera and Hou 2004; Melhem 2004; Moyo and Omenzetter *et al*. 2004; Ovanesova and Suarez 2004; Kim and Rucka and Wilde 2006; Hester and González 2012; Cantero

and Basu 2015). However, there has been little literature about the application of WT to systematically pre-processing the long-term SHM data.

An automatic and efficient wavelet-based methodology is proposed in this chapter to pre-process the long-term SHM data, in terms of denoising, despiking and decomposing. Strain and displacement data acquired by the long-term SHM system deployed on the TMB are employed to demonstrate this methodology. The remainder of this chapter is organized as follows. Section 3.2 reviews the WT theory and existing methodologies of wavelet-based denoising and despiking. Section 3.3 proposes the wavelet-based signal pre-processing methodology for long-term SHM data. In section 3.4, the proposed methodology is illustrated and demonstrated using the long-term strain and displacement data measured from the TMB. Finally, a summary of this chapter is given in section 3.5.

3.2 Wavelet Theory and Existing Methodologies for Signal Pre-Processing

3.2.1 Wavelet Transform

The continuous WT (CWT) of a signal is defined as the convolution of the signal $f(t)$ and a mother wavelet function $\psi(t)$ (Rioul and Vetterli 1991)

$$W_{a,b} = \frac{1}{\sqrt{a}} \int_{-\infty}^{+\infty} f(t)\, \bar{\psi}\left(\frac{t-b}{a}\right) dt \tag{3.1}$$

where a and b are scale and translation parameters, respectively. The bar over $\psi(t)$ indicates its complex conjugate. The mother wavelet $\psi(t)$ is a function of finite energy and zero integral,

$$\int_{\mathbb{R}} \psi(t)\, dt = 0 \tag{3.2}$$

The mother wavelet should ensure the existence of the inverse wavelet transform. That is

$$C_{\psi} = \int_{-\infty}^{+\infty} \frac{\left|F_{\psi}(\omega)\right|^2}{\left|\omega\right|} d\omega < \omega \tag{3.3}$$

where $F_{\psi}(\omega)$ denotes the Fourier transform of $\psi(t)$. Then the signal $f(t)$ can be reconstructed by an inverse CWT (ICWT)

$$f(t) = \frac{1}{C_{\psi}} \int_{-\infty}^{+\infty} \int_{-\infty}^{+\infty} \frac{1}{a^2} W_{a,b}\, \psi\left(\frac{t-b}{a}\right) da\, db \tag{3.4}$$

The CWT requires much calculation effort to find the wavelet coefficients corresponding to every single value of the dilation and translation parameters. To process signals more efficiently, a discrete version of WT is often employed. The

discrete WT (DWT) discretizes the scale parameter a and the translation parameter b. Generally, the dyadic values of a and b are used

$$a = 2^j; \quad b = 2^j k \qquad j,k \in Z \tag{3.5}$$

where Z indicates sets of positive integers. The corresponding discretized wavelets $\{\psi_{j,k}\}$, which are

$$\psi_{j,k}(t) = 2^{j/2}\psi(2^j t - k) \tag{3.6}$$

constitute an orthogonal basis. The wavelet expression of a signal $f(t)$ is defined using the orthogonal basis as

$$f(t) = \sum_j \sum_k \alpha_{j,k}\, \psi_{j,k}(t) \tag{3.7}$$

The coefficients of the wavelet expansion are

$$\alpha_{j,k} = \int_{-\infty}^{+\infty} f(t)\, \overline{\psi}_{j,k}(t)\, dt \tag{3.8}$$

For faster algorithm, the Mallat's decomposition scheme (Mallat 1989) is mostly adopted in practice. In this scheme, the DWT can be interpreted as a filter bank. The signal is passed through a series of high-pass filters and low-pass filters, usually denoted as $h(k)$ and $g(k)=(-1)^k h(1-k)$, respectively. Using these filters, the signal is decomposed into a set of low and high-frequency components

$$\begin{cases} a_{j,k} = \sum_m h(2k-m)\, a_{j-1,m} \\ d_{j,k} = \sum_m g(2k-m)\, a_{j-1,m} \end{cases} \tag{3.9}$$

where $a_{j,k}$ is the approximation coefficients, which represent the low-frequency components of signals; $d_{j,k}$ is the detail coefficients, which correspond to the high-frequency components of signals; and m is the number of wavelet coefficients. The approximation and detail coefficients at level j are obtained by convolving the approximation coefficients at the previous level (j-1) with the low-pass and high-pass filter coefficients, respectively. By inverse DWT (IDWT), the approximations and details at different levels will be reconstructed using the corresponding wavelet coefficients. The signal $f(t)$ is a sum of the approximation at level J and details at level J and lower levels

$$f(t) = A_J + \sum_{j \le J} D_j \tag{3.10}$$

where A_J is the approximation at level J, and D_j is the detail at level j. More details about the wavelet theory can be found in many books and papers (Rioul and Vetterli 1991; Daubechies 1992; Mallat and Zhang 1993; Strang and Nguyen 1996; Mallat 1999; Fugal 2009; Chui 2014).

The CWT has very high resolution but creates an increase in computational time and memory. It is better used to analyze the features in a signal. The DWT has improved computational efficiency, even faster than the fast FT (FFT). However, it comes to a

sparse representation of the signal, which goes against finding signal features. It is widely applied in signal compression and denoising.

3.2.2 Wavelet Denoising

Signal denoising can be described as a process of extracting useful information from raw data. In a broad sense, noise is any signal of no interest. Thus, spikes, trends and any other signal sources irrelevant to the desired signal all can be considered as noises. Nevertheless, each signal source has unique characteristics; consequently, different processing methods are required. Therefore, throughout this thesis the noise is limited to Gaussian white noise.

Based on the domain of analysis, the signal denoising methods can in general be divided into three categories: the time-domain method, frequency-domain method and time-frequency domain method. The time-domain method is often called smoothing method, in which averaging is usually used (Braun 2011). It is most suitable to analyze a strictly periodic signal. The frequency-domain method is also called filtering method, in which band-pass filtering is typically used (Antoni 2007). This method only considers narrow band information, whereas the noises may span a wide frequency band. Moreover, if noises have similar frequencies to the underlying signal, filtering out noises will cause noticeable loss of useful information. Therefore, these two methods cannot effectively remove noises in the long-term SHM data. The time-frequency domain method combines information of time and frequency, addressing

some limitations of them (Papandreou-Suppappola 2002). The DWT-based denoising method is a well-accepted time-frequency domain method (Lin and Qu 2000; Beheshti *et al*. 2005; Zhu *et al*. 2009).

In the DWT-based denoising procedure, noises are usually modelled as stationary independent Gaussian variables (Moulin and Liu 1999; Alfaouri and Daqrouq 2008). The noisy signal $f(t)$ is represented by

$$f(t) = s(t) + \delta\varepsilon(t) \tag{3.11}$$

where $s(t)$ is the real signal, $\varepsilon(t)$ is standard white noise $N(0,1)$, δ is the intensity of the noise. Because of the orthogonality of the set of wavelet basis in the DWT, wavelet coefficients of the white noise are also independent $N(0,1)$ random variables. Therefore, the empirical approximation coefficients $\hat{a}_{j_0,k}$ and detail coefficients $\hat{d}_{j,k}$ of the noisy signal $f(t)$ can be written as

$$\begin{cases} \hat{a}_{j_0,k} = a_{j_0,k} + \delta\varepsilon_{j_0,k} & k = 0,1,...,2^{j_0}-1 \\ \hat{d}_{j,k} = d_{j,k} + \delta\varepsilon_{j,k} & j = j_0,...,J-1 \qquad k = 0,1,...,2^{j}-1 \end{cases} \tag{3.12}$$

where $\varepsilon_{j,k}$ are independent $N(0,1)$ variables; j_0 is the primary resolution level, e.g. $j_0=\log_2(\ln(n))+1$, where n is the signal length (Härdle *et al*. 2012); and $J=\log_2(n)$. The approximation coefficients $a_{j_0,k}$ represent low-frequency terms, which usually contain important information about the desired real signal $s(t)$ (Antoniadis *et al*. 2001).

Therefore, they are advised to be kept intact in the denoising process. On the other hand, mostly only a few relatively large detail coefficients $d_{j,k}$ contain information of $s(t)$, while the small coefficients $d_{j,k}$ are attributed to noises (Antoniadis *et al*. 2001). To remove the noises, thresholds are needed to define the "large" and "small" detail coefficients.

The classical DWT-based denoising approach is the data-adaptive wavelet thresholding method provided by Donoho and his co-workers (Donoho and Johnstone 1994, 1995; Donoho 1995; Donoho *et al.* 1995, 1998). In this approach, the detail coefficients with absolute values below a certain threshold level are set to zero, and then the de-noised data is obtained by an IDWT to the modified coefficients. The threshold estimation as well as the thresholding policies are two of the most important issues. Donoho and his co-workers proposed several threshold estimations, such as minimax, universal, translation invariant (TI), and Stein's unbiased risk estimate (SURE), and several thresholding policies. Other scholars also proposed various threshold estimations and thresholding policies (Nason 1996; Wang 1996). This classical wavelet denoising approach is easy to understand and efficient, and widely applied in various fields (Cai and Harrington 1998; Lin and Qu 2000; Wachowiak *et al*. 2000; Beheshti *et al*. 2005; Zhu *et al*. 2009; Madadi *et al*. 2013). Different threshold estimations and thresholding policies may lead to different denoising results. A comprehensive overview of various wavelet thresholding methods for signal denoising is given by Nason (1995) and Antoniadis *et al.* (2001).

Motivated by the intrinsic connections of threshold estimation with the Bayesian approach, the problem of wavelet denoising can also be approached from a Bayesian standpoint. Various Bayesian methods for wavelet denoising have been proposed (Chipman *et al*. 1997; Vidakovic 1998; Clyde and George 2000; Percival and Walden 2006). A prior distribution is assumed for the wavelet coefficients first. Then by applying a suitable Bayesian rule to the posterior distribution of the wavelet coefficients, the real signal is estimated. It has been shown that the Bayesian method outperforms the classical one in terms of mean square error (MSE) in some situations (Antoniadis *et al.* 2001). However, it is also argued that this method has a large computation cost and less ad-hoc than the classical method.

3.2.2.1 Classical method

There are three steps in the classical method of DWT-based denoising: (1) to forwardly transform the signal to the wavelet domain using the DWT; (2) to eliminate or shrink detail coefficients below a threshold; and (3) to reconstruct the signal using the approximation coefficients and the remaining detail coefficients. In this procedure, four factors should be considered: wavelet selection and decomposition level in step 1; and threshold estimation and thresholding policy in step 2.

The wavelet coefficients represent how well the dilated (or contracted) and shifted wavelet basis matches the signal. Thus, in general it is superior to choose a wavelet basis which is as similar as possible to the signal. A suitable wavelet may significantly enhance the denoising effect. Theoretically, there exist an infinite set of wavelets,

among which the Haar, Daublets, Coiflets, and Symmlets are widely applied in signal processing. The trial-and-error method is often employed to select the wavelet basis, because so far there has been no quantitative criterion for it. It is ill-advised to indulge in the wavelet hunting too much when a wavelet works very well (Fugal 2009). The larger the decomposition level is, the smoother the de-noised signal would be; however, a decomposition level too large would eliminate some useful information along with the denoising. Just as the case of wavelet selection, there is no quantified approach to determine the decomposition level, so the trial-and-error method is also widely accepted.

There are various threshold estimations, and four of them commonly used are minimax (Donoho and Johnstone 1994), universal (Donoho and Johnstone 1994), translation invariant (TI) (Coifman and Donoho 1995), and Stein's unbiased risk estimate (SURE) (Stein 1981).

When a threshold is available, what should be considered subsequently is how to apply the threshold to the detail coefficients, i.e. the thresholding policy. There are several policies, such as hard thresholding, soft thresholding, non-negative garrote thresholding, and firm thresholding (Fodor and Kamath 2003). Hard thresholding removes all detail coefficients with magnitude lower than the threshold. Soft thresholding removes all detail coefficients below the threshold as well as shrinks all those above it (Donoho 1995). Hard thresholding may introduce discontinuities into the de-noised signal. Nonetheless, it has smaller MSE than soft thresholding. Soft

thresholding usually gives a smoother de-noised signal, but tends to over-smooth abrupt changes and broaden sharp peaks. Both non-negative garrote and firm thresholding policies attempt to moderate the limitations of hard thresholding and soft thresholding. Non-negative garrote thresholding removes small detail coefficients and shrinks large coefficients by a nonlinear continuous function (Breiman 1995; Gao 1998). Firm thresholding has two thresholds, λ_1 and λ_2. The detail coefficients are partitioned into three treatments: (1) to retain those with magnitude larger than λ_2, (2) to remove the small ones with magnitude lower than λ_1, and (3) to linearly shrink the middle ones with magnitude between λ_1 and λ_2 (Gao and Bruce 1997). However, hard thresholding and soft thresholding are still most commonly applied in practice because of their efficiency and reliability.

Because the DWT is multilevel transform, different thresholds may be applied at each level. The global threshold and level-dependent threshold can be adopted depending on the cases. Global threshold means that a single threshold is applied to detail coefficients at all levels. On the other hand, level-dependent threshold is to select individual thresholds for different levels.

3.2.2.2 Bayesian method

It is usually assumed that the empirical approximation coefficients $\hat{a}_{j_0,k}$ conditional on $a_{j_0,k}$ and σ^2 are independent variables subjected to normal distributions. A scale mixture of two distributions: one corresponding to negligible coefficients, and the other to significant coefficients, is the popular prior model for each detail coefficient

$d_{j,k}$. The two distributions are usually two normal distributions, or one normal distribution and the other a point mass at zero (George and McCulloch 1993). An important distinction between the two mixtures is the type of shrinkage obtained. Further modifications of the basic thresholding were also suggested by considering wavelet block thresholding, which means that the detail coefficients are thresholded in blocks rather than term-by-term (Hall *et al.* 1998; Cai 1999). It has been shown that the block thresholding has better MSE performance compared with the term-by-term way sometimes (Antoniadis *et al*. 2001). Nevertheless, the computation cost would be tremendous when it is applied to large data.

Though various threshold estimations and thresholding policies have been proposed, none of the wavelet denoising approaches always outperform others (Wachowiak *et al.* 2000; Messer *et al.* 2001). The choice of the optimal denoising method depends on the characteristics of the signals and the requirement of the actual research.

3.2.3 Wavelet Despiking

A spike is usually defined as freak data whose amplitude is significantly different from that of the immediate surrounding data. A straightforward removal of the spikes could be achieved by a time-domain method, or low-pass filters if their frequencies are sufficiently high to separate them from the signal. In the time-domain method, spikes are identified as supra-threshold deviations from the local median absolute deviations. They are suppressed to zero or the level of local mean or median, or replaced by a

linear interpolation. When frequencies of the spikes overlap those of the underlying signals, the low-pass filters would fail. Moreover, it has been proven that even when spike frequencies are far higher, the low-pass filter may still not be entirely sufficient to isolate the wanted signal (Zanos *et al.* 2011).

The traditional wavelet-based despiking method removes the spikes by reversing the normal denoising procedure, which means cancelling all wavelet coefficients that exceed the threshold. However, it has been proven that this approach significantly underestimates the initial amplitude in the case of spike series (Costabel and Müller-Petke 2014). To remove the effects of in-scanner head movement on functional magnetic resonance imaging (fMRI), Patel *et al*. (2014) develop a new wavelet-based despiking algorithm. It defines spikes as chains of scale-invariant maximal or minimal wavelet coefficients. This wavelet despiking algorithm does not simply interpolate values at the time of spikes, but rather removes spikes only in their occurrence frequencies, retaining information from any unaffected frequency. It is unsupervised, data-driven, and spatially-adaptive. Thus, it is a preferable method to remove the spikes in long-term SHM data. However, the computational expense was found to be extremely significant, when an attempt was made to remove the spikes in a long sequence of data.

3.3 Methodology to Pre-Process Long-Term SHM Data

3.3.1 Denoising

No denoising approach dominates in all aspects, so the denoising method should be tailored in line with the actual signals based on their characteristics. Recognizing that long-term SHM data is complex, level dependent threshold is suggested to be applied. To be more computationally efficient, between the two methods: the classical method and the Bayesian method, the classical one is preferred; among the four estimators: minimax, universal, TI, and SURE, TI is unwanted; for the block and term-by-term thresholding, the term-by-term thresholding is suggested; for different thresholding policies, the hard thresholding and soft thresholding would be superior. Various denoising methods should be tried and compared to select an optimal one, which is both effective and efficient.

3.3.2 Despiking

Maxima and minima chain search is employed to find the spikes in the wavelet despiking algorithm as suggested by Patel *et al.* (2014). It leads to an unacceptable cost in computation, when a signal with a large amount of data is analyzed. Therefore, a fast spike detection method is desired before applying this despiking algorithm. There exist dozens of spike detection algorithms, which can be classified as manual

and automated, supervised and unsupervised. Manual methods are especially time consuming; and supervised methods require template matching or prior knowledge of "typical" spike shape. Thus, spike detection methods that are automated and unsupervised are of particular interest.

A totally automatic spike detection method was proposed by Yand and Shamma (1988) based on the discrete Haar transformation, which is essentially a wavelet idea. Spike waveforms do not only have average amplitude exceeding a certain baseline level, but also have a characteristic shape and duration. However, this method used inverse wavelet transformation, which may be unnecessarily time consuming. Other approaches to spike detection using wavelet bases can be found (Frisch and Messer 1992; Liu and Fraser-Smith 2000). These methods apply dyadic wavelets and mainly detect a single spike in the signal, but cannot estimate parameters such as arrival times of spikes. Nenadic and Burdick (2005) proposed a novel wavelet-based spike detection methodology. It consists of a combination of several techniques, including multiresolution wavelet decomposition, statistics, detection theory (sequential hypothesis testing) and estimation theory (occurrence times of spikes are the parameters of interest). By comparing its performance to many commonly used spike detection methods, this method was demonstrated to perform better than the traditional methods such as amplitude or power thresholding methods in many situations. Therefore, this method can be adopted to detect spike transients in the long-term SHM data. It can be achieved by the following five steps: (1) to perform CWT of the signal;

(2) to de-noise if noises contaminate the signal; (3) to perform Bayesian hypothesis testing at different scales, assessing the presence of spikes; (4) to combine the decisions at individual scales; and (5) to estimate the arrival times of individual spikes.

Subsequently, the spikes can be removed by the wavelet despiking method, focusing on the time domain immediately surrounding the spike. If a spike is significantly damaging, there may still be a peak or valley trend close to the instant it occurs in the de-spiked signal. Then a DWT can be applied to remove this trend.

3.3.3 Decomposing

Based on the characteristics of frequency and magnitude, the long-term SHM data collected from civil structures can generally be divided into the following two cases: (i) the signal sources can be discriminated by frequencies; and (ii) the signal sources overlap in frequency but can be discriminated by magnitudes.

For the first case, if there is a prior knowledge about the frequency information of the signal components, different signal sources can be reconstructed from the corresponding scales in the wavelet domain. For example, there is an apparent low-frequency component in the daily strain data measured from a bridge, which is caused by the daily fluctuation of temperature. It can be estimated that this signal source is the approximation at a certain wavelet decomposition level. Thus, it can be separated by the DWT directly. Otherwise, if there is not any prior knowledge about the signal

sources, the joint WT and FT approach proposed by Hong and Liang (2007) can be employed. The main idea of this method is to extract the information pertinent to each signal source from the wavelet scales using the FT. The overall procedure can be divided into six steps.

(1) To apply CWT to the signal mixture to obtain the wavelet decomposed signals W_a.

(2) To perform FT of W_a, and to obtain the frequency spectrum FW_a for each scale.

(3) To find the dominant frequency f_a, which associates with the highest peak, for each scale.

(4) To check feasibility condition for all f_a and to find feasible dominant frequencies f_i. The number of f_i is taken as the number of signal sources, N_s.

(5) To calculate contribution ratios of the wavelet decomposed signals to the source signals, and to reconstruct each signal source using

$$r_{i,a} = \frac{\left|FW_a(f_i)\right|}{\sum_{j=1}^{N_s}\left|FW_a(f_j)\right|}, \quad S_{i,a}(t) = r_{i,a}W_a(t) \qquad (i = 1,2,...,N_s,\ a = 1,2,...,L) \qquad (3.9)$$

where $r_{i,a}$ is the contribution ratios, $\left|FW_a(f_i)\right|$ is the peak magnitude at feasible frequency f_i in scale a, $S_{i,a}(t)$ is the reconstructed source signal i in scale a at time t.

(6) Reconstruct signal sources $s_i(t)$.

When it comes to the second case, the signal sources with obviously larger magnitudes can be considered as spikes. Consequently, the adaptive wavelet despiking algorithm can be used to achieve signal source separation.

3.3.4 Signal Pre-Processing Scheme

To avoid the influence of noises on despiking and decomposing, denoising is set as the first step in the pre-processing procedure. And then, spikes embedded in the signals are removed. If there are only a few spikes in a signal, to improve computational efficiency, the spikes should be identified before implementing the wavelet despiking algorithm. Afterwards, the clean signal is separated into different components. Finally, refined denoising can be carried out for those signal sources that are still contaminated with noises. The signal pre-processing scheme for the long-term SHM data collected from civil structures is briefly illustrated in Figure 3.1.

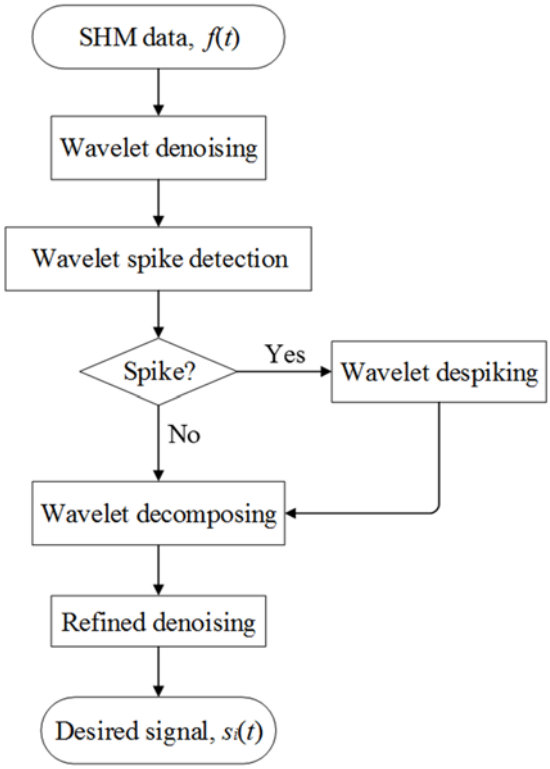

Figure 3.1 Signal pre-processing scheme for long-term SHM data

3.4 Application to Real Data Collected from TMB

3.4.1 Characteristics of Strain and Displacement Data

In the TMB, a total of 110 dynamic strain gauges are installed at critical locations of the stiffening deck system. Level sensors, which are sophisticated pile-line systems consisting of oil and water pipelines throughout the bridge alignment, are also fixed on the deck to measure the vertical displacement by pressure difference. The sampling rate of the strain monitoring is 25.6 Hz before 2001, but has been increased to 51.2 Hz since 2002; and that of the displacement monitoring is 2.56 Hz.

When there is no strong typhoon or monsoon, the measured strain and displacement are mainly due to highway traffic, railway traffic, and temperature. An obvious trend exists in the time history of daily strain and displacement, as shown in Figure 3.2. This trend is induced by the daily cycle of temperature. As shown in the close-up view, the salient peaks are due to railway traffic, whereas the oscillations with much lower magnitudes are due to highway traffic. The signals are contaminated with noises due to the monitoring system itself and the operational environment (Figure 3.3). Furthermore, it is found that occasionally spikes are corrupted in the signals (Figure 3.4).

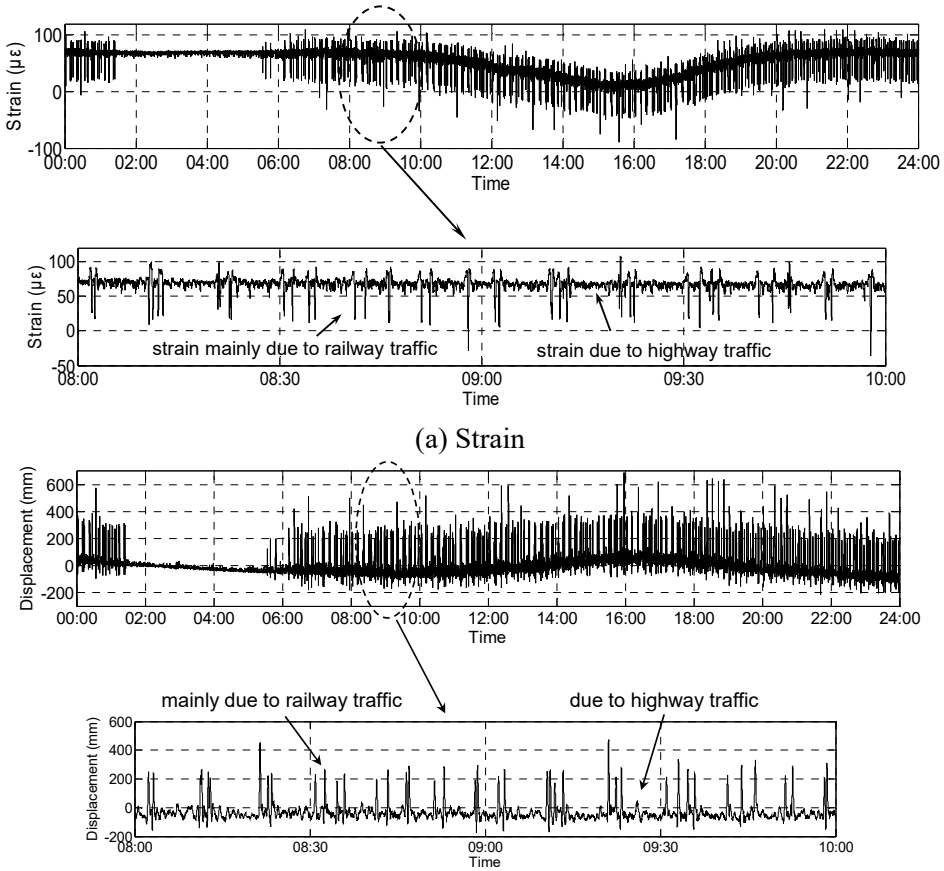

(a) Strain

(b) Displacement

Figure 3.2 Time history of daily strain and displacement with close-up view of 2-hour data

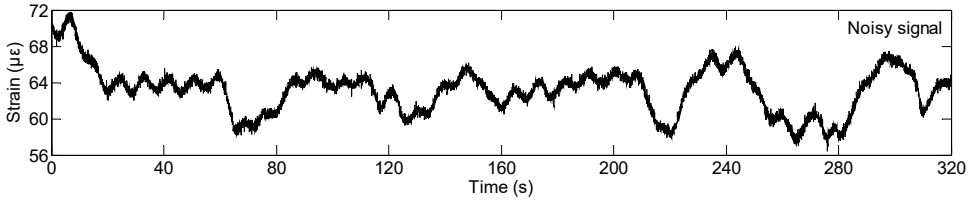

Figure 3.3 Noisy strain signal

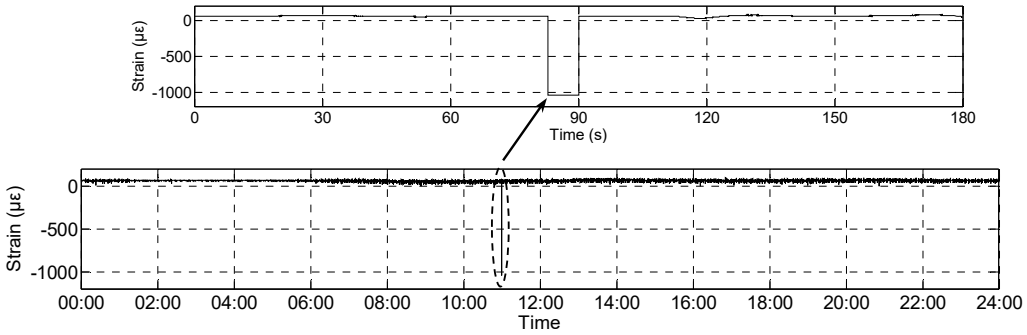

Figure 3.4 Time history of daily strain with a spike

3.4.2 Denoising

The wavelet basis selected for both the classical and Bayesian methods is Symmlet 8. The decomposition level was set as seven. In the classical method, the four threshold estimations introduced in section 3.2.2.1: minimax, universal, TI, and SURE, were used. To obtain smoother denoised signals, which are desired in the research next step, soft thresholding was adopted. Furthermore, because the signal in study is complicated, level dependent threshold is applied. For easy discrimination, the classical approaches corresponding to the four threshold estimations are denoted by MINIMAX, UNI, TI and SURE, respectively.

The following four threshold estimations are employed in the Bayesian method: the single posterior mean estimator (Clyde and George 2000), single posterior median estimator (Abramovich *et al.* 1998), blocking posterior mean estimator (Abramovich *et al.* 1998), and Bayesian hypothesis testing estimator (Vidakovic 1998; Abramovich and Sapatinas 1999). These four threshold estimators are all level-dependent. The Bayesian approaches corresponding to these four threshold estimators are denoted as SINGLMEAN, SINGLMED, BLMEAN and SINGLHYP, respectively.

Unlike the previous comparative studies which are based on simulation (Wachowiak *et al.* 2000; Antoniadis *et al.* 2001; Messer *et al.* 2001) where the signals were generated by simulation and known, the real signals in this study are not definite. Therefore, some denoising evaluation criteria previously employed, such as the signal-to-noise ratio (SNR), mean square error (MSE), root mean square error (RMSE), and maximum deviation (MD), are not applicable. In this study, the performance of the wavelet denoising approach is evaluated by three criterion: (1) the graphical output is as smooth as possible (facilitating the subsequent study which concerns the equivalent static effects of traffic loads); (2) most of the signal components with frequencies larger than 0.5 Hz are eliminated (there is a discrepancy between the traffic-induced strain and Gaussian noises); (3) the computational cost (both time and memory occupation) is as low as possible.

The graphic outputs of the de-noised signal corresponding to Figure 3.3 are shown in Figure 3.5. On smoothness, it can be observed that the results of the SURE approach

and all the Bayesian approaches, are inferior to those of other approaches. Among the classical approaches, the MINIMAX, UNI and TI all performs well. Taking the denoising results of the UIN and SURE methods as an example, Figure 3.6 shows the raw strain and denoised strain in the frequency domain. It can be observed that the UNI method removes noises more radically. The computer employed in this study has a CPU of Intel core i7-3770 with a basic frequency of 3.40 GHz, and a memory of 16 GB. The computation time it took to remove the noises in the strain data of one day using the approaches: MINIMAX, UNI, TI, SURE, SINGLMEAN, SINGLMED, and SINGLHYP, is 1.03 s, 0.88 s, 97.38 s, 1.28 s, 2.13 s, 2.12 s, and 3.72 s respectively. However, the program stopped when the signal was de-noised by the BLMEAN approach, because the computer was out of memory. Thus, the block thresholding is more computationally expensive than the term-by-term thresholding. In computational efficiency, the approaches of MINIMAX and UNI outperform others. The UNI approach is adopted as the denoising method for the long-term strain data measured from the TMB.

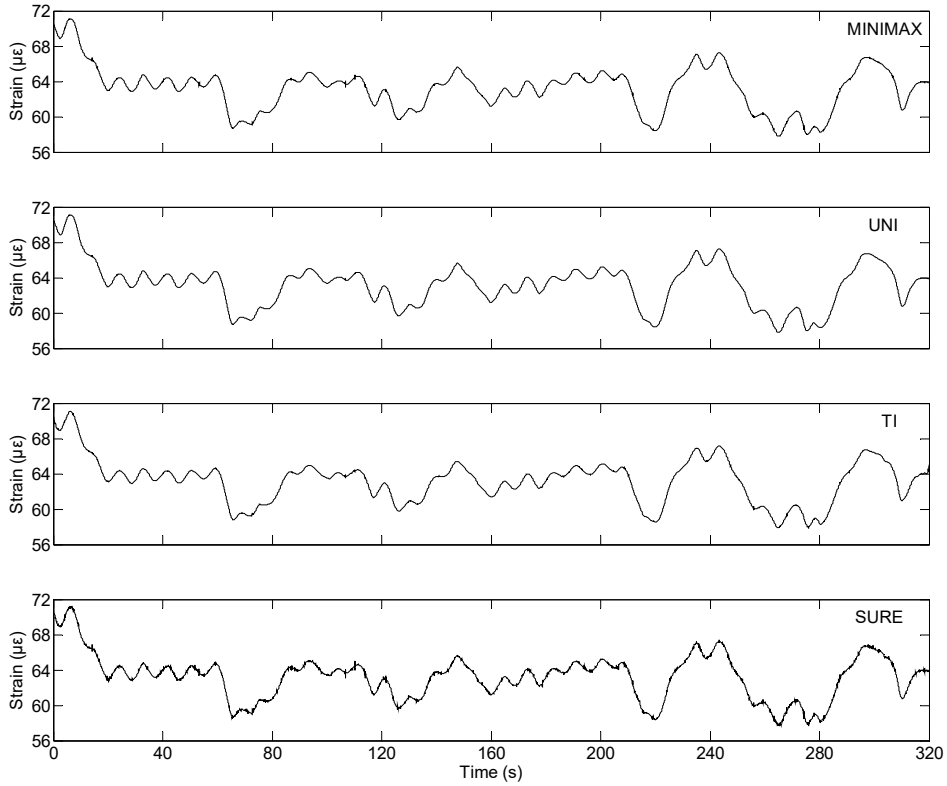

(a) Denoised signals by classical method

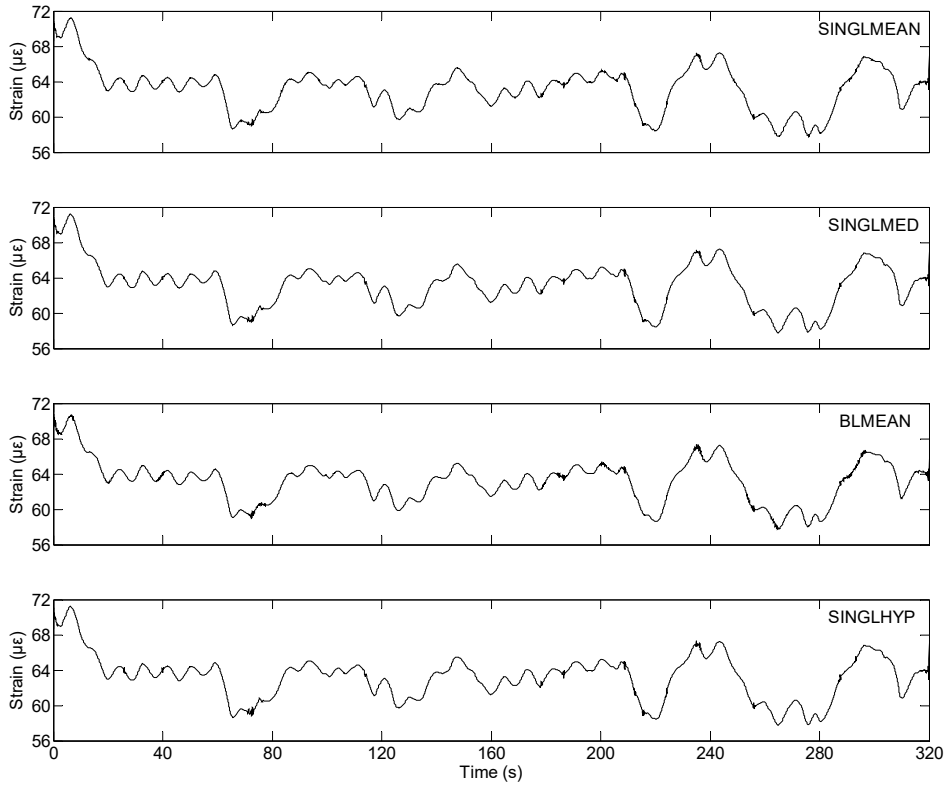

(b) Denoised signals by Bayesian method

Figure 3.5 Wavelet denoising results

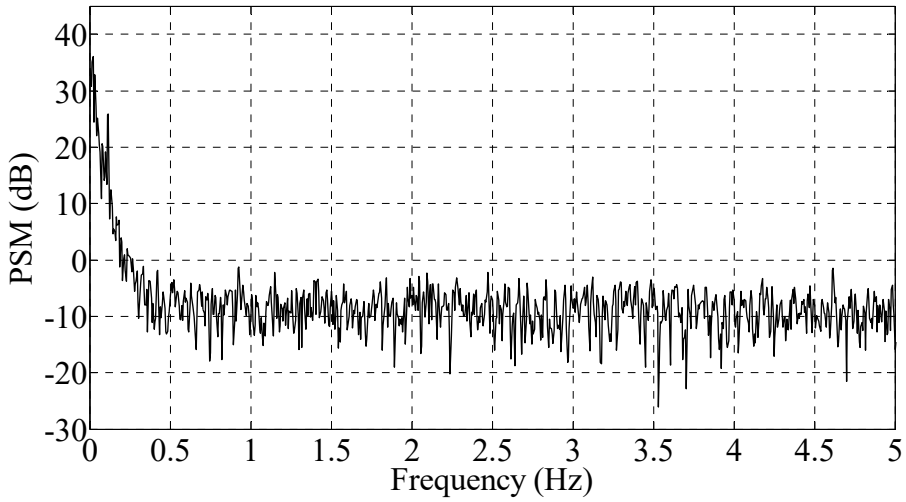

(a) Raw strain

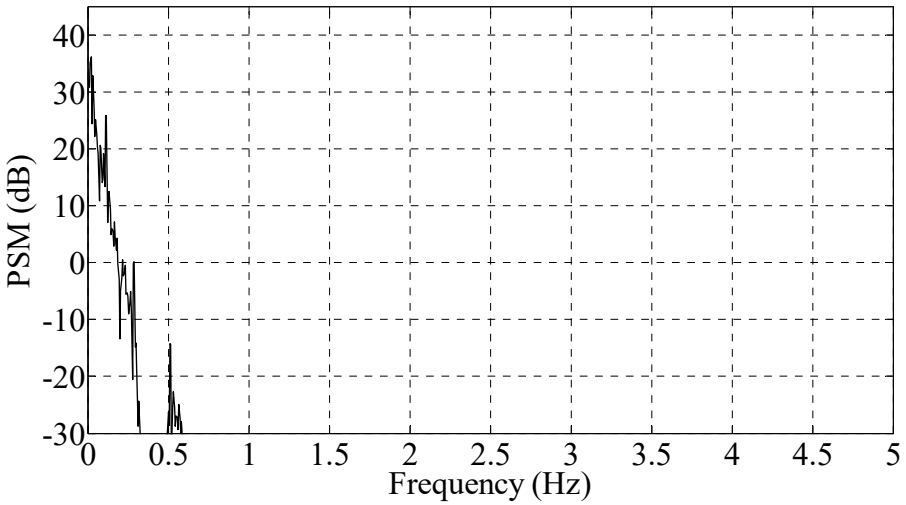

(b) Signal denoised by UNI

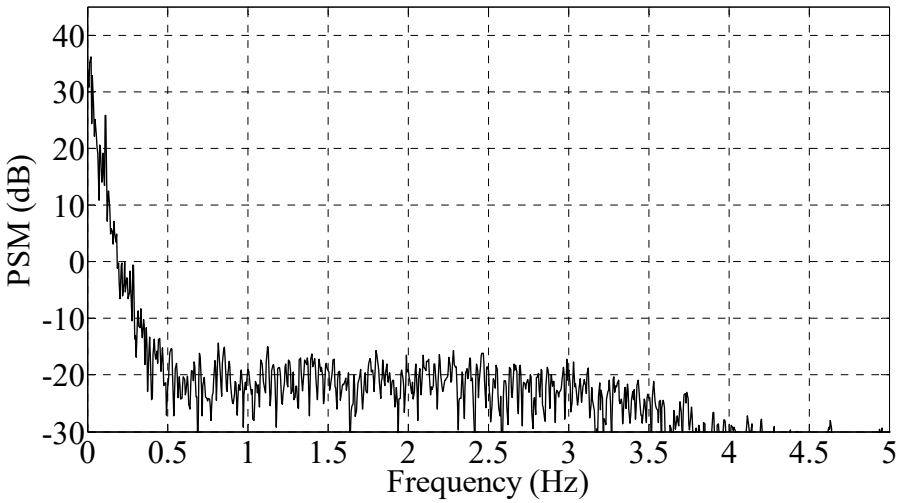

(c) Signal denoised by SURE

Figure 3.6 Comparison of denoised strain signals in frequency domain

3.4.3 Despiking

Using the wavelet detection method proposed by Nenadic and Burdick (2005), the spike embedded in the signal, as shown in Figure 3.4, was automatically detected (Figure 3.7). The wavelet used is Haar, which is spike-like. The occurrence time of the spike is detected at 10:59:56:24, which coincides with that identified manually. Subsequently, this spike was removed by the wavelet despiking algorithm developed by Patel *et al*. (2014), focusing on the time domain close to the spike. The primary despiking result is not satisfactory, because there is still a valley trend (Figure 3.8(b)) near the previous instant of the spike. To eliminate this trend, a DWT is further conducted for the primarily de-spiked signal, and then the spike is completely removed, with other data points nearly unaffected (Figure 3.8(c)).

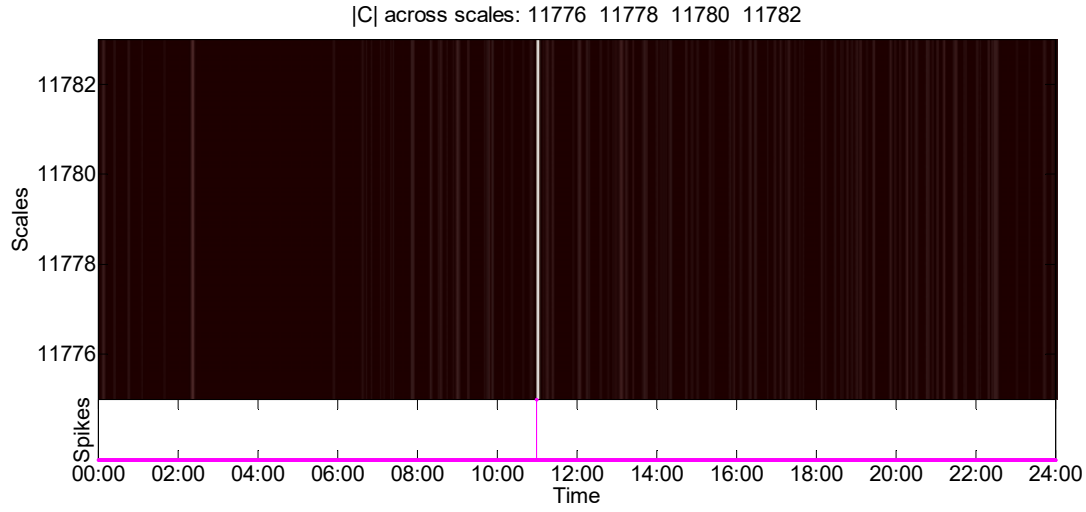

Figure 3.7 Automatically detected spike

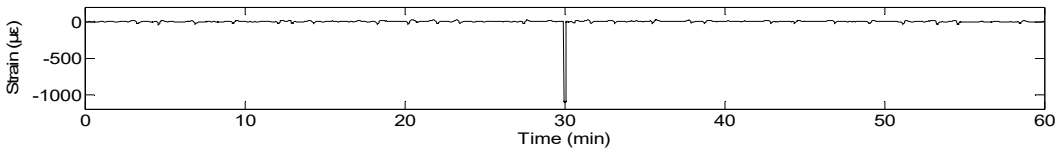

(a) Raw data

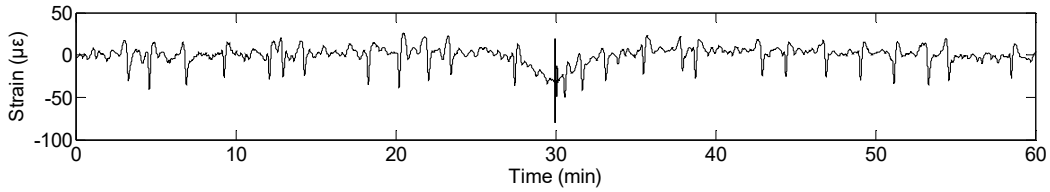

(b) Primary despiking result using wavelet despiking algorithm directly

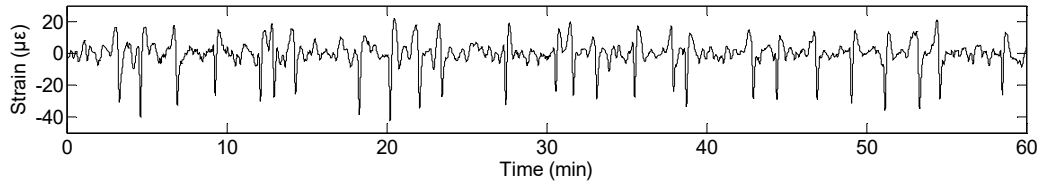

(c) Despiking result after de-trending by the DWT

Figure 3.8 Wavelet despiking results

Combining the wavelet despiking algorithm with the wavelet spike detection method can greatly improve the computational efficiency. It took the computer more than 400 s to remove the spike as shown in Figure 3.4 using the wavelet despiking algorithm directly; while the time consumed by the combined method is only 3 s.

3.4.4 Decomposing

3.4.4.1 Extraction of thermal strain

There is no quantified approach to determine the decomposition level for signal separation, so the trial-and-error method is approached. The approximations at levels 12, 16 and 22, i.e. A12, A16 and A22, are shown in Figure 3.11(b-d). There are still

noises in A12; on the other hand, A22 is distorted. Thus, a decomposition level of 16 is selected to separate the thermal strain. Frequency filters were also tried to extract this signal component which has an apparently low frequency. However, edge effect was discovered (Figure 3.9), so the advantage of WT is reflected.

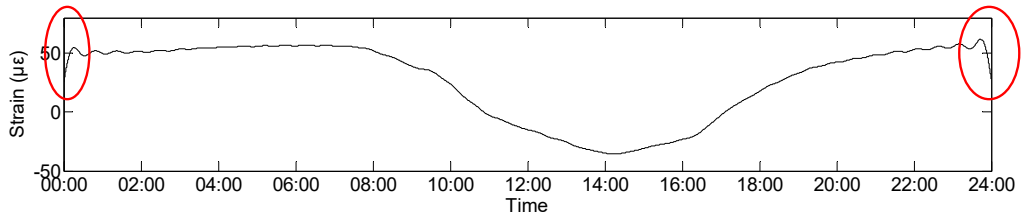

Figure 3.9 Edge effect of frequency filter

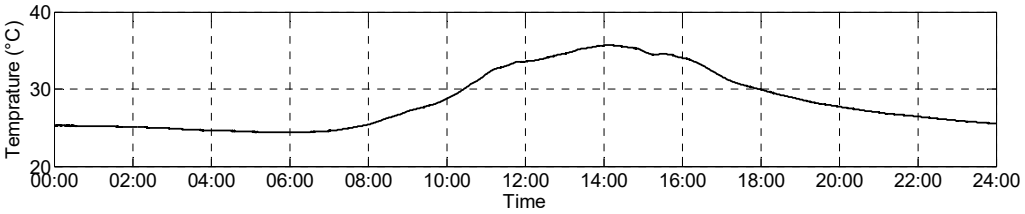

(a) Effective temperature

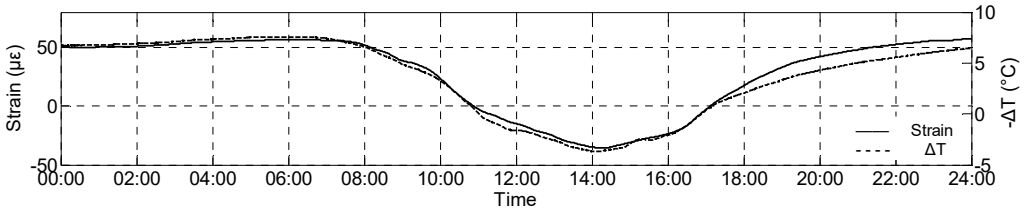

(b) A16 and ΔT

Figure 3.10 Pattern coincidence between A16 and ΔT

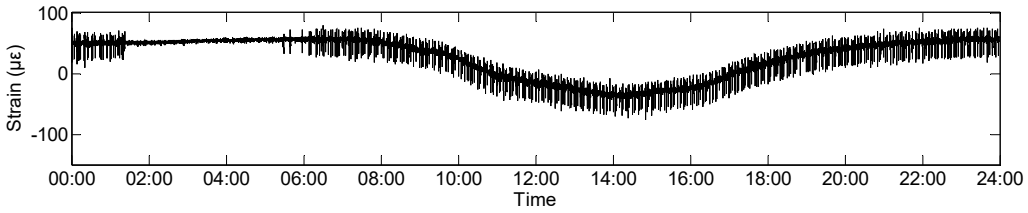

(a) Strain signal with noises and spikes removed

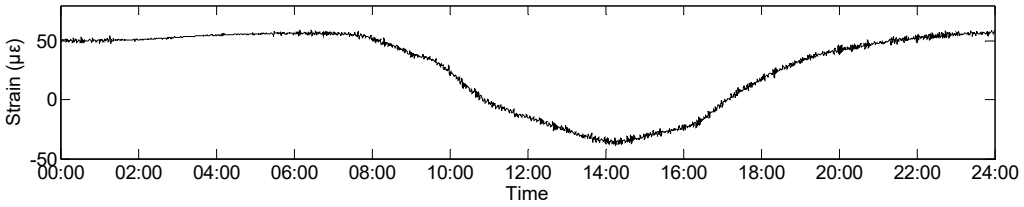

(b) Approximation at level 12, A12

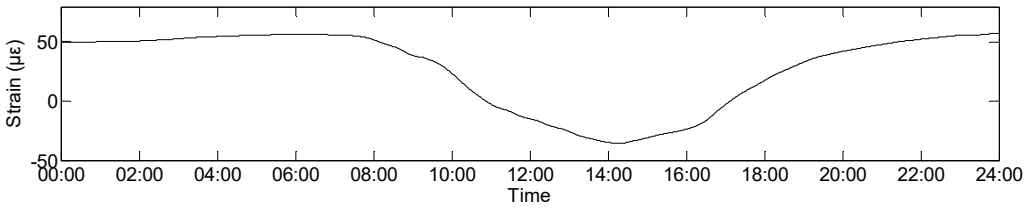

(c) Approximation at level 16, A16

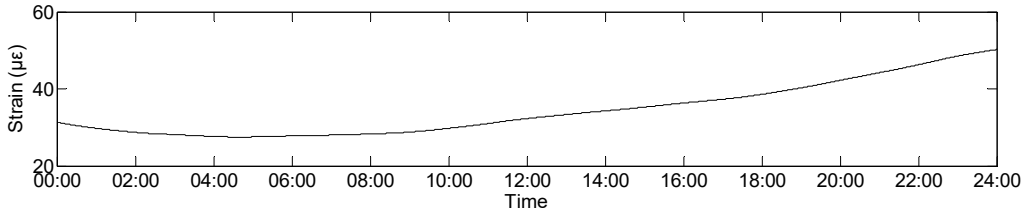

(d) Approximation at level 22, A22

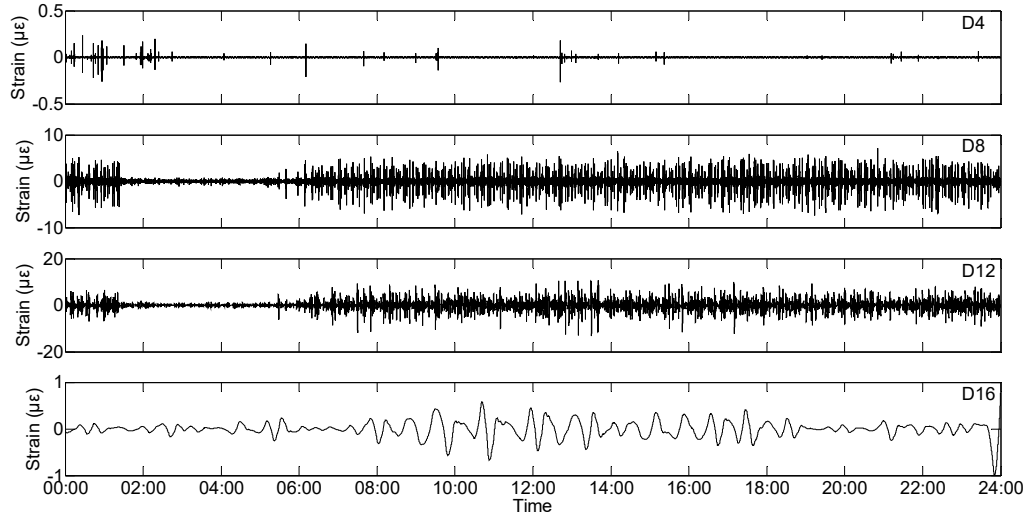

(e) Example of details

Figure 3.11 16-level decomposition of typical daily strain using DWT

In physical explanation, A16, which is the trend of the original signal, is the strain induced by temperature variation, which is verified below. Temperature in the deck's cross-section can be decomposed into effective temperature and differential temperature (Li *et al.* 2004; Ni *et al*. 2007). The effective temperature is distributed in a cross-section uniformly, inducing the bridge deck to move; on the other hand, the differential temperature means the temperature differences between the top surface and other levels in the cross-section, leading to supplementary internal axial forces when the ends of the deck are restrained (Maes *et al.* 1992; Ni *et al*. 2007). There is an expansion joint on one abutment of the TMB, which is designed to accommodate the longitudinal displacement of the deck due to temperature. The movement Δ_T of the deck due to effective temperature T can be calculated by

$$\Delta_T = \alpha L(T - T_0) = \alpha L \times \Delta T \tag{3.14}$$

where α is the thermal expansion coefficient for structural steel, L is the length of the deck, T_0 is the reference temperature, and ΔT is the difference between the effective temperature and the reference temperature. Assuming that the thermal strain ε_T is uniformly distributed along the longitudinal direction of the deck, the thermal strain can be roughly evaluated by

$$\varepsilon_T = \alpha(T - T_0) = \alpha \times \Delta T \tag{3.15}$$

It can be concluded from Eq. (3.15) that the thermal strain is proportional to ΔT, implying that the variation of the thermal strain should have the same pattern as ΔT. Based on the temperature data collected from the deck, the pattern coincidence between A16 and ΔT is confirmed as shown in Figure 3.10. Therefore, it is validated that A16 is the thermal strain. Examples of this pattern coincidence for data of other days are shown in Figure 3.12.

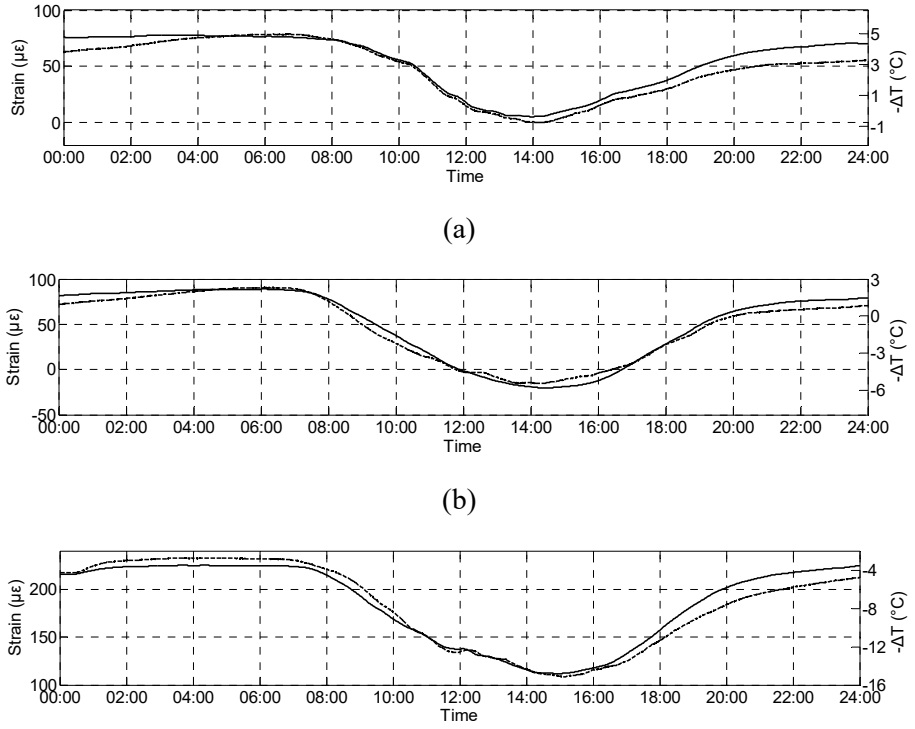

Figure 3.12 Examples of pattern coincidence between A16 and ΔT

3.4.4.2 Separation of strain due to different traffic loads

With thermal strain extracted, the remaining signal, as shown in Figure 3.13, is mainly due to highway traffic and railway traffic. However, since the frequencies of the two signal sources overlap each other, it is difficult to discriminate them directly in the

wavelet domain. Fortunately, there is apparent disparity between amplitudes of these two signal sources. The strain induced by the railway traffic can be tentatively regarded as spikes. Therefore, the wavelet despiking algorithm (Patel *et al*. 2014) is used to separate these two signal sources. An example of the separation results is shown in Figure 3.15. Figure 3.15 (a) is the strain due to traffic during 5:00-6:00 in the morning. Figure 3.15 (b)-(c) shows the effectiveness of the signal decomposing method. The railway traffic passing the TMB starts at about 5:30 every morning, and stops at about 12:00 in the night. Thus, there is no railway traffic from 5:00 to about 5:30, as shown in Figure 3.15 (b). In further research, refined denoising may be required for the strain due to highway traffic (Figure 3.15 (c)). The zoom in view of the signal decomposition result is shown in Figure 3.14.

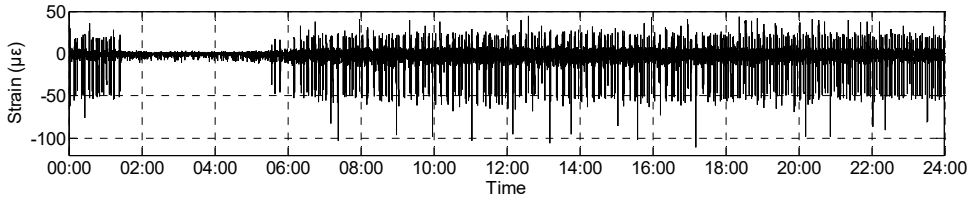

Figure 3.13 Daily strain due to highway traffic and railway traffic

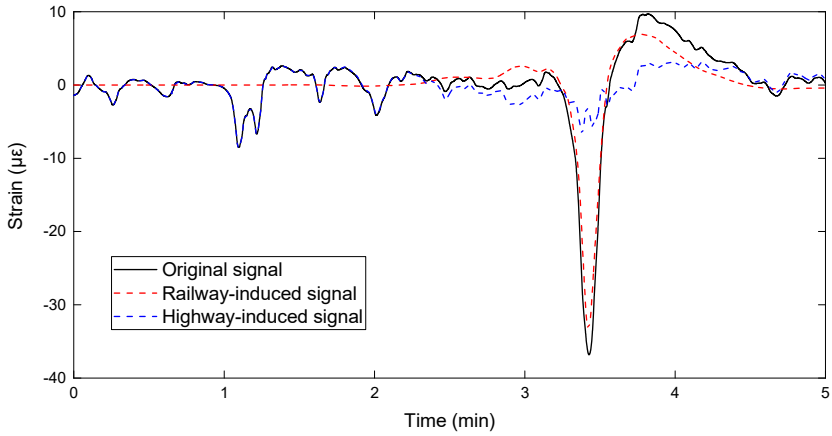

Figure 3.14 Zoom-in view of signal decomposition

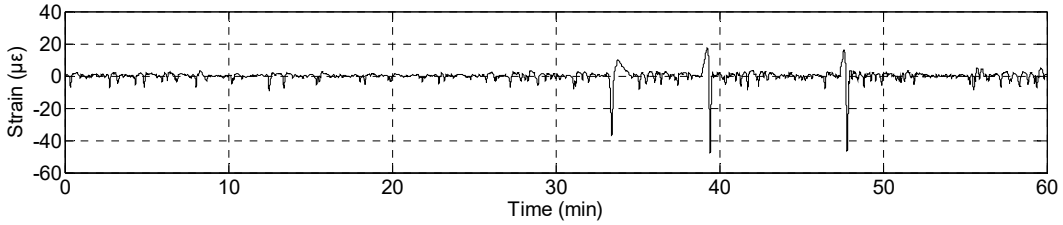

(a) Original strain

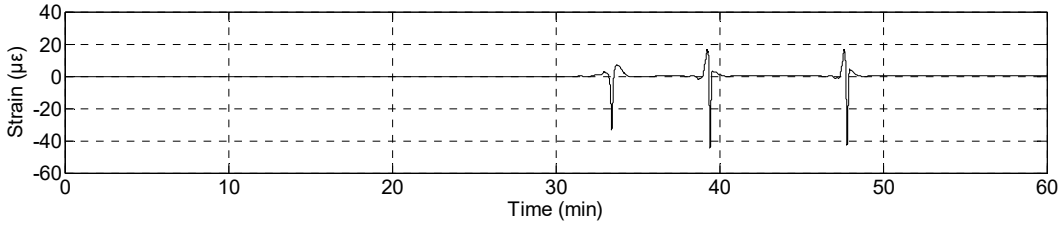

(b) Strain due to railway traffic

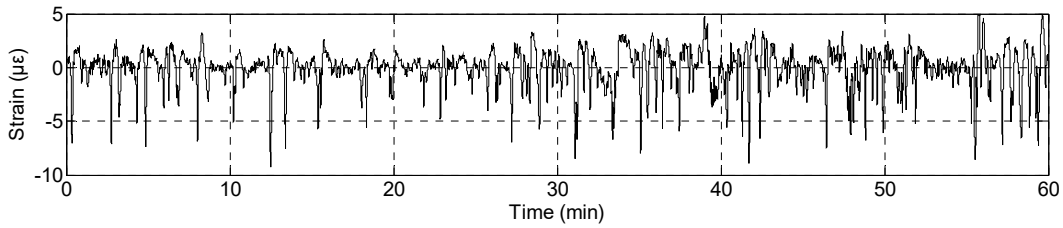

(c) Strain due to highway traffic

Figure 3.15 Wavelet decomposing results

3.5 Summary

When evaluating the conditions of civil structures based on long-term SHM data, it is essential to automatically and efficiently pre-process these data. A novel technique is required to remove the noises and spikes corrupted in signals, and to separate different signal sources. Motivated by this necessity, a wavelet-based signal pre-processing scheme is proposed for denoising, despiking and decomposing. Recognizing the enormous amount of data, automation and efficiency of the method, in addition to effectiveness, are especially considered.

The wavelet denoising method should be tailored for signals in hand, because none of the existing methods outperform others in all aspects. If there are only a few spikes in signals, the procedure of identifying the spikes first and then focusing on their neighboring time domain to eliminate them by the wavelet despiking algorithm, is more efficient than applying the wavelet despiking algorithm directly. DWT is a filter bank in a sense; hence different signal sources could be separated straightforwardly using DWT if there is an apparent gap between their frequencies. For those signal sources with overlapped frequencies but distinct magnitudes, they can be separated by the wavelet despiking algorithm.

The proposed signal pre-processing method is illustrated and demonstrated using the strain and displacement data collected from the TMB. The noises and spikes in the signals were eliminated efficiently, and different signal sources, i.e., strain or displacement due to the respective effect of temperature, railway traffic, and highway traffic, was separated as expected.

CHAPTER 4

EXTREME VALUE DISTRIBUTIONS OF TRAFFIC LOAD EFFECTS

4.1 Introduction

It is nearly impossible that sensors are installed on every component of a monitored bridge, limited by practical problems such as cost, accessibility, consumption of time and human power in installation, difficulty in data management and processing, etc. The FEM of a bridge is expedient for the evaluation of the load carrying capacity of the structural components without sensors. To employ the FEM, the live load models are prerequisite. The load effects due to cars and other relatively light vehicles are unconcerned, because they are usually not the dominant factor which threatens the serviceability and safety of bridges. On the contrary, the extreme load effects arising under scenarios such as heavy vehicles crossing, several vehicles meeting or overtaking, and traffic jam are of the greatest interest. To provide critical stress level for the development of live load models, the probability distribution of extreme traffic load effects (TLEs) should be studied in the first place.

In the context of probabilistic modeling, extreme values correspond to the tails of probabilistic distributions. The extreme value theory (EVT) develops techniques and models to describe these tails, and provides a framework to predict the characteristic values and probabilities of rare events on the basis of historical data. It has been widely applied in many fields such as hydrology, climate forecasting, finance and so on (Tawn 1990; Harris 1996; Tsimplis and Blackman 1997; Holmes and Moriarty 1999; Poon *et al.* 2004; Gilli *et al.* 2006). The EVT has also been applied in bridge engineering to extrapolate extreme traffic loads or load effects (O'Brien *et al*. 1995; Bailey 1996; Cooper 1997; Crespo-Minguillón and Casas 1997; Bailey and Bez 1999; Grave *et al*. 2000; O'Connor 2001; Grave 2002; Getachew 2003; James 2003; Caprani 2005; Caprani *et al*. 2008; Siegert *et al*. 2008; Enright 2010; Treacy *et al*. 2014). Among the EVT-based tail fitting approaches, two are particularly popular: block maxima (BM), and peaks-over-threshold (POT) (Simiu *et al*. 2001; Katz *et al*. 2002; Getachew 2003; James 2003; Messervey *et al*. 2011).

In almost all of the previous studies, the investigators addressed TLEs by generating the traffic loads based on weigh-in-motion data collected during a short period and then predicting the load effects with the use of influence lines. The short-term data are unlikely to capture extreme events. On the other hand, the reliability of extreme values obtained by simulation techniques such as the Monte Carlo method is doubtful. Some uncertainties such as the dynamic impact of vehicles, the roughness of the road, and properties of structural materials are difficult to simulate in this procedure.

Investigations on the extreme TLEs of bridges based on long-term monitoring data of structural response were scarcely reported.

Strain monitoring data provides the most direct link to the load effect, and avoids the difficulty in uncertainty modeling. In the present study, the long-term strain data collected from the TMB are used to study the extreme traffic load effects on the bridge. The TMB with a main span of 1,377 m is currently the world's longest suspension bridge that carries both highway and railway traffic. It is the key linkage of the most important transport network in Hong Kong, which connects the international airport to the commercial centers. As a result, the traffic on this bridge is relatively busy and heavy. With the long-term strain data collected from the stiffening deck system of the TMB, the extreme value distributions of the stresses induced by the highway and railway traffic respectively are evaluated. Characteristic values of the extreme stresses with a return period of five and 120 years (the design life of the bridge) are extrapolated, respectively. The extreme stresses with these two return periods will be used in the development of live load models for bridge condition assessment under the respective serviceability limit state (SLS) and the ultimate limit state (ULS). Both the BM and POT approaches are employed to extrapolate the extreme stresses. The parameters of the fitted probability distributions and the corresponding return levels of extreme stresses are estimated by the likelihood-based method including maximum likelihood and profile likelihood method, and the Bayesian estimation method, respectively. The results are compared and discussed. To evaluate the extrapolated

extreme stresses and roughly assess the operational condition of the TMB, the characteristic values corresponding to a return period of 120 years are further compared with the stresses generated by design traffic loads, which are computed with the help of a 3D FEM of the bridge.

The remainder of this chapter is organized as follows. Section 4.2 outlines the theoretical background of using the EVT to study extreme value distributions and extrapolate extreme TLEs. Section 4.3 briefs the TMB and the deployed sensors for strain monitoring. In section 4.4, the strain monitoring data continuously collected in nine years are presented to observe long-term variations of the structural stresses caused by highway and railway traffic, respectively. In section 4.5, the extreme value distributions of the extreme stresses are studied, and the characteristic values with five-year and 120-year return periods are extrapolated. The parameters of the data-driven extreme value distributions and the extrapolated return levels are compared and discussed. Finally, a summary is given in section 4.6.

4.2 Extreme Value Theory and Methodology

The BM and POT approaches are the two most popular methods adopted in the EVT. These two approaches have their own pros and cons. The BM approach has the advantage of time referencing, which is necessary in calculating probabilities of exceedance during the lifetime of a structure. However, only the maximum values in

given blocks of time (days, months, years, etc.) are taken into account in this approach. Even if several very large values were recorded, only one value in each time-block is considered, so a lot of useful data might be wasted. The POT approach accounting for the peaks which exceed a specified threshold can address the above issue, but its time reference is not as clear as the BM approach. The BM and POT data are in general fitted to the generalized extreme value (GEV) distribution and the generalized Pareto (GP) distribution, respectively (Coles 2001, Beirlant et al. 2006). The EVT and its engineering applications can be found in the literature (Gumbel 1958; Castillo 1988; Coles 2001; Reiss *et al.* 2001; Leadbetter *et al.* 2012).

4.2.1 BM and POT Approach

4.2.1.1 BM approach

The BM approach focuses on the statistical behavior of

$$M_n = \max\left(X_1, X_2, \ldots, X_n\right) \tag{4.1}$$

where ($X_1, X_2, \ldots, X_n$) is a sequence of independent random variables with a common distribution function F. The distribution of M_n can be derived by (Coles 2001):

$$P(M_n \le z) = P(X_1 \le z, ..., X_n \le z) = P(X_1 \le z) \times ... \times P(X_n \le z) = F^n(z) \tag{4.2}$$

To calculate $F^n(z)$, a practical approach is to estimate $F^n(z)$ based on extreme data only. To overcome the difficulty that $F^n(z)$ degenerates to 0 as n tends to infinity, the following linear renormalization of the variable M_n is adopted:

$$M_n^* = \frac{M_n - b_n}{a_n} \tag{4.3}$$

where $\{a_n\}$ and $\{b_n\}$ are sequences of constants with $a_n>0$. The limit distribution for M_n^* is given by the *extreme types theorem* (Jenkinson 1955): if sequences of constants $\{a_n\}$ and $\{b_n\}$ exist, such that

$$P\{(M_n - b_n)/a_n \le z\} \xrightarrow{n\to\infty} G(z) \tag{4.4}$$

where G is a non-degenerate distribution function, then G is a distribution of the GEV family:

$$G(z)=\exp\left\{-\left(1+\xi\left(\frac{z-\mu}{\sigma}\right)\right)^{-1/\xi}\right\} \tag{4.5}$$

defined on z such that $1+\xi(z-\mu)/\sigma>0$, where $-\infty<\mu<\infty$, $\sigma>0$ and $-\infty<\xi<\infty$.

The three parameters μ, σ, and ξ are location, scale and shape parameters, respectively. Eq. (4.5) is called the GEV distribution. The cases $\xi=0$, $\xi>0$, and $\xi<0$ are named the extreme value distribution (EVD) with types *I*, *II* and *III*, which are also widely known as Gumbel, Fréchet and Weibull families, respectively. The three types of EVDs have

different forms of tail behavior. The upper bound is finite for the Weibull distribution while it is infinite for the Fréchet and Gumbel distributions.

4.2.1.2 POT approach

The POT approach studies those data that surpass a threshold level u, and then the conditional probability

$$F_u(y) = P(X \le u + y \,|\, X > u) = \frac{F(u+y) - F(u)}{1 - F(u)} \tag{4.6}$$

is interested. For a u large enough, when $M_n = \max\{X_1, X_2, \ldots, X_n\}$ satisfying the conditions to be approximated by a GEV, the distribution function of $(X–u)$ conditional on $X>u$, is approximately

$$H(y) = 1 - \left(1 + \xi y / \tilde{\sigma}\right)^{-1/\xi} \tag{4.7}$$

defined on $\left\{y / y>0 \text{ and } (1+\xi y/\tilde{\sigma}) > 0\right\}$, where

$$\tilde{\sigma} = \sigma + \xi(u - \mu) \tag{4.8}$$

The family of distributions defined by Eq. (4.7) is called the GP distribution. This theorem implies that if the block maxima of a dataset have an approximating GEV distribution, the threshold excesses can be fitted to a GP distribution with parameters associated with the GEV distribution. Particularly, the shape parameter ξ in Eq. (4.7)

is equal to that of the corresponding GEV distribution. As that in the GEV distribution, this ξ also determines the upper bound of the GP distribution.

4.2.2 Return Level and Return Period

The quantile function z_p of the GEV distribution is

$$z_p = \begin{cases} \mu - (\sigma / \xi)(1 - (-\log(1-p))^{-\xi}) & \text{for} \quad \xi \neq 0 \\ \mu - \sigma \log(-\log(1-p)) & \text{for} \quad \xi = 0 \end{cases} \tag{4.9}$$

where $G(z_p)=1-p$. z_p is the return level corresponding to the return period $1/p$. The return period is important in engineering due to the fact that it is usually used as a design criterion. By defining $y_p=-\log(1-p)$, Eq. (4.9) is expressed as

$$z_p = \begin{cases} \mu - (\sigma / \xi)(1 - y_p^{-\xi}) & \text{for} \quad \xi \neq 0 \\ \mu - \sigma \log y_p & \text{for} \quad \xi = 0 \end{cases} \tag{4.10}$$

The graph of z_p against $\log y_p$ is called return level plot. It is linear when $\xi=0$, is convex when $\xi<0$, and is concave in the case of $\xi>0$. It is particularly convenient and useful for model presentation and validation.

In the case of the GP distribution, when $\xi\neq0$ the return level x_m that is exceeded once on average for every m observations is

$$x_m = u + \frac{\sigma}{\xi}\left(\left(m\varsigma_u\right)^{\xi} - 1\right) \tag{4.11}$$

and when ξ=0 the return level x_m is

$$x_m = u + \sigma \log\left(m\varsigma_u\right) \tag{4.12}$$

where $\varsigma_u = P\{X > u\}$. As the return level plot for the GEV model, plotting x_m against m on a logarithmic scale produces the same qualitative features: linearity if ξ=0; concavity if ξ>0; and convexity if ξ<0. For the m observations corresponding to n_y observations per year,

$$m = N \times n_y \tag{4.13}$$

the N-year return level is

$$z_N = u + \frac{\sigma}{\xi}\left(\left(Nn_y\varsigma_u\right)^{\xi} - 1\right) \tag{4.14}$$

for $\xi \neq 0$, and is

$$z_N = u + \sigma \log\left(Nn_y\varsigma_u\right) \tag{4.15}$$

for ξ=0.

4.2.3 Parameter Estimation

There are several methods for parameter estimation of GEV and GP distribution functions. In general the methods can be divided into likelihood-based method and Bayesian method. The maximum likelihood estimation (MLE), profile likelihood estimation (PLE) and Bayesian estimation (BE) are considered in the present study.

4.2.3.1 Likelihood-based estimation

The MLE is often adopted to estimate the parameters of the fitted model of extreme values. For the GEV model, the log-likelihood for the distribution when $\xi \neq 0$ is

$$L(\mu,\sigma,\xi) = -m\log\sigma - (1+1/\xi)\sum_{i=1}^{m}\log\left(1+\xi\frac{z_i-\mu}{\sigma}\right) - \sum_{i=1}^{m}\left(1+\xi\frac{z_i-\mu}{\sigma}\right)^{-1/\xi} \quad (4.16)$$

provided that

$$\left(1+\xi\frac{z_i-\mu}{\sigma}\right) > 0 \quad (4.17)$$

When Eq. (4.17) is violated, the likelihood is zero and the log-likelihood is minus infinity. For the Gumbel case ($\xi=0$), the log-likelihood is

$$L(\mu,\sigma) = -m\log\sigma - \sum_{i=1}^{m}\left(\frac{z_i-\mu}{\sigma}\right) - \sum_{i=1}^{m}\exp\left(-\frac{z_i-\mu}{\sigma}\right) \quad (4.18)$$

For the GP distribution, denoting the k excesses over the threshold u by $y_1, y_2, \ldots, y_k$, the log-likelihood function in the case of $\xi \neq 0$ is:

$$L(\sigma,\xi) = -k\log\sigma - (1+1/\xi)\sum_{i=1}^{k}\log(1+\xi y_i/\sigma) \tag{4.19}$$

when $(1+\xi y_i/\sigma) > 0$; otherwise, $L(\sigma,\xi) = -\infty$. For $\xi = 0$,

$$L(\sigma,\xi) = -k\log\sigma - \sigma^{-1}\sum_{i=1}^{k} y_i \tag{4.20}$$

By maximizing the log-likelihood functions as defined in Eqs. (4.16) and (4.18)-(4.20), the MLEs of the model parameters are obtained.

Parameters obtained from MLEs are point estimators. Confidence intervals (CIs) for the estimated parameters and associated return levels can be obtained by normal approximation, profile likelihood (PL), and parametric bootstrap. It should be noted that the normal approximation may be poor, especially for the shape parameter and return levels corresponding to long return periods. Therefore, to allow for skewed intervals that may better match the sampling distribution functions of these parameters, it is often better to obtain their CIs from the PL method (Coles 2001; Gilleland and Katz 2016).

To obtain the PL for any of the individual parameters, numerical evaluation is made as follows. The first step is to fix the evaluated parameter and maximize the

corresponding log-likelihood in Eqs. (4.16) and (4.18)-(4.20) with respect to the remaining parameters. Then a range of values of the evaluated parameter is repeated in this way. The maximized log-likelihood values constitute the profile log-likelihood for the evaluated parameter, from which the approximate CIs are obtained. The CIs for any specified return level can be obtained by re-parameterizing of the GEV model to make the return level as one of the model parameters based on Eqs. (4.9) and (4.10).

4.2.3.2 Bayesian estimation

The Bayesian technique offers an alternative for parameter estimation in extreme value models, and it is often preferable. Different from those in the MLE, parameters of the distribution functions in the Bayesian estimation are treated as random variables, not constant ones. That is, the Bayesian approach reflects uncertainties of the parameters. Based on the Bayes' Theorem, the posterior PDF of parameters $\boldsymbol{\theta}$ is

$$f(\boldsymbol{\theta}|\boldsymbol{x}) = \frac{f(\boldsymbol{x}|\boldsymbol{\theta}) f'(\boldsymbol{\theta})}{\int_{\Theta} f(\boldsymbol{x}|\boldsymbol{\theta}) f'(\boldsymbol{\theta}) d\boldsymbol{\theta}} \tag{4.21}$$

where $f'(\boldsymbol{\theta})$ and $f(\boldsymbol{x} \mid \boldsymbol{\theta})$ are the prior PDF and likelihood function for $\boldsymbol{\theta}$, respectively. If the data x_i are independent, then

$$f(\boldsymbol{x}|\boldsymbol{\theta}) = \prod_{i=1}^{n} f(x_i;\boldsymbol{\theta}) \tag{4.22}$$

Bayesian inference involves the balance of uncertainties associated with both the prior information and new observation information, to obtain a posterior estimation. The prior information is regarded as the greatest strength and also main pitfall of Bayesian inference (Coles 2001). It supplements the observed data, which is often very limited. In contrast, different analysts would specify different priors, which may lead conclusions to being meaninglessly subjective. In other words, to do Bayesian estimation the price of having to specify prior information must be accepted.

When the posterior distribution $f(\boldsymbol{\theta} \mid \boldsymbol{x})$ in Eq. (4.21) is in the same family as the prior probability distribution $f'(\boldsymbol{\theta})$, the prior and posterior are then called conjugate distributions, and the prior is called a conjugate prior for the likelihood. For example, the Gaussian family is self-conjugate with respect to a Gaussian likelihood function. However, conjugate prior distributions may not even be possible in practice. Non-conjugate prior distributions can make computation of posterior inferences intractable using conventional techniques. This difficulty can be tackled by the MCMC algorithms.

Predictions can also be handled by the Bayesian inference. The predictive PDF of a future observation z given $\boldsymbol{x}$ is

$$f(z|\boldsymbol{x}) = \int_{\Theta} f(z|\boldsymbol{\theta}) f(\boldsymbol{\theta}|\boldsymbol{x}) d\boldsymbol{\theta} \tag{4.23}$$

where $f(z \mid \boldsymbol{\theta})$ is the PDF of z, and $f(\boldsymbol{\theta} \mid \boldsymbol{x})$ is the posterior PDF of $\boldsymbol{\theta}$ obtained based on observed data $\boldsymbol{x}$. If z is the return level corresponding to a return period N, by solving

$$\mathrm{P}\{Z \le z \mid \boldsymbol{x}\} = \int_{\Theta} \mathrm{P}\{Z \le z \mid \boldsymbol{\theta}\} f(\boldsymbol{\theta} \mid \boldsymbol{x}) d\boldsymbol{\theta} = 1 - 1/N \tag{4.24}$$

the N-year return level can be obtained. When the posterior PDF of $\boldsymbol{\theta}$ has been estimated by the MCMC algorithm, the sample of the stationary distribution $f(\boldsymbol{\theta} \mid \boldsymbol{x})$ obtained by deleting the values generated in the settling period can be used to solve Eq. (4.24) easily

$$\mathrm{P}\{Z \le z \mid \boldsymbol{x}\} = \frac{1}{s} \sum_{i=1}^{s} \mathrm{P}\{Z \le z \mid \theta_i\} \tag{4.25}$$

4.2.3.3 Model checking

There are four data-based plots to assess the accuracy of the extreme value model fitted to the data: probability plot, quantile plot, return level plot and density plot. A probability plot is a comparison of the empirical and fitted probabilities of the extreme values. A successful probability plot should lie close to the unit diagonal. A weakness of the probability plot is that it provides the least information in the most concerned region, which corresponds to extremes with long return periods. This deficiency is avoided by the quantile plot. A quantile plot is a comparison of the empirical and fitted quantiles of the extreme values. Departure from linearity in the quantile plot also indicates model failure. The return level plot has been introduced in section 4.2.2. Empirical estimates of the return level are added to the plot. If the fitted model is

suitable for the data, the model-based curve and empirical estimates should be in reasonable agreement. Confidence intervals can be added to the plot to increase its informativeness. For completeness, another diagnostic plot, the density plot which is based on the density function, is also adopted. By comparing the PDF of the fitted model with the histogram of the data, the fitted model can be validated. It is generally less informative than the previous plots, because the histogram can vary substantially with the choice of size of blocks or threshold of peaks.

4.2.4 Threshold Selection for POT Model

Like the choice of block size in the BM approach, the threshold selection in the POT approach is also subjective. The selection implies a trade-off between bias and variance. When the threshold level is too low, the fitted model of extreme values is quite poor, leading to bias in estimation and extrapolation. On the other hand, too high threshold levels generate only few data to derive the model, leading to large estimation variance. Two methods are popular to select the threshold (O'Brien *et al*. 2015): one is an exploratory technique carried out prior to model estimation, the other is an assessment of the stability of parameter estimates. The first method builds the mean residual life plot representing the points

$$\left(u, \sum_{i=1}^{n_u} \left(x_{(i)} - u \right) \Big/ n_u \right) \qquad u < x_{\max} \tag{4.26}$$

where $x_{(i)}$ is the n_u observation that exceeds u, and $x_{\max}$ is the maximum observation in the data set. Then the value above which the plot is approximately linear in u is chosen as the threshold. The representation of CIs can help to determine this point. Sometimes it is difficult to select threshold using mean residual life plots. Another technique is to look for stability of parameter estimates over a range of thresholds. The lowest value of u for which the parameter estimates of the GP model remain near-constant is selected as the threshold.

4.3 Tsing Ma Bridge (TMB) and Monitoring of Strain

4.3.1 TMB

The TMB is the key linkage of the most important transport network in Hong Kong, which connects the international airport to the urban area. As shown in Figure 4.1 (a), the TMB is a two-span suspension bridge with an overall length of 2,160 m and a main span of 1,377 m between the Tsing Yi tower in the east and the Ma Wan tower in the west. It is currently the world's longest suspension bridge that carries both highway and railway traffic. Each concrete portal tower has a length of 195 m. The two main cables accommodated by four saddles at the top of the tower legs are 36 m apart in the north and south. Each set of suspenders is composed of four 75 mm diameter twisted-wire strands. At the main span and the Ma Wan side span, the deck is suspended from the main cables at 18 m intervals. In the longitudinal direction, the bridge deck

continuously expands from the Ma Wan abutment to the Tsing Yi abutment. The supports for the deck at the end of Ma Wan span, Ma Wan tower, Tsing Yi tower, the end of Tsing Yi span, and piers are hinged support, rocker bearings, sliding bearings, roller support basing on a highway movement joint at upper deck and a railway movement joint at lower deck, and sliding bearings, respectively. The movement joint at the end of Tsing Yi span was designed to accommodate the longitudinal displacement of the deck due to temperature.

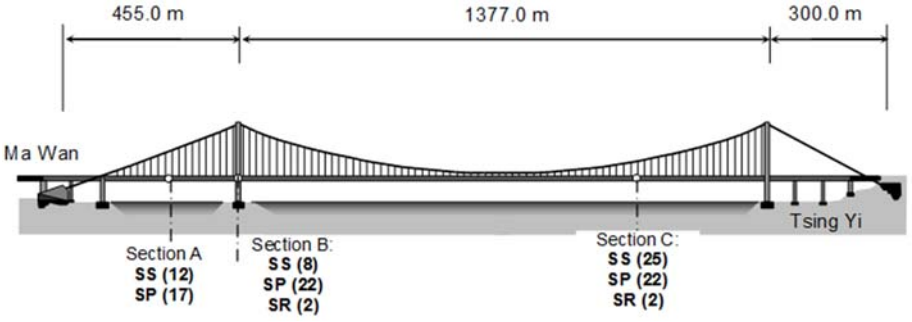

(a) Elevation view

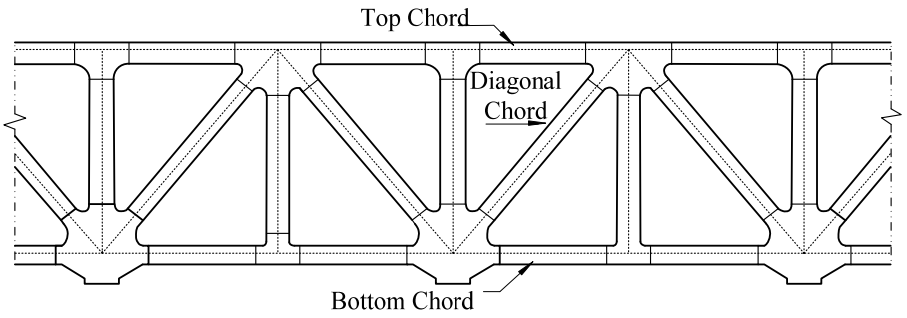

(b) Warren truss

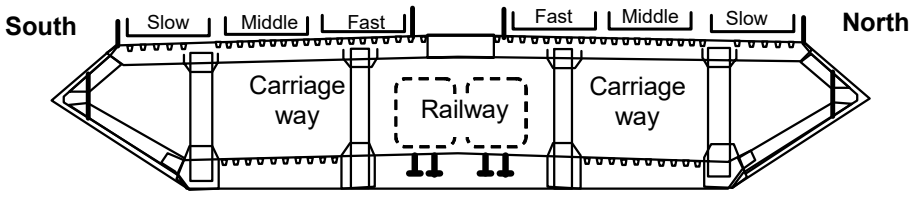

(c) Vierendeel truss

Figure 4.1 General structural features of TMB

The key structural feature of the TMB lies in the stiffening deck system (Beard and Young 1995), which is a streamlined box-shaped and continuous truss girder with a central air-gap. It has a continuous length of 2,160 m and a total steel weight of 49,000 tons. There is a minimum of 62 m for shipping channel below the deck. The geometrical features of streamlined box-shape and central air-gap are respectively used to reduce the wind dragging forces acting on the bridge-deck and to increase the aerodynamic stability of the bridge-deck under fluctuating winds. The truss girder is composed of the Warren truss (longitudinal) and the Vierendeel truss (transverse) (Figure 4.1(b)-(c)). The two longitudinal trusses act as the main girder of the bridge. As shown in Figure 4.1(b), the deck has two levels: the upper level carries a dual three-lane highway, and the lower level carries two railway tracks and two single-lane carriage ways. The two directions of traffic are called the Airport bound way and the Kowloon bound way, respectively.

The TMB serves a port and airport complex, so it carries a particularly large amount of heavy lorries. In normal days, the highway traffic is on the upper deck; while when there is a strong typhoon, the traffic on the upper deck will be closed and the two carriageways on the lower deck will be used for emergency. The vehicles running on the bridge are classified into eight categories according to their main features including the number of axles, magnetic vehicle length, axle distance, and gross vehicle weight (GVW). The highway traffic on the TMB is governed by the Hong Kong road traffic regulations (HKRTR), so the maximum GVW and axle load of the vehicles are

regulated. Before 2003, most trains passing through the TMB were 7-car trains; however, with the increasing demand of passenger flow, most trains had become 8-car trains since the end of 2005. The years between 2003 and 2005 were a transition period with 7-car and 8-car trains running concurrently. The railway traffic is managed by the MTR Corporation Limited, Hong Kong. The maximum distribution of bogie loads in an 8-car MTRC train is regulated, and the maximum gross train weight (GTW) allowed to pass the TMB is 498 tonnes.

4.3.2 WASHMS

A Wind And Structural Health Monitoring System (WASHMS) was instrumented on the TMB after the completion of its construction. The system started operation in 1997, and it has worked continuously and successfully for about 20 years up to now. The objectives of the WASHMS are (Ko and Ni 2005): (i) to monitor and evaluate the structural health of the bridge; (ii) to provide information for the planning of inspection and maintenance activities; and (iii) to verify design assumptions and parameters for future design and construction of similar bridges around Hong Kong. The WASHMS is composed of 283 sensors in eight types (Ni and Xia 2016), namely, 6 anemometers, 19 servo-type accelerometers, 115 temperature sensors, 110 welded foil-type strain gauges (or dynamic strain gauges), 14 global positioning system (GPS) receivers, two displacement transducers, 10 level sensing stations, and seven dynamic weigh-in-motion (WIM) stations. The general layout of these sensors and their associated data-

acquisition outstations is shown in Figure 4.2 (Wong 2007). The seven dynamic WIM stations are not shown in the figure because they are installed about 2 km away from Ma Wan Anchorage.

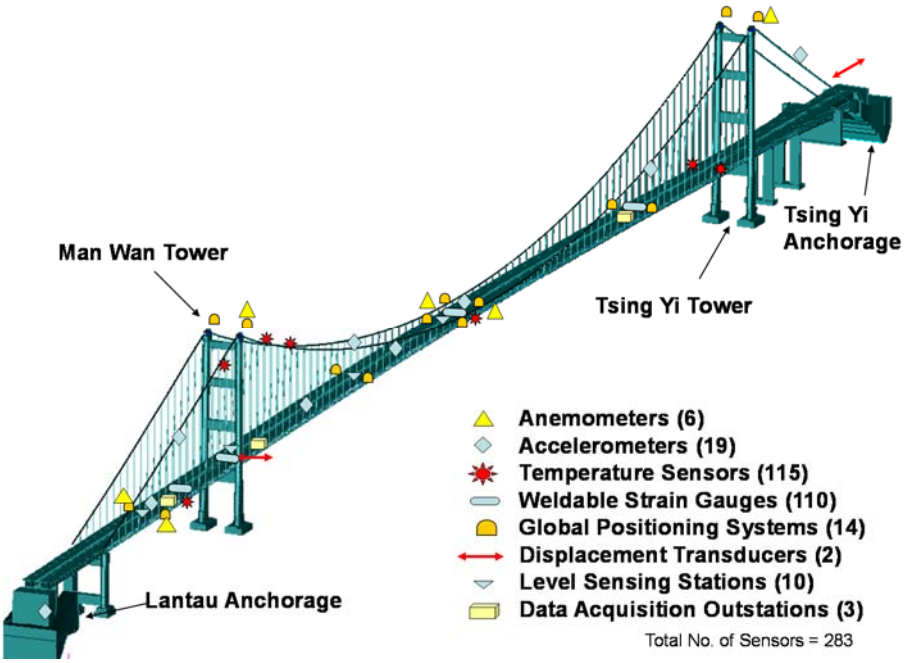

Figure 4.2 Layout of sensors and data acquisition stations on TMB (Wong 2007)

4.3.3 Strain Monitoring

As an important part of this system, a total of 110 strain gauges have been installed in three selected deck sections, i.e., sections A, B and C, as shown in Figure 4.1. The strains of critical chords, plan bracings, deck trough and rocker bearings, in these three sections are measured. The strain gauges installed are in three types of configuration: single strain sensor (SS), pair strain sensor (SP), and rosette strain sensor (SR). Figure 4.3 illustrates the deployment of the strain gauges on the north and south longitudinal

trusses at the main span. The sampling rate of the strain measurement was 25.6 Hz before 2001, but has increased to 51.2 Hz since 2002.

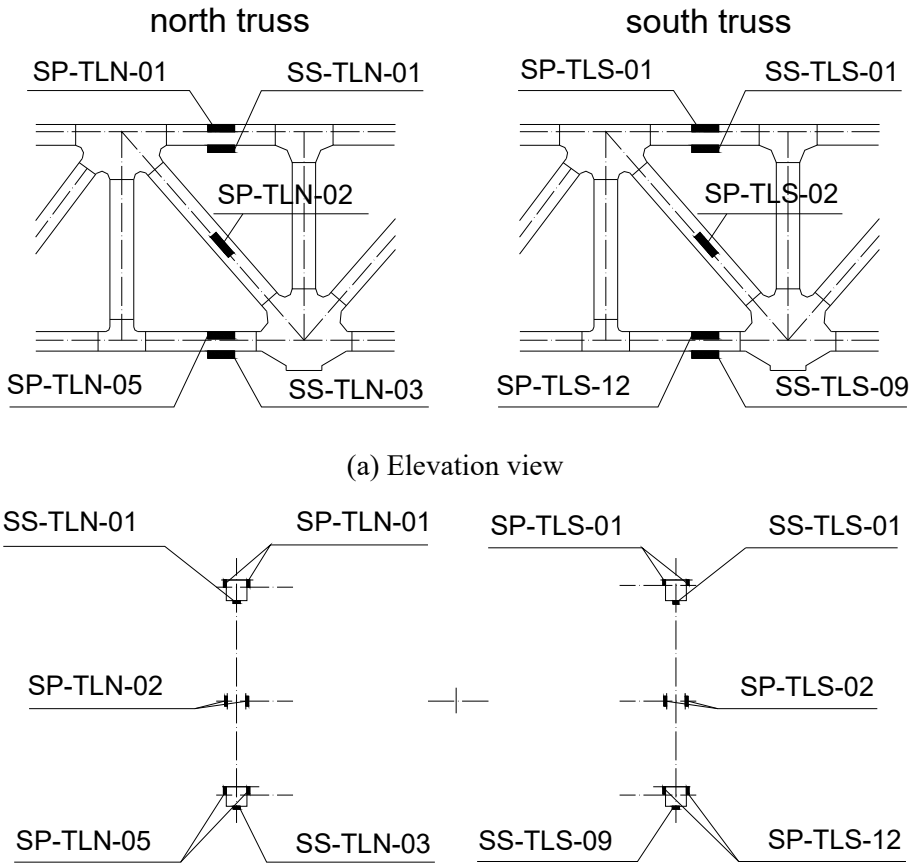

(a) Elevation view

(b) Cross-section view

Figure 4.3 Strain gauges installed on longitudinal trusses at main span

4.4 Variation Tendency of Long-Term Stresses

The monitored strain from the TMB deck is mainly due to four effects: highway traffic, railway traffic, wind, and temperature. The static strain resulting from initial dead loads is not measurable because the strain gauges were installed after the completion

of bridge construction. The temperature-induced strain, although fairly large, contributes little to the stress because the majority of it is released by free movement of the bridge deck at the expansion joints on the Tsing Yi abutment. Therefore, under normal conditions, i.e. when there are no events such as typhoon, the stress of the bridge deck is mainly due to highway and railway traffic. Recognizing the fact that the bridge performs in elastic stage under normal in-service conditions, the stress experienced by the steel trusses can be obtained by the Hook's Law.

Recognizing the fact that the two longitudinal trusses acting as the main girder of the bridge, the stresses measured from a bottom longitudinal truss were concerned. Characteristics of the strain measured at the three deck sections can be found in Ni and Xia (2016). It was found through statistical analysis of one-year strain data that the traffic-induced stresses in the longitudinal trusses at sections A and C (Figure 4.1) are close to each other, while those at section B are smaller. For sections A and C, the bottom chords experienced larger stress than the top and diagonal chords. In addition, for the north and south bottom chords that are symmetric to each other against the longitudinal axis of the deck, the daily maximum stresses are close to each other. In the present study, the strain measured by the strain gauge SSTLS09 (Figure 4.3), which is a single strain gauge installed at the bottom of the longitudinal truss at section C, is selected to investigate the extreme TLEs on the TMB.

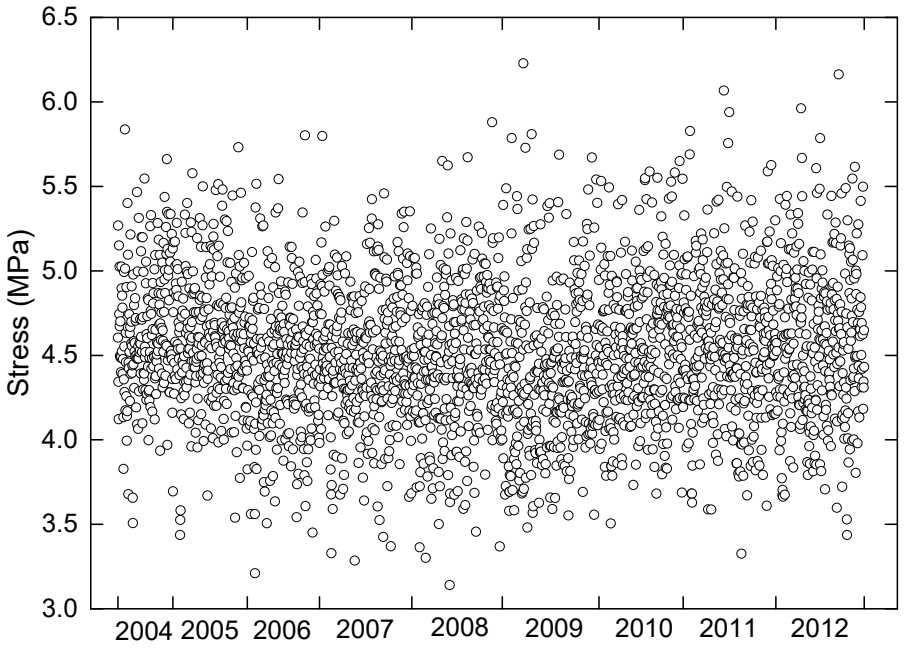

(a) Highway-induced stress

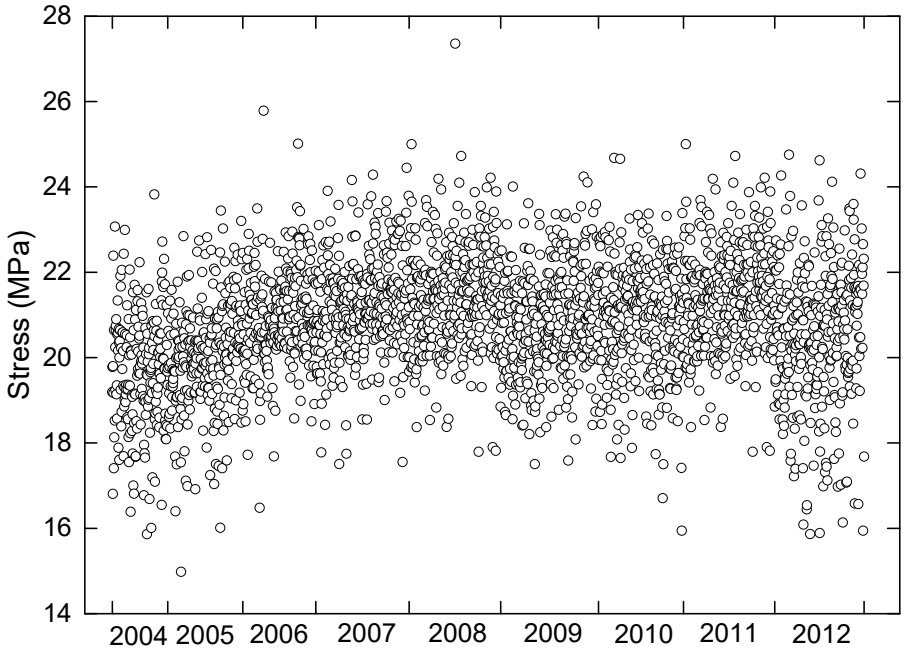

(b) Railway-induced stress

Figure 4.4 Scatter plots of daily maximum tensile stresses due to highway and railway traffic

The monitored strain data are contaminated with noises, spikes and trends. Furthermore, to study the respect effect of highway and railway traffic, the strain should be decomposed accordingly. The wavelet-based signal pre-processing method

in terms of denoising, despiking and decomposing proposed in Chapter 3 was applied to obtain the desired ingredients. Figure 4.4 shows the scatter plots of the daily maximum tensile stresses induced by the highway and railway traffic, respectively. The data shown were measured during the period from April 2004 to December 2012, and have excluded those collected during typhoons and strong monsoons. It is found that the stresses due to highway traffic do not change much during the observed period. On the other hand, the railway-induced stresses have an increase during April 2004 to December 2006, but afterward there is no significant change. It is because 2005 is the critical year of pattern transition of the railway traffic on the TMB. Between 2003 and 2005, both 7-car and 8-car trains ran concurrently on the TMB, while after 2005 most of the trains running on the TMB were 8-car trains.

4.5 Extreme Value Distribution and Characteristic Values

4.5.1 Results Based on BM Approach

The block-size to study the extreme stresses using the BM approach is selected as one-month. The scatter plot of the monthly maximum tensile stresses measured by the strain gauge SSTLS09 during April 2004 to December 2012 is shown in Figure 4.5: (a) is the highway-induced stress, and (b) is the railway-induced stress. It is observed that the monthly maximum tensile stresses due to both the highway and railway traffic can be considered as statistically independent and identically distributed. Therefore,

the asymptotic distributions of these monthly maximum stresses are the GEV distribution.

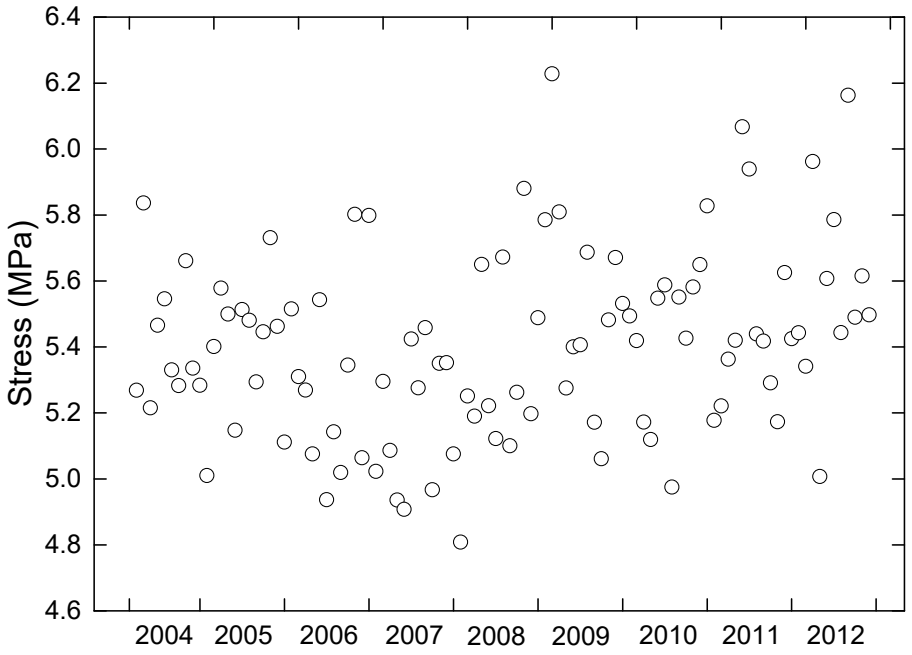

(a) Highway-induced stresses

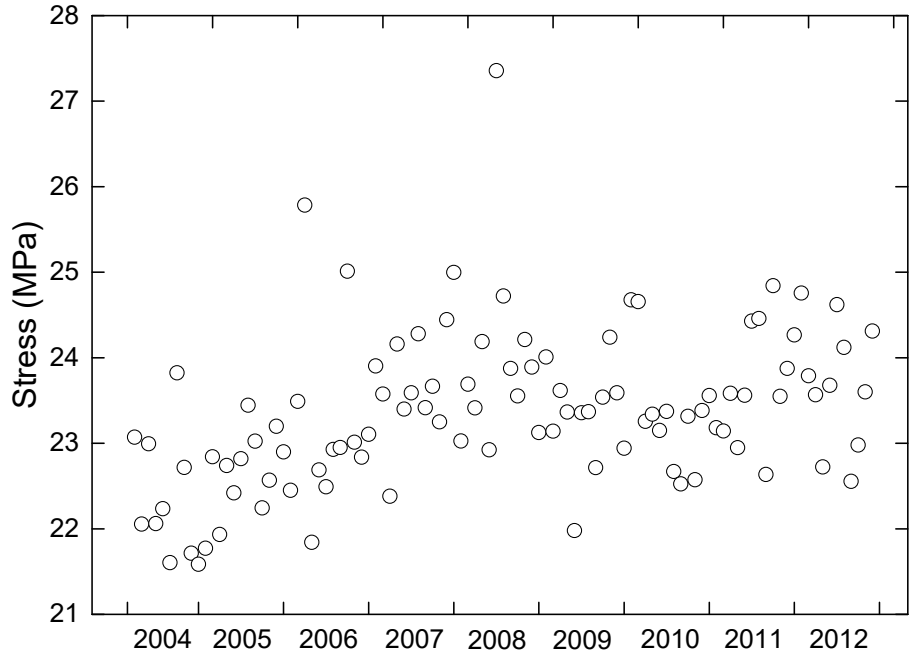

(b) Railway-induced stresses

Figure 4.5 Scatter plots of monthly maximum tensile stresses

The parameters of the distribution are estimated by the MLE, PLE and BE methods, respectively. The diagnostic plots (probability plot, quantile plot, return level plot and density plot) for the GEV fits to the extreme stresses based on MLE are shown in Figure 4.6. In the return level plot, the 95% CIs based on normal approximation are also shown (grey dashed lines). It can be observed from Figure 4.6 that the monthly maxima of both the highway and railway induced stresses are well fitted to the GEV distribution. Because the normal approximation may be poor for the parameters of fitted the GEV model and the corresponding return levels, especially the shape parameter and the return levels associated with long return periods, i.e., their CIs are likely to be skewed, the CIs are preferred to be estimated by the PLE method. As an example, the PL plots for the parameters of the GEV model fitted to the railway-induced stresses and the return level of 120 years are shown in Figure 4.7. In the PL plots, the vertical long dashed lines in bold are the estimates of CIs, and the vertical short dashed line shows the location of the MLE for the corresponding parameter or return level. The skewness of the CIs for the shape parameter and 120-year return level can be easily observed.

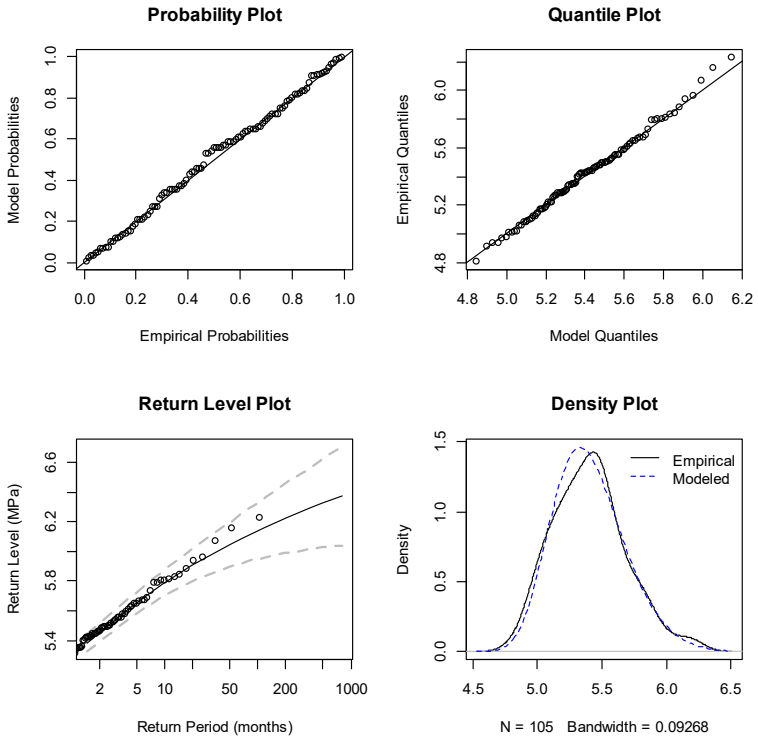

(a) Highway-induced case

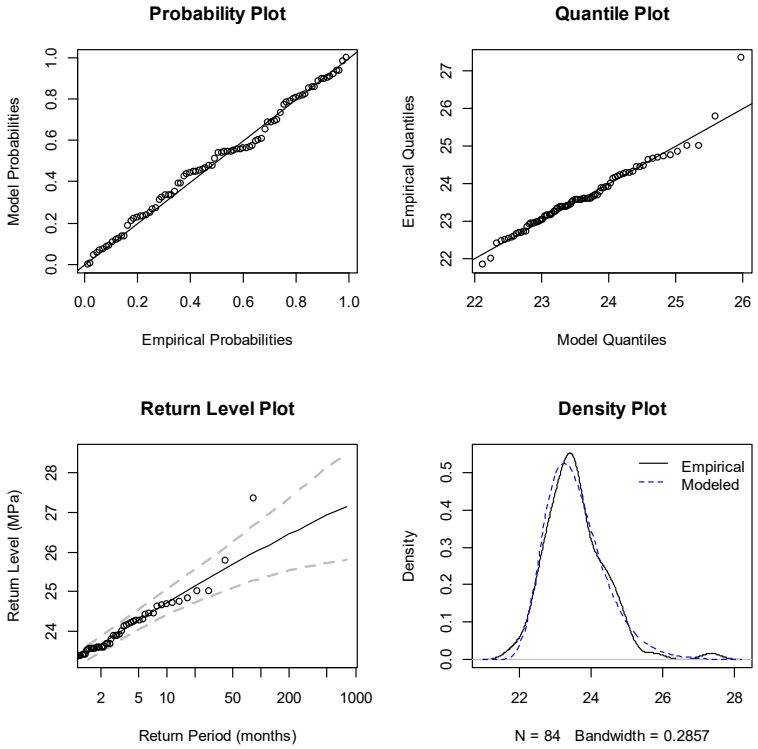

(b) Railway-induced case

Figure 4.6 Diagnostic plots for GEV fit to traffic-induced stresses

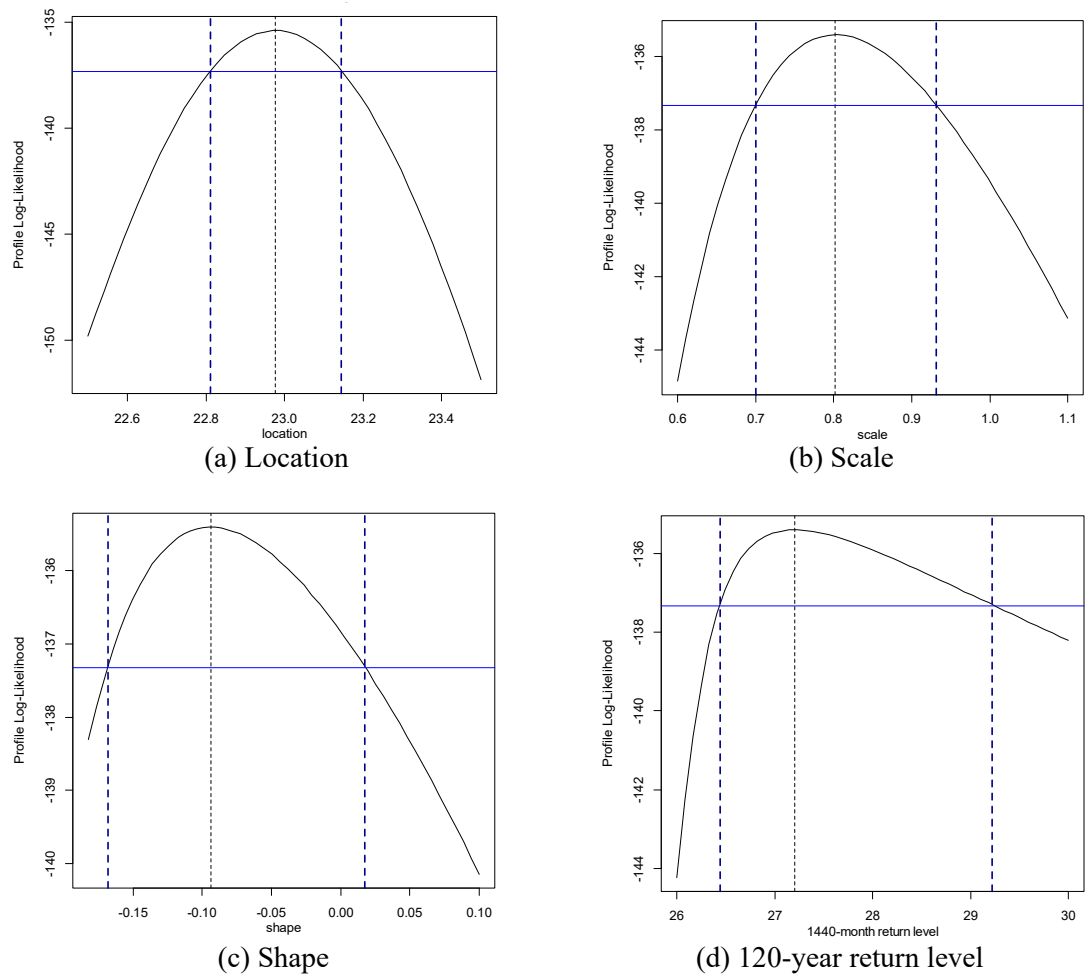

(a) Location (b) Scale

(c) Shape (d) 120-year return level

Figure 4.7 PL plots for parameters of GEV model fitted to monthly maximum stresses induced by railway traffic and 120-year return level

In the Bayesian estimation, the likelihood function is

$$z_i \sim \mathrm{GEV}(\mu, \sigma, \xi) \tag{4.27}$$

where z_i is the monthly maximum stress indexed by i. To respect the positivity on σ, $\phi = \log\sigma$ is stetted. Under the prerequisite that the parameters are independent with each other, the prior density function

$$f(\mu,\phi,\xi) = f_{\mu}(\mu) f_{\phi}(\phi) f_{\xi}(\xi) \tag{4.28}$$

where $f_{\mu}(\mu)$, $f_{\phi}(\ \phi)$, and $f_{\xi}(\xi)$ are normal PDFs, is chosen. To estimate the parameters of the GEV fitting to the extreme stresses by Bayesian estimation, the price of subjective conclusions produced by prior information should be accepted, as stated in section 4.2.3.2. Figure 4.8 shows the comparison of GEV fittings to the railway-induced extreme stresses based on relatively non-informative and informative prior information, respectively. Figure 4.8 (a) corresponds to the prior information of μ~N(25,1000), σ~N(1, 1000), and ξ~N(0, 1000), while Figure 4.8 (b) corresponds to that of μ~N(25,1), σ~N(1,0.1), and ξ~N(0,0.1). It is observed that with non-informative prior information, the fitted extreme value model mostly depends on the data; while with prior information relatively informative, the fitting of the GEV model to the data is apparently not good, which implies the subjective prior information has played an important role in the conclusion. The deviance information criteria (DIC) for the two fittings are 821 and 953, respectively.

When newly collected data are available, the posterior PDF of the parameters (μ, σ, ξ) can be obtained by the Bayes' theorem

$$f(\mu,\sigma,\xi\,|\,\boldsymbol{Z}) = \frac{f(\boldsymbol{Z}\,|\,\mu,\sigma,\xi)\ f'(\mu,\sigma,\xi)}{\int_{\Theta} f(\boldsymbol{Z}\,|\,\mu,\sigma,\xi)\ f'(\mu,\sigma,\xi)\ \mathrm{d}\mu\ \mathrm{d}\sigma\ \mathrm{d}\xi} \tag{4.29}$$

where $f(\mu,\sigma,\xi|\boldsymbol{Z})$ is the posterior PDF of the parameters, $\boldsymbol{z}$ represents the monthly maximum live load demand obtained from strain data, $f'(\mu,\sigma,\xi)$ is the prior PDF of the parameters; and $f(\boldsymbol{Z}|\mu,\sigma,\xi)$ is the likelihood function

$$\begin{aligned} f(\boldsymbol{Z}|\mu,\sigma,\xi) = L(\mu,\sigma,\xi|\boldsymbol{Z}) &= \prod_{i=1}^{m} f(z_i;\mu,\sigma,\xi) \\ &= \prod_{i=1}^{m} \frac{1}{\sigma}\left[1+\xi\frac{(z_i-\mu)}{\sigma}\right]^{-1/\xi-1} \exp\left\{-\left[1+\xi\frac{(z_i-\mu)}{\sigma}\right]^{-1/\xi}\right\} \\ &= \frac{1}{\sigma^n}\exp\left\{-\sum_{i=1}^{m}\left[1+\xi\frac{(z_i-\mu)}{\sigma}\right]^{-1/\xi}\right\}\prod_{i=1}^{m}\left[1+\xi\frac{(z_i-\mu)}{\sigma}\right]^{-1/\xi-1} \end{aligned} \tag{4.30}$$

where $f(z_i;\mu,\sigma,\xi)$ is the GEV function. In recognition of the fact that there is no expert information to formulate a reliable prior distribution, the non-informative prior information is preferred in this study.

The prior PDF is a three-dimensional joint distribution of the parameters (μ, σ, ξ). The likelihood function and the posterior are also three-dimensional joint distributions of (μ, σ, ξ). There is no analytical solution of the joint posterior distribution presented in Eq. (4.29). This problem can be overcome by the MCMC algorithms (Gilks 2005). To specify the prior, a parametrization of ϕ=ln σ is made to constrain σ to be positive. When non-informative priors are given, the variances of the normal priors are set large enough to make the distributions almost flat. Since this is a multivariate density, the Gibbs sampling is adopted, and a Metropolis step with random walk updates is employed to simulate from the full conditionals. The interested posterior is

$$f(\mu,\sigma,\xi\,|\,\boldsymbol{Z}) \propto L(\mu,\phi,\xi\,|\,\boldsymbol{Z})\; f'(\mu,\phi,\xi) \tag{4.31}$$

thus the posterior is of the form

$$L(\mu,\phi,\xi\,|\,\boldsymbol{Z})\; f'(\mu,\phi,\xi) = f_{\mu}(\mu) f_{\phi}(\phi) f_{\xi}(\xi) L(\mu,\phi,\xi\,|\,\boldsymbol{Z}) \tag{4.32}$$

and the full conditionals are of the form

$$\begin{aligned} f(\mu\,|\,\phi,\xi) &= f_{\mu}(\mu) L(\mu,\phi,\xi\,|\,\boldsymbol{Z}) \\ f(\phi\,|\,\mu,\xi) &= f_{\phi}(\phi) L(\mu,\phi,\xi\,|\,\boldsymbol{Z}) \\ f(\xi\,|\,\mu,\phi) &= f_{\xi}(\xi) L(\mu,\phi,\xi\,|\,\boldsymbol{Z}) \end{aligned} \tag{4.33}$$

The three transition densities are denoted by q_{μ}, q_{ϕ} and q_{ξ}, respectively, and the proposed values for the parameters are given in random walks

$$\begin{aligned} \mu^{*} &= \mu + \varepsilon_{\mu} \\ \phi^{*} &= \phi + \varepsilon_{\phi} \\ \xi^{*} &= \xi + \varepsilon_{\xi} \end{aligned} \tag{4.34}$$

where ε_{μ}, ε_{ϕ}, and ε_{ξ} are normally distributed variables with zero means and variances of ω_{μ}, ω_{ϕ}, and ω_{ξ}. The procedures of the algorithm are as follows:

(1) To initialize the chain at $\boldsymbol{\theta}^{(0)}=(\mu^{(0)}, \phi^{(0)}, \xi^{(0)})$ and the counter at j=1.

(2) To simulate $\varepsilon_{\mu}\sim N(0, \varepsilon_{\mu})$.

(3) To set $\mu^{*}=\mu^{(j-1)}+\varepsilon_{\mu}$.

(4) To accept $\mu^{(j)}=\mu^*$ with probability $a(\mu^{(j-1)}, \mu^*)=\min\{1,A\}$ where

$$A=\frac{f(\mu^*\left|\phi^{(j-1)},\xi^{(j-1)}\right.)q_\mu(\mu^{(j-1)},\mu^*)}{f(\mu^{(j-1)}\left|\phi^{(j-1)},\xi^{(j-1)}\right.)q_\mu(\mu^*,\mu^{(j-1)})} \tag{4.35}$$

and $\mu^{(j)}=\mu^{(j-1)}$ otherwise. Then $q_\mu(\mu^{(j-1)},\mu^*)=f_{\varepsilon_\mu}(\mu^{(j-1)}-\mu^*)$, where $f_{\varepsilon\mu}(\cdot)$ is the PDF of ε_μ. The distribution of ε_μ is symmetric about zero, $q_\mu(\mu^{(j-1)},\mu^*)=q_\mu(\mu^*,\mu^{(j-1)})$, so

$$A=\frac{f(\mu^*\left|\phi^{(j-1)},\xi^{(j-1)}\right.)}{f(\mu^{(j-1)}\left|\phi^{(j-1)},\xi^{(j-1)}\right.)} \tag{4.36}$$

(5) To simulate $\varepsilon_\phi \sim N(0, \varepsilon_\phi)$.

(6) To set $\phi^*=\phi^{(j-1)}+\varepsilon_\phi$.

(7) To accept $\phi^{(j)}=\phi^*$ with probability $a(\phi^{(j-1)}, \phi^*)=\min\{1,A\}$ where

$$A=\frac{f(\phi^*\left|\mu^{(j-1)},\xi^{(j-1)}\right.)}{f(\phi^{(j-1)}\left|\mu^{(j-1)},\xi^{(j-1)}\right.)} \tag{4.37}$$

and$\varphi^{(j)}=\varphi^{(j-1)}$ otherwise.

(8) To simulate $\varepsilon_\xi \sim N(0, \varepsilon_\xi)$.

(9) To set $\xi^*=\xi^{(j-1)}+\varepsilon_\xi$.

(10) To accept $\xi^{(j)}=\xi^*$ with probability $a(\xi^{(j-1)},\xi^*)=\min\{1,A\}$ where

$$A=\frac{f(\xi^*\left|\mu^{(j-1)},\phi^{(j-1)}\right.)}{f(\xi^{(j-1)}\left|\mu^{(j-1)},\phi^{(j-1)}\right.)} \tag{4.38}$$

and $\zeta^{(j)}=\zeta^{(j-1)}$ otherwise.

(11) To increase counter from j to $j + 1$ and return to step 2.

The resulting chain of the parameters will converge to the posterior distribution after an initial "burn-in" period. With the MCMC algorithm, the posterior probability densities of the estimated parameters and trace plots generated by 10,000 iterations of the chain are shown in Figure 4.9.

The MLE, PLE and BE-obtained estimations of GEV parameters and return levels, including point estimators and 95% CIs, for the extreme stresses induced by railway and highway traffic respectively, are shown in Table 4.1. The CIs estimated by the MLE are based on the normal approximation of the parameters; and the point estimators for the PLE and BE are the MLE and the mode (the value that appears most often in a set of data) of the posterior parameters, respectively. z_{p_5} means the return level corresponding to a return period of 5 years, and z_{p_120} means that corresponding to a return period of 120 years. It is found that the point estimates of the evaluated parameters of the GEV distributions fitted to the data and extrapolated return levels are robust to the estimation methods (non-informative prior information was adopted in the BE method, so the results more depend on the data). The difference in the skewness of the CIs for the shape parameter and return levels, which were estimated based on the normal approximation and the profile likelihood respectively, can also be observed.

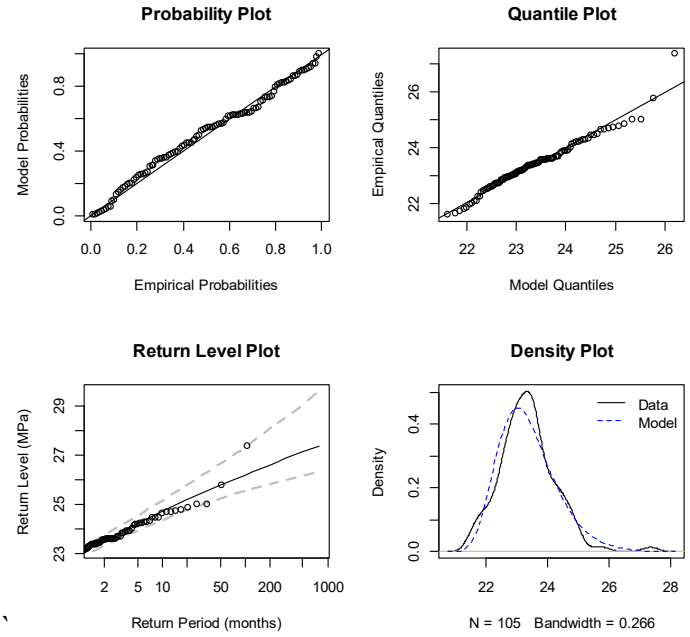

(a) Based on prior information relatively non-informative

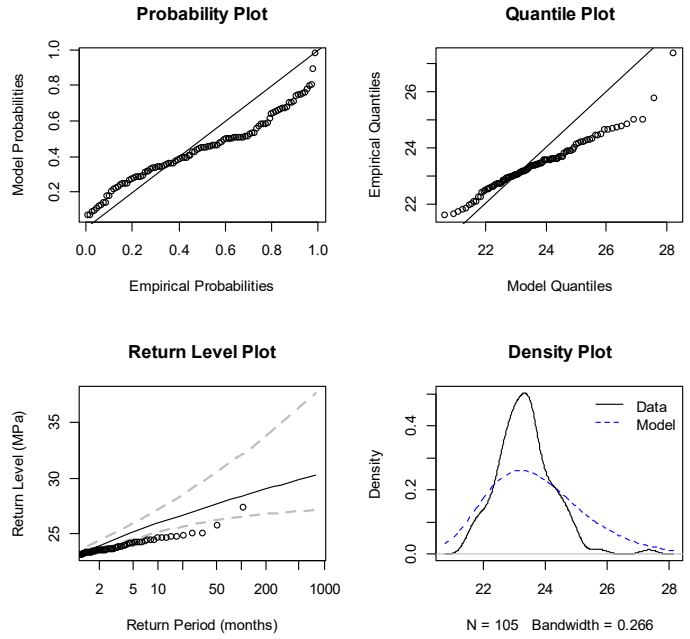

(b) Based on prior information relatively informative

Figure 4.8 GEV fittings to railway-induced extreme stresses based on non-informative and informative prior information

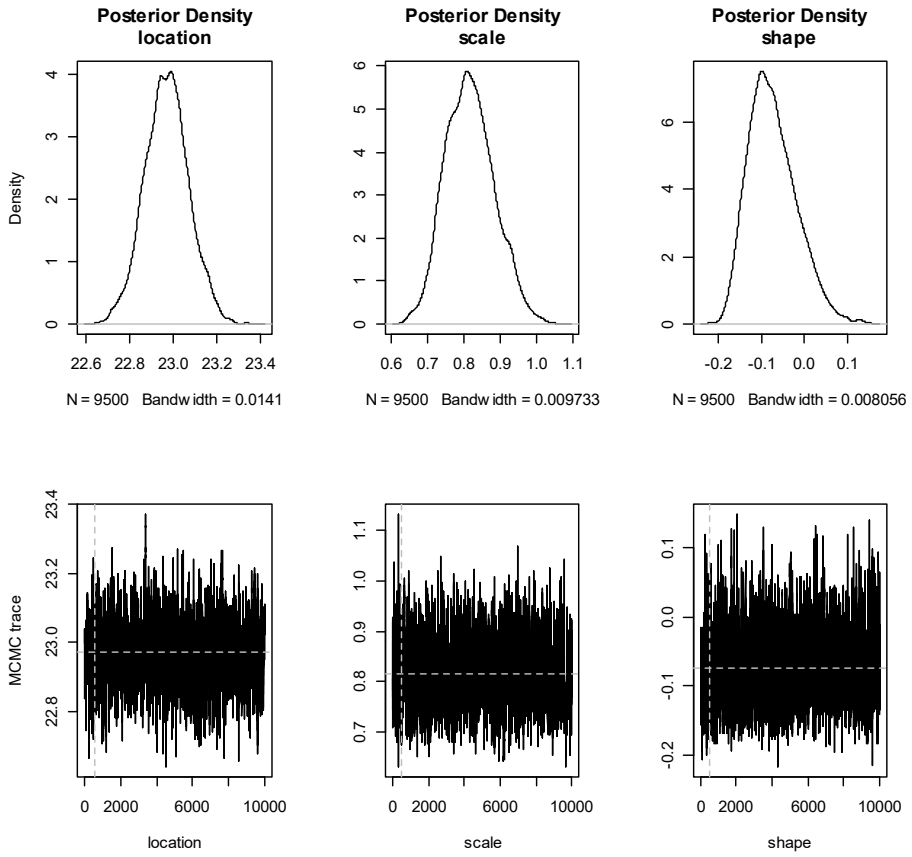

Figure 4.9 MCMC posterior parameter densities and trace plots from fitting GEV distribution function to monthly maximum values of railway-induced stresses using Bayesian estimation

Table 4.1 Parameter and return level estimates based on BM approach

			μ	σ	ξ	$z_{p\ 5}$ (MPa)	$z_{p\ 120}$ (MPa)
Highway	MLE	Point	5.29	0.26	-0.15	6.07	6.43
		CI	(5.24,5.35)	(0.22,0.29)	(-0.28,-0.02)	(5.91,6.23)	(6.05,6.80)
	PLE	Point	5.29	0.26	-0.15	6.07	6.43
		CI	(5.24,5.35)	(0.22,0.30)	(-0.27,0.00)	(5.95,6.31)	(6.20,7.07)
	BE	Point	5.29	0.26	-0.13	6.12	6.54
		CI	(5.23,5.35)	(0.22,0.31)	(-0.25,0.02)	(5.97,6.37)	(6.20,7.23)
Railway	MLE	Point	22.98	0.8	-0.09	25.70	27.21
		CI	(22.81,23.14)	(0.69,0.92)	(-0.19,0.00)	(25.18,26.22)	(26.02,28.39)
	PLE	Point	22.98	0.8	-0.09	25.70	27.21
		CI	(22.81,23.14)	(0.70,0.93)	(-0.17,0.02)	(25.29,26.45)	(26.44,29.22)
	BE	Point	22.97	0.82	-0.07	25.87	27.68
		CI	(22.77,23.17)	(0.70,0.95)	(-0.16,0.05)	(25.31,26.76)	(26.49,30.17)

4.5.2 Results Based on POT Approach

The two threshold-selection techniques introduced in section 4.2.4 are employed to select thresholds for extreme extrapolation using the POT approach. The plots used to select the threshold of the daily maximum railway-induced stresses are shown in Figure 4.10: (a) is the mean residual life plot, and (b) is the threshold range plot. The threshold is selected as 22 MPa. Similarly, the threshold for the POT model of the daily maximum highway-induced stresses is selected as 5 MPa.

The diagnostic plots for the MLE-obtained GP fittings to the POT of traffic-induced stresses are shown in Figure 4.11. It can be observed that the POTs of both the highway-induced and railway-induced stresses are well fitted to the GP distribution. The MLE, PLE and BE-obtained estimations of GP parameters and return levels, including point estimators and 95% CIs, for the extreme stresses induced by railway and highway traffic respectively, are shown in Table 4.2. The BE is also based on non-informative prior information because of the absence of reliable expert knowledge. It can be found from Table 4.2 that the parameters and return levels are not sensitive to the estimation methods.

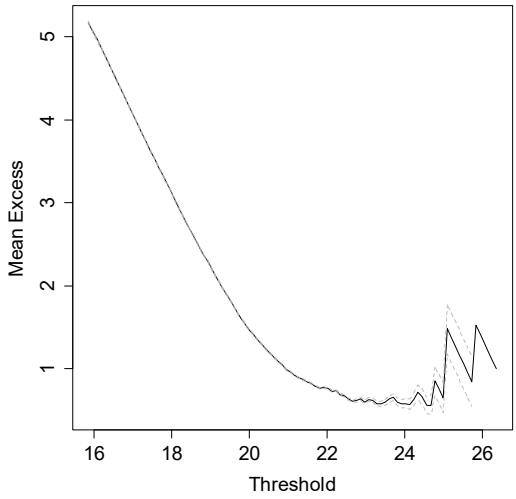

(a) Mean residual life plot

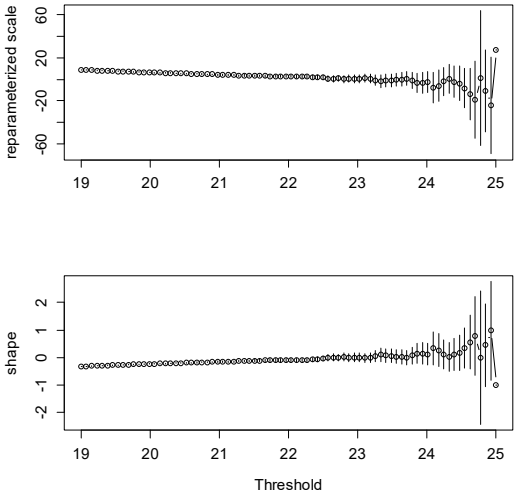

(b) Threshold range plot

Figure 4.10 Threshold selection for POT model of daily maximum railway-induced stresses

Table 4.2 Parameter and return level estimates based on POT approach

			σ	ξ	$z_{p\ 5}$ *(MPa)*	$z_{p\ 120}$ *(MPa)*
Highway	MLE	Point	0.24	-0.15	6.05	6.36
		CI	(0.18,0.30)	(-0.31,0.00)	(5.88,6.22)	(5.99,6.74)
	PLE	Point	0.24	-0.15	6.05	6.36
		CI	(0.19,0.31)	(-0.25,0.04)	(5.94,6.29)	(6.17,7.10)
	BE	Point	0.24	-0.10	6.11	6.56
		CI	(0.18,0.30)	(-0.27,0.13)	(5.96,6.42)	(6.19,7.67)
Railway	MLE	Point	0.79	-0.09	25.65	26.97
		CI	(0.71,0.88)	(-0.15,-0.03)	(25.20,26.09)	(26.06,27.88)
	PLE	Point	0.79	-0.09	25.65	26.97
		CI	(0.71,0.88)	(-0.14,-0.02)	(25.31,26.23)	(26.35,28.31)
	BE	Point	0.79	-0.08	25.75	27.22
		CI	(0.70,0.88)	(-0.13,0.00)	(25.35,26.36)	(26.42,28.72)

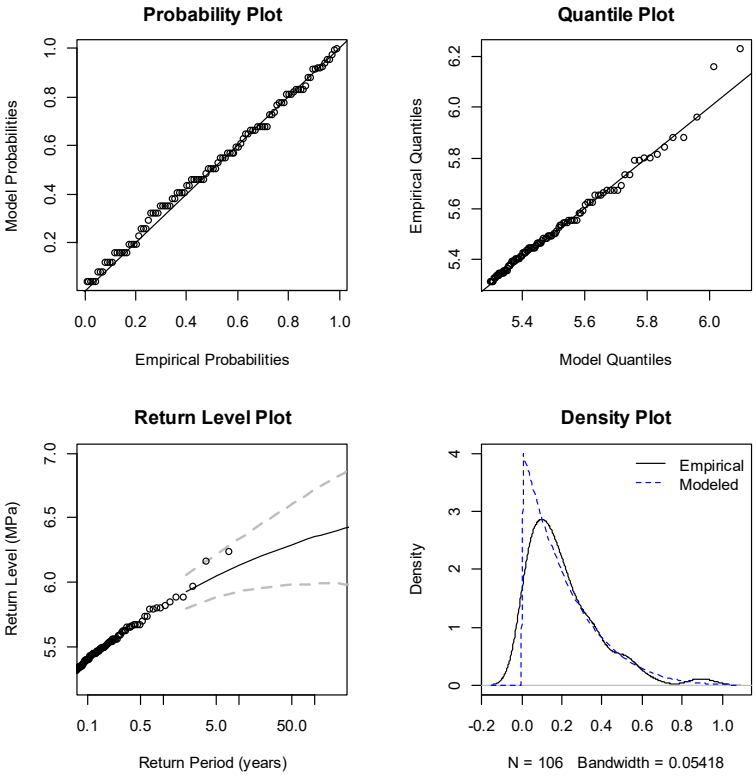

(a) Highway-induced case

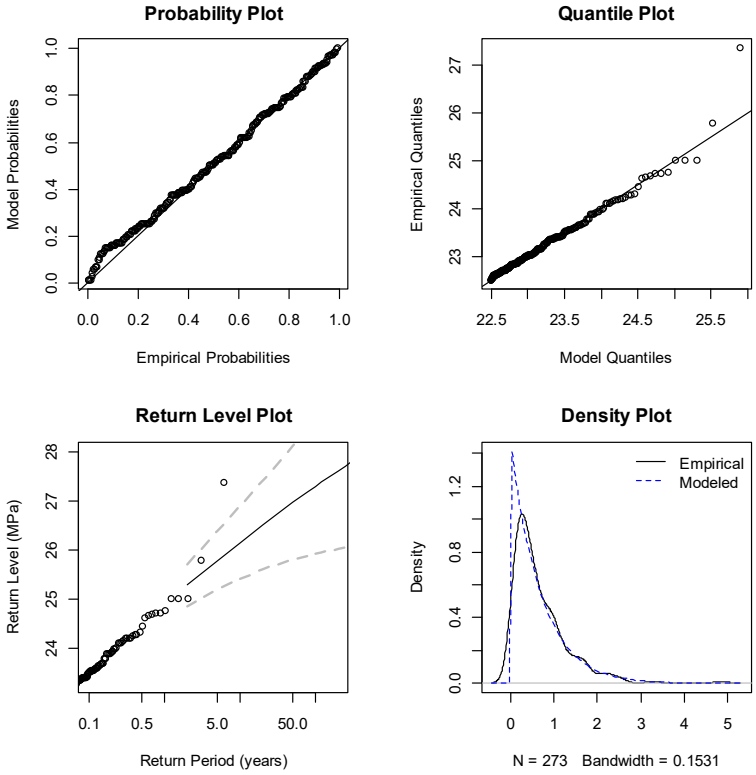

(b) Railway-induced case

Figure 4.11 Diagnostic plots for GP fit to traffic-induced extreme stresses

4.5.3 Comparisons and Discussions

4.5.3.1 Comparison of extremes extrapolated by BM and POT approaches

Recognizing that when there is no reliable prior information, the parameters of the fitted EVDs and the return levels are not so sensitive to the estimation methods, as shown in Tables 4.1 and 4.2, the MLE-based point estimators and the PLE-based CIs will be used in the subsequent study of this thesis. A summary of the BM-obtained highway- and railway-induced extreme stresses with a return period of five and 120 years respectively, which are point estimates obtained by the MLE, is given in Table 4.3. It is observed that the extreme stresses extrapolated by the two methods are very close to each other, though the POT method uses more data. This can also be found in the return plots shown in Figure 4.12. It implies that the extrapolated extreme values are robust to the extrapolation techniques. This conclusion coincides with that drawn by O'Brien *et al*. (2015) who concluded that the accuracy of the extrapolated characteristic value is more dependent on data quality and less on extrapolation technique adopted.

Table 4.3 Point estimates of extremes with five- and 120-year return periods estimated by BM and POT approaches

Return period (years)	Stress type	Estimate (MPa)		Difference (%)
		BM	POT	
5	Highway-induced	6.07	6.05	0.33
	Railway-induced	25.70	25.65	0.19
120	Highway-induced	6.43	6.36	1.09
	Railway-induced	27.21	26.97	0.88

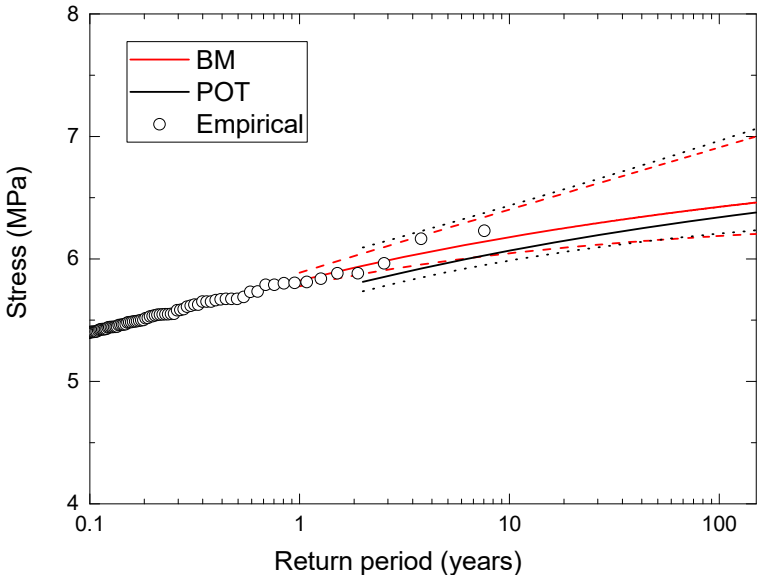

(a) Highway-induced case

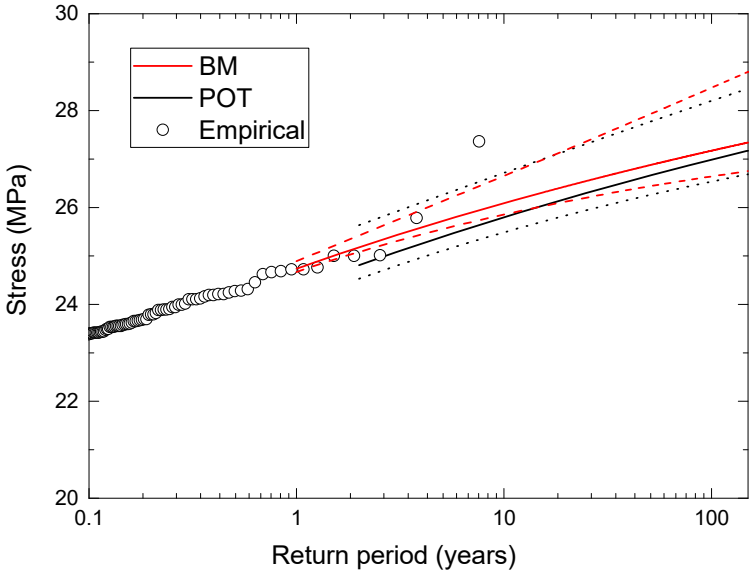

(b) Railway-induced case

Figure 4.12 Return level plots for extreme values of traffic-induced stresses estimated by BM and POT approaches and measured strain data (red dash and black dot lines are PLE-based 95% CIs of BM- and POT-obtained return levels respectively)

4.5.3.2 Comparison of extrapolated extremes with design values

The design live loads of the TMB are determined by the United Kingdom Department of Transport Standard BD 37/88 with amendments to suit the traffic conditions predicted for the TMB. The highway load adopted is HA and 45 units of HB loading

applied to the roadway deck in the severest configuration. The design railway load for the TMB is an 8-car train with a gross weight of 544 tonnes. These two kinds of design live loads are applied respectively to a 3D FEM of the TMB to obtain the stress responses.

The influence line of stress at the deck location with the strain gauge SSTLS09 is shown in Figure 4.13. The positive value means tensile strain. It is obtained by a vehicle with a gross weight of 1 tonne running on the upper deck in the lane closest to SSTLS09. The influence lines owing to a vehicle passing over other lanes and the railway tracks can be obtained in a similar way. It can be observed from Figure 4.13 that the length of distributed load to generate large load effect (stress) in the concerned point is approximately 250 m (100 m on the left and 150 m on the right). The portion of influence line spanning this length is sharp, so the most adverse condition is when heavy vehicles are positioned at the desired region.

When the design highway loads are then applied to the six lanes on the upper deck only in the adverse area, the calculated design stress is 76.77 MPa. However, in daily operation, the vehicles are mostly distributed along the whole length of the bridge, rather than just along the adverse region. When the design highway loading is applied to the whole length of the bridge, the calculated stress at the same deck location is only 2.79 MPa. The reason for such a small value is that the stress generated by the uniform distribution load (UDL) of HA loading along the adverse length has been nearly offset by that generated by UDL along the favorable length. The stress is mainly caused by

the HB loading or the knife edge load (KEL) multiplied by proper HA lane factors as suggested in the design code. This implies that when assessing in-service condition of the bridge, it may not be appropriate to use the 45 units of HB loading or the KEL of 120 kN as adopted in the design. The HB loading or the KEL is preferably determined according to the loads and distributions of site-specific heavy trucks. A live load model for in-service condition assessment of the TMB will be developed in the next chapter.

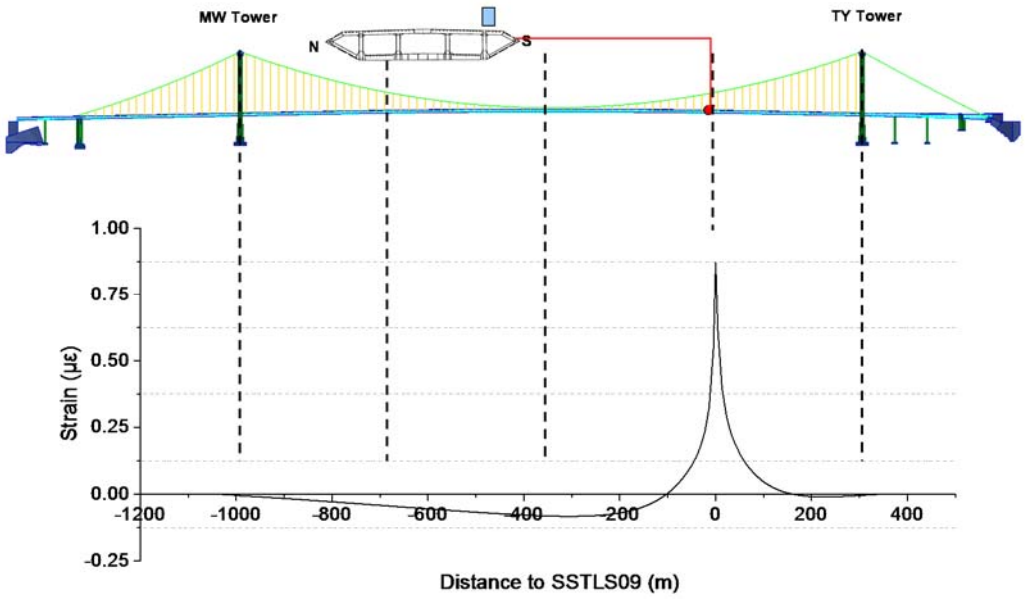

Figure 4.13 Influence line of stress at deck location with strain gauge SSTLS09

In the FEM, loads simulating two 8-car trains are applied on the rail tracks side by side. The axle distances and axle loads of the trains comply with the specifications of BD 37/88. The computed stress in the deck location with SSTLS09 is 38.98 MPa. As such, the extrapolated railway-induced extreme stress with a return period of 120 years is about 70% of the design value.

4.5.3.3 Discussions

As stated in section 4.2.1, the GEV and GP distributions resulting from the same dataset are intimately related and share the same shape parameter ξ. That is to say, the estimated parameter ξ in the GEV and GP models should be the same theoretically. Probably because of the richness and good quality of the monitoring data, the estimated values of ξ for the GEV and GP distributions of the extreme stresses in this study are exactly the same. The shape parameter in the two extreme value models for the highway-induced stresses is -0.15, and it is identically -0.09 in the two models for the railway-induced stresses.

For the railway-induced stresses, an "extreme of extremes" is observed (Figure 4.5 (b)). After checking the strain data measured at the rail waybeams, it is found that this extreme was caused by two relatively heavy trains concurrently running near the measured deck section. Being a true extreme data point, it was not excluded from the extreme stress dataset.

Based on the monitoring data, the extrapolated highway- and railway-induced extreme stresses with a return period of 120 years are not significantly larger than the maximum data values collected in the measurement periods (nine years). The maximum highway- and railway-induced stresses measured are 6.23 and 27.36 MPa respectively, while the extrapolated extremes for these two types of stresses obtained by the BM approach are 6.43 MPa with a 95% CI of (6.20, 7.07) and 27.21 MPa with a 95% CI of (26.44, 29.22). Because the EVDs and the corresponding return levels of the stress

were obtained based on monitoring data of only nine years, these extrapolated characteristic values can be updated if more data showing increase of traffic load effects are collected in the future, or there is reliable expert information to prove that the stresses will increase significantly in the future.

The data used in this study were collected during the first 15 years of the bridge life, during which the bridge works under the elastic state and there is nearly no deterioration. Therefore, the data in a certain block size (one day or one month in this study) used are considered to be independent with each other in the time domain. The structural degradation is an external interference which will make the extreme values time-dependent. This effect can be considered into the extreme value study, but because this study is based on the limited data available, EVDs and extreme value extrapolations taking this effect into account are out of the scope of this chapter.

Two or more strain gauges have been installed on each of the instrumented truss members of the TMB; thus the inner forces experienced in each truss member and experienced by the whole cross-section of the deck can be further evaluated from the measured strain data. The EVDs of them are valuable information for structural reliability analysis, which will be carried out in Chapter 6.

4.6 Summary

To provide critical stress levels for the development of site-specific live load models, which will be conducted in the next chapter, this chapter studied the EVDs and characteristic values of the TLEs on bridges based on long-term strain data using the EVT. Strain data was selected for the study because it provides most direct link to the load effect. Nine-year strain data collected from the TMB were used to study the extreme TLEs.

The two most popular approaches, the BM and POT approaches, were explored. The parameters for the EVDs (GEV for the BM approach and GP for the POT approach) of the stresses and the return levels were estimated by the likelihood-based methods, including the MLE and PLE, and the BE method. Because no reliable expert knowledge can be used as prior information, the results of the BE inference was largely dominated by the data. The results obtained by the three estimation methods were compared, and it was found that the point estimation result is almost regardless of the estimation method used. The PLE method outperforms the normal approximation, which was adopted in the MLE method, when it is used to estimate the CIs of parameters or return levels, especially the shape parameter and return levels with longer return period.

The characteristic values of the stresses, which mean the extreme stresses with a return period of five and 120 years respectively, were extrapolated. The extrapolation results obtained by the BM and POT approaches respectively are found to be close to each other. It implies that the extreme values are robust to the extrapolation techniques. Extreme stresses corresponding to a five- or 120 year return period can be used for the development of a live load model for bridge condition assessment under the SLS and ULS, respectively.

CHAPTER 5

DEVELOPMENT OF SITE-SPECIFIC LIVE LOAD MODELS FOR BRIDGE CONDITION ASSESSMENT

5.1 Introduction

To evaluate existing bridges, live load of traffic is one of the most variable parameters, because traffic varies with time and is different from site to site. Various live load models have been provided in bridge codes worldwide, such as the ASCE Recommended Design Loads for Bridges (Buckland 1981), Eurocode 1 (CEN 2002), Canadian Highway Bridge Design Code (CSA 2006), British Standard 5400 (BSI 2006), and AASHTO LRFD Bridge Design Specifications (AASHTO 2015). The generic live load models in the codes are inherently conservative. The reason is that by their very nature, they have to be applicable to a large range of bridge types and spans under the most aggressive traffic. Thus, it is probable that the design live load models are not valid to the bridge condition assessment. Inaccurate bridge evaluation results will bring about economic losses and even casualties. Results too conservative may lead to unnecessary bridge closure and maintenance works. Even worse, an underestimation could make sudden damage of a bridge without any warning.

Therefore, a site-specific live load model is essential for accurate condition assessment, as well as cost-effective and safety-ensured bridge maintenance.

The live load models in most of the bridge design codes were developed for short and median span bridges. There are live load models for long span bridges in some codes (Buckland 1981; BDT 1989). However, these models are mainly extrapolated from those of the shorter-span bridges, other than based on measured data in-situ. Though several large-scale bridges with span of more than 1000 m have been built worldwide, up to now the knowledge of design traffic loading for long-span bridges is still limited (Enright *et al*. 2013). The most widely known research of live loading on long-span bridges may be that conducted by Buckland and his co-workers (Buckland *et al*. 1978, 1980; Buckland 1991). A recent research on the design live load model for long-span bridges is the one conducted by Lutomirska (2009). This research concludes that the AASHTO live load model: HL-93 load, is valid for spans up to 1500 m.

The highway loads are usually modelled by a combination of a uniform distribution load (UDL) and concentrated loads in the bridge design codes (Buckland 1981; OHBDC 1991; CEN 2002; BSI 2006; CSA 2006; AASHTO 2015). The UDL represents the normal traffic flow, and the concentrated loads represent overloaded freights. The factors considered in developing the live load models for short-span and long-span bridges respectively are different in some ways. Firstly, the detail characteristics of individual vehicles, such as axle loads and axle configuration, are important parameters for short and median span bridges. On contrary, these parameters

are usually not of great concern for the long, especially super long bridges. Those deserving attentions for long-span bridges include the number of vehicles, the proportion of heavy trucks, and distribution of vehicles on the bridge in both transverse and longitudinal directions. Besides, the UDL usually decreases while concentrated load increases as loaded length increases (Buckland *et al*. 1978, 1980; Lutomirska 2009). Moreover, dynamic impact of vehicles due to factors such as roughness of the roadway, dynamic characteristics of the bridge and vehicles, vehicle number and speed, can be ignored for long-span bridges (Buckland 1981, 1991; BDT 1989; Lutomirska 2009).

SHM data provide important information to develop live load models for bridge evaluation. For example, the WIM stations provide data such as the gross weight and axle distributions of the vehicles, and proportion of different vehicles on each lane. The CCTV shows the view of traffic situations on the deck, from which the distance between vehicles can be roughly judged. Data measured from strain gauges installed beneath the rail waybeams can be used to derive the information of railway traffic, including speed, number of bogies, bogie weight, and bogie spacing of the trains. Once an SHM-based live load model is established, it is possible not only to update an existing model, but also to track changes as the structure ages (Messervey 2008; Frangopol 2011). The advances in the extrapolation of variables to long return periods engender confidence in lifetime estimation of live load models.

The rich data obtained by the WASHMS of the TMB provides a valuable opportunity to study the site-specific traffic load models. For more accurate condition assessment of the TMB, live load models are developed in this chapter by taking advantage of the long-term SHM data. To evaluate the bridge performance in SLS and ULS, the live load model is developed respectively. The developed railway and highway load models consider extreme traffic situations. However, the worst conditions of these two types of traffic rarely occur concurrently. Thus, the combination of these two types of loads is also studied. To validate the developed highway load models, they are compared with the ASCE load model (Buckland 1981), BD 37/88 load model (BDT 1989), and AASHTO HL-93 load model (AASHTO 2015) which is suggested to be used in the design of long-span bridges recently (Lutomirska 2009). The railway load model is compared with the model specified in BD 37/88, based on which the TMB was designed. The uncertain factors in developing the highway load model are much more than those in developing the railway model. Thus, the developed highway load model should be compared with its counterparts to get a more reliable conclusion. What are compared include the load magnitudes and load effects.

The remainder of this chapter is organized as follows. Section 5.2 introduces the regulations of the railway and highway traffic on the TMB. Section 5.3 gives a briefing of traffic-load monitoring for the TMB. The statistical characteristics of long-term traffic data, such as the daily average of total number and proportion of different vehicles passing the bridge and each lane, and the daily average of total number and

composition of train classes, are described in section 5.4. Section 5.5 develops the load models for both railway and highway traffic based on the long-term WIM data, CCTV recordings of the traffic on the bridge, and extreme value of stresses extrapolated in Chapter 4. The combination of these two load types is also studied. The developed live load models are validated in section 5.6. Finally, section 5.7 summarizes the study carried out in this chapter.

5.2 Regulations of Traffic on TMB

5.2.1 Highway Traffic

The three lanes for each traffic direction on the upper level are divided into slow, middle and fast lane (Figure 4.1 (c)). Vehicles with different speeds usually running on their corresponding lane, so the heavy goods vehicles usually run on the slow lane. The TMB serves a port and airport complex; thus, the traffic on it is busy, and sometimes it carries a particularly large amount of heavy lorries. In normal days, the highway traffic is on the upper deck; while when there is a strong typhoon, the traffic on the upper deck will be closed and the two carriage ways on the lower deck will be used for emergency. The vehicles running across the bridge are classified into eight categories (Table 5.1) according to their main features, including the number of axles, magnetic vehicle length, axle distance, and also gross vehicle weight (GVW) (HKTD

1997). The highway traffic on the TMB, for example, the maximum GVW and axle load of the vehicles, is governed by the HKRTR (HKTD 2012).

Table 5.1 Eight-class vehicle classification system (HKTD 1997)

Class	Vehicle category	Number of axles	Magnetic vehicle length	Axle distance (1 to 2)	GVW (tonnes)
1	Motor cycles	2	< 2 plus magnetic contour analysis		< 0.6
2	Cars, vans or taxis	2, 3, 4	< 6.3 m		< 3
3	Public service vehicles		Magnetic contour analysis	< 5.5m	< 4
4	Light goods vehicles	2, 3, 4	≥ 6.3m, < 10m	< 3.5m	< 5.5
5	Medium goods vehicles	2, 3, 4 ,5, 6, 7, 8	-	≥ 3.5m, <7.8m	< 24
6	Rigid heavy goods vehicles	2, 3, 4, 5, 6, 7, 8	-	≥ 3.5m, <7.8m	< 38
7	Articulated heavy goods vehicles	2, 3, 4, 5, 6, 7, 8	-	≥ 3.5m, <7.8m	< 44
8	Buses and coaches	2, 3, 4	Magnetic contour analysis	≥ 7.8m	< 24

5.2.2 Railway Traffic

The passenger railway began to operate in June 1998. As mentioned in section 4.4 of Chapter 4, before 2003 most trains passing through the TMB have seven cars. However, with the increasing demand of passenger flow, most trains have become the

eight-car train since the end of 2005. The years between 2003 and 2005 are a transition period with seven-car and eight-car train running concurrently. After 2005, most trains running on the TMB are eight-car train. The design railway load model for the TMB is the eight-car train. The railway traffic is managed by the MTR Corporation Limited, Hong Kong. The distribution of maximum bogie loads for an eight-car MTRC train is shown in Figure 5.1. The maximum GTW allowed is 498 tonnes.

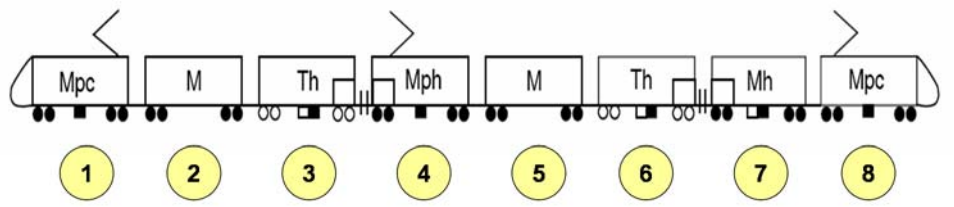

Distribution of Maximum Axle-Load, Bogie-Load and Car-Load in the 8-Car MTRC Train

Car No.	1	2	3	4	5	6	7	8
Car Type	Mpc	M	Th	Mph	M	Thu	Mh	Mpc
Axle-Load (Crush) in kg	A1 = 17169 A2 = 17140 A3 = 16107 A4 = 16107	A1 = 15221 A2 = 15221 A3 = 15219 A4 = 15219	A1 = 14259 A2 = 14259 A3 = 14448 A4 = 14448	A1 = 16027 A2 = 16207 A3 = 16026 A4 = 16026	A1 = 15221 A2 = 15221 A3 = 15219 A4 = 15219	A1 = 14259 A2 = 14259 A3 = 14448 A4 = 14448	A1 = 15923 A2 = 15923 A3 = 16223 A4 = 16223	A1 = 17169 A2 = 17140 A3 = 16107 A4 = 16107
Bogie-Load (Crush) in kg	B1 = A1 + A2 = 34309 B2 = A3 + A4 = 32214	B1 = A1 + A2 = 30442 B2 = A3 + A4 = 30438	B1 = A1 + A2 = 28518 B2 = A3 + A4 = 28896	B1 = A1 + A2 = 32414 B2 = A3 + A4 = 32052	B1 = A1 + A2 = 30442 B2 = A3 + A4 = 30438	B1 = A1 + A2 = 28518 B2 = A3 + A4 = 28896	B1 = A1 + A2 = 31851 B2 = A3 + A4 = 32446	B1 = A1 + A2 = 34309 B2 = A3 + A4 = 32214
Car-Load (Crush) in kg	Car = B1 +B2 = 66523	Car = B1 + B2 = 60880	Car = B1 + B2 = 57414	Car = B1 + B2 = 64466	Car = B1 + B2 = 60880	Car = B1 + B2 = 57414	Car = B1 + B2 = 64297	Car = B1 + B2 = 66523

Figure 5.1 Distribution of bogie loads in 8-car MTRC train (Wong 2007)

5.3 Monitoring of Traffic Loads

The highway loads are monitored by WIM stations, installed about 2 km away from one anchorage of the TMB. As shown in Figure 5.2, each WIM station is composed of two bending path pads and two magnetic loop detectors (Xu and Xia 2011). The two bending path pads are used to measure the weight of vehicles. The two magnetic

loop detectors measure the axle length, axle numbers, and vehicle speed. The WIM stations have measured the highway traffic on the bridge since August 1998.

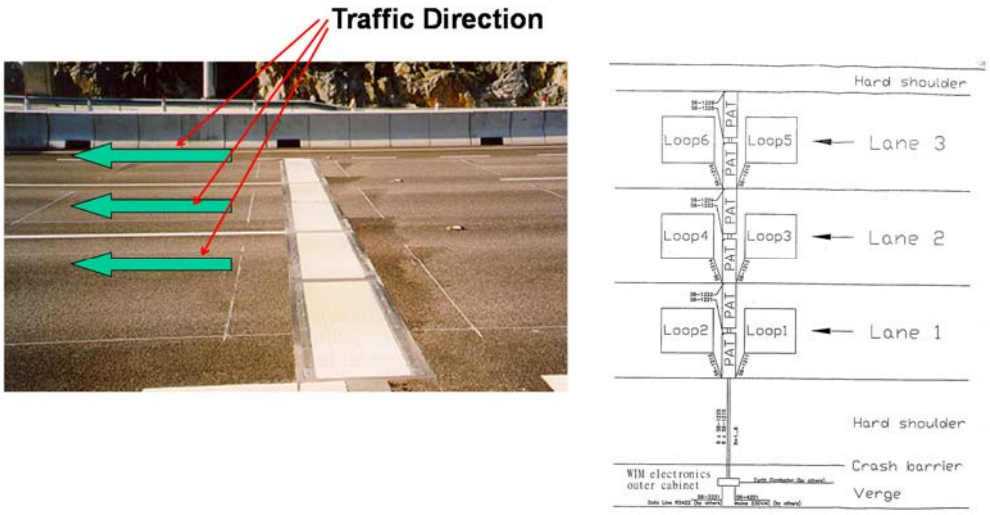

Figure 5.2 WIM station

The rail way beam on the TMB is composed of two inverted T-beams welded to a top flange plate (Ni *et al*. 2011). At the section of the instrumented railway beam, 50 mm from the midway between the cross frames, the dynamic strain gauges are arranged to measure the railway traffic. The layout of these strain gauges is shown in Figure 5.3. The strain data have been converted into information of railway traffic, including the speed, class, number of bogies, bogie-weight, and bogie spacing of the trains.

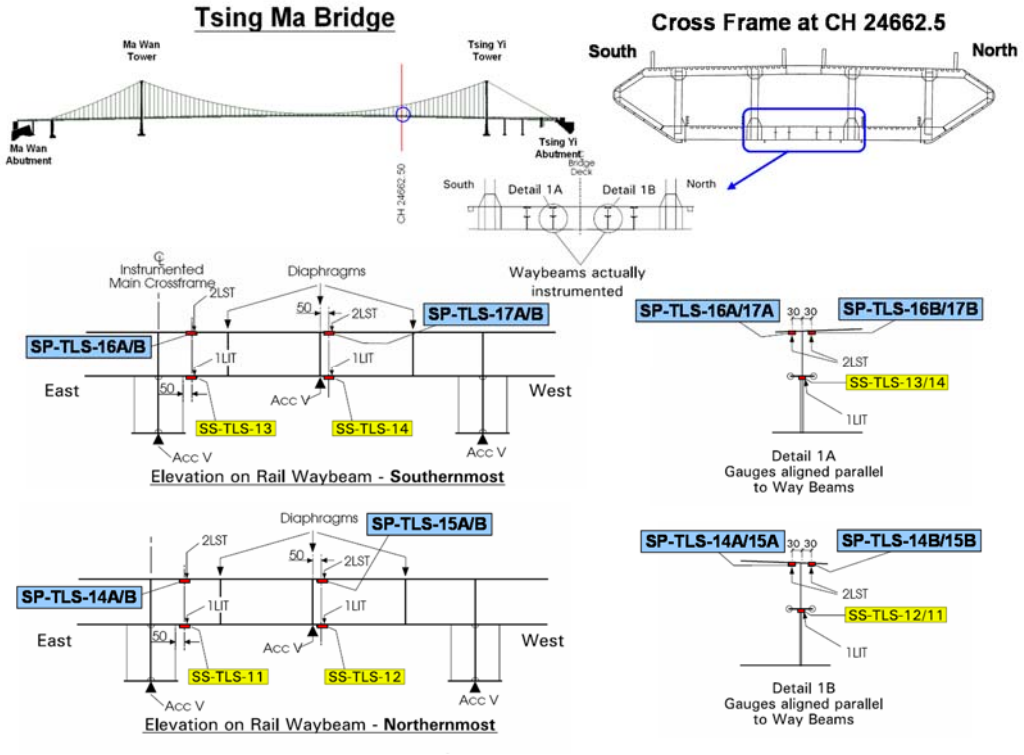

Figure 5.3 instrumented railway beam

5.4 Statistics of Long-Term Traffic Data

5.4.1 Highway Traffic

The WIM database contains information about date and time, lane, speed, vehicle category, number of axles, spacing between axles, and axle weight. To study the highway loads, the vehicles on the TMB are usually simplified into four classes based on the GVW (Xu and Xia 2011). These four classes include: vehicles with GVW less than 3.00 tonnes, 3.00-5.49 tonnes, 5.50-23.99 tonnes, and equaling to or more than 24.00 tonnes. They are denoted by Cars, LGV (light goods vehicle), MGV (median

goods vehicle) and HGV (heavy goods vehicle), respectively. The proportions of these four types of vehicles in the traffic flow are shown in Figure 5.4. Overall, most of the vehicles passing the TMB are Cars and LGV, which takes up more than 70% of the total vehicle count.

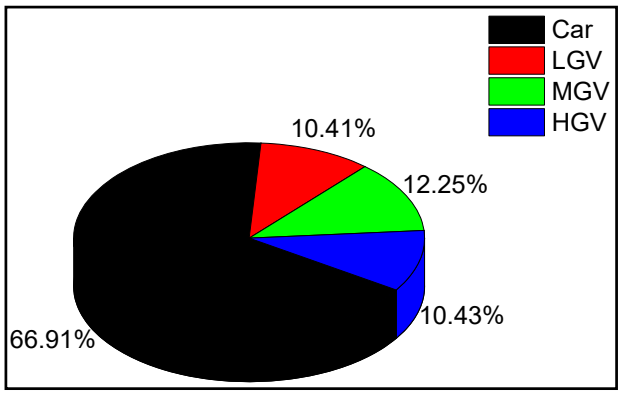

Figure 5.4 Proportion of different vehicles

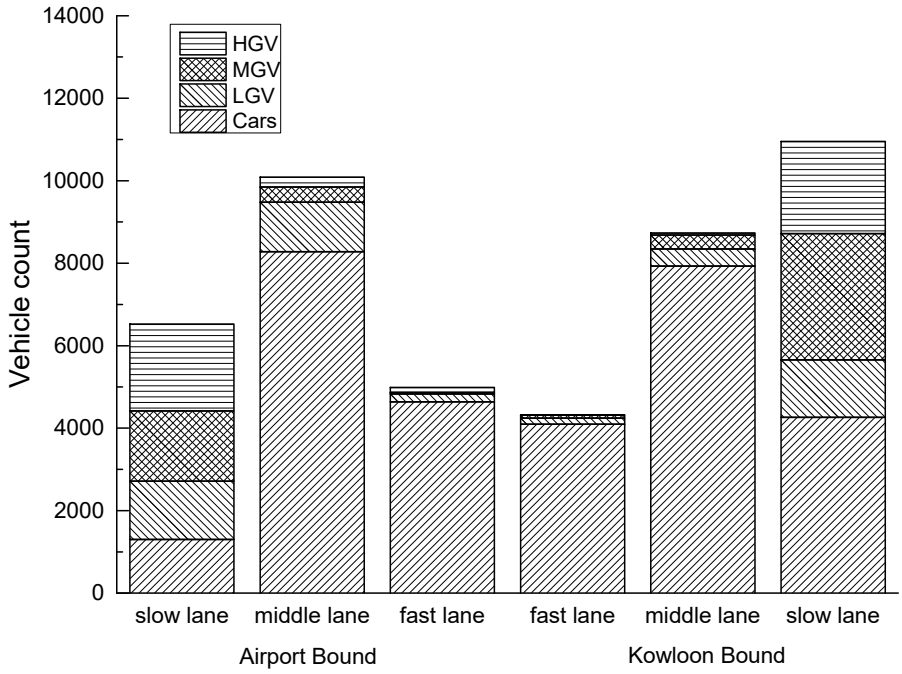

Figure 5.5 Average daily vehicle counts with composition of vehicle classes for each lane

The average daily vehicle count as well as the composition of different vehicle classes for the six lanes of the upper deck is shown in Figure 5.5. It can be observed that most of the heavy vehicles run on the slow lanes, while most cars and light goods vehicles run on the fast and middle lanes. On the slow lane, the percentage of MGV and HGV is about 60%; on the middle lane, it is around 5%; and on the fast lane, it is only about 2%.

5.4.2 Railway Traffic

The average daily train count with composition of four classes of trains (trains with less than seven cars, seven cars, eight cars and more than eight cars, respectively) during the years from 2003 to 2012 is shown in Figure 5.6. The transition of the train from seven-car class to eight-car class can be observed easily from this figure. The count of trains passing the bridge seems to have no significant increase during the studied years. However, as expected, the GTW increased after the transition. The recorded maximum GTW in 2003 is 374.2 tonnes, while that measured in 2007 is 420.2 tonnes. And the recorded mean GTWs during these two years are 330.1 tonnes and 347.4 tonnes, respectively. This increase has been reflected in the structural responses such as stress, which is shown in Figure 4.4.

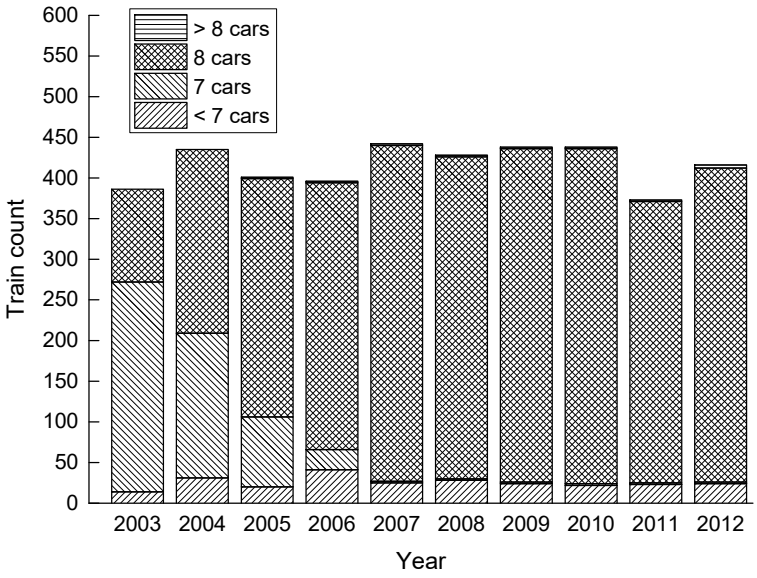

Figure 5.6 Average daily train count with composition of train classes (2003-2012)

5.5 Live Load Models

5.5.1 Highway Load Model

The TMB was designed based on the British code, BD 37/88 (BDT 1989), with amendments to suit the traffic conditions predicted for the bridge. In the BD 37/88 live load model, the highway traffic load is modelled as a UDL representing the normal traffic flow, and a single concentrated force called KEL, which simulates an extremely heavy vehicle. The live load model for the condition assessment of the TMB is also modelled as a combination of UDL and KEL.

5.5.1.1 UDL

To calculate the UDL for bridge condition assessment, the vehicles are presumed to be distributed on each lane and along the whole length of the bridge one after another by a certain spacing. The inter-vehicle gap is an important parameter. However, this information is not included in the WIM data. The inter-vehicle gap is usually represented by the headway or clearance. The headway means the distance between the back axle of the leading vehicle to the front axle of the following vehicle (Nowak and Hong 1991); and the clearance refers to the distance between the back bumper of the leading vehicle and the front bumper of the following vehicle (Caprani 2012). Nowak and Hong (1991) used headways of 4.57 m and 9.14 m, respectively. Vrouwenvelder and Waarts (1993) adopted headways of 5.5 m for simply distributed lanes, and 4-10 m for full congested lanes. In the background studies to Eurocode, a headway of 5 m was used (Bruls *et al.* 1996; Flint and Jacob 1996). Bailey (1996) used beta distributions to model the distance between vehicles for different speeds. Normally distributed clearances were generated using traffic microsimulation by Caprani (2012) to replicate different traffic compositions and flow rates. As for long-span bridges, a simple gap model would be attractive, because it is computationally efficient and could be used by practitioners (Caprani 2012). For example, Lutomirska (2009) adopted a clearance of 4.57 m.

Clearance is used as the measure of inter-vehicle spacing in this study. Considering the traffic jam scenario, the clearances in the design model are generally in the range

of 1.8-6.4 m (Lutomirska 2009). The live load model developed in this study is mainly for bridge condition assessment, thus, the inter-vehicle spacing may be not as dense as that adopted in the design model. However, although no serious traffic jam has happened up to now, the highway traffic on the TMB is relatively dense sometimes, as shown in Figure 5.7. Therefore, a clearance of 10.0 m (approximately equaling to length of an HGV) and 5.0 m (approximately equaling to length of a Car) is adopted for the SLS and ULS evaluation models, respectively.

(a) Record on June 29, 2007 (b) Record on May 2, 2008

Figure 5.7 CCTV record of highway traffic on TMB

The information of vehicles for developing the UDL model is listed in Table 5.2. In this table, the maximum length means the maximum vehicle length limited by the HKRTR (HKTD 2012); and the axle length means the distance between the front and rear axles of the vehicles. The total length of the vehicles is determined by adding the front and back overhangs to the axle distances measured by the WIM stations, as well as referring to the legal vehicle lengths. The total length for front and back overhangs of a car is about 2 m, and that for a 5-axle truck is about 3 m (Lutomirska 2009). For the SLS evaluation, the proportion of different vehicles on each lane is determined based on the WIM data. On the other hand, all the vehicles on the slow lanes are

assumed to be MGV and HGV (each taking up 50% percentage) for the ULS evaluation. Therefore, for the SLS evaluation, the UDL of the slow, middle and fast lane is 9.04 kN/m, 2.53 kN/m and 1.91 kN/m, respectively; and the UDL of these three lanes is 16.48 kN/m, 3.28 kN/m and 2.54 kN/m respectively for the ULS evaluation. These values are considered as the mean values of the UDL, which is presumed to be normally distributed variables with a coefficient of variance (CoV, defined as the standard deviation divided by the mean) of 0.10.

Table 5.2 Vehicle information for UDL model

	GVW (tonnes)	Maximum length (m)	Axle distance (m)	Vehicle length (m)	Percentage on each lane (%)		
					slow	middle	fast
Car	1.83	6.3	2.82	5.0	20	85	95
LGV	4.01	10.0	3.56	6.5	25	10	5
MGV	11.43	11.0	5.87	9.0	25	3	0
HGV	28.78	13.0	6.62	10.0	30	2	0

5.5.1.2 KEL

The KEL is inversely calculated by a full 3D FEM of the bridge, targeting a stress level obtained in Chapter 4, which was extrapolated based on long-term strain data. A full 3D FEM of the TMB, as shown in Figure 5.8, is built in ABAQUS to complement the WASHMS in bridge condition assessment. To obtain precise analytical results and be more easily correlated with the measured results, all structural components are modelled delicately. The connections and boundary conditions are modelled properly. For example, to model the stiffening deck system, full truss girder modeling approach is used instead of the modeling approach of single spinal beam. In the FEM, four types of elements were used: the 12-degree-of-freedom (DOF) bar element, the 14-DOF beam element, the 20-DOF plate-bending element, and 12-DOF rigid bar element. The

cables, suspenders, towers, piers and horizontal cross-bracings in the bridge-deck are modelled by bar elements; the longitudinal truss members, cross-frame members and rail waybeams are modelled by the beam elements; the upper and lower orthotropic deck trough structures are modelled by the plate bending elements; the bearings between bridge-deck and towers/piers and the connection between the center-lines of orthogonal deck and longitudinal truss members are modelled by the rigid bar elements. About half-million elements are used in the FEM.

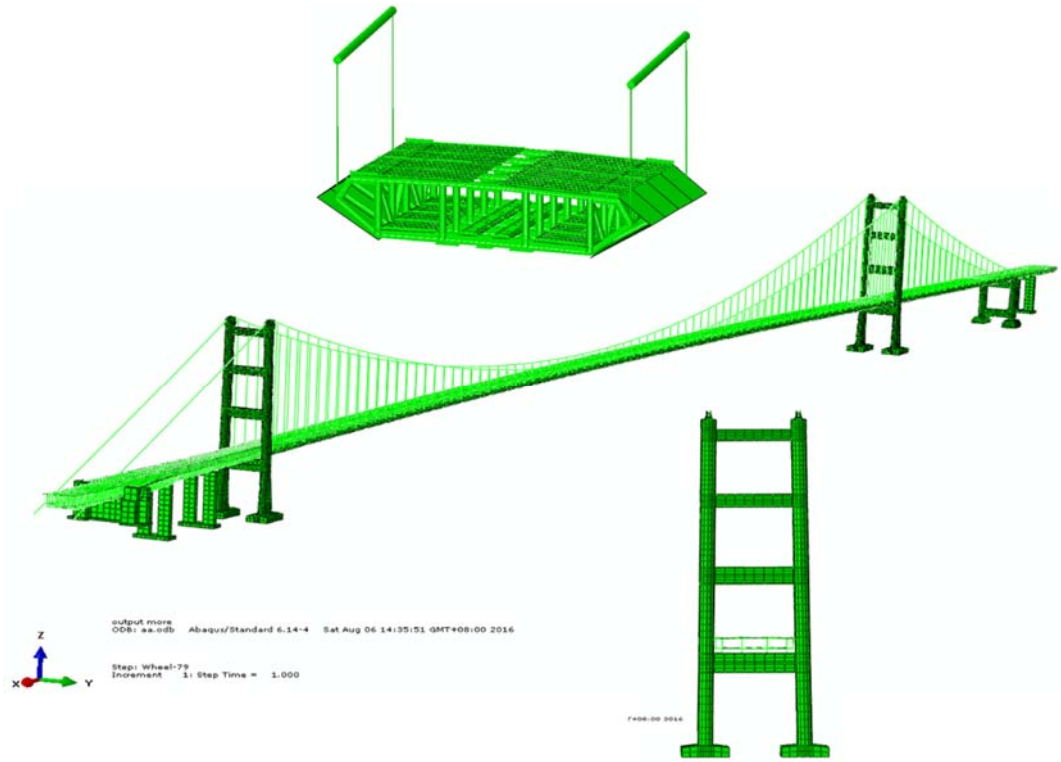

Figure 5.8 Full 3D FEM of TMB

This FEM was verified by comparing modal frequencies predicted by it and those identified using acceleration data, as shown in Table 5.3. It can be found that the

difference is relatively low, and the maximum difference is only 7.67%. The examples of mode shapes identified by the FEM are shown in Figure 5.9.

Table 5.3 Comparison of mode frequencies

Mode Order	FEM	Measured	E (%)	Mode No.*
LF-D-1	0.0716	0.0688	-4.07	1
VF-D-1	0.1173	0.1125	-4.27	2
VF-D-2	0.1438	0.1375	-4.58	3
LF-D-2	0.1678	0.1578	-6.34	4
LF-D-3	0.1919	0.1955	1.84	5
L-C-4	0.2019	0.1977	-2.12	6
L-C-6	0.2163	0.2091	-3.44	7
L-C-7	0.2252	0.2227	-1.12	8
LF-D-4	0.2329	0.2406	3.20	9
T-D-1	0.2424	0.2438	0.57	10
VF-D-4	0.2477	0.2375	-4.29	11
T-D-2	0.2569	0.2656	3.28	12
VF-D-5	0.2932	0.2800	-4.71	13
LF-D-6	0.2947	0.2875	-2.50	14
L-C-14	0.3218	0.3273	1.68	15
V-C-6	0.3329	0.3281	-1.46	16
VF-D-6	0.3380	0.3281	-3.02	17
L-C-15	0.3563	0.3636	2.01	18
LF-D-8	0.3742	0.3906	4.20	19
L-C-20	0.3774	0.3750	-0.64	20
V-C-10	0.3819	0.3841	0.57	21
T-D-3	0.3862	0.3819	-1.13	23
VF-D-7	0.42682	0.4175	-2.23	27
LongF-T-1	0.4366	0.4055	-7.67	28
L-C-22	0.4748	0.4759	0.23	30

Notes:
1. FEM = Analyzed Frequency from FEM
2. Measured = Measured Frequency from WASHMS
3. LF-D-* Lateral flexural deck modes
4. VF-D-* Vertical flexural deck modes
5. L-C-* Lateral cable modes
6. T-D-* Torsional deck modes
7. V-C-* Vertical cable modes
8. LongF-T-* Longitudinal flexural tower modes
9. E = (FEM- Measured)/Fx 100%
10. Mode No.* = ABAQUS's mode number

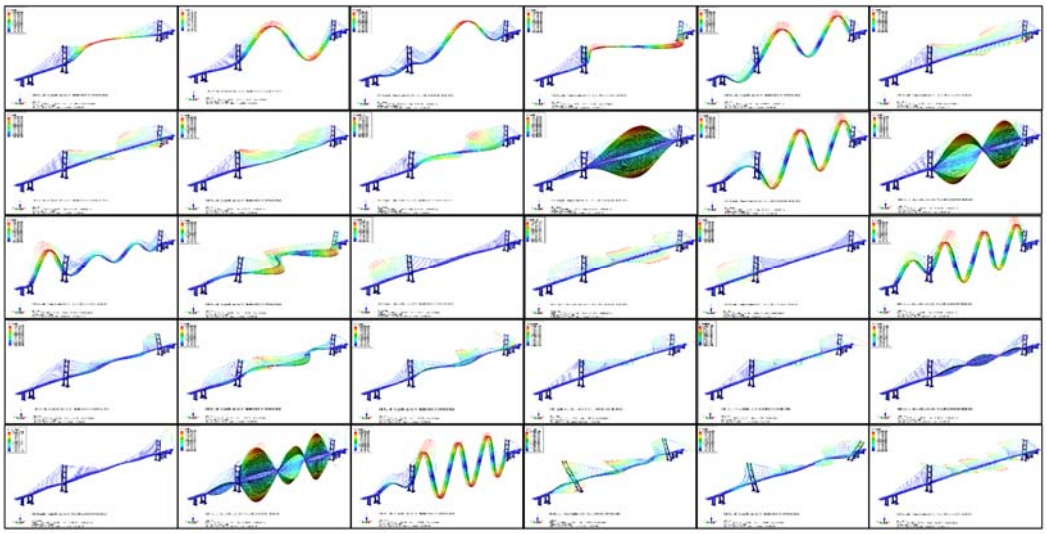

Figure 5.9 Examples of mode shapes identified by FEM

To realize this, the UDL and KEL loads were imposed simultaneously on the six lanes, as shown in Figure 5.10. The KEL corresponding to the stress with a return period of five years will be used for the SLS evaluation, while that corresponding to the stress with a 120-year return period will be used for the ULS evaluation. The extreme stress extrapolated by the BM approach is used. According to the results obtained in Chapter 4, these two stress levels are 6.07 MPa with a 95% CI of (5.95, 6.31), and 6.43 MPa with a 95% CI of (6.20, 7.07), respectively. Therefore, the KEL for the SLS evaluation is 253 kN with a 95% confidence interval of (248, 263), and that for the ULS evaluation is 342 kN with a 95% CI of (330, 376). The probabilistic distribution of the KEL is the GEV.

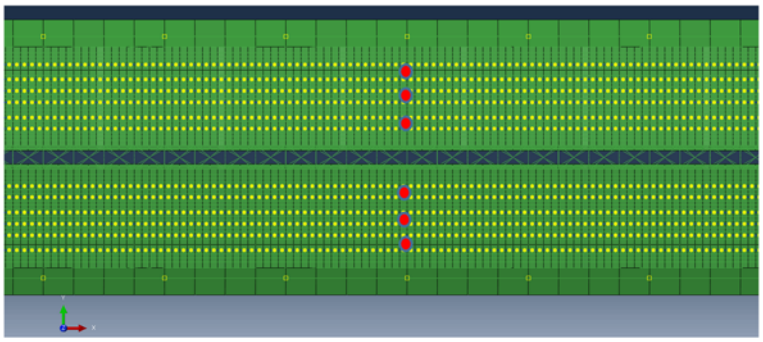

(a) Plan view

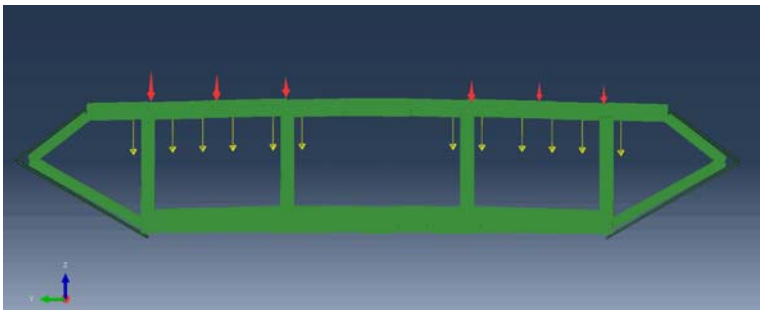

(b) Side view

Figure 5.10 Imposition of UDL and KEL on lanes

5.5.1.3 Multilane factor

It is unusual that all the lanes are loaded with heavy vehicles. Hence, in the bridge design or condition assessment, the highway loadings are usually applied to the lanes after being multiplied by appropriate multilane reduction factors. The multilane factors could be very site specific. These factors for the TMB are calculated based on the data-driven UDL, i.e. they are 1.0, 0.3, and 0.2 for the slow, middle, and fast lane, respectively.

5.5.1.4 Dynamic impact

When vehicles cross a bridge, the interaction of the dynamic characteristics of the bridge, the characteristics of vehicles such as the GVW and speed, and the roughness of the road surface, may induce the dynamic response of a bridge. To take this into

account, a dynamic amplification is usually added as a percentage to static effects. This is applicable for the short and median span bridges. However, for a long span bridge, the dynamic amplification is small and can be neglected in the structural analysis. Therefore, the dynamic factor is not considered in the live load model developed in this study. Actually, because the KEL was calculated inversely based on the measured stress, the dynamic amplification had been taken into account if there is any. The highway load model developed for the condition assessment of the TMB in this study is listed in Table 5.4.

Table 5.4 Highway load model for evaluation of TMB

Bound	Lane	UDL (kN/m)		KEL (kN)	
		SLS	ULS	SLS	ULS
Airport Bound	Slow	N (9.04, 0.90)	N (16.48, 1.65)	GEV (220, 10.66, -0.15)	GEV (282, 13.62, -0.15)
	Middle	N (2.53, 0.25)	N (3.28, 0.33)	GEV (66, 3.20, -0.15)	GEV (85, 4.09, -0.15)
	Fast	N (1.91, 0.19)	N (2.54, 0.25)	GEV (44, 2.13, -0.15)	GEV (56, 2.72, -0.15)
Kowloon Bound	Fast	N (1.91, 0.19)	N (2.54, 0.25)	GEV (44, 2.13, -0.15)	GEV (56, 2.72, -0.15)
	Middle	N (2.53, 0.25)	N (3.28, 0.33)	GEV (66, 3.20, -0.15)	GEV (85, 4.09, -0.15)
	Slow	N (9.04, 0.90)	N (16.48, 1.65)	GEV (220, 10.66, -0.15)	GEV (282, 13.62, -0.15)

5.5.2 Railway Load Model

The railway load model developed for the condition assessment of the TMB is a series of concentrated forces, which represent the wheel loads of an eight-car train. The eight-car train is selected because it has a dominant proportion in the railway traffic, as stated in section 5.4.2. In the model, the distribution of the wheel loads follows the train regulation of the MTR Corporation of Hong Kong. Similar to the KEL, the GTW

for the train load model is also inversely calculated by the full 3D FEM of the bridge, targeting an extreme stress level, as shown in Figure . The GTW corresponding to an extreme stress with a return period of five years will be used in the SLS evaluation, and that corresponding to a stress with a return period of 120 years will be used in the ULS evaluation. Similar to the highway case, the extreme stress predicted using the BM approach is adopted. According to the results obtained in Chapter 4, these two stress levels are 25.70 MPa (95% CI: (25.29, 26.45)) and 27.21 MPa (95% CI: (26.44, 29.22)), respectively. The extreme stress was induced by two side-by-side trains. Thus, the weight of two trains is 674 tonnes with a 95% CI of (663, 693) for the SLS evaluation, and 713 tonnes with a 95% CI of (697, 766) for the ULS evaluation. Then the GTW was distributed to each wheel of the two trains following the configuration of the MTR standard train to get the railway load model. The weight of the two trains is subjected to a GEV distribution: for the SLS evaluation, it is GEV (674, 23.46, -0.09); while for the ULS evaluation, it is GEV (713, 24.82, -0.09).

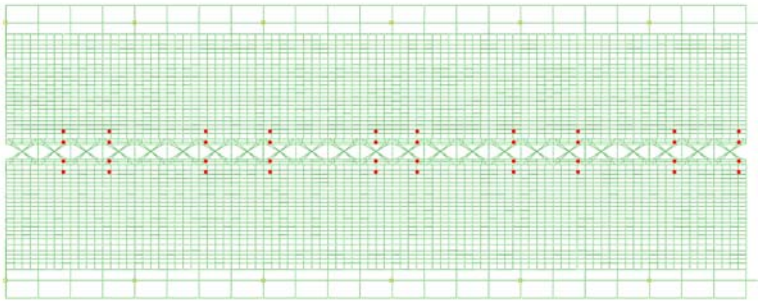

(a) Plan view

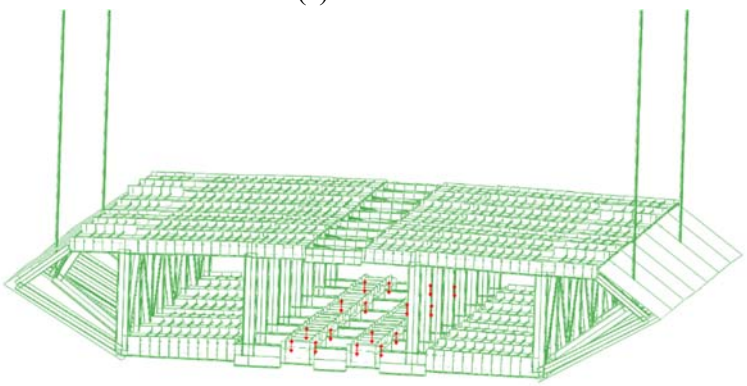

(c) Side view

Figure 5.11 Imposition of train loads on tracks

5.6 Validation of Developed Live Load Model and Discussions

To validate the developed highway load models, they are compared with the existing models for long-span bridges, which include the ASCE load model, BD 37/88 load model, and AASHTO HL-93 load model. The ASCE loading specifies three levels of live load depending on the average percentage of heavy vehicles in traffic flow: 7.5%, 30%, and 100%. The live load is represented by a uniform load and a concentrated load. The uniform load decreases while the concentrated load increases as load length increases. The British standard, BD 37/88, designs the bridge to resist more severe effects of either HA loading or HA loading combined with HB loading. The AASHTO

HL-93 load model is defined as a uniformly distributed model with an additional design truck or tandem.

The UDL and KEL of the developed live load model are compared with those of ASCE, BD 37/88, and AASHTO, as shown in Table 5.6. For the ASCE load model, the case of 30% heavy vehicles is considered. It is found in Table 5.4 that though it is developed for bridge evaluation, the UDL of the developed model is relatively large comparing with that for the bridge design. The reason is that the TMB serves a port and airport complex, so the traffic on the TMB is very dense sometimes and the proportion and GVW of the heavy vehicles on the slow lane are extremely large as well. Based on the statistical analysis of the WIM data, the median GVW of the MGV and HGV is 11.43 and 28.78 tonnes, respectively. However, the heavy vehicles defined in the compared code models have smaller GVW. For example, the GVW of the heavy vehicle defined in the ASCE loading is only 5.44 tonnes. Nevertheless, the multilane factors determined based on the data-driven UDL are smaller than those of the design models, as shown in Table 5.5. For the TMB, lanes 1 and 2 are slow lanes, 3 and 4 are middle lanes, and 5 and 6 are fast lanes.

Table 5.5 Comparison of multilane factors

Load model	Number of lanes					
	1	2	3	4	5	6
ASCE	1.00	0.70	0.40	0.40	0.40	0.40
BD 37/88	1.00	1.00	0.60	0.60	0.60	0.60
AASHTO	1.20	1.00	0.85	0.65	0.65	0.65
TMB	1.00	1.00	0.30	0.30	0.20	0.20

Table 5.6 Comparison of different live load models

Load model	UDL (kN/m)	Concentrated load (kN)
ASCE	8.76	809
BD 37/88	14.85	120 (HA) 450+450+450+450 (HB)
AASHTO	9.3	35+145+145 (design truck) 113+113 (design tandem)
TMB_SLS	9.04	253
TMB_ULS	16.48	342

According to BD 37/88 (BDT 1989), the GTW of the design train is 544 tonnes. The stress induced by two side-by-side design trains (1088 tonnes) is 41.49 MPa. Therefore, the gross weight of the train for the developed railway load model is much smaller than that of the design train.

The developed live load model can be applied to the FEM of the bridge to analyze the inner forces or deformation of each structural component, no matter there is sensor installed or not. Therefore, it will be helpful in the objective condition rating and cost-effective management of the bridge. For example, the tension force of the main cables, which suspend all the dead and live loads on the bridge deck, can be calculated by applying the developed live load models to the FEM, as shown in Figure 5.12. To show the load effect obviously, the vertical displacement of the deck has been magnified 50 times. The calculated tensional forces of the main cable, in both SLS and ULS, at the right-hand side span are listed in Table 5.7. In the table, LL represents tension induced by live load only, DL+LL means tension induced by the combination

of dead load and live load. And then, the results can be incorporated into a three-dimensional bridge condition rating system, to generate a more accurate and objective bridge condition assessment result, which will be illustrated in Chapter 7.

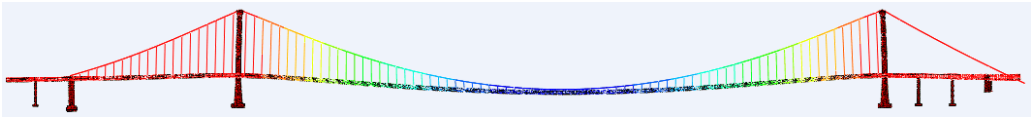

Figure 5.12 Application of live load model to bridge FEM

Table 5.7 Tension of main cable calculated based on developed live load model

State	LL (kN)	DL+LL (kN)	Permissible tension (kN)
SLS	25494	444538	522878
ULS	42148	476997	654665

5.7 Summary

This chapter developed site-specific live load models for bridge condition assessment. Based on the continuously measured data, especially the WIM, strain data and the CCTV recording of the traffic on the TMB, the highway and railway load models were developed. The highway load is modelled as a UDL representing the traffic flow, with an additional KEL which simulates an overloaded vehicle. The UDL is determined based on the WIM data, including the GVW and axle distance of the vehicles, proportion of different vehicles, and the CCTV recording of the traffic. The KEL is calculated inversely by the full 3D FEM of the bridge, targeting a certain stress level

in a typical point of the deck. The KEL corresponding to an extreme stress with a five-year return period is used in the SLS evaluation; while that corresponding to a stress with a return period of 120 years is used in the ULS evaluation. The multi-lane factors of the highway loads are determined by the data-driven UDL, and the dynamic impact factor is ignored based on the conclusions of the previous studies.

The railway load is modelled by a series of concentrated forces representing the wheel loads of an eight-car train. Similar to the KEL, the GTW is also calculated inversely by the FEM of the bridge, targeting a certain stress level for the SLS and ULS evaluation, respectively. The GTW is distributed to each wheel of the train following the configuration of the standard train defined by the MTR Cooperation of Hong Kong. To validate the developed live load models, they are compared with the existing ones specified in the design codes or suggested by the recent research. And the results demonstrate that the developed models are reasonable.

CHAPTER 6

STRUCTURAL RELIABILITY ANALYSIS BASED ON LONG-TERM STRAIN DATA

6.1 Introduction

The load and structural resistance models contain many uncertainties. As a result, bridge condition assessment is an estimation, rather than an exact conclusion (Rakoczy and Nowak 2014). The structural reliability theory is perhaps the best tool to integrate the long-term SHM data into bridge condition assessment. The reason is that it has a capability to accommodate the uncertainties in load effects and resistance-related parameters, as reflected in long-term SHM data. The theory and applications of structural reliability have been reviewed in section 2.1.3 of Chapter 2.

The use of measured structural responses has eliminated a substantial portion of modeling uncertainties in live load characterization (Bhattacharya *et al.* 2005). As reviewed in section 2.3 of Chapter 2, strain is one of the most important structural responses and plays an important role in SHM-based condition assessment of bridges. Researchers have made efforts to conduct bridge condition assessment using long-

term strain monitoring data; for example, Cardini and DeWolf (2008) developed an envelope of maximum distribution factors, peak strains and neural axis location to determine if change in the structural behavior of a bridge had happened.

Bridges deteriorate over time under aggressive environment and live loads, which leads to a reduction of the structural reliability. On the other hand, prior service loads reduce the uncertainty associated with bridge resistance and increase the reliability. These two contrary factors vary with time and may negate each other, so the reliability of a bridge is time-dependent. SHM data provide information about the bridge resistance, and continuously proves that the resistance is higher than the maximum load experienced already. Thus, the lower tail of the structural resistance distribution can be progressively truncated as survival age increases (Hall 1988). In addition, SHM data provide useful information of site-specific loads, load effects and even resistance models. Consequently, the structural reliability of the bridge can be updated using the Bayesian approach continuously. In the bridge design or evaluation, the target reliability index is based on a time reference period, such as 75 or 120 years. Hence, it is more meaningful to update the reliability year by year considering prior service loads for a bridge and use the updated structural reliability as a reference for decision making on bridge maintenance (Stewart and Val 1999).

In this chapter, an evolutionary reliability-based framework is established for bridge condition assessment in the context of statistical inference, based on the long-term strain data measured from the stiffening deck system of the TMB. Owing to the

deliberate design of strain gauge arrays, reliability indices at both structural component and deck cross-section level are estimated. A probabilistic model considering uncertainties of time-variant structural resistance and loads of the bridge is proposed. Some associated uncertainties can be quantified by the long-term SHM data. Both the point-in-time and updated annual reliabilities of the instrumented steel chords and deck sections are estimated. Taking corrosion of steel into account, this study also tries to describe the lifetime probability profile of the bridge. A target reliability index is specified to provide a decision-making reference for the bridge management activities, such as inspection, repair, or replacement.

The remainder of this chapter is organized as follows. Section 6.2 introduces the methodology for strain-based structural reliability analysis. The structural reliability of the TMB is studied in section 6.3, including both the point-in-time reliability and updated reliability obtained from the new data-driven live load demand distributions. Section 6.4 describes the profile of the lifetime structural reliability. And finally, the summary of this chapter is given in section 6.5.

6.2 Strain-Based Structural Reliability

The structural reliability theory, including the fundamental concepts, reliability index estimation, and time-dependent reliability, has been reviewed in section 2.1.3 of Chapter 2. The methodology for reliability evaluation based on strain data induced by

live loads is stated below. If the strain gauges were installed before the completion of the bridge's construction, the dead load effect should be taken into account correspondingly.

6.2.1 Limit State Function

The generalized limit state function g associated with the SHM data at time t, can be written as

$$g(t) = R(t) - (1 + E) \times Q_M(t) \tag{6.1}$$

where $R(t)$ is the structural resistance (capacity) corresponding to a limit state; $Q_M(t)$ is the live load demand derived from the measured strain based on the mechanical equilibrium; and E is the uncertainties associated with the sensors. The linear or nonlinear relationships between the measured strain and corresponding stress should be studied carefully before applying the strength theories to the failure analysis of structures.

6.2.2 Structural Resistance Models

Because only live load demands are considered, the structural resistance can be determined by maximum allowable stresses due to live loads, which is obtained by structural analysis. The maximum allowable stresses estimated based on different operational criteria of the bridge, such as serving under ULS or SLS live loads defined

by the design code, would be used in structural reliability analysis corresponding to different limit states.

The structural resistance is time-dependent because of deterioration. Corrosion is one of the most important causes of deterioration for steel bridges (Czarnecki and Nowak 2008). The effect of corrosion on steel bridges was studied in (Albrecht and Naeemi 1984; McCrum R. *et al*. 1985; Kayser 1988; Kayser and Nowak 1989a, b). Rate and progress of corrosion are the important issues to be addressed. However, it is nearly impossible to predict the corrosion rate accurately, because there are many factors influencing it but the available data is too limited to establish the analytical models (Czarnecki and Nowak 2008). Thus, the corrosion rate is usually estimated with approximate empirical formulas. Albrecht and Naeemi (1984) studied the performance of different types of steel exposed to environments of urban, rural, industrial, and marine. The section loss induced by corrosion penetration is considered as the main deterioration factor throughout the lifetime of the bridge in this study. The corrosion propagation model for the steel bridges is (Albrecht and Naeemi 1984)

$$C(T) = A \times T^{B} \tag{6.2}$$

where $C(T)$ is the average penetration in micrometers, and T is time in years, A and B are site-specific parameters. In case of marine environment, A=70.6 μm with the COV of 0.66, and B=0.789 with the COV of 0.49 (Albrecht and Naeemi 1984).

The loss of cross-section can cause an increase of stress under a given load, and reduction of section modulus or slenderness ratio. Consequently, the structural resistance to load effects like bending moment and axial forces, will be reduced. Based on the corrosion propagation models, mean value and standard deviation of relevant parameters, such as neural axis location and the elastic section modulus can be estimated.

6.2.3 Probabilistic Models of Live Load Demands

Arrays of strain gauges are usually designed deliberately for inner force evaluation of installed components, so the live load demands can be obtained easily. Statistics of extreme live load demands is suggested because of the following advantages. Firstly, extreme load demands are dominant factors associated with the structural reliability. Besides, statistics of extremes can prevent the miscellaneous modeling of variables engendered by many intricate processes, such as traffic, wind, and temperature, which occur at different and varying frequencies. This makes it an efficient way to manage data. Another advantage is that it provides a mechanism to incorporate time effects, i.e. return period (Messervey 2008). The extreme statistics are based on the EVT, which has been illustrated using the strain data measured from the TMB in Chapter 4.

6.2.4 Estimation of Reliability Index

If the structural resistance $R(t)$, the live load demand $Q_M(t)$, and uncertainties associated with the sensors E are independent with each other, for a certain time t the probability of structural failure corresponding to the limit state function in Eq. (6.1) is

$$P_f = \iiint_{g(t)\le 0} f_{R(t)}(r) f_{\mathrm{Q}_M(t)}(q_M) f_E(e)\,\mathrm{d}r\,\mathrm{d}q_M\,\mathrm{d}e \tag{6.3}$$

where $f_{R(t)}(\cdot)$, $f_{Q(t)}(\cdot)$, and $f_E(\cdot)$ are the PDF of $R(t)$, $Q_M(t)$, and E, respectively. The structural resistance $R(t)$ usually obeys the lognormal distribution; the live load demand $Q_M(t)$ has a GEV distribution because extreme values statistics are done based on long-term strain data; and E is often subject to a normal distribution with a zero mean. It is difficult to calculate the failure probability P_f due to the difficulty in integration of the PDFs. Therefore, indirect evaluation of this probability, i.e., the reliability index, is adopted. As reviewed in section 2.1.3 of Chapter 2, there are generally two methods to calculate the reliability index: (1) numerical approximation method (e.g. FOSM), and (2) simulation method (e.g. MC).

6.2.4.1 First-order second-moment (FOSM) method

The numerical approximation method is based on uncorrelated and normally distributed variables. However, for the case studied in this chapter, both the structural resistance $R(t)$ and the live load demand $Q_M(t)$ are not normally distributed. Thus, equivalent normalization should be carried out for these two variables. The equivalent

normal distribution for an individual non-normal variate can be obtained by making the cumulative probability and the probability density ordinate of the equivalent normal distribution equal to those of the corresponding non-normal distribution at the appropriate point on the failure surface (Paloheimo and Hannus 1974). Taking the structural resistance $R(t)$ as an example, what stated above means

$$\Phi\left(\frac{r^*(t)-\mu_{R(t)}^N}{\sigma_{R(t)}^N}\right)=F_{R(t)}(r^*(t)) \tag{6.4}$$

and

$$\frac{1}{\sigma_{R(t)}^N}\phi\left(\frac{r^*(t)-\mu_{R(t)}^N}{\sigma_{R(t)}^N}\right)=f_{R(t)}(r^*(t)) \tag{6.5}$$

where the superscript N denotes normal distribution. Eqs. (6.4)-(6.5) yield

$$\mu_{R(t)}^N=r^*(t)-\sigma_{R(t)}^N\Phi^{-1}[F_{R(t)}(r^*(t))] \tag{6.6}$$

and

$$\sigma_{R(t)}^N=\frac{\phi\{\Phi^{-1}[F_{R(t)}(r^*(t))]\}}{f_{R(t)}(r^*(t))} \tag{6.7}$$

After the non-normal variables are normalized, all the variables are converted to standard normal variables. For example, the standard normal variable for the structural resistance $R(t)$ is

$$R'(t) = \frac{R(t) - \mu_{R(t)}}{\sigma_{R(t)}} \tag{6.8}$$

The limit state equation, Eq. (6.1), would be

$$g(\sigma_{R(t)} R'(t) + \mu_{R(t)}, \sigma_{Q_M(t)} Q'_M(t) + \mu_{Q_M(t)}, \sigma_E E' + \mu_E) = 0 \tag{6.9}$$

Then the reliability index, which is the minimum distance between the failure surface and the origin, can be calculated by

$$\beta = D_{\min} = \frac{-\sum_i x'^*_i \left(\frac{\partial g}{\partial X'_i} \right)_*}{\sqrt{\sum_i \left(\frac{\partial g}{\partial X'_i} \right)^2_*}} \tag{6.10}$$

where the derivatives $\partial g / \partial X'_i$ are evaluated at $(x'^*_1, x'^*_2, ..., x'^*_n)$, and X'_i means the standard normalized $R(t)$, $Q_M(t)$ and E, respectively. This reliability estimation method only uses the constant term and first-order Taylor derivative, and the first and second moment of the variables, hence it is often called first-order second-moment (FOSM) method.

6.2.4.2 Monte Carlo (MC) method

The simulation technique of Monte Carlo (MC) is another usual method to estimate structural reliability indirectly. The probability of failure is estimated as (Shinozuka 1983)

$$P_f = \frac{A}{N}\sum_{i=1}^{N}\frac{\delta_i}{(2\pi)^{n/2}}\exp(-\frac{1}{2}\boldsymbol{t}_i^T\boldsymbol{t}_i) \tag{6.11}$$

with

$$\delta_i = \begin{cases} 0 & \text{if } g(\boldsymbol{t}_i) > 0 \\ 1 & \text{if } g(\boldsymbol{t}_i) \le 0 \end{cases} \tag{6.12}$$

where $\boldsymbol{t}_i$ is the ith realization of $\boldsymbol{x}$ generated by a computer simulation of the n independent, uniformly distributed random variables over an appropriate multidimensional square with an area of A. The shape and size for such a square depend on the location of the design point and the geometry of the limit state surface relative to this point. Therefore, it is desired that this area contains a region of high likelihood around the design point.

The total number of samples required depends on the magnitude of failure probability: the smaller the failure probability is, the larger the required number of samples will be. The direct sampling method is the simplest MC simulation, but not the most efficient (Melchers 1999). It takes samples from the region with highest probability, but this region is generally near the point corresponding to mean values of the variables, which contribute little to the failure of the structure. Thus, it is possible that even hundreds of thousands samplings have been done, the estimated failure probability is still 0. Even worse, the computer may stop work because of out of memory. In other words, the computational cost of this method is tremendously expensive. To improve the

efficiency of the MC method, several techniques have been developed (Melchers 1990; McKay *et al*. 2000; Rubinstein and Kroese 2011), which include: (1) Latin hypercube sampling, (2) importance sampling, (3) stratified sampling, (4) adaptive sampling, (5) directional sampling, (6) antithetic variates method, and (7) conditional & generalized conditional expectation method. The importance sampling technique is adopted in this study.

The basic idea of importance sampling is to change the center point of the sampling and get samples having a higher chance of falling in the failure region, or contributing to the probability of failure. The failure probability of the structure can be written as (Rubinstein and Kroese 2011)

$$P_f = \int_{-\infty}^{\infty} \frac{I[g_X(\boldsymbol{v})]f_X(\boldsymbol{v})}{p_V(\boldsymbol{v})} p_V(\boldsymbol{v})d\boldsymbol{v} = E\left\{\frac{I[g_X(\boldsymbol{v})]f_X(\boldsymbol{v})}{p_V(\boldsymbol{v})}\right\} \tag{6.13}$$

where $I[g_X(\boldsymbol{v})]$ is the indicator function of $g_X(\boldsymbol{v})$ (when $g_X(\boldsymbol{v})<0$, $I[g_X(\boldsymbol{v})]=1$, else, $I[g_X(\boldsymbol{v})]=0$); $g_X(\boldsymbol{v})$ is the limit sate function; $f_X(\boldsymbol{v})$ is the joint PDF of the random variables; $p_V(\boldsymbol{v})$ is the importance sampling PDF. Using $p_V(\boldsymbol{v})$ to take samples from the vector of variables, $\boldsymbol{V}$, the estimate of P_f is

$$\hat{P}_f = \frac{1}{N}\sum_{i=1}^{N} \frac{I[g_X(v_i)]f_X(v_i)}{p_V(v_i)} \tag{6.14}$$

6.2.5 Reliability Updating

If a bridge has survived for T years of service, it demonstrates immediately that its resistance is greater than any of the prior loads (Hall 1988; Ellingwood 1996; Stewart and Val 1999). Thus, the uncertainty of the bridge resistance can be reduced, and the reliability of the bridge is increased. The live load demands may increase as the service life of the bridge goes on, so the structural reliability would decrease correspondingly. Structural damage or deterioration may be discovered from the monitored data, which also leads to a decrease in structural reliability. The probabilistic distributions of both the structural resistance and live load demands can be updated continuously based the new collected data.

6.2.5.1 Updating PDF of structural resistance

After T years of service, the bridge survived from a maximum load effect q^*, which is a deterministic value obtained from the strain data. Then the PDF of the structural resistance at time T is updated to

$$\begin{cases} f_R''(r) = \dfrac{f_R'(r)}{1\text{-}F_R'(q^*)} & r > q^* \\ f_R''(r) = 0 & r \le q^* \end{cases} \tag{6.15}$$

where $f''_R(\cdot)$ is the updated PDF, $f'_R(\cdot)$ is the prior PDF, $F'_R(\cdot)$ is the prior CDF of the structural resistance. After updating, the lower tail of the resistance distribution is removed.

6.2.5.2 Updating PDF of live load demands

The PDF of the live load demands for this study is the GEV distribution, because the extreme values of live load demands are sampled considering the advantages stated in section 6.2.3. The GEV distribution has three parameters, the location parameter μ, the scale parameter σ and the shape parameter ξ, respectively. To update these parameters, both the Bayesian method and the classical frequentist method can be employed. One major philosophical difference between these two techniques is the notion of probability. The frequentist methods are rooted in the notion of probability as the limiting relative frequency of an event in a repeated series of trials, while the cornerstone of Bayesian methods is the notion of subjective probability (Hamada *et al*. 2008). As samples become large, the differences between these two types of methods often become negligible.

The Bayesian method requires a prior distribution of the parameters (μ, σ, ξ), which is expected to represent beliefs about parameter values before the data is available. In most cases such knowledge is absent, so arbitrary distributions with a large variance are usually adopted. For this study which is based on long-term strain data, the parameters estimated based on past data can be used as the prior information. For the first analyzed year, non-informative prior can be given if there is no reliable expert knowledge or other valuable information. The Gibbs sampling is adopted, and a Metropolis step with random walk updates is employed to simulate from the full conditionals.

In the frequentist method, all the measured data available, including data measured in the studied year as well as those collected in the previous years, form a large sample and then the GEV parameters are estimated using the likelihood-based estimation method as introduced in Chapter 4. With more and more new collected data integrated, the GEV parameters can be updated by this means.

The main difference between these two updating approaches is how to take the cumulative effects of data measured in the previous years into account. In the frequentist method, the effects of past data are considered by integrating the data in to the sample directly; while in the Bayesian method, these effects are taken into account in the form of prior information.

The revised distributions of structural resistance and live load demands can be used to calculate the updated structural reliability using either the FOSM or MC method subsequently. The outcome of the Bayesian updating method is a distribution of the parameter rather than just a point estimate, which represents a considerable advantage over the frequentist method. To evaluate the results of these two methods, a simple summary statistic of the posterior, the mode, is selected to be compared with the point estimate of the frequentist method.

6.3 Structural Reliability Evolution of TMB

In this study, the data-driven structural reliability is estimated in the following way. Based on a predefined lognormal distribution of the structural resistance, and the GEV distribution of the live load demands obtained from the daily maximum strain data measured in each year, the annual reliability index, i.e. point-in-time reliability, is calculated first. And then the probabilistic models for both the structural resistance and live load demands are updated based on the continuously collected data, and new reliability indices for each year are obtained consequently. To take the degradation of structural resistance into account, the corrosion propagation model for the steel bridges as introduced in section 6.2.2 is adopted.

6.3.1 Strain-Based Limit State Functions

6.3.1.1 Data-driven live load demands

The strain monitoring of the TMB focuses on the stiffening deck system, which has been introduced in section 4.3.3 of Chapter 4. In recognition of the fact that the longitudinal trusses act as the main girder and are the load resistance framework of the deck, this chapter focuses on the structural reliability of the longitudinal trusses. As shown in Figure 4.3, two or more strain gauges have been installed on the cross-section of each of the instrumented chords, and also been intentionally deployed on all the truss members across the cross-section. The internal forces experienced in both the

chords and the full deck sections can be readily obtained for reliability-based assessment. Therefore, two levels of structural behaviors are considered in the structural reliability analysis of this study: (1) the structural component level, i.e., the compression or tension of individual chords; and (2) the cross-section level, e.g. the flexure, shear or torsion of the whole cross-sections of the stiffening deck system.

Most of the temperature-induced strain in the stiffening deck system has been released by the free movement of the expansion joint. Thus, it contributes little to the stress and inner forces experienced by the deck. After extracting the thermal strain from the original signals using the WT-based method stated in Chapter 3, the live-load-induced inner forces of the instrumented chords and deck cross-sections, i.e. live load demands, can be calculated. Taking the bottom chord as an example, its internal forces can be calculated by (Ni and Xia 2016)

$$N = A\sigma_a = A(\sigma_T Z_T + \sigma_B Z_B)/(Z_T + Z_B) \tag{6.16}$$

and

$$M = Z_B \sigma_{bB} = (\sigma_T - \sigma_B)/(1/Z_T + 1/Z_B) \tag{6.17}$$

where N is the axial force, M is the vertical bending moment, A is the area of the cross section, σ_a is the average stress in the cross section, σ_T and σ_B are the stresses derived from strains measured at the top and bottom of the chord respectively, Z_T and Z_B are the section moduli corresponding to the positions of the strain gauges, and σ_{bB} is the

bending stress at the bottom of the cross section. For trusses, the axial forces of individual chords are dominant inner forces, so the bending moments are often not considered. The detailed procedure for calculating the deck cross-sectional internal forces, such as the axial force, vertical and transverse bending moment, and vertical shear, can be found in (Ni *et al.* 2011). The time histories of all the internal forces can be readily obtained by synthesizing the monitored strain time histories of the relevant chords.

6.3.1.2 Limit state functions

The structural analysis was carried out by the Highway Department of Hong Kong to estimate the allowable stresses in the steel chords of the stiffening deck system when live loads corresponding to SLS and ULS are imposed on the bridge respectively. Under operational loads the TMB has behaved in the elastic state up to now, and consequently the strain data which will be used in the structural reliability analysis correspond to this state. Thus, the limit state considered in the data-driven structural reliability analysis carried out in this chapter is the SLS. The maximum allowable stress induced by lived loads in the SLS is 60 MPa for the top and bottom chords, and 30 MPa for the diagonal chords (Wong 2007).

The limit state function for the failure of individual chords is

$$g_N(t) = A(t) \times f_N - (1+e) \times A(t) \times \sigma_M(t) \tag{6.18}$$

where $A(t)$ is the individual chords' cross-section area; f_N is the maximum allowable stress induced by lived loads; e is the uncertainty associated with the sensors (the standard deviation of the sensors' uncertainties, σ_e, is 5%); $\sigma_M(t)$ is the daily maximum stresses induced by live loads. Similarly, the limit state functions for the failure of deck cross-sections, are

$$g_M(t) = R_M(t) - (1+e) \times M_M(t) \tag{6.19}$$

for flexural failure, and

$$g_V(t) = R_V(t) - (1+e) \times V_M(t) \tag{6.20}$$

for shear failure. In Eq. (6.19), $R_M(t)$ is the flexural resistance of the section, which is

$$R_M(t) = \frac{h(t)}{2} \times \{[A_{nb}(t) \times f_{Nnb} + A_{sb}(t) \times f_{Nsb}] - [A_{nt}(t) \times f_{Nnt} + A_{st}(t) \times f_{Nst}]\} \tag{6.21}$$

for vertical bending, where $h(t)$ is the effective height of the cross-section, A_{nb}, A_{sb}, A_{nt}, and A_{nt} are the cross-section areas of the bottom chords and top chords at the north and south side of the deck, and f_{N*} is the maximum allowable stress induced by lived loads for the relevant chords; and $M_M(t)$ is the bending moment derived based on the strain data, which is

$$\begin{aligned} M_M(t) = \frac{h(t)}{2} \times \{&[A_{nb}(t) \times \sigma_{Mnb}(t) + A_{sb}(t) \times \sigma_{Msb}(t)] \\ &- [A_{nt}(t) \times \sigma_{Mnt}(t) + A_{st}(t) \times \sigma_{Mst}(t)]\} \end{aligned} \tag{6.22}$$

for vertical bending, where $\sigma_{M^*}(t)$ is the measured average stress for relevant chords. In Eq. (6.20), $R_V(t)$ is the shear resistance of the section, which is

$$R_V(t) = [A_{nd}(t) \times f_{Nnd} + A_{sd}(t) \times f_{Nsd}] \times \frac{L_v}{\sqrt{L^2_v + L^2_l}} \tag{6.23}$$

for vertical shear, where A_{nd} and A_{sd} are the cross-section areas of the diagonal chords, L_v and L_l are the effective length of the vertical and lateral chords ; and $V_M(t)$ is shear force calculated using monitored strain, which is

$$V_M(t) = [A_{nd}(t) \times \sigma_{nd}(t) + A_{sd}(t) \times \sigma_{sd}(t)] \times \frac{L_v}{\sqrt{L^2_v + L^2_l}} \tag{6.24}$$

for vertical shear.

6.3.2 Annual Probabilistic Distribution of Live Load Demands

The daily maximum axial forces experienced by the chords are fitted to the GVE distributions. Figure 6.1 shows the GEV fitting to a chord's daily maximum axial forces measured in 2009. This chord is the one on which the strain sensor SSTLS09 (Figure 4.3) is installed. It can be observed from this figure that the daily maximum axial forces of the chord are well fitted to the GEV model. The annual probabilistic distributions of this daily maximum axial force for other representative years, i.e. 2004, 2006, 2008, 2010 and 2012, are shown in Figure 6.2. The annual probabilistic distributions for all the years during the period of 2004-2012 were derived, but for

clearer view only those of the selected years are shown. It is observed that median value of the axial forces measured in 2004 is smaller than that for other years, which is due to the transition of trains from seven-car to eight-car, as mentioned in section 5.2.2 of Chapter 5.

The statistical analyses of inner forces for the deck cross-sections are conducted in the similar way. Figure 6.3 shows the box-plot of the daily maximum bending moments for section C (Figure 4.1). It is found that the bending moments have an obvious increase during the years of 2004-2006, which is due to the transition of train type passing the bridge. Figure 6.4 is the GEV fitting to the daily maximum bending moments of the year 2011.

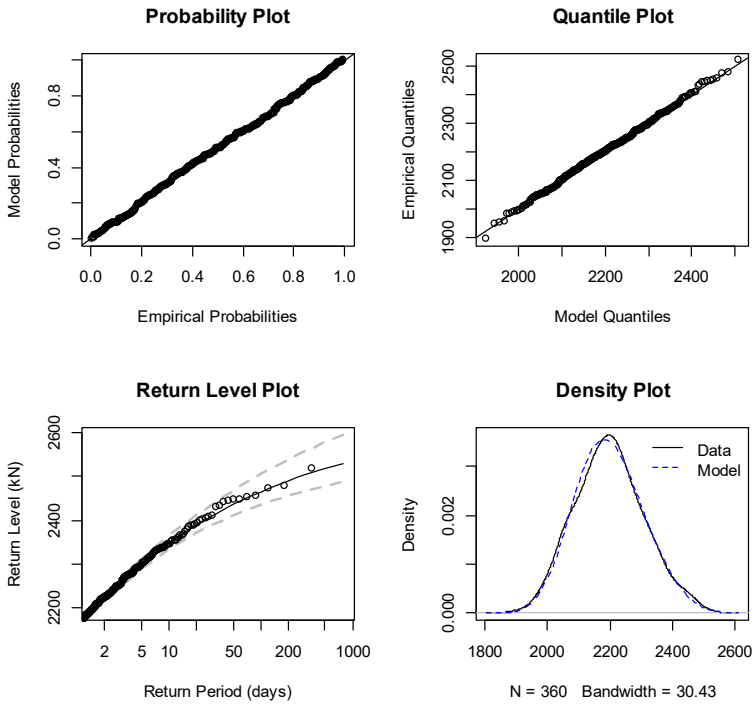

Figure 6.1 Diagnostic plots of GEV fitting to a chord's daily maximum inner forces obtained from strain data measured in 2009

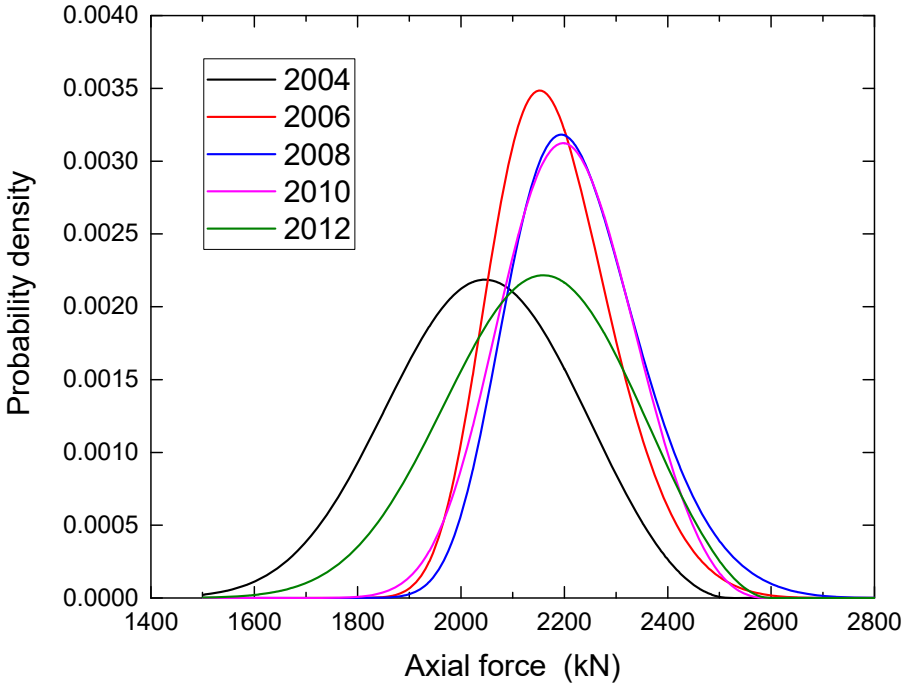

Figure 6.2 GEV fitting to daily maximum inner forces of a chord based on strain data measured in 2004, 2006, 2008, 2010, and 2012

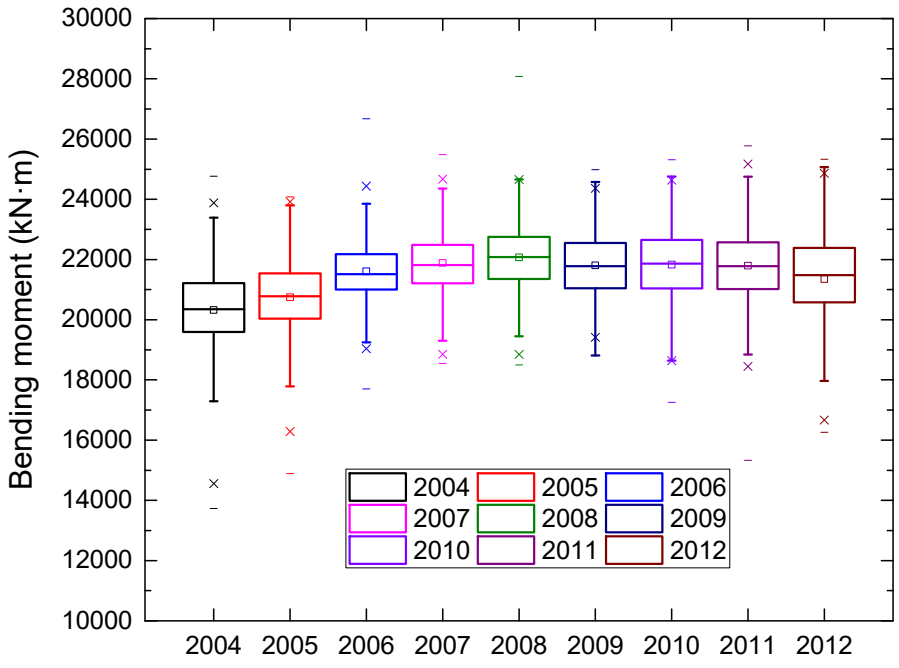

Figure 6.3 Box-plots of bending moment for deck cross-section

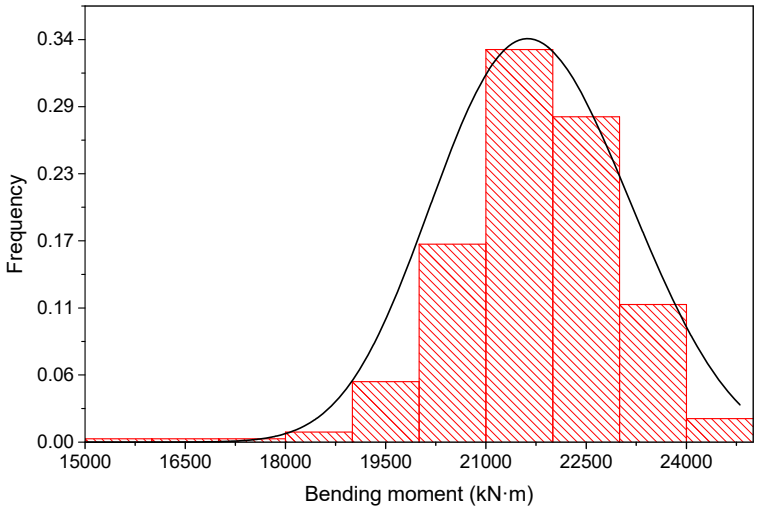

Figure 6.4 GEV fitting to daily maximum bending moment of 2011

6.3.3 Structural Resistance Models

The resistances of the steel chords to live loads is considered as lognormal random variables. As mentioned in section 6.3.1.2, the maximum allowable stress induced by lived loads in the SLS is 60 MPa for the top and bottom chords, and 30 MPa for the diagonal chords. Due to the uncertainties of the analytical models and methods, these values are not definite. Thus, they are assumed to be lognormal variables with mean values as stated above, and a COV of 0.15. The growing section loss caused by corrosion is considered in the structural resistance model. The TMB is in the marine environment, so high corrosion rate is adopted and the values of A and B in Eq. (6.2) are selected correspondingly. Corrosion is assumed to occur on the whole surface of the chords over the entire span of the bridge.

6.3.4 Structural Reliability Analysis

6.3.4.1 Point-in-time reliability

Reliability of individual chords

The reliability indices in this study are estimated using two methods introduced in section 6.2.4, FOSM (a numerical approximation method) and MC (a simulation method), respectively. In the FOSM method, the equivalent normal distribution of the non-normal variables, in Eq. (6.18), i.e. the maximum allowable stress induced by lived loads, f_N, which is lognormal variable, and the daily maximum stress induced by live loads, $\sigma_M(t)$, which obeys GEV distribution, are derived first based on Eqs. (6.4)-(6.7). Then these equivalent normal variables as well as the real normal variables are converted to standard normal variables using Eq. (6.8). The failure surface is transformed to the standard normal coordinate as presented in Eq. (6.9) consequently. The structural reliability indices are estimated in the standard normal coordinate using the first-order Taylor derivative of the limit state function based on Eq. (6.10). Recognizing that the failure probability is very small and large samples are needed to produce a stable result, the importance sampling as introduced in section 6.2.4.2 is adopted in the MC method to ensure the computational efficiency.

Figure 6.5 shows a chord's structural reliability indices estimated using both the FOSM and MC method. This chord is also the one on which the strain gauge SSTLS09 is installed because of its typicality and criticality. It can be observed that the results

obtained by these two methods match each other well, though the values calculated by the FOSM method is smaller. The point-in-time reliability of this chord has a decrease after the year 2005 because of the transition of train types from seven-car to eight-car, as mentioned in chapters 4 and 5.

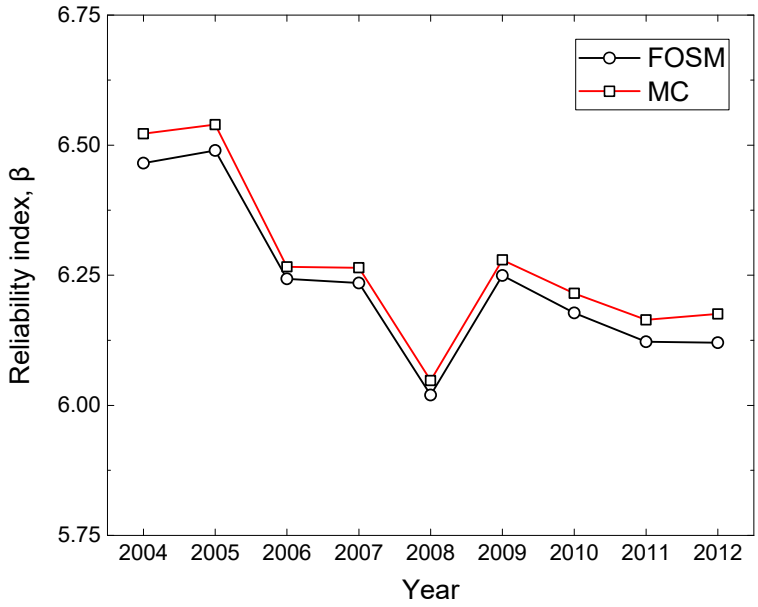

Figure 6.5 Structural reliability indices estimated by FOSM and MC methods

Reliability of deck sections

The cross-section of the deck is considered to fail when any chord in the section loses function. Therefore, if this cross-section is considered as a system, it is a series system, for which the probability of failure must satisfy (Nowak and Collins 2012)

$$p_{f_i,\max} \le P_f \le 1-(1-p_{f_i,\max})^n \tag{6.25}$$

where p_{fi} is the failure probability of element i. The upper bound is the failure probability when all elements are uncorrelated, and the lower bound corresponds to the case when all elements are fully correlated (ρ_{ij} =1). Due to the strong mechanical relationship, the reliabilities of the chords in the same cross-section of the TMB deck are strongly correlated to each other, with a correlation factor close to 1 based on the data. Therefore, the reliability of the deck section is the lowest reliability of the constituent elements. For instance, the vertical bending dominates the failure modes of the instrumented section C (Figure 4.1), and the bottom chords are the most critical truss members. The reliability of the cross-section should be equal to that of the bottom chords.

Based on the limit state functions of Eqs. (6.18)-(6.20), the reliabilities of the instrumented deck sections can be evaluated for the vertical bending and shear, which are important failure modes for bridge deck under traffic loads. Figure 6.6 presents the section C's point-in-time reliability indices corresponding to the failure modes of vertical bending, comparing with the reliability indices of the south bottom chord with tensile failure mode. All these structural reliability indices were calculated by the MC method. It can be observed that the reliability indices of the cross-section is nearly equal to those of the bottom chord. Because the reliability indices were estimated based on daily maximum strain data, which were mainly induced by two trains running side by side, there is nearly no eccentric strain responses for the north and south bottom

chords. Therefore, the annual reliability indices of the deck section coincides very well with those of the arbitrarily selected chord, i.e. the south chord.

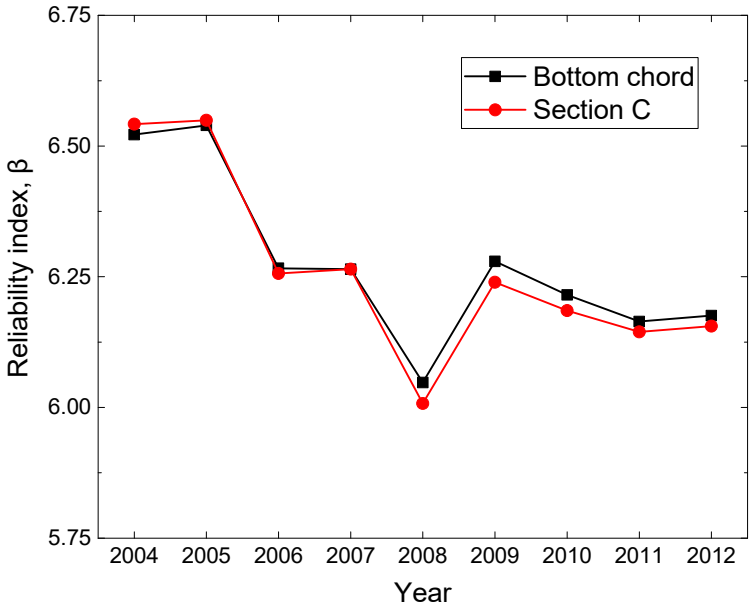

Figure 6.6 Comparison of reliability indices for deck section and bottom chord

6.3.4.2 Updated reliability

It was found that the load histories the bridge has survived from have no significant influence on the structural reliability indices. It is because that the load effect is relatively small comparing with the structural resistance. Taking the chord where the strain gauge SSTLS09 (Figure 4.3) is installed as an example, the PDF of the maximum allowable stress induced by lived loads is shown in Figure 6.7. However, the maximum stress experienced by this chord is less than 30 MPa, as analyzed in Chapter 4. It is easy to understand that this small load effect nearly has no influence on the estimated structural reliability.

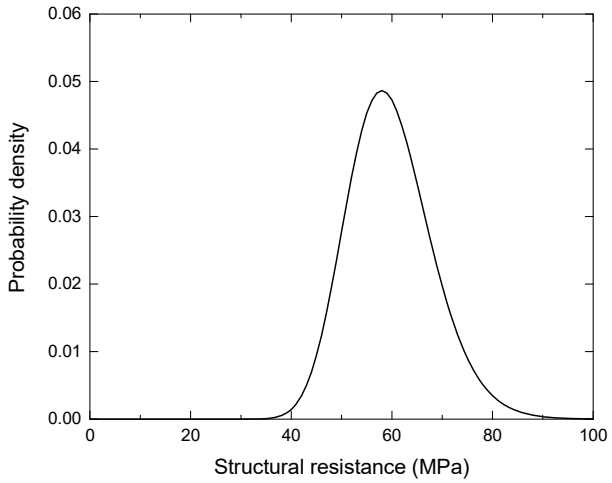

Figure 6.7 Structural resistance PDF of a typical chord

The annual GEV distributions fitting to the daily maximum live load demands which were obtained from the strain data are updated using both the Bayesian method and the classical frequentist method introduced in section 6.2.5.2. To update using the Bayesian method, a prior should be given. For the first analyzed year, 2004, weakly informative prior is given by assigning large variances to the three GEV parameters (μ, σ, ξ). For example, the variances of these three parameters for the axial forces of the chord SSTLS09 is installed on are 10,000, 1000, and 100, respectively. The means of these parameters are set to be 2000, 150, and 0 on the basis of the author's experience of data analysis. The priors for the following years adopt the distributions of the parameters estimated based on the past data. For the axial force mentioned above, the prior for 2005 is μ~N(1979, 3.16), σ~N(178, 9.5), and ξ~N(-0.33, 0.024). And then the MCMC algorithm introduced in section 6.2.5.2 is applied to estimate the posterior parameters when newly collected data are available. The Gibbs sampling is run for 10,000 iterations, of which the first 1000 were discarded.

Benefitting from the continuous operation of the SHM system, new strain data are collected unceasingly and the database becomes larger and larger. The GEV of the live load demands can also be updated based on the large dataset containing all the past data the new data collected in each individual year by the classical frequentist method. The parameters of the GEV distributions are estimated by the MLE.

With the new GEV distributions of the live load demands, the structural reliability indices of each year are updated subsequently. The updated structural reliability indices of the chord associated with the strain gauge SSTLS09 are shown in Figure 6.8, comparing with the corresponding point-in-time reliability indices. The shown reliability indices were estimated by the MC method. The change of reliability profile (or the reliability evolution) after updating can be easily observed. Because of the randomness in the annual probabilistic distributions of live load demands, the point-in-time reliability profile is a little uneven. In contrast, with all past data integrated, the updated results are more balanced and the resulting reliability profile is smoothed a little. The updated reliability profile has a continuous descending trend, which meets the general case of the bridges.

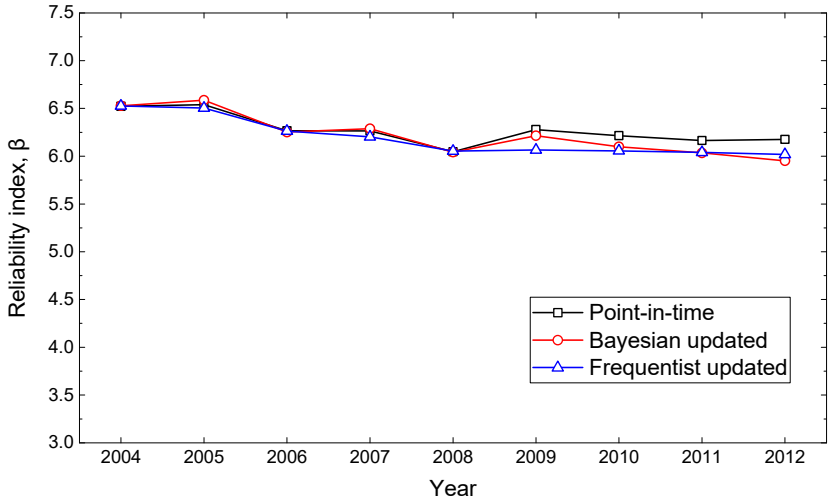

Figure 6.8 Updated reliability using Bayesian updating and classical frequentist methods

6.4 Profile of Lifetime Structural Reliability

The live load demand model used is the GEV fitting to the daily maximum values obtained from all the strain data measured from 2004 to 2012. The lifetime reliability profile of the typical chord studied above is shown in Figure 6.9. As exposure time goes on, the section loss due to corrosion increases, and the structural resistance is reduced continuously as a result. Therefore, the structural reliability decreases in the lifetime of the bridge. Because of more uncertainties in the structural deterioration, i.e. larger deviation of section loss, after 60 years of service it can be observed from Figure 6.9 that the decrease of structural reliability becomes fast afterward. What can also be observed from Figure 6.9 is that the effect induced by the transition of railway traffic from seven-car train to eight-car train on the structural reliability index can be observed clearly in the figure, which has surpassed that of the steel corrosion. Since the year 2006 (corresponding to the third box on the left) most of the trains have

changed to eight-car class, the reliability indices tends to be stable in the following years, i.e. 2007-2012 (corresponding to the fourth to the ninth box on the left).

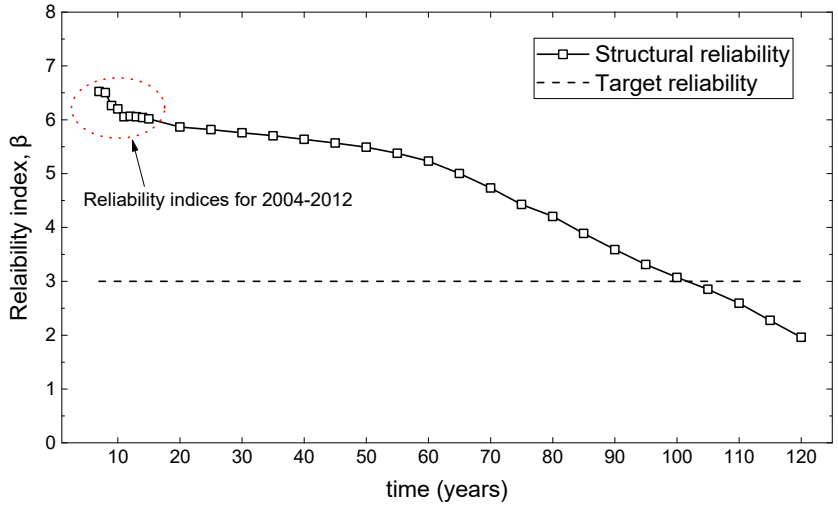

Figure 6.9 Lifetime reliability profile of a typical chord

The structural reliability profile provides an important reference for the bridge management activities, such as inspection and maintenance actions. A structural component needs repair when its system reliability falls below a prescribed minimum value. Therefore, a minimum reliability index, which is usually called target reliability index, needs to be specified. The target reliability index, β_T, for a given failure mode is intended to ensure that the concerned structural component has an adequate level of safety up to the end of a reference period (Bhattacharya *et al.* 2008).

The specification of target reliability index is a decision making, which should consider both bridge safety and economic saving, optimizing the total cost related to an assumed remaining working life of a structure. A risk-cost-benefit analysis can be

applied to assist the decision-making (Stewart and Val 1999). Time parameters should be taken into account; that is, the target reliability index is commonly related to a reference period. This reference period is understood as a chosen period of time used as a basis for statistically assessing time-variant basic variables such as wind, traffic, or temperature actions, and the corresponding probability of failure (Sykora et al. 2017). The design working life is a period of time for which a structure is to be used for its intended purpose without any major repair work being necessary. The concept of reference period is fundamentally different from that of design working life. ISO 2394:2015 indicates that the remaining working life can be adopted as a reference period for the SLS and fatigue limit states, while a shorter reference period might be used for the ULS.

Some bridge design or evaluation guidelines have specified target reliability indices. For example, the target reliability index used implicitly in the LRFD of new bridge components in flexure is 3.5 with a typical design life of 75 years (NCHRP 1999a, b). For bridge condition assessment, the target reliability index is suggested to be 2.5, corresponding to a typical inspection interval of five years (NCHRP 1998; Ghosn 2000). This suggestion is mainly based on economic considerations. Bhattacharya *et al.* (2005) proposed target reliability indices for two different levels of bridge rating: (1) yield limit stat for a reference period not exceeding 2 years, and (2) plastic collapse (i.e. ULS) over any duration up to the end of service life. The target reliability index for the first rating level is 2.5, and that for the second level is 3.5.

The TMB is an important asset and a key linkage connecting the international airport to the urban area; thus, it is of great significance for Hong Kong, and its failure consequence would be great. Taking this into account and adopting the remaining working life of 20 years as a reference period, the target reliability index for the evaluated structural components of this bridge is set as 3.0. Special inspection should be conducted for the evaluated component when the reliability index is less than 3.0 and repair or replacement should be done if serious damage is observed during inspection. The interval for reliability estimation of the structural component in Figure 6.9 is five years. When the reliability index is less than 3.0, the interval for routine inspections and detail condition rating can be narrowed to two years.

In this reliability prediction analysis, the deterioration model of steel structures is based on the existing model and not sufficiently accurate. Moreover, the live load demand model used was established based on the statistics of the existing SHM data, but it may change in the future. Furthermore, absence of maintenance was assumed. However, maintenance activities such as painting, repair or replacement will be taken when structural damage is detected. As a result, the structural reliability will be increased. Therefore, the derived lifetime reliability profile above needs to be updated as time lasts based on the new SHM data, inspection results, and maintenance records, etc. It can only be employed as a reference in the bridge management.

6.5 Summary

To incorporate the long-term SHM data into bridge condition assessment, a reliability-based framework is proposed in this chapter, based on nine years of strain data measured from the stiffening deck system of the TMB. With a predefined lognormal distribution of the structural resistance, and the GEV distribution of the live load demands obtained from the daily maximum strain data measured in each individual year, the point-in-time reliability was calculated first. To obtain a more balanced and reasonable structural reliability profile, the probabilistic models of the live load demands were updated using both the Bayesian and the classical frequentist method. And then the annual reliability indices were updated and the evolution of the structural reliability during the studied years is learned. In both the point-in-time and updated reliability analysis, an existing corrosion propagation model for the steel bridges was adopted to consider the degradation of structural resistance.

To predict the future reliabilities, the profile of lifetime reliability for the instrumented members was studied subsequently. The annual probabilistic distribution of daily maximum load effects estimated based on all the nine years of data was used as the load demand model. To facilitate the decision-making for bridge management based upon the lifetime reliability profile, a target reliability index can be selected. To optimize the bridge management targeting both bridge safety and economic saving, a risk-cost-benefit analysis is suggested to assist the decision-making. The profile only

provides a broad outline, and needs to be updated unremittingly with new information such as SHM data, inspection results, and maintenance records.

CHAPTER 7

AN SHM-BASED BRIDGE CONDITION RATING SYSTEM

7.1 Introduction

To make it convenient for the bridge engineers and decision-makers to determine the maintenance priority and strategy, results of bridge condition assessment are preferred to be represented by indices in certain metric scales. This process is called bridge condition rating (BCR). A relatively accurate and comprehensive BCR system can help bridge managers to make effective budget allocation for bridge maintenance. However, the complexity of bridge structures and imprecision of the condition data makes the BCR not so reliable (Sasmal and Ramanjaneyulu 2008).

Currently, the BCR is either based on visual inspections or structural analysis. In visual inspections, the bridge inspectors assess the condition of each element based on the experience, intuition and personal judgment. The inspection-based BCR systems all over the world and the shortcomings of visual inspections can be found in section 2.2.1 of Chapter 2. The analytical method can also be called load carrying capacity rating,

which is evaluated based on the load and the resistance of the bridge components; for example, the LRFR method in the AASHTO MBE (AASHTO 2008) as introduced in section 2.2.2 of Chapter 2. The problem with this method is that a generalized live load model representing bridges nationwide, is adopted to calculate the load capacity. Nevertheless, this defined model may not be applicable to the concerned bridge. The involved condition factors which are used to determine the structural capacity are also relatively subjective.

Providing a wealth of high-quality in-situ data, SHM can effectively complement the traditional BCR methods. The compelling advantages of SHM technologies include but not limited to updating existing models for the structural resistance and load effect, and showing performance variations over time and warning against threshold levels. It makes the bridge condition assessment more efficiently and simply. As a result, it has a potential to save cost in bridge management, including repair, rehabilitation and inspection. However, limited by practical problems such as budget and difficulty of deployment, only a necessary number of sensors are installed at discrete points of a bridge. Critical locations of a structure are time-dependent, because of the changes of loads, environment, and development of damage states. Consequently, the monitored structural responses may not always represent the critical data. Furthermore, it is difficult for sensors to access to all critical locations of the bridges, such as the connections or articulations. Besides, though great progress has been made, it is still difficult for large-scale bridges to identify the damage or to determine the structural

deterioration based on the SHM data. Therefore, it seems that only incomplete SHM data are not enough to evaluate the bridge condition.

A full 3D-FEM can reliably simulate the global and local structural characteristics of a bridge; thus, it is a valuable tool to provide structural information for bridge condition assessment. Its advantages include: (1) simulation of diverse loading scenarios is enabled; (2) all the structural components including the joints or articulations can be analyzed, so structural responses which are difficult to measure can be obtained; (3) the failure mechanisms and sequences of failure modes, which are difficult to analyze using the conceptual methods or manual mechanical approaches, can be studied. Therefore, a precise FEM is an ideal substitute for the traditional analytical approach based on simple structural analysis using a defined live load model. It can be considered as a powerful complement to SHM technology.

Although the visual inspection has inherent drawbacks, it has capabilities which SHM may not possess. For instance, some initial damage such as stripping of painting, spalling of concrete, visible cracks or wear, which cannot be sensed by an SHM system, may be discovered in visual inspections. Information such as the as-built report and maintenance record of the bridge is also essential in bridge condition assessment. Therefore, a comprehensive BCR system incorporating all the relevant information, is desired.

Attempt to integrate the WASHMS monitoring results into the bridge inspection and maintenance has been made (Wong 2006). A BCR system composed of criticality rating and vulnerability rating was used to assess the bridge condition based on SHM data, as-built report, and maintenance record. Observations of inspections were not included, and the FEM of the bridge was not truly used. In addition, by using a strength utilization factor, which is a semi-probabilistic index, this rating system does not have the capability of making full use of the SHM data.

A three-dimensional BCR system in terms of criticality rating, vulnerability rating and inspection-based rating is proposed in this chapter. The criticality rating is to evaluate the resistance surplus and failure consequence of the structural components, based on the mechanical concept, SHM data or 3D FEM of the bridge. The vulnerability rating estimates the exposure or degree of protection to adverse effects such as deterioration, damage and wear mainly based on the as-built report and maintenance records. The inspection-based rating assesses the current situation of deterioration, crack and wear based on inspections. A database for storage, retrieval, enquiry, tracing, and updating of all the data and information in this BCR system is developed by IBM's DB2. Thus, the information of the structural components is stored well and can be enquired easily. Furthermore, the condition rating results can be updated when any data associated with SHM, FEM, inspection, or maintenance records changes. Therefore, the developed condition rating system can be used in the life-cycle management of bridges. This BCR system is illustrated by taking the TMB as an example.

The remainder of this chapter is organized as follows. Section 7.2 explains the concept of the proposed three-dimensional BCR system. The procedure of this system is introduced in section 7.3. The development of database which will be used to manage and update the data and rating results of this system is described in section 7.4. The application of the proposed system to the TMB is presented in section 7.5. Finally, section 7.6 summarizes the main works of this chapter.

7.2 Concept of Three-Dimensional BCR System

The three-dimensional BCR system includes three aspects, criticality rating (CR), vulnerability rating (VR), and inspection-based rating (IR). The CR involves the resistance surplus associated with the ultimate and fatigue strength, and consequence of failure. It is determined based on four criticality factors, namely, structural reliability index, fatigue life, known defects, and failure consequence. Table 7.1 gives the definitions, subdivided ranges and corresponded points for each criticality factor.

For the structural components installed with strain gauges, the structural reliability indices are estimated using the methods introduced in Chapter 6. The probabilistic model of live load demands can be determined based on the interval of bridge condition assessment. For the structural components without strain gauges, the live load demands are obtained by applying the live load models developed in Chapter 5 to the FEM of the bridge. The fatigue life of instrumented structural elements is

evaluated using the measured strain based on relevant fatigue codes such as BS 5400-10. The FEM is employed to estimate the fatigue life of those un-instrumented components. Defects such as construction errors may lead to stress concentration. The information of known or discovered defects is from the as-built report of the bridge. Among the three failure consequences, catastrophic collapse means the failure partial or total failure which would endanger the lives of those on or under the bridge; partial collapse refers to major deformations and discontinuities which would affect the traffic on or under the bridge; and structural damage refers to localized failure, such as excessive deformation or cracking in structural components.

Table 7.1 Definitions, range and points of criticality factors

Criticality factor	Definition	Range	Points
C1	Structural reliability index, β	$\beta < 6.0$	2
		$6.0 \leq \beta \leq 8.0$	1
		$\beta > 8.0$	0
C2	Fatigue life	< 200 years	2
		200-300 years	1
		> 300 years or not applicable	0
C3	Known or discovered defects but not serious enough to affect performance	Any, non-repairable	2
		Any, repairable	1
		None	0
C4	Failure consequence	Catastrophic collapse	2
		Partial collapse	1
		Structural damage	0

The VR evaluates the fragility of bridge components to the environment, based on the as-built report and bridge maintenance records. It is calculated by three vulnerability factors, namely, deterioration, damage, and wear. Table 7.2 gives the definitions, subdivided ranges and corresponded points for each vulnerability factor. What deserves notice is that besides the exposure degree, the vulnerability rating is also associated with the likelihood of detection in superficial inspection. The rating results are the product of the points for these two aspects. That is to say, even the exposure degree of a bridge component is high, if it is very easy for superficial inspection, the vulnerability rating of this component is low, and vice versa.

As the name suggests, the IR assesses the current condition of the bridge components based on the inspection results. It is calculated by three factors, including current situation of deterioration, crack, and wear, as illustrated in Table 7.3.

Every evaluated element has a cumulative point for each rating, CR, VR, or IR. This cumulative point is transformed into percentage which ranges from 0-100% based on the following equations:

$$CR = \frac{\sum_{i=1}^{4} Ci}{8} \times 100\% \tag{7.1}$$

$$VR = \frac{\prod_{i=1}^{2} VAi + \prod_{i=1}^{2} VBi + \prod_{i=1}^{2} VCi}{12} \times 100\% \tag{7.2}$$

$$IR = \frac{\sum_{i=1}^{3} Ii}{6} \times 100\% \tag{7.3}$$

Table 7.2 Definitions, range and points of vulnerability factors

Vulnerability factor	Definition	Range	Points
A. Deterioration			
VA1	Exposure or degree of protection	Internal or adequate	0
		Partial or average	1
		Extreme or none	2
VA2	Likelihood of detection in superficial inspection	Likely	0
		Possible	1
		Unlikely	2
B. Damage			
VB1	Exposure to damage	None	0
		Medium	1
		High	2
VB2	Likelihood of detection in superficial inspection	Likely	0
		Possible	1
		None	2
C. Wear			
VC1	Relative wear rate per annum	Low	0
		Medium	1
		High	2
VC2	Likelihood of detection in routine maintenance	Likely	0
		Medium	1
		Unlikely	2

Table 7.3 Definitions, range and points of inspection-based condition factors

Inspection-based condition factor	Definition	Range	Points
I1	Current situation of deterioration	Little	0
		Medium	1
		Severe	2
I2	Current situation of crack	Little	0
		Medium	1
		Severe	2
I3	Current situation of wear	Little	0
		Medium	1
		Severe	2

Then the percentages will be put into a 3D coordinate system: CR% as X-axis, VR% as Y-axis, and IR% as Z-axis, to form a rating cube, as illustrated in Figure 7.1. Setting 50% as the border, the cube is divided into eight quadrants: Quadrant 1 (Q1) to Quadrant 8 (Q8). This eight-quadrant cube is used as a guidance in the bridge management system to determine the priorities of the maintenance or inspection of bridge components. CR takes the highest priority, and VR takes the lowest priority in the rating results. Therefore, in the scheduling of inspection and maintenance for bridge components, the priority sequence is in the order of Q1, Q2, Q3, Q4, Q5, Q6, Q7, and Q8.

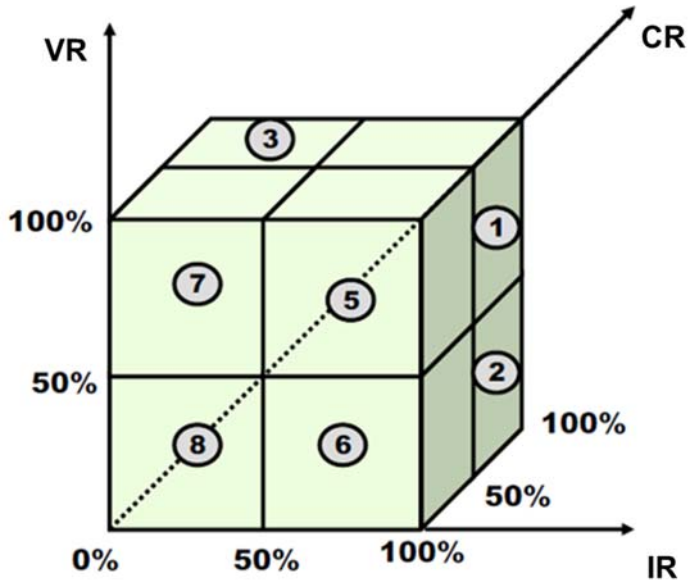

Figure 7.1 BCR cube

7.3 Procedure of Three-Dimensional BCR System

The following three steps should be taken to implement the proposed three-dimensional BCR system: (i) systematic categorization of structural components; (ii) structural analysis in terms of reliability index and fatigue life based on SHM data and FEM of the bridge; (iii) calculation of CR, VR, and IR, and formation of the three-dimensional rating cube; (iv) decision-making for priorities of activities for bridge inspection and maintenance.

The systematic categorization of structural components is a fundamental element. A well-devised categorization system will minimize the time of searching, and speed up the efficiency of the BCR. The structural reliability indices associated with all the main failure modes such as the axial, shear, flexural and torsional failure of structural

components should be analyzed. The minimum reliability index will be used in the CR. Based on strain measured by the SHM system or simulated by the FEM, stress histories of structural components or connections can be evaluated by the rain-flow method to get the stress cycles and range spectra, which will be used to estimate the fatigue life based on the Miner's Rule or any other more advanced technique.

7.4 Development of Database for BCR System

There are so many components of different types and structural characters in a bridge, as well as a large amount of required data for condition rating. To manage the bulk of information and make the BCR more efficiently, a database which is a logically coherent collection of data with some inherent meaning (Elmasri 2008) is necessary. The database is created and maintained by a database management system (DBMS), a computer software application interacting with the user, other applications, and the database itself to capture and analyze data (Wikipedia 2016). The DBMS allows users to create new databases and specify the logical structure of the data; to query and modify the data; supports the storage of very large amounts of data; to access to data with isolation and atomicity (Garcia-Molina 2008). The examples of DBMS include DB2, Oracle, FileMaker Pro, Microsoft Access, Microsoft's SQL Server, SAP and MySQL. SQL (Structured Query Language) is a widely used standard language for making interactive queries from and updating a database. As one of the DBMS, IBM's DB2 has the characteristics of integrated, open, virtualized and automatic (Chong *et*

al. 2013). It is adopted in this study to establish the database for the bridge condition rating system of the TMB.

Using the “CREATE DATABASE” command, a database for the BCR can be created. Tablespaces should then be created to store tables containing different information for the BCR, for example, the categorizations, geometric and design strength of the structural components, the BCR strategies, data associated with CR, VR and IR, metric of CR, VR and IR and the rating result, recommendations for bridge management and so on. All the information is stored in different tables or different columns of the tables. To discriminate the tablespaces and tables, comments should be made for them using the “COMMENT ON” command. Type of data listed in tables should be defined in the command of “CREATE TABLE”. All the data can be enquired easily and efficiently by the SQL in the command line processor (CLP) using the command of “SELECT”. Furthermore, the data can be modified using “UPDATE”, which makes it feasible to update any data in the BCR system and get a new result. The command “UPDATE” is also used to correlate the data in different columns of the tables based on certain qualifications or mathematical equations. Therefore, the condition rating can be executed and updated semi-automatically, and this database can be used as a reference or even guidance in the life-cycle bridge management.

7.5 Application to TMB

7.5.1 Systematic Categorization of Structural Components

The structural components of the TMB are classified into four groups: (1) suspension system group (SSG), (2) vertical structure group (VSG), (3) horizontal structure group (HSG), and (4) foundation group (FDG). The SSG includes suspension cables and suspenders; the VSG includes towers and piers; the HSG refers to the stiffening deck system which includes outer-longitudinal trusses, inner-longitudinal trusses, main cross-frames, intermediate cross-frames, plan bracings, deck, rail waybeams, bearings, movement joints, and the Tsing Yi approach deck; and the FDG includes the anchorages and foundations of towers and piers. All these structural types are further divided into structural components, as illustrated in Table 7.4.

For inventory, each structural component is assigned with a tag-name, which provides three or four types of information, namely, group name, structural type, element and location. These different types of information are separated by the "_" sign, for example, SSG_SC_MC_N means the north main cable in the suspension system group, and VSG_T_NL_MW means the north leg of Ma Wan tower in the vertical structure group.

Table 7.4 Classification of structural components of TMB

Name of Group	Name of Component
Suspension cables	Main cables Strand shoes Shoe anchor rods Anchor bolts Cable clamps & bands
Suspenders	Hangers Hanger connections: stiffeners Hanger connections: bearing plates
Towers	Legs Portals Saddles
Anchorages	Chambers Pre-stressing anchors Saddles
Piers: M1, M2, T1, T2, T3	Legs Cross-beams
Outer-longitudinal trusses	Top chord Diagonal Vertical post Bottom chord
Inner-longitudinal trusses	Top chord Diagonal Vertical post Bottom chord
Main cross-frames	Top web Sloping web Bottom web Bottom chord
Intermediate cross-frames	Top web Sloping web Bottom web Bottom chord
Plan bracings	Upper-deck Lower-deck

(Continued Table 7.4)

Name of Group	Name of Component
Deck	Troughs
	Plates
Rail waybeams	T-sections
	Top flanges
	Connections
Bearings	Rocker bearings at Ma Wan Tower
	PTFE bearings at Tsing Yi Tower
	PTFE bearings at Pier T1
	PTFE bearings at Pier T2
	PTFE bearings at Pier T3
	PTFE bearings at Tsing Yi anchorage
	Rocker bearings at M2
	PTFE bearings at M1
	Hinge bearing at Lantau anchorage
Movement joints	Highway movement joint
	Railway movement joint
Tsing Yi approach deck	Top chord
	Diagonals
	Vertical post
	Bottom chord
	Diagonals (k-bracings)

7.5.2 Structural Analysis Based on SHM Data and FEM

Based on the methodology introduced in Chapter 6, structural reliability of the longitudinal trusses and cross frames in the three instrumented sections of the stiffening deck system can be analyzed using the measured strain directly. For other structural members, the reliability should be analyzed with the help of the 3D FEM of the bridge using the site-specific live load model developed in Chapter 5. Taking the main cable as an example, the reliability analysis using the FEM is illustrated below.

The influence line for the tension of the main cable at the Tsing Yi side span is shown in Figure 7.2. Thus, the critical live load case for the main cable is that the vehicles are distributed on all lanes along the full length of the bridge, and the heavy vehicles and trains are located 530 m from the Tsing Yi tower. If the condition rating is done in detail every five years, the highway and railway load model corresponds to a return period of five years developed using the methodology introduced in Chapter 5 can be used to analyze the structural responses. For the TMB, the UDL is a normal variable with a mean value and standard deviation of 9.04 kN/m and 0.90 kN/m; the KEL is a random variable with a GEV distribution whose location, scale and shape parameters are 220 kN, 10.66 and -0.15, respectively; the weight of each of the side-by-side trains is a GEV variable with location, scale and shape parameters of 674 tonnes, 23.46 and -0.09. The lane distribution factors are 1.0, 0.3, and 0.2 for the slow, middle, and fast lane, respectively. Applying these loads to the 3D FEM of the bridge, the tension forces experienced by the studied main cable are obtained.

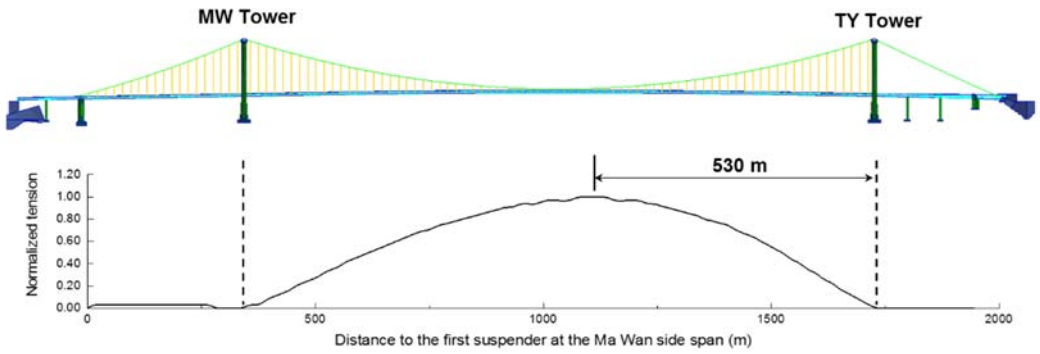

Figure 7.2 Influence line for tension force of main cable

Taking the south cable as an example, the limit state function is

$$g_T(t) = T_L - (1+e_1)T_{UDL} - (1+e_2)T_{KEL} - (1+e_3)T_{train} \quad (7.4)$$

where T_L is the maximum allowable tension strength for the cable, which is a lognormal variable, lognormal (11.16, 0.10) (corresponding to SLS); T_{UDL} is the tension induced by the UDL, which is a normal variable, normal (24876, 2488); T_{KEL} is the tension induced by the KEL, which is a GEV variable, GEV (729, 35.32,-0.15); T_{train} is the tension induced by the train, which is a GEV variable, GEV (7401, 257.61,-0.09); and e_1, e_2, and e_3 are the uncertainties associated with the FEM-obtained tensions, which are considered as normal variables which have a mean value of 0 and standard deviation of 5%. Then using the MC method, the reliability index is estimated as 6.00. Thus, the criticality factor C1 for this main cable is 1.

7.5.3 Execution of BCR

The factors of CR and VR for the structural components of the TMB are listed in Table 7.5. In inspections, the same type of structural components at different locations, such as bottom chords at the north and south side of the deck, may have different conditions. But in VR and CR up to present, when the bridge has operated for less than 20 years, they have the same point. Thus, unlike in the IR and the database, the structural components in this table are not classified by locations further, and are not indicated by a tag name as introduced in section 7.5.1. This is also for the sake of easy understanding.

In the evaluation of C3, most of them are zero except those of the PTFE bearings, in which minor repairable defects were discovered after the completion of the bridge's construction. The inspection reports are not available for this study now, and all the factors of IR are all assumed to be zero considering that the bridge is still young now comparing with its design life. After the CR, VR, and IR are estimated, the rating results, i.e. the coordinates in the BCR cube, of the structural components is obtained, and the decisions for bridge management can be made. As stated in section 7.2, the inspection and maintenance of the bridge components can be scheduled in the order of Q1, Q2, Q3, Q4, Q5, Q6, Q7, and Q8. The decision for bridge management should be specific in practice. For example, the structural components evaluated to fall in Q1 may need replacement; those fall in Q4 may need repair and special inspection; and those fall in Q8 may be considered as intact and just need routine inspection. It is a balance between structural safety and cost, which should be determined by an optimization analysis.

A database is built by IBM's DB2 to store all the information relevant to the BCR, as well as the strategy. The CR, VR, and IR of the structural components can be calculated automatically following the strategy, and the rating results can be enquired easily. The priority of maintenance and inspection can be obtained by sorting the results of quadrants in ascending order in the database. The decision for bridge management can be provided by this database as well if the guidelines are imported to the database. Using the command "UPDATE", each factor and the rating results can

be modified easily. Thus, this database can be used to assist the bridge management throughout the lifetime of the bridge.

Table 7.5 CR and VR for structural components of TMB

Name of group	Name of component	Criticality factor				CR	Vulnerability factor						VR
		C1	C2	C3	C4	(%)	VA1	VA2	VB1	VB2	VC1	VC2	(%)
Suspension cables	Main cables	1	0	0	2	37.5	1	2	2	2	0	2	50
	Strand shoes	0	0	0	0	0	2	2	1	2	0	2	50
	Shoe anchor rods	0	0	0	0	0	2	2	1	2	0	2	50
	Anchor bolts	0	0	0	0	0	2	2	1	2	0	2	50
	Cable clamps & bands	0	0	0	0	0	2	1	1	1	0	1	25
Suspenders	Hangers	1	1	0	1	38	1	1	2	1	0	1	25
	Hanger connections: stiffeners	1	0	0	0	13	2	1	2	1	0	1	33
	Hanger connections: bearing plates	1	0	0	0	13	2	1	2	1	0	1	33
Towers	Legs	0	0	0	2	25	2	2	0	1	0	1	33
	Portals	0	0	0	2	25	2	2	0	1	0	1	33
	Saddles	0	0	0	2	25	2	1	0	1	0	1	17
Anchorages	Chambers	0	0	0	2	25	1	2	0	2	0	2	17
	Pre-stressing anchors	1	0	0	2	38	1	2	0	2	0	2	17
	Saddles	0	0	0	2	25	1	2	0	2	0	2	17
Piers: M1, M2, T1, T2, T3	Legs	0	0	0	1	13	1	2	2	1	0	1	33
	Cross-beams	0	0	0	1	13	1	2	2	1	0	1	33

(Continued Table 7.5)

Name of group	Name of component	Criticality factor				CR (%)	Vulnerability factor						VR (%)
		C1	C2	C3	C4		VA1	VA2	VB1	VB2	VC1	VC2	
Outer-longitudinal trusses	Top chord	0	0	0	1	13	1	2	1	2	0	2	33
	Diagonal	1	1	0	1	38	1	2	1	2	0	2	33
	Vertical post	1	1	0	1	38	1	2	1	2	0	2	33
	Bottom chord	1	1	0	1	38	1	2	1	2	0	2	33
Inner-longitudinal trusses	Top chord	0	0	0	1	13	1	2	1	2	0	2	33
	Diagonal	0	1	0	1	25	1	2	1	2	0	2	33
	Vertical post	0	1	0	1	25	1	2	1	2	0	2	33
	Bottom chord	0	1	0	1	25	1	2	1	2	0	2	33
Main cross-frames	Top web	0	0	0	1	13	1	2	1	2	0	2	33
	Sloping web	0	1	0	1	25	1	2	1	2	0	2	33
	Bottom web	0	1	0	1	25	1	2	1	2	0	2	33
	Bottom chord	1	1	0	1	38	1	2	1	2	0	2	33
Intermediate cross-frames	Top web	0	0	0	1	13	1	2	1	2	0	2	33
	Sloping web	0	1	0	1	25	1	2	1	2	0	2	33
	Bottom web	0	1	0	1	25	1	2	1	2	0	2	33
	Bottom chord	1	1	0	1	38	1	2	1	2	0	2	33
Plan bracings	Upper-deck	1	0	0	1	25	2	1	1	1	0	1	25
	Lower-deck	1	0	0	1	25	2	1	1	1	0	1	25

(Continued Table 7.5)

Name of group	Name of component	Criticality factor				CR	Vulnerability factor						VR
		C1	C2	C3	C4	(%)	VA1	VA2	VB1	VB2	VC1	VC2	(%)
Deck	Troughs	1	1	0	1	38	1	2	1	2	0	2	33
	Plates	1	1	0	1	38	1	2	1	2	0	2	33
Rail waybeams	T-sections	0	2	0	2	50	2	1	1	1	0	1	25
	Top flanges	0	2	0	2	50	2	1	1	1	0	1	25
	Connections	0	2	0	2	50	2	1	1	1	0	1	25
Bearings	Rocker bearings at Ma Wan Tower	1	0	0	1	25	2	1	1	1	1	1	33
	PTFE bearings at Tsing Yi Tower	1	0	1	1	38	2	2	2	2	1	2	83
	PTFE bearings at Pier T1	1	0	1	1	38	2	2	2	2	1	2	83
	PTFE bearings at Pier T2	1	0	1	1	38	2	2	2	2	1	2	83
	PTFE bearings at Pier T3	1	0	1	1	38	2	2	2	2	1	2	83
	PTFE bearings at Tsing Yi anchorage	1	0	1	1	38	2	2	2	2	1	2	83
	Rocker bearings at M2	1	0	0	1	25	2	1	1	1	1	1	33
	PTFE bearings at M1	1	0	1	1	38	2	2	2	2	1	2	83
	Hinge bearing at Lantau anchorage	1	0	0	1	25	2	2	1	2	1	2	67
Movement joints	Highway movement joint	0	2	0	1	38	1	2	2	2	1	2	67
	Railway movement joint	0	2	0	1	38	1	2	2	2	1	2	67

(Continued Table 7.5)

Name of group	Name of component	Criticality factor				CR (%)	Vulnerability factor						VR (%)
		C1	C2	C3	C4		VA1	VA2	VB1	VB2	VC1	VC2	
Tsing Yi approach deck	Top chord	0	0	0	1	13	1	2	1	2	0	2	33
	Diagonals	1	1	0	1	38	1	2	1	2	0	2	33
	Vertical post	1	1	0	1	38	1	2	1	2	0	2	33
	Bottom chord	1	1	0	1	38	1	2	1	2	0	2	33
	Diagonals (k-bracings)	0	1	0	1	25	1	2	1	2	0	2	33

7.6 Summary

To incorporate the SHM data into the bridge management system and provide guidelines for bridge maintenance and inspection, this chapter proposed an SHM-based bridge condition rating system. This system includes criticality rating, vulnerability rating, and inspection-based rating. The criticality rating estimates the strength surplus of the structural components and the consequence of their failure, based on SHM data and the FEM of the bridge. The live load models obtained based on long-term SHM data are applied to the FEM to analyze the structural performance. The vulnerability rating estimates the exposure of the structural components to the adverse effects, and the likelihood of detection in visual inspections. The as-built report and maintenance record are important information for vulnerability rating. The inspection-based rating assesses the current deterioration, crack and wear of the structural components according to the observations of inspections. The SHM data, FEM, inspection results, as-built report, and maintenance record of the bridge are integrated into this bridge rating system, thus a more objective and accurate bridge condition rating will be obtained. A database is developed for this system, in order that all the data and rating results can be enquired and updated efficiently throughout the life-cycle bridge management. Benefiting from the proposed condition rating system, the bridge managers can schedule the priorities of bridge inspection and maintenance activities under a limited budget.

CHAPTER 8

CONCLUSIONS AND RECOMMENDATIONS

8.1 Conclusions

A wealth of high-quality SHM data has been collected from the TMB, which is currently the world's longest suspension bridge carrying both highway and railway traffic, since the completion of its construction in 1997. Taking advantage of the data measured from the TMB, this thesis studied how to integrate the long-term SHM data into the bridge condition assessment and bridge management system. The major contributions of the work are as follows.

(i) Development of an efficient and automatic wavelet-based signal preprocessing methodology in terms of denoising, despiking, and decomposing for long-term SHM data

With the merit of multi-resolution and time-frequency scale, the WT is a potential tool to process the long-term SHM data. A wavelet-based signal preprocessing methodology was proposed to remove the noises, spikes, and trends embedded in the signals, and separate different signal sources to meet needs of some specific researches.

Besides effectiveness, automation and computational efficiency of the signal preprocessing techniques were especially considered due to the enormous amount of long-term SHM data.

It has been proven that none of the existing methods outperform others in all aspects, thus the two types of wavelet denoising approaches: the classical threshold method and the Bayesian method, were studied and compared to remove the noises in the data.

As the usual case is, there are only a few spikes in the SHM signals at a certain time interval, say, one day. Identifying the spikes first and then focusing on their neighboring time domain to eliminate them by the wavelet despiking algorithm, was found to be far more computationally efficient than using the wavelet despiking algorithm directly. A novel wavelet-based spike detection methodology was adopted to identify the spikes in the long-term SHM data. This methodology consists of a combination of several techniques, including multiresolution wavelet decomposition, statistics, detection theory and estimation theory. A wavelet despiking algorithm was adopted to eliminate spikes in the long-term SHM data. This algorithm does not simply interpolate values at the time of spikes, but removes spikes only in their occurrence frequencies, retaining information from any unaffected frequency. Furthermore, it is unsupervised, data-driven, and spatially-adaptive.

Taking the characteristics of different signals into account, different signal source separation methods were proposed. For the signal sources with frequencies easy to

discriminate, they could be separated straightforwardly using the DWT, because the DWT is a filter bank in a sense. For those with overlapped frequencies but distinct magnitudes, they can be separated by the wavelet despiking algorithm, considering the sources with large magnitudes as spike-like signals.

(ii) Study of extreme value distribution of live load effects and extrapolation of characteristic values

Both the BM and POT approaches were adopted to study the extreme values of live load effects based on nine years of strain data, including to establish the probabilistic models and to extrapolate the characteristic values. The parameters for the EVDs and corresponding return levels were estimated by the likelihood-based methods (MLE and PLE) and BE method. It was found that the accuracy of the extrapolated characteristic value of extremes is more dependent on data quality than the extrapolation technique adopted. Thus, taking the advantage of time referring into consideration, the BM approach is selected to establish probabilistic models of extreme variables for structural reliability analysis. The characteristic values of the stresses with different return periods can be used to develop live load models for the FEM-based bridge condition assessment corresponding to different limit states, such as ULS and SLS.

(iii) Development of site-specific live load models

The highway and railway load models were developed based on the continuously collected data, especially the WIM data, strain data and the CCTV recordings of the traffic on the bridge. The highway load is modelled as a combination of a UDL and a KEL. The UDL represents the traffic flow, and the KEL simulates an overloaded vehicle. The UDL is determined based on the WIM data, including the gross vehicle weight and axle distance of the vehicles, proportion of different vehicles, and CCTV recordings of the traffic. The KEL is calculated inversely by the full 3D FEM of the bridge, targeting a certain stress level in a typical point of the deck, which was obtained by extreme value extrapolation conducted in (ii). The KEL corresponding to an extreme stress with a five-year return period was used in the SLS evaluation of the bridge; and that corresponding to a stress with a return period of 120 years was used in the ULS evaluation. The multi-lane factors of the highway loads were determined by the data-driven UDL, while the dynamic impact factor was ignored based on the conclusions of previous studies.

The railway load was modelled by a series of concentrated forces representing the wheel loads of an eight-car train. Similar to the KEL, the gross train weight (GTW) was also calculated inversely by the FEM of the bridge, targeting a certain stress level for the SLS and ULS evaluation, respectively. The GTW was distributed to each wheel of the train following the configuration of the standard train defined by the MTR Cooperation of Hong Kong.

(iv) Investigation of evolution of structural reliability based on long-term strain data

Based on nine years of strain data measured from the stiffening deck system of the TMB, a reliability-based framework was proposed to incorporate the long-term SHM data into bridge condition assessment. With the annual probabilistic models of daily maximum load effects, the point-in-time reliability indices were estimated for each year first. The corrosion model proposed by previous studies for structural steel was adopted, focusing on the case of marine environment and high corrosion rate. The reliability indices were estimated using both the FOSM and MC method, and a good match was found. Recognizing the positive effect of the service-proven load history and the variation of probability distributions for annual load effects, the annual structural reliabilities were updated subsequently. Both the Bayesian updating and the classical frequentist approaches were employed. After updating, a more balanced result was obtained. Owing to the deliberate arrangement of sensor arrays, reliability indices at both the structural component level and deck section level were studied. To get a knowledge of the future reliabilities, the lifetime reliability profiles for instrumented members were also studied. The annual PDF of daily maximum load effects estimated based on all the nine years of data is used as the load demand model. A target reliability index is suggested to be selected to facilitate the decision-making for bridge management.

(v) Establishment of an SHM-based bridge condition rating system

Results of bridge condition assessment are preferred to be represented by explicit indices. This bridge condition rating (BCR) system makes it easy for the bridge managers to optimize the bridge maintenance priority and strategy. An SHM-based BCR system was developed to integrate the SHM data into the bridge management system. It consists of criticality rating, vulnerability rating, and inspection-based rating. The criticality rating estimates the spare strength of the structural components and the consequence of their failure. For the instrumented structural components, the SHM data are made full use; for those without sensors, a full 3D FEM of the bridge is employed to conduct structural analysis using the live load models obtained in (iv). The vulnerability rating estimates the exposure of the structural components to the adverse effects, and the likelihood of detection in visual inspections. To do vulnerability rating, the as-built report and maintenance record are important information. The inspection-based rating assesses the current condition of the structural components according to the observations of inspections. Because the SHM data, FEM, inspection results, as-built report, and maintenance record of the bridge are incorporated into this bridge rating system, a more objective and accurate bridge condition rating can be obtained. A database was developed for this system, so that all the data and rating results can be enquired and updated efficiently during the life-cycle bridge management.

8.2 Recommendations

The developed methodology to integrate the SHM data into bridge condition assessment is still in its infancy. To improve the proposed methodology and make the bridge managers benefit more from the high-tech but costly SHM systems, more research is expected to be carried out in the future. The recommendations for the future research are as follows.

(i) Multi-hazard risk assessment of the bridge

The TMB has operated for about 20 years up to now, but is at a young age in comparison with its design life, 120 years. During this period, only two typhoons of signal number 10 can be regarded as a challenge for the bridge. However, based on the measured data, the bridge performed well in these two typhoons due to the rational design of the bridge (e.g., adopting the stiffening deck system composed of a streamlined box-shaped steel truss girder with a central air-gap) (Xia 2014). As the bridge ages, its sensitivity to the extreme events will increase. Multi-hazard including strong typhoon, overloaded traffic, ship collision, and earthquake should be taken into consideration in the safety evaluation of the bridge.

(ii) Damage detection algorithm based on long-term data using techniques such as statistical pattern recognition and data fusion

This thesis mainly develops a methodology to integrate long-term SHM data into bridge condition assessment. The long-term variation in load-carrying capacity, i.e., the structural reliability, was focused, but detection of structural damage was not addressed. However, a high expectation put on the SHM technology is to detect damage in structures. The large amount of high-quality, long-term, and multi-sensed SHM data collected from the TMB provides a unique opportunity to study this problem and verify the existing algorithms. The statistical pattern recognition and data fusion techniques can be applied, and new specific methods may be developed based on the data.

(iii) Development of a mathematical framework to incorporate costs into a life-cycle bridge management system

The budget for bridge management is usually very limited, thus the life-cycle bridge management is an optimization problem. The SHM-based BCR system provides the indices about the structural safety or serviceability, but decisions such as how many structural components should be considered in the condition rating, whether the imperfect structural component should be repaired or leave it as it is, the intervals between inspections and detail condition assessment and so on, should be made taking the economic factor into account. In addition, though the long-term SHM technology has a potential to provide revolutionary improvement for the bridge design and assessment, it is very costly in both instrument and management. Thus, methods to reduce the SHM cost such as the optimized layout of the sensors should be studied.

(iv) Establishment of a linkage to connect SHM technology, and bridge design and assessment standards

Due to the absence of information about load and structural behaviors, the existing bridge design and evaluation standards use some empirical models or factors, and they are still in the stage of semi-probabilistic solution. With the rapid development of SHM technologies and increasing applications to bridges, performance-based bridge design and assessment may be realized. Profiting from the existing SHM experience, the standards or specifications can be formulated through the collaboration of researchers and engineers worldwide in this field.

REFERENCES

AASHTO. (2003). *Guide Manual for Condition Evaluation and Load and Resistance Factor Rating (LRFR) of Highway Bridges*. Washington, D.C.

AASHTO. (2008). *Manual for Bridge Evaluation*. Washington, D.C.

AASHTO. (2011). *Manual for Bridge Evaluation*. Washington, D.C.

AASHTO. (2015). *LRFD Bridge Design Specifications*. Washington, D.C.

Abe, M., and Fujino, Y. (2009). "Bridge monitoring in Japan." *Encyclopedia of Structural Health Monitoring*, Wiley Online Library.

Abramovich, F., and Sapatinas, T. (1999). "Bayesian approach to wavelet decomposition and shrinkage." *Bayesian Inference in Wavelet-Based Models*, Springer, 33–50.

Abramovich, F., Sapatinas, T., and Silverman, B. W. (1998). "Wavelet thresholding via a Bayesian approach." *Journal of the Royal Statistical Society: Series B (Statistical Methodology)*, Wiley Online Library, 60(4), 725–749.

Addison, P. S. (2005). "Wavelet transforms and the ECG: a review." *Physiological Measurement*, IOP Publishing, 26(5), 155-199.

Akgül, F., and Frangopol, D. M. (2004a). "Bridge rating and reliability correlation: Comprehensive study for different bridge types." *Journal of Structural Engineering*, American Society of Civil Engineers, 130(7), 1063–1074.

Akgül, F., and Frangopol, D. M. (2004b). "Time-dependent interaction between load rating and reliability of deteriorating bridges." *Engineering Structures*, Elsevier, 26(12), 1751–1765.

Aktan, A. E., Farhey, D. N., Brown, D. L., Dalal, V., Helmicki, A. J., Hunt, V. J., and Shelley, S. J. (1996). "Condition assessment for bridge management." *Journal of Infrastructure Systems*, American Society of Civil Engineers, 2(3), 108–117.

Albrecht, P., and Naeemi, A. H. (1984). "Performance of weathering steel in bridges." *NCHRP Report*, (272), Transportation Research Board, National Research Council, Washington, D.C.

Alfaouri, M., and Daqrouq, K. (2008). "ECG signal denoising by wavelet transform thresholding." *American Journal of Applied Sciences*, 5(3), 276–281.

Ang, A. H.-S., and Cornell, C. A. (1974). "Reliability bases of structural safety and design." *Journal of the Structural Divisio*n, 100(9), 1755-1769.

Ang, A. H.-S., and Tang, W. H. (1975). *Probability Concepts in Engineering Planning and Design. Vol. I, Basic Principles*. Wiley, New York.

Ang, A. H.-S., and Tang, W. H. (1984). *Probability concepts in engineering planning and design, Volume II, Decision, Risk and Reliability*. Wiley, New York.

Ang, A. H.-S., and Tang, W. H. (2007). *Probability Concepts in Engineering Planning and Design*. Wiley, New York.

Antoni, J. (2007). “Fast computation of the kurtogram for the detection of transient faults.” *Mechanical Systems and Signal Processing*, Elsevier, 21(1), 108–124.

Antoniadis, A., Bigot, J., and Sapatinas, T. (2001). “Wavelet estimators in nonparametric regression: a comparative simulation study.” *Journal of Statistical Software*, 6(6), 1-83.

ASCE. (2013). Report card for America’s Infrastructure. Retrieved October 18, 2014, from *http://www.infrastructurereportcard.org/*.

Ayyub, B. M., and McCuen, R. H. (2011). *Probability, Statistics, and Reliability for Engineers and Scientists*. CRC press.

BA35/90. (1990). “The Inspection and repair of concrete highway structures.” *Design Manual for Roads and Bridges. Vol. 3, Section 3, Part 2*, Highways Agency, London UK.

BA63/94. (1994). *Inspection of Highway Structures. Design Manual for Roads and Bridges. Vol. 3, Section 1, Part 5*. Highways Agency, London, U.K.

Bailey, S. F. (1996). “Basic Principles and Load Models for the Structural Safety Evaluation of Existing Road Bridges.” Ph.D. thesis, University of Southampton, UK.

Bailey, S. F., and Bez, R. (1999). “Site specific probability distribution of extreme traffic action effects.” *Probabilistic Engineering Mechanics*, Elsevier, 14(1), 19–26.

Bakht, B., and Jaeger, L. G. (1990). “Bridge testing-a surprise every time.” *Journal of Structural Engineering*, American Society of Civil Engineers, 116(5), 1370-1383.

Basheer, P., Chidiact, S., and Long, A. (1996). “Predictive models for deterioration of concrete structures.” *Construction and Building Materials*, Elsevier, 10(1), 27–37.

BD63/94. (1994). “Inspection of highway structures.” *Design Manual for Roads and Bridges. Vol. 3, Section 1, Part 4*. Highways Agency, London, U.K.

BD79/13. (2013). “The Management of sub-standard highway structures.” *Design Manual for Roads and Bridges. Vol. 3, Section 4, Part 18*. Highways Agency, London, U.K.

BDT. (1989). *Departmental Standard BD 37/88, Loads for Highway Bridges*. Department of British Department of Transport, South Ruislip, Middlesex, England.

Beard, A., and Young, J. (1995). “Aspect of the design of the Tsing Ma Bridge.” *Proceedings of International Conference on Bridge into 21st Century, Impressions Design & Print Ltd., Hong Kong*, 93–100.

Beck, J. L., and Au, S.-K. (2002). “Bayesian updating of structural models and reliability using Markov chain Monte Carlo simulation.” *Journal of Engineering Mechanics*, American Society of Civil Engineers, 128(4), 380–391.

Beheshti, S., Dahleh, M., and others. (2005). “A new information-theoretic approach to signal denoising and best basis selection.” *Signal Processing, IEEE Transactions on*, IEEE, 53(10), 3613–3624.

Beirlant, J., Goegebeur, Y., Segers, J., and Teugels, J. (2006). *Statistics of Extremes: Theory and Applications*. John Wiley & Sons.

Benjamin, J. R., and Cornell, C. A. (1970). *Probability, Statistics, and Decision for Civil Engineers*. McGraw Hill, Inc.

Berger, J. O. (2013). *Statistical Decision Theory and Bayesian Analysis*. Springer Science & Business Media.

Bernardo, J. M., and Smith, A. F. (2009). *Bayesian Theory*. John Wiley & Sons.

Bhattacharya, B., Li, D., and Chajes, M. (2008). "Bridge rating using in-service data in the presence of strength deterioration and correlation in load processes." *Structure and Infrastructure Engineering*, Taylor & Francis, 4(3), 237–249.

Bhattacharya, B., Li, D., Chajes, M., and Hastings, J. (2005). "Reliability-based load and resistance factor rating using in-service data." *Journal of Bridge Engineering*, American Society of Civil Engineers, 10(5), 530–543.

Blakelock, R., Day, W., and Chadwick, R. (1999). *Bridge Condition Index*. Thomas Telford, London.

Boller, C., Chang, F.-K., and Fujino, Y. (2009). *Encyclopedia of Structural Health Monitoring*. John Wiley.

Box, G. E., and Tiao, G. C. (2011). *Bayesian Inference in Statistical Analysis*. John Wiley & Sons.

Braun, S. (2011). "The synchronous (time domain) average revisited." *Mechanical Systems and Signal Processing*, Elsevier, 25(4), 1087–1102.

Brechet, L., Lucas, M.-F., Doncarli, C., and Farina, D. (2007). "Compression of biomedical signals with mother wavelet optimization and best-basis wavelet packet selection." *Biomedical Engineering, IEEE Transactions on*, IEEE, 54(12), 2186–2192.

Breiman, L. (1995). "Better subset regression using the nonnegative garrote." *Technometrics*, Taylor & Francis Group, 37(4), 373–384.

Brooman, H., and Wootton, N. (2000). "Management of bridge maintenance-a local authority perspective." *Bridge Management 4: Inspection, Maintenance, Assessment and Repair*, 753–761.

Brown, J. H. (1987). *The Performance of Concrete in Practice :A Field Study of Highway Bridges*. Department of Transport, UK.

Brownjohn, J. M. (2007). "Structural health monitoring of civil infrastructure." *Philosophical Transactions of the Royal Society of London A: Mathematical, Physical and Engineering Sciences*, The Royal Society, 365(1851), 589–622.

Bruls, A., Croce, P., Sanpaolesi, L., and Sedlacek, G. (1996). "ENV 1991-Part 3: Traffic loads on bridges Calibration of road load models for road bridges." *IABSE Reports*, International Association for Bridge, 439–454.

BSI. (2006). *BS 5400: Steel, Concrete and Composite Bridges*. British Standards Institution, London.

Buckland, P. G. (1981). "Recommended design loads for bridges." *Journal of the Structural Division*, American Society of Civil Engineers, 107(7), 1161–1213.

Buckland, P. G. (1991). "North American and British long-span bridge loads." *Journal of Structural Engineering*, American Society of Civil Engineers, 117(10), 2972–2987.

Buckland, P. G., McBryde, J. P., Navin, F. P., and Zidek, J. V. (1978). "Traffic loading

of long span bridges." *Transportation Research Record*, 2, 146-154.
Buckland, P. G., McBryde, J. P., Zidek, J. V., and Navin, F. P. (1980). "Proposed vehicle loading of long-span bridges." *Journal of the Structural Division*, American Society of Civil Engineers, 106(4), 915–932.
Cai, C., and Harrington, P. de B. (1998). "Different discrete wavelet transforms applied to denoising analytical data." *Journal of Chemical Information and Computer Sciences*, ACS Publications, 38(6), 1161–1170.
Cai, T. T. (1999). "Adaptive wavelet estimation: a block thresholding and oracle inequality approach." *Annals of Statistics*, 27(3), 898–924.
Cantero, D., and Basu, B. (2015). "Railway infrastructure damage detection using wavelet transformed acceleration response of traversing vehicle." *Structural Control and Health Monitoring*, Wiley Online Library, 22(1), 62–70.
Caprani, C. C. (2005). "Probalistic analysis of highway bridge traffic loading." Ph.D. thesis, Dublin Institute of Technology, Dublin, Ireland.
Caprani, C. C. (2012). "Calibration of a congestion load model for highway bridges using traffic microsimulation." *Structural Engineering International*, International Association for Bridge and Structural Engineering, 22(3), 342–348.
Caprani, C. C., OBrien, E. J., and McLachlan, G. J. (2008). "Characteristic traffic load effects from a mixture of loading events on short to medium span bridges." *Structural Safety*, Elsevier, 30(5), 394–404.
Carden, E. P., and Fanning, P. (2004). "Vibration based condition monitoring: a review." *Structural Health Monitoring*, SAGE Publications, 3(4), 355–377.
Cardini, A., and DeWolf, J. T. (2008). "Long-term structural health monitoring of a multi-girder steel composite bridge using strain data." *Structural Health Monitoring*, SAGE Publications 8(1), 47-58.
Carlin, B. P., and Louis, T. A. (2008). *Bayesian Methods for Data Analysis*. CRC Press.
Castillo, E. (1988). *Extreme Value Theory in Engineering*. Academic Press, San Diego.
Castillo, E. (2012). *Extreme Value Theory in Engineering*. Elsevier.
Catbas, F. N., and Aktan, A. E. (2009). "Development of a Monitoring System for a Long-span Cantilever Truss Bridge." *Encyclopedia of Structural Health Monitoring*, Wiley Online Library.
Catbas, F. N., Susoy, M., and Frangopol, D. M. (2008). "Structural health monitoring and reliability estimation: Long span truss bridge application with environmental monitoring data." *Engineering Structures*, Elsevier, 30(9), 2347–2359.
Cattan, J., and Mohammadi, J. (1997). "Analysis of bridge condition rating data using neural networks." *Computer-Aided Civil and Infrastructure Engineering*, Wiley Online Library, 12(6), 419–429.
CEN. (2002). *Eurocode 1: Actions on Structures*. European Committee for Standardization, Brussels, Belgium.
Chajes, M. J., Mertz, D. R., and Commander, B. (1997). "Experimental load rating of a posted bridge." *Journal of Bridge Engineering*, American Society of Civil Engineers, 2(1), 1–10.
Chan, T. H., Miao, T., and Ashebo, D. B. (2005). "Statistical models from weigh-in-motion data." *Structural Engineering and Mechanics*, Taejon, Korea: Techno-

Press, c1993-, 20(1), 85–110.
Chang, P. C., Flatau, A., and Liu, S. (2003). “Review paper: health monitoring of civil infrastructure.” *Structural health monitoring*, Sage Publications, 2(3), 257–267.
Chen, N.-Z. (2016). “Hull girder reliability assessment for FPSOs.” *Engineering Structures*, Elsevier, 114, 135–147.
Chen, Z. W. (2010). “Fatigue and reliability analyses of multiload suspension bridges with WASHMS.” Ph.D. Dissertation, The Hong Kong Polytechnic University.
Chipman, H. A., Kolaczyk, E. D., and McCulloch, R. E. (1997). “Adaptive Bayesian wavelet shrinkage.” *Journal of the American Statistical Association*, Taylor & Francis, 92(440), 1413–1421.
Chong, R. F., Dang, M., Snow, D. R., and Wang, X. (2013). *Introduction to DB2*. Retrieved.
Chryssanthopoulos, M., and Sterritt, G. (2002). “Integration of deterioration modeling and reliability assessment for reinforced concrete bridge structures.” *First ASRANet International Colloquium*, Citeseer.
Chui, C. K. (2014). *An Introduction To Wavelets*. Academic press.
Clyde, M., and George, E. I. (2000). “Flexible empirical Bayes estimation for wavelets.” *Journal of the Royal Statistical Society: Series B (Statistical Methodology)*, Wiley Online Library, 62(4), 681–698.
Coifman, R. R., and Donoho, D. L. (1995). *Translation-Invariant Denoising*. Springer.
Coles, S. (2001). *An Introduction to Statistical Modeling of Extreme Values*. Springer.
Congdon, P. (2002). *Bayesian Statistical Modeling*. IOP Publishing.
Cooper, D. I. (1997). “Development of short span bridge-specific assessment live loading.” *Safety of Bridges*, P. C. Das, ed., Thomas Telford, London, 64–89.
Cornell, C. A. (1967). “Bounds on the reliability of structural systems.” *Journal of the Structural Division*, 93(1), 171–200.
Costabel, S., and Müller-Petke, M. (2014). “Despiking of magnetic resonance signals in time and wavelet domains.” *Near Surface Geophysics*, 12(2), 185–197.
Crespo-Minguillón, C., and Casas, J. R. (1997). “A comprehensive traffic load model for bridge safety checking.” *Structural Safety*, Elsevier, 19(4), 339–359.
CSA. (2006). *Canadian Highway Bridge Design Code*. Canadian Standards Association, CSA International, Toronto, Canada.
Czarnecki, A. A., and Nowak, A. S. (2008). “Time-variant reliability profiles for steel girder bridges.” *Structural Safety*, Elsevier, 30(1), 49–64.
Das, P. C. (1998a). “New developments in bridge management methodology.” *Structural Engineering International*, International Association for Bridge and Structural Engineering, 8(4), 299–302.
Das, P. C. (1998b). “Application of reliability analysis in bridge management.” *Engineering Structures*, Elsevier, 20(11), 957–959.
Das, P. C. (1999). “Prioritization of bridge maintenance needs.” *Case Studies in Optimal Design and Maintenance Planning of Civil Infrastructure Systems*, ASCE, Reston, Virginia, 26–44.
Daubechies, I. (1992). *Ten Lectures on Wavelets*. SIAM.
De Moortel, I., and Hood, A. (2000). “Wavelet analysis and the determination of

coronal plasma properties." Astronomy and Astrophysics, 363, 269–278.
DeWolf, J. T., Lauzon, R. G., and Culmo, M. P. (2002). "Monitoring bridge performance." *Structural Health Monitoring*, SAGE Publications, 1(2), 129–138.
Doebling, S. W., Farrar, C. R., Prime, M. B., and Shevitz, D. W. (1996). *Damage Identification and Health Monitoring of Structural And Mechanical Systems from Changes in Their Vibration Characteristics: A Literature Review*. Los Alamos National Lab., USA.
Donoho, D. L. (1995). "Denoising by soft-thresholding." *Information Theory, IEEE Transactions on*, IEEE, 41(3), 613–627.
Donoho, D. L., and Johnstone, I. M. (1995). "Adapting to unknown smoothness via wavelet shrinkage." *Journal of the American Statistical Association*, Taylor & Francis Group, 90(432), 1200–1224.
Donoho, D. L., Johnstone, I. M., Kerkyacharian, G., and Picard, D. (1995). "Wavelet shrinkage: asymptopia?" *Journal of the Royal Statistical Society. Series B (Methodological)*, 57(2), 301–369.
Donoho, D. L., Johnstone, I. M., and others. (1998). "Minimax estimation via wavelet shrinkage." *The Annals of Statistics*, Institute of Mathematical Statistics, 26(3), 879–921.
Donoho, D. L., and Johnstone, J. M. (1994). "Ideal spatial adaptation by wavelet shrinkage." *Biometrika*, Biometrika Trust, 81(3), 425–455.
Draper, N. R., and Smith, H. (2014). *Applied Regression Analysis*. John Wiley & Sons.
Dubin, E. E., and Yanev, B. S. (2001). "Managing the East River bridges in New York City." *The 6th Annual International Symposium on NDE for Health Monitoring and Diagnostics*, International Society for Optics and Photonics, 60–74.
Ehrentreich, F. (2002). "Wavelet transform applications in analytical chemistry." *Analytical and Bioanalytical Chemistry*, Springer, 372(1), 115–121.
Ellingwood, B. (1980). *Development of a Probability based Load Criterion for American National Standard A58: Building Code Requirements for Minimum Design Loads in Buildings and Other Structures*. USA Department of Commerce, National Bureau of Standards.
Ellingwood, B., MacGregor, J. G., Galambos, T. V., and Cornell, C. A. (1982). "Probability based load criteria: load factors and load combinations." *Journal of the Structural Division*, American Society of Civil Engineers, 108(5), 978–997.
Ellingwood, B. R. (1996). "Reliability-based condition assessment and LRFD for existing structures." *Structural Safety*, Elsevier, 18(2), 67–80.
Ellingwood, B. R. (2000). "LRFD: implementing structural reliability in professional practice." *Engineering Structures*, Elsevier, 22(2), 106–115.
Elmasri, R. (2008). *Fundamentals of Database Systems*. Pearson Education India.
Enright, B. (2010). "Simulation of traffic loading on highway bridges." Ph.D. thesis, Dublin Institute of Technology, Dublin, Ireland.
Enright, B., Carey, C., and Caprani, C. C. (2013). "Microsimulation evaluation of Eurocode load model for American long-span bridges." *Journal of Bridge Engineering*, 18(12), American Society of Civil Engineers, 1252-1260.
Enright, M. P., and Frangopol, D. M. (1998). "Service-life prediction of deteriorating

concrete bridges." *Journal of Structural Engineering*, American Society of Civil Engineers, 124(3), 309–317.
Enright, M. P., and Frangopol, D. M. (1999a). "Condition prediction of deteriorating concrete bridges using Bayesian updating." *Journal of Structural Engineering*, American Society of Civil Engineers, 125(10), 1118–1125.
Enright, M. P., and Frangopol, D. M. (1999b). "Reliability-based condition assessment of deteriorating concrete bridges considering load redistribution." *Structural Safety*, Elsevier, 21(2), 159–195.
Estes, A. C. (1997). *A System Reliability Approach to The Lifetime Optimization of Inspection and Repair of Highway Bridges.* DTIC Document.
Estes, A. C., and Frangopol, D. M. (1999). "Repair optimization of highway bridges using system reliability approach." *Journal of Structural Engineering*, American Society of Civil Engineers, 125(7), 766–775.
Estes, A. C., and Frangopol, D. M. (2003). "Updating bridge reliability based on bridge management systems visual inspection results." *Journal of Bridge Engineering*, American Society of Civil Engineers, 8(6), 374–382.
Faber, M. H., Val, D. V., and Stewart, M. G. (2000). "Proof load testing for bridge assessment and upgrading." *Engineering Structures*, Elsevier, 22(12), 1677–1689.
Farrar, C. R., and Worden, K. (2007). "An introduction to structural health monitoring." *Philosophical Transactions of the Royal Society of London A: Mathematical, Physical and Engineering Sciences*, The Royal Society, 365(1851), 303–315.
FHWA. (2014). National Bridge Inventory. Retrieved October 18, 2014, from *https://www.fhwa.dot.gov/bridge/nbi/ascii.cfm*.
Flint, A., and Jacob, B. (1996). "Extreme traffic loads on road bridges and target values of their effects for code calibration." *IABSE Reports*, IABSE International Association for Bridge, 469–478.
Fodor, I. K., and Kamath, C. (2003). "Denoising through wavelet shrinkage: an empirical study." *Journal of Electronic Imaging*, International Society for Optics and Photonics, 12(1), 151–160.
Foster, G. (1996). "Wavelets for period analysis of unevenly sampled time series." *The Astronomical Journal*, 112(4), 1709-1729.
Frangopol, D. M (2011). "Life-cycle performance, management, and optimisation of structural systems under uncertainty: accomplishments and challenges 1." *Structure and Infrastructure Engineering*, 6 (2011), 389-413.
Frangopol, D. M., and Estes, A. C. (1997). "Lifetime bridge maintenance strategies based on system reliability." *Structural Engineering International*, International Association for Bridge and Structural Engineering, 7(3), 193–198.
Frangopol, D. M., Kong, J. S., and Gharaibeh, E. S. (2001). "Reliability-based life-cycle management of highway bridges." *Journal of Computing in Civil Engineering*, American Society of Civil Engineers, 15(1), 27–34.
Frangopol, D. M., and Liu, M. (2007). "Maintenance and management of civil infrastructure based on condition, safety, optimization, and life-cycle cost." *Structure and Infrastructure Engineering*, Taylor & Francis, 3(1), 29–41.
Frangopol, D. M., Strauss, A., and Kim, S. (2008). "Bridge reliability assessment

based on monitoring." *Journal of Bridge Engineering*, American Society of Civil Engineers, 13(3), 258–270.
Freudenthal, A. M. (1956). "Safety and the probability of structural failure." *American Society of Civil Engineers Transactions*, 121, 1337-1397.
Frisch, M., and Messer, H. (1992). "The use of the wavelet transform in the detection of an unknown transient signal." *Information Theory, IEEE Transactions on*, IEEE, 38(2), 892–897.
Friswell, M. I. (2007). "Damage identification using inverse methods." *Philosophical Transactions of the Royal Society of London A: Mathematical, Physical and Engineering Sciences*, The Royal Society, 365(1851), 393–410.
Fugal, D. L. (2009). *Conceptual Wavelets in Digital Signal Processing: An In-Depth, Practical Approach for the Non-Mathematician*. Space & Signals Technical Pub.
Fujino, Y., Siringoringo, D. M., and Abe, M. (2009). "The needs for advanced sensor technologies in risk assessment of civil infrastructures." *Smart Structures and Systems*, Techno-Press, 5(2), 173–191.
Gamerman, D., and Lopes, H. F. (2006). *Markov Chain Monte Carlo: Stochastic Simulation for Bayesian Inference*. CRC Press.
Gao, H.-Y. (1998). "Wavelet shrinkage denoising using the non-negative garrote." *Journal of Computational and Graphical Statistics*, Taylor & Francis, 7(4), 469–488.
Gao, H.-Y., and Bruce, A. G. (1997). "WaveShrink with firm shrinkage." *Statistica Sinica*, 855–874.
Garcia-Molina, H. (2008). *Database Systems: the Complete Book*. Pearson Education India.
Gelman, A., Carlin, J. B., Stern, H. S., and Rubin, D. B. (2014). *Bayesian Data Analysis*. Taylor & Francis.
Geman, S., and Geman, D. (1984). "Stochastic relaxation, Gibbs distributions, and the Bayesian restoration of images. " *IEEE Transactions on Pattern Analysis and Machine Intelligence*, PAMI-6(6), 721-741.
George, E. I., and McCulloch, R. E. (1993). "Variable selection via Gibbs sampling." *Journal of the American Statistical Association*, Taylor & Francis Group, 88(423), 881–889.
Getachew, A. (2003). "Traffic load effects on bridges, statistical analysis of collected and Monte Carlo simulated data." Royal Institute of Technology, Stockholm, Sweden.
Ghosn, M. (2000). "Development of truck weight regulations using bridge reliability model." *Journal of Bridge Engineering*, American Society of Civil Engineers, 5(4), 293–303.
Ghosn, M., Moses, F., and Wang, J. (2003). *Design of Highway Bridges for Extreme Events*. Transportation Research Board.
Gilks, W. R. (2005). *Markov Chain Monte Carlo*. Wiley Online Library.
Gilleland, E., and Katz, R. W. (2011). "New software to analyze how extremes change over time." *Eos, Transactions American Geophysical Union*, Wiley Online Library, 92(2), 13–14.

Gilleland, E., and Katz, R. W. (2016). “Extremes 2.0: an extreme value analysis package in R.” Journal of Statistical Software, 72(8), 1-39.

Gilli, M., and others. (2006). “An application of extreme value theory for measuring financial risk.” *Computational Economics*, Springer, 27(2-3), 207–228.

Grave, S. (2002). “Modeling of site-specific traffic loading on short to medium span bridges.” Trinity College Dublin, Dublin, Ireland.

Grave, S., O’Brien, E., and O’Connor, A. (2000). “The determination of site-specific imposed traffic loadings on existing bridges.” *Bridge Management 4-Inspection, Maintenance, Assessment and Repair*.

Gumbel, E. J. (1958). *Extreme Value Theory*. Columbia University Press, New York, USA.

Guo, Q. L. (2001). “Development of risk analysis models for decision-making in project management.” Ph.D. Dissertation, Napier University.

Gurley, K., and Kareem, A. (1999). “Applications of wavelet transforms in earthquake, wind and ocean engineering.” *Engineering Structures*, 21(2), 149–167.

Hafez, A. G., Khan, M. T. A., and Kohda, T. (2010). “Clear P-wave arrival of weak events and automatic onset determination using wavelet filter banks.” *Digital Signal Processing*, Elsevier, 20(3), 715–723.

Hall, P., Kerkyacharian, G., Picard, D., and others. (1998). “Block threshold rules for curve estimation using kernel and wavelet methods.” *The Annals of Statistics*, Institute of Mathematical Statistics, 26(3), 922–942.

Hall, W. B. (1988). “Reliability of service-proven structures.” *Journal of Structural Engineering*, American Society of Civil Engineers, 114(3), 608–624.

Hamada, M. S., Wilson, A., Reese, C. S., and Martz, H. (2008). *Bayesian Reliability*. Springer Science & Business Media.

Härdle, W., Kerkyacharian, G., Picard, D., and Tsybakov, A. (2012). *Wavelets, Approximation, and Statistical Applications*. Springer Science & Business Media.

Harris, R. (1996). “Gumbel re-visited-a new look at extreme value statistics applied to wind speeds.” *Journal of Wind Engineering and Industrial Aerodynamics*, Elsevier, 59(1), 1–22.

Hasofer, A., Lind, N. (Niels C., and Waterloo. Solid Mechanics Division, U. of. (1973). *An Exact and Invariant First-Order Reliability Format*. University of Waterloo, Solid Mechanics Division,.

Hastings, W. K. (1970). “Monte Carlo sampling methods using Markov chains and their applications.” *Biometrika*, Biometrika Trust, 57(1), 97–109.

Hawk, H., and Small, E. P. (1998). “The BRIDGIT bridge management system.” *Structural Engineering International*, International Association for Bridge and Structural Engineering, 8(4), 309–314.

Hearn, G., Puckett, J., Friedland, I., Everett, T., Hurst, K., Romack, G., Christian, G., Shepard, R., Thompson, T., and Young, R. (2005). *Bridge Preservation and Maintenance in Europe and South Africa*. Federal Highway Administration (FHWA), Washington, D.C., USA.

Hera, A., and Hou, Z. (2004). “Application of wavelet approach for ASCE structural health monitoring benchmark studies.” *Journal of Engineering Mechanics*,

American Society of Civil Engineers, 130(1), 96–104.
Hester, D., and González, A. (2012). “A wavelet-based damage detection algorithm based on bridge acceleration response to a vehicle.” *Mechanical Systems and Signal Processing*, Elsevier, 28, 145–166.
Hibbit, H., Karlsson, B., and Sorensen, P. (2005). “ABAQUS user’s manual.” *Theory Manual Version*, 4.
HKTD. (1997). *Road Traffic (Construction and Maintenance of Vehicles) Regulations*. Hong Kong Transport Department, Hong Kong.
HKTD. (2012). *Road Traffic (Construction and Maintenance of Vehicle) Regulations*. Hong Kong Transport Department, Hong Kong.
Hohenbichler, M., and Rackwitz, R. (1988). “Improvement of second-order reliability estimates by importance sampling.” *Journal of Engineering Mechanics*, American Society of Civil Engineers, 114(12), 2195–2199.
Holmes, J., and Moriarty, W. (1999). “Application of the generalized Pareto distribution to extreme value analysis in wind engineering.” *Journal of Wind Engineering and Industrial Aerodynamics*, Elsevier, 83(1), 1–10.
Hong, H., and Liang, M. (2007). “Separation of fault features from a single-channel mechanical signal mixture using wavelet decomposition.” *Mechanical Systems and Signal Processing*, Elsevier, 21(5), 2025–2040.
Hua, X. G. (2006). “Structural health monitoring and condition assessment of bridge structures.” Ph.D. thesis, The Hong Kong Polytechnic University, Hong Kong.
Iversen, G. R. (1984). *Bayesian Statistical Inference*. SAGE.
James, G. (2003). “Analysis of traffic load effects an railway bridges.” Royal Institute of Technology, Sweden.
Jenkinson, A. F. (1955). “The frequency distribution of the annual maximum (or minimum) values of meteorological elements.” *Quarterly Journal of the Royal Meteorological Society*, Wiley Online Library, 81(348), 158–171.
Kantz, H., and Schreiber, T. (2004). *Nonlinear Time Series Analysis*. Cambridge University Press.
Katz, R. W., Parlange, M. B., and Naveau, P. (2002). “Statistics of extremes in hydrology.” *Advances in Water Resources*, Elsevier, 25(8), 1287–1304.
Kawamura, K., Miyamoto, A., Frangopol, D. M., and Kimura, R. (2003). “Performance evaluation of concrete slabs of existing bridges using neural networks.” *Engineering Structures*, Elsevier, 25(12), 1455–1477.
Kayser, J. R. (1988). “The Effects of Corrosion on the Reliability of Steel Girder Bridges.” University of Michigan.
Kayser, J. R., and Nowak, A. S. (1989a). “Capacity loss due to corrosion in steel-girder bridges.” *Journal of Structural Engineering*, American Society of Civil Engineers, 115(6), 1525–1537.
Kayser, J. R., and Nowak, A. S. (1989b). “Reliability of corroded steel girder bridges.” *Structural Safety*, Elsevier, 6(1), 53–63.
Khadra, L., Al-Fahoum, A., and Al-Nashash, H. (1997). “Detection of life-threatening cardiac arrhythmias using the wavelet transformation.” *Medical and Biological Engineering and Computing*, Springer, 35(6), 626–632.

Kim, H., and Melhem, H. (2004). “Damage detection of structures by wavelet analysis.” *Engineering Structures*, Elsevier, 26(3), 347–362.

Ko, J. M., and Ni, Y. Q. (2005). “Technology developments in structural health monitoring of large-scale bridges.” *Engineering structures*, Elsevier, 27(12), 1715–1725.

Koo, I., Zhang, X., and Kim, S. (2011). “Wavelet-and Fourier-transform-based spectrum similarity approaches to compound identification in gas chromatography/mass spectrometry.” *Analytical Chemistry*, ACS Publications, 83(14), 5631–5638.

Krieger, J., and Haardt, P. (2000). “Management of bridge in Germany.” *Bridge Management 4: Inspection, Maintenance, Assessment and Repair*, 5–13.

Lapin, L. L. (1983). *Probability and Statistics for Modern Engineering*. Thomson Brooks/Cole.

Leadbetter, M. R., Lindgren, G., and Rootzén, H. (2012). *Extremes and Related Properties of Random Sequences and Processes*. Springer Science & Business Media.

Leemis, L. M. (1995). *Reliability: Probabilistic Models and Statistical Methods*. Prentice-Hall, Inc.

Li, C., Zheng, C., and Tai, C. (1995). “Detection of ECG characteristic points using wavelet transforms.” *Biomedical Engineering, IEEE Transactions on*, IEEE, 42(1), 21–28.

Li, D., Maes, M. A., and Dilger, W. H. (2004). “Thermal design criteria for deep prestressed concrete girders based on data from Confederation Bridge.” *Canadian Journal of Civil Engineering*, NRC Research Press, 31(5), 813–825.

Li, Y. (2004). “Effects of spatial variability on maintenance and repair decisions for concrete structures.” Delft University of Technology.

Liang, M.-T., Wu, J.-H., and Liang, C.-H. (2001). “Multiple layer fuzzy evaluation for existing reinforced concrete bridges.” *Journal of Infrastructure Systems*, American Society of Civil Engineers, 7(4), 144–159.

Lin, J., and Qu, L. (2000). “Feature extraction based on Morlet wavelet and its application for mechanical fault diagnosis.” *Journal of Sound and Vibration*, Elsevier, 234(1), 135–148.

Lin, S., and McFadden, P. (1997). “Gear vibration analysis by B-spline wavelet-based linear wavelet transform.” *Mechanical Systems and Signal Processing*, Elsevier, 11(4), 603–609.

Liu, M., Frangopol, D. M., and Kim, S. (2009). “Bridge system performance assessment from structural health monitoring: a case study.” *Journal of Structural Engineering*, American Society of Civil Engineers, 135(6), 733–742.

Liu, T. T., and Fraser-Smith, A. C. (2000). “Detection of transients in 1/f noise with the undecimated discrete wavelet transform.” *IEEE Transactions on Signal Processing*, Institute of Electrical and Electronics Engineers, 48(5), 1458–1462.

Lutomirska, M. (2009). “Live load models for long span bridges.” Ph.D. thesis, University of Nebraska - Lincoln, USA.

Madadi, Z., Anand, G. V., and Premkumar, A. B. (2013). “Signal Detection in

Generalized Gaussian Noise by Nonlinear Wavelet Denoising." *Circuits and Systems I: Regular Papers, IEEE Transactions on*, IEEE, 60(11), 2973–2986.
Madsen, H. O., Krenk, S., and Lind, N. C. (2006). *Methods of Structural Safety*. Courier Corporation.
Maeck, J., Peeters, B., and De Roeck, G. (2001). "Damage identification on the Z24 bridge using vibration monitoring." *Smart Materials and Structures*, IOP Publishing, 10(3), 512.
Maes, M. A., Dilger, W. H., and Ballyk, P. D. (1992). "Extreme values of thermal loading parameters in concrete bridges." *Canadian Journal of Civil Engineering*, NRC Research Press, 19(6), 935–946.
Mahalakshmi, M., Hariharan, G., and Kannan, K. (2013). "The wavelet methods to linear and nonlinear reaction–diffusion model arising in mathematical chemistry." *Journal of Mathematical Chemistry*, Springer, 51(9), 2361–2385.
Mallat, S. (1999). *A wavelet tour of signal processing*. Academic press.
Mallat, S. G. (1989). "A theory for multiresolution signal decomposition: the wavelet representation." *Pattern Analysis and Machine Intelligence, IEEE Transactions on*, Ieee, 11(7), 674–693.
Mallat, S. G., and Zhang, Z. (1993). "Matching pursuits with time-frequency dictionaries." *Signal Processing, IEEE Transactions on*, IEEE, 41(12), 3397–3415.
Maraki, A. (2003). "Development of a universal bridge management system." Department of Civil Engineering, University of Surrey.
Martis, R. J., Acharya, U. R., and Min, L. C. (2013). "ECG beat classification using PCA, LDA, ICA and Discrete Wavelet Transform." *Biomedical Signal Processing and Control*, Elsevier, 8(5), 437–448.
Martz, H., Wailer, R., and Fickas, E. (1988). "Bayesian reliability analysis of series systems of binomial subsystems and components." *Technometrics*, Taylor & Francis Group, 30(2), 143–154.
McCrum R., Arnold C.J., and R.P., D. (1985). *Current Status Report Effect of Corrosion on Unpainted Weathering Steel Bridges: Testing and Research Division*. Research Report No. R-1255, Michigan Department of Transportation;
McKay, M. D., Beckman, R. J., and Conover, W. J. (2000). "A comparison of three methods for selecting values of input variables in the analysis of output from a computer code." *Technometrics*, Taylor & Francis Group, 42(1), 55–61.
Melchers, R. (1990). "Search-based importance sampling." *Structural Safety*, Elsevier, 9(2), 117–128.
Melchers, R. E. (1999). *Structural Reliability Analysis and Prediction*. John Wiley & Son Ltd.
Mendenhall, W., Sincich, T., and Boudreau, N. S. (1996). *A Second Course in Statistics: Regression Analysis*. Prentice Hall Upper Saddle River eNew Jersey New Jersey.
Messer, S. R., Agzarian, J., and Abbott, D. (2001). "Optimal wavelet denoising for phonocardiograms." *Microelectronics Journal*, Elsevier, 32(12), 931–941.
Messervey, T. B. (2008). "Integration of structural health monitoring into the design,

assessment, and management of civil infrastructure." Ph.D. Thesis, University of Genoa, Italy.
Messervey, T. B., Frangopol, D. M., and Casciati, S. (2011). "Application of the statistics of extremes to the reliability assessment and performance prediction of monitored highway bridges." *Structure and Infrastructure Engineering*, Taylor & Francis, 7(1-2), 87–99.
Mészárosová, H., Karlick, M., Rybák, J., and Jiricka, K. (2009). "Tadpoles in Wavelet Spectra of a Solar Decimetric Radio Burst." *The Astrophysical Journal Letters*, IOP Publishing, 697(2), L108.
Miao, T., and Chan, T. H. (2002). "Bridge live load models from WIM data." *Engineering Structures*, Elsevier, 24(8), 1071–1084.
Micic, T., Chryssanthopoulos, M., and Baker, M. (1995). "Reliability analysis for highway bridge deck assessment." *Structural Safety*, Elsevier, 17(3), 135–150.
Montgomery, D. C., Peck, E. A., and Vining, G. G. (2012). *Introduction to Linear Regression Analysis*. John Wiley & Sons.
Mori, Y., and Ellingwood, B. R. (1993). "Reliability-based service-life assessment of aging concrete structures." *Journal of Structural Engineering*, American Society of Civil Engineers, 119(5), 1600–1621.
Moses, F., Lebet, J. P., and Bez, R. (1994). "Applications of field testing to bridge evaluation." *Journal of Structural Engineering*, American Society of Civil Engineers, 120(6), 1745–1762.
Moss, R., and Matthews, S. (1995). "In-service structural monitoring. a state of the art review." *Structural Engineer*, 73(2).
Moulin, P., and Liu, J. (1999). "Analysis of multiresolution image denoising schemes using generalized Gaussian and complexity priors." *Information Theory, IEEE Transactions on*, IEEE, 45(3), 909–919.
Moyo, P., and Brownjohn, J. (2002). "Detection of anomalous structural behaviour using wavelet analysis." *Mechanical Systems and Signal Processing*, Elsevier, 16(2), 429–445.
Mufti, A. A. (2002). "Structural health monitoring of innovative Canadian civil engineering structures." *Structural Health Monitoring*, SAGE Publications, 1(1), 89–103.
Nason, G. (1995). "Choice of the threshold parameter in wavelet function estimation." *Wavelets and Statistics*, Springer, 261–280.
Nason, G. P. (1996). "Wavelet shrinkage using cross-validation." *Journal of the Royal Statistical Society. Series B (Methodological)*, 58(2), 463–479.
NCHRP. (1998). "Manual for bridge rating through load testing." *Research Results Digest No. 234*, Transportation Research Board, National Research Council, Washington, DC.
NCHRP. (1999a). "Calibration of LRFD bridge design." *Report 368*, Transportation Research Board, National Research Council, Washington, DC.
NCHRP. (1999b). "Manual for condition evaluation and load and resistance factor rating of highway bridges." *NCHRP 12, Pre-Final Draft*, Transportation Research Board, National Research Council, Washington, DC.

Neild, S., McFadden, P., and Williams, M. (2003). “A review of time-frequency methods for structural vibration analysis.” *Engineering Structures*, Elsevier, 25(6), 713–728.

Nenadic, Z., and Burdick, J. W. (2005). “Spike detection using the continuous wavelet transform.” *Biomedical Engineering, IEEE Transactions on*, IEEE, 52(1), 74–87.

Neves, L. A., Frangopol, D. M., and Cruz, P. J. (2006a). “Probabilistic lifetime-oriented multiobjective optimization of bridge maintenance: single maintenance type.” *Journal of Structural Engineering*, American Society of Civil Engineers, 132(6), 991–1005.

Neves, L. A., Frangopol, D. M., and Petcherdchoo, A. (2006b). “Probabilistic lifetime-oriented multiobjective optimization of bridge maintenance: Combination of maintenance types.” *Journal of Structural Engineering*, American Society of Civil Engineers, 132(11), 1821–1834.

Neves, L. C., and Frangopol, D. M. (2005). “Condition, safety and cost profiles for deteriorating structures with emphasis on bridges.” *Reliability Engineering & System Safety*, Elsevier, 89(2), 185–198.

Ng, S., and Moses, F. (1996). “Prediction of bridge service life using time-dependent reliability analysis.” *Bridge Management*, 3, 26–32.

Ni, Y. Q., Hua, X. G., Wong, K. Y., and Ko, J. M. (2007). “Assessment of bridge expansion joints using long-term displacement and temperature measurement.” *Journal of Performance of Constructed Facilities*, American Society of Civil Engineers, 21(2), 143-151.

Ni, Y. Q., and Wong, K. Y. (2012). “Integrating bridge structural health monitoring and condition-based maintenance management.” In *Civil Structural Health Monitoring Workshop, International Society for Structural Health Monitoring of Intelligent Infrastructure*, Winnipeg, Canada.

Ni, Y. Q., Xia, H. W., Wong, K. Y., and Ko, J. M.(2011). “In-service condition assessment of bridge deck using long-term monitoring data of strain response.” *Journal of Bridge Engineering*, American Society of Civil Engineers, 17(6), 876–885.

Ni, Y. Q., Xia, Y., Liao, W., and Ko, J. M. (2009). “Technology innovation in developing the structural health monitoring system for Guangzhou New TV Tower.” *Structural Control and Health Monitoring*, Wiley Online Library, 16(1), 73–98.

Ni, Y. Q., and Xia, Y. X. (2016). “Strain-based condition assessment of a suspension bridge instrumented with structural health monitoring system.” *International Journal of Structural Stability and Dynamics*, 16(04), 1640027.

Ni, Y. Q., Ye, X. W., and Ko, J. M. (2011). “Modeling of stress spectrum using long-term monitoring data and finite mixture distributions. ” *Journal of Engineering Mechanics*, American Society of Civil Engineers, 138(2), 175-183.

Nowak, A. S., and Collins, K. R. (2012). *Reliability of Structures*. CRC Press.

Nowak, A. S., and Eamon, C. D. (2008). “Reliability analysis of plank decks.” *Journal of Bridge Engineering*, American Society of Civil Engineers, 13(5), 540–546.

Nowak, A. S., and Hong, Y.-K. (1991). “Bridge live-load models.” *Journal of*

Structural Engineering, American Society of Civil Engineers, 117(9), 2757–2767.
Nowak, A. S., and Lind, N. C. (1979). "Practical bridge code calibration." *Journal of the Structural Division*, ASCE, 105(12), 2497–2510.
Nowak, A. S., Yamani, A. S., and Tabsh, S. W. (1994). "Probabilistic models for resistance of concrete bridge girders." *Structural Journal*, 91(3), 269–276.
O'Brien, E., Schmidt, F., Hajializadeh, D., Zhou, X.-Y., Enright, B., Caprani, C., Wilson, S., and Sheils, E. (2015). "A review of probabilistic methods of assessment of load effects in bridges." *Structural Safety*, Elsevier, 53, 44–56.
O'Brien, E., Sloan, T., Butler, K., and Kirkpatrick, J. (1995). "Traffic load'fingerprinting'of bridges for assessment purposes." *Structural Engineer*, Institution of Structural Engineers, 73, 320–320.
O'Connor, A. J. (2001). "Probabilistic traffic load modeling for highway bridges." Ph.D. Thesis, Trinity College Dublin.
OHBDC. (1991). *Ontario Highway Bridge Design Code*. Ontario Ministry of Transportation, Downsview, Ontario.
Omenzetter, P., Brownjohn, J. M. W., and Moyo, P. (2004). "Identification of unusual events in multi-channel bridge monitoring data." *Mechanical Systems and Signal Processing*, Elsevier, 18(2), 409–430.
Ou, J., and Li, H. (2009). "Structural health monitoring research in China: trends and applications." *Structural Health Monitoring of Civil Infrastructure Systems.* Cambridge: Woodhead Publishing.
Ovanesova, A., and Suarez, L. (2004). "Applications of wavelet transforms to damage detection in frame structures." *Engineering Structures*, Elsevier, 26(1), 39–49.
Paloheimo, E., and Hannus, M. (1974). "Structural design based on weighted fractiles." *Journal of the Structural Division*, ASCE, 100(7), 1367–1378.
Papandreou-Suppappola, A. (2002). *Applications in Time-Frequency Signal Processing*. CRC press.
Park, C., and Nowak, A. (1997). "Lifetime reliability model for steel girder bridges." *Safety of Bridges*, Thomas Telford Publications London, 189–202.
Patel, A. X., Kundu, P., Rubinov, M., Jones, P. S., Vértes, P. E., Ersche, K. D., Suckling, J., and Bullmore, E. T. (2014). "A wavelet method for modeling and despiking motion artifacts from resting-state fMRI time series." *NeuroImage*, Elsevier, 95, 287–304.
Peng, Z., and Chu, F. (2004). "Application of the wavelet transform in machine condition monitoring and fault diagnostics: a review with bibliography." *Mechanical Systems and Signal Processing*, Elsevier, 18(2), 199–221.
Percival, D. B., and Walden, A. T. (2006). *Wavelet Methods for Time Series Analysis*. Cambridge university press.
Phares, B. M., Washer, G. A., Rolander, D. D., Graybeal, B. A., and Moore, M. (2004). "Routine highway bridge inspection condition documentation accuracy and reliability." *Journal of Bridge Engineering*, American Society of Civil Engineers, 9(4), 403–413.
Pines, D., and Aktan, A. E. (2002). "Status of structural health monitoring of long-span bridges in the United States." *Progress in Structural Engineering and*

Materials, Wiley Online Library, 4(4), 372–380.
Poon, S.-H., Rockinger, M., and Tawn, J. (2004). "Extreme value dependence in financial markets: Diagnostics, models, and financial implications." *Review of Financial Studies*, Soc Financial Studies, 17(2), 581–610.
Rackwitz, R., and Flessler, B. (1978). "Structural reliability under combined random load sequences." *Computers & Structures*, Elsevier, 9(5), 489–494.
Rafiee, J., Rafiee, M., Prause, N., and Schoen, M. (2011). "Wavelet basis functions in biomedical signal processing." *Expert Systems with Applications*, Elsevier, 38(5), 6190–6201.
Rafiq, M. I. (2005). "Health monitoring in proactive reliability management of deteriorating concrete bridges." Ph.D. Thesis, University of Surrey.
Rakoczy, A. M., and Nowak, A. S. (2014). "Reliability-based strength limit state for steel railway bridges." *Structure and Infrastructure Engineering*, Taylor & Francis, 10(9), 1248–1261.
Ravindra, M. K., and Galambos, T. V. (1978). "Load and resistance factor design for steel." *Journal of the Structural Division*, ASCE, 104(9), 1337–1353.
RDevelopmentCoreTeam. (2014). "R: A language and environment for statistical computing. R Foundation for Statistical Computing." Vienna, Austria.
Reiss, R.-D., Thomas, M., and Reiss, R. (2001). *Statistical Analysis of Extreme Values*. Springer.
Rioul, O., and Vetterli, M. (1991). "Wavelets and signal processing." *IEEE Signal Processing Magazine*, Institute of Electrical and Electronics Engineers, 8(LCAV-ARTICLE-1991-005), 14–38.
Robert, C., and Casella, G. (2013). *Monte Carlo Statistical Methods*. Springer Science & Business Media.
Robertson, A. N., and Basu, B. (2009). "Wavelet analysis." *Encyclopedia of Structural Health Monitoring*, Wiley Online Library.
Robertson, D. C., Camps, O. I., Mayer, J. S., and Gish, W. B. (1996). "Wavelets and electromagnetic power system transients." *Power Delivery, IEEE Transactions on*, IEEE, 11(2), 1050–1058.
Rosenblatt, M. (1952). "Remarks on a multivariate transformation." *The Annals Of Mathematical Statistics*, 23(3), 470–472.
Rubinstein, R. Y., and Kroese, D. P. (2011). *Simulation and the Monte Carlo Method*. John Wiley & Sons.
Rucka, M., and Wilde, K. (2006). "Application of continuous wavelet transform in vibration based damage detection method for beams and plates." *Journal of Sound and Vibration*, Elsevier, 297(3), 536–550.
Ryall, M. J. (2001). *Bridge Management*. Butterworth-Heinemann, Oxford.
Sasmal, S., and Ramanjaneyulu, K. (2008). "Condition evaluation of existing reinforced concrete bridges using fuzzy based analytic hierarchy approach." *Expert Systems with Applications*, Elsevier, 35(3), 1430–1443.
Shinozuka, M. (1983). "Basic analysis of structural safety." *Journal of Structural Engineering*, American Society of Civil Engineers, 109(3), 721-740.
Siegert, D., Estivin, M., Billo, J., Barin, F., and Toutlemonde, F. (2008). "Extreme

effects of the traffic loads on a prestressed concrete bridge." *International Conference on Heavy Vehicles HVParis 2008*, Wiley Online Library, 499–509.
Simiu, E., Heckert, N., Filliben, J., and Johnson, S. (2001). "Extreme wind load estimates based on the Gumbel distribution of dynamic pressures: an assessment." *Structural Safety*, Elsevier, 23(3), 221–229.
Small, E. P., and Cooper, J. (1998). "Condition of the Nation's Highway Bridges: A Look at the Past, Present, and Future." *TR News*, (194).
Sohn, H., Farrar, C. R., Hemez, F. M., Shunk, D. D., Stinemates, D. W., Nadler, B. R., and Czarnecki, J. J. (2004). *A Review of Structural Health Monitoring Literature: 1996-2001*. Los Alamos National Laboratory Los Alamos, NM.
Starck, J.-L., and Murtagh, F. (1994). "Image restoration with noise suppression using the wavelet transform." *Astronomy and Astrophysics*, 288, 342–348.
Staszewski, W., and Tomlinson, G. (1994). "Application of the wavelet transform to fault detection in a spur gear." *Mechanical Systems and Signal Processing*, Elsevier, 8(3), 289–307.
Stein, C. M. (1981). "Estimation of the mean of a multivariate normal distribution." *The Annals of Statistics*, 9(6), 1135–1151.
Stewart, M. G., and Val, D. V. (1999). "Role of load history in reliability-based decision analysis of aging bridges." *Journal of Structural Engineering*, American Society of Civil Engineers, 125(7), 776–783.
Stojanovic R., Knezevic S., Karadaglic D. and Devedzic G. (2013). "Optimization and implementation of the wavelet based algorithms for embedded biomedical signal processing." *Computer Science and Information Systems*, 10(1), 503-523.
Strang, G., and Nguyen, T. (1996). *Wavelets and Filter Banks*. SIAM.
Sundararajan, C. R. (2012). *Probabilistic Structural Mechanics Handbook: Theory and Industrial Applications*. Springer Science & Business Media.
Sykora, M., Diamantidis, D., Holicky, M., and Jung, K. (2017). Target reliability for existing structures considering economic and societal aspects. *Structure and Infrastructure Engineering*, 13(1), 181-194.
Systèmes, D. (2007). "ABAQUS analysis user's manual." Simulia Corpration. Providence, RI, USA.
Tabsh, S. W., and Nowak, A. S. (1991). "Reliability of highway girder bridges." *Journal of Structural Engineering*, American Society of Civil Engineers, 117(8), 2372–2388.
Tawn, J. A. (1990). "Modeling multivariate extreme value distributions." *Biometrika*, Biometrika Trust, 77(2), 245–253.
Thoft-Christensen, P. (1993). "Reliability-based expert systems for optimal maintenance of concrete bridges." *Structural Engineering in Natural Hazards Mitigation*, ASCE, 1053–1058.
Thoft-Christensen, P. (1997). *Lifetime Reliability Assessment of Concrete Slab Bridges*. Department of Building Technology and Structural Engineering.
Thoft-Christensen, P. (1998). "Assessment of the reliability profiles for concrete bridges." *Engineering Structures*, Elsevier, 20(11), 1004–1009.
Thoft-Christensen, P., and Baker, M. J. (1982). *Structural Reliability Theory and Its*

Applications. Springer Science & Business Media.
Thoft-Christensen, P., Jensen, F., Middleton, C., and Blackmore, A. (1996). *Assessment of the Reliability of Concrete Slab Bridges*. Department of Building Technology and Structural Engineering.
Thoft-Christensen, P., and Murotsu, Y. (2012). *Application of Structural Systems Reliability Theory*. Springer Science & Business Media.
Thompson, P. D., Small, E. P., Johnson, M., and Marshall, A. R. (1998). "The Pontis bridge management system." *Structural Engineering International*, International Association for Bridge and Structural Engineering, 8(4), 303–308.
Treacy, M. A., Brühwiler, E., and Caprani, C. C. (2014). "Monitoring of traffic action local effects in highway bridge deck slabs and the influence of measurement duration on extreme value estimates." *Structure and Infrastructure Engineering*, Taylor & Francis, 10(12), 1555–1572.
Tsimplis, M., and Blackman, D. (1997). "Extreme sea-level distribution and return periods in the Aegean and Ionian Seas." *Estuarine, Coastal and Shelf Science*, Elsevier, 44(1), 79–89.
TutorialsPoint. (2016). *DB2 Tutorial*. Tutorials Point (I) Pvt. Ltd.
Val, D., Bljuger, F., and Yankelevsky, D. (1997). "Reliability evaluation in nonlinear analysis of reinforced concrete structures." *Structural Safety*, Elsevier, 19(2), 203–217.
Val, D. V., Stewart, M. G., and Melchers, R. E. (1998). "Effect of reinforcement corrosion on reliability of highway bridges." *Engineering Structures*, Elsevier, 20(11), 1010–1019.
Val, D. V., Stewart, M. G., and Melchers, R. E. (2000). "Life-Cycle Performance of RC Bridges: Probabilistic Approach." *Computer-Aided Civil and Infrastructure Engineering*, Wiley Online Library, 15(1), 14–25.
Vidakovic, B. (1998). "Nonlinear wavelet shrinkage with Bayes rules and Bayes factors." *Journal of the American Statistical Association*, Taylor & Francis, 93(441), 173–179.
Vrouwenvelder, A., and Waarts, P. (1993). "Traffic loads on bridges." *Structural Engineering International*, International Association for Bridge and Structural Engineering, 3(3), 169–177.
Wachowiak, M. P., Rash, G. S., Quesada, P. M., and Desoky, A. H. (2000). "Wavelet-based noise removal for biomechanical signals: A comparative study." *Biomedical Engineering, IEEE Transactions on*, IEEE, 47(3), 360–368.
Walczak, B. (2000). *Wavelets in Chemistry*. Elsevier.
Walczak, B., Den Bogaert, B. van, and Massart, D. L. (1996). "Application of wavelet packet transform in pattern recognition of near-IR data." *Analytical Chemistry*, ACS Publications, 68(10), 1742–1747.
Wallbank, E. J. (1989). *The Performance of Concrete in Bridges: A Survey of 200 Highway Bridges*. The Department of Transport, London.
Wang, P., Youn, B. D., Xi, Z., and Kloess, A. (2009). "Bayesian reliability analysis with evolving, insufficient, and subjective data sets." *Journal of Mechanical Design*, American Society of Mechanical Engineers, 131(11), 111008.

Wang, Y. (1996). “Function estimation via wavelet shrinkage for long-memory data.” *The Annals of Statistics*, Institute of Mathematical Statistics, 24(2), 466–484.

Weber, P., and Jouffe, L. (2006). “Complex system reliability modeling with dynamic object oriented Bayesian networks (DOOBN).” *Reliability Engineering & System Safety*, Elsevier, 91(2), 149–162.

Wenzel, H. (2008). *Health Monitoring of Bridges*. John Wiley & Sons.

Wikipedia (2016). Database. Retrieved August 3 2016, from *https://en.wikipedia.org/wiki/Database*.

Wong, K. Y. (2006). “Criticality and vulnerability analyses of Tsing Ma Bridge.” *Proceedings of the International Conference on Bridge Engineering*, Hong Kong, China.

Wong, K. Y. (2007). “Stress and traffic loads monitoring of Tsing Ma Bridge.” *Proceedings of the China Bridge Congress 2007*, China Highway and Transportation Society, Beijing.

Wong, K. Y. (2003). “Structural identification of Tsing Ma bridge.” *HKIE Transactions*, Taylor & Francis, 10(1), 38–47.

Wong, K. Y. (2004). “Instrumentation and health monitoring of cable-supported bridges.” *Structural Control and Health Monitoring*, Wiley Online Library, 11(2), 91–124.

Worden, K., and Manson, G. (2007). “The application of machine learning to structural health monitoring.” *Philosophical Transactions of the Royal Society of London A: Mathematical, Physical and Engineering Sciences*, The Royal Society, 365(1851), 515–537.

Xia H. W. (2012). “SHM-based condition assessment of in-service bridge structures using strain measurement.” Ph.D. Thesis, Department of Civil and Environmental Engineering, The Hong Kong Polytechnic University, Hong Kong.

Xia, Y. X., Ni Y. Q., and Zhang C. (2014). “Evaluation of torsional response of a long-span suspension bridge under railway traffic and typhoons based on SHM data.” *Structural Monitoring and Maintenance*, 1(4), 371–392.

Xu, Y. L., and Xia, Y. (2011). *Structural Health Monitoring of Long-Span Suspension Bridges*. CRC Press.

Yan, R., Gao, R. X., and Chen, X. (2014). “Wavelets for fault diagnosis of rotary machines: A review with applications.” *Signal Processing*, Elsevier, 96, 1–15.

Yanev, B., and Testa, R. B. (1997). “Life-cycle performance of bridge components in New York City.” *Recent Advances in Bridge Engineering*, EMPA Dubendoiff, Switzerland, 385–392.

Yang, X., and Shamma, S. A. (1988). “A totally automated system for the detection and classification of neural spikes.” *Biomedical Engineering, IEEE Transactions on*, IEEE, 35(10), 806–816.

Yokoyama, K., Sato, H., Ogihara, K., and Toriumi, R. (1996). “Development of a bridge management system in Japan.” *Bridge Management 3. Inspection, Maintenance and Repair*.

Yu, D. C., Nguyen, T. C., and Haddawy, P. (1999). “Bayesian network model for reliability assessment of power systems.” *Power Systems, IEEE Transactions on*,

IEEE, 14(2), 426–432.
Yun, C.-B., Lee, J.-J., and Koo, K.-Y. (2011). “Smart structure technologies for civil infrastructures in Korea: recent research and applications.” *Structure and Infrastructure Engineering*, Taylor & Francis, 7(9), 673–688.
Zacks, S. (1971). *The theory of Bayesian Statistical Inference*. Wiley New York.
Zanos, T. P., Mineault, P. J., and Pack, C. C. (2011). “Removal of spurious correlations between spikes and local field potentials.” *Journal of Neurophysiology*, Am Physiological Soc, 105(1), 474–486.
Zhang, R., and Mahadevan, S. (2000). “Model uncertainty and Bayesian updating in reliability-based inspection.” *Structural Safety*, Elsevier, 22(2), 145–160.
Zheng, R., and Ellingwood, B. R. (1998). “Role of non-destructive evaluation in time-dependent reliability analysis.” *Structural Safety*, Elsevier, 20(4), 325–339.
Zhu, Z., Yan, R., Luo, L., Feng, Z., and Kong, F. (2009). “Detection of signal transients based on wavelet and statistics for machine fault diagnosis.” *Mechanical Systems and Signal Processing*, Elsevier, 23(4), 1076–1097.
Žnidaric, A., Turk, G., and Zupan, E. (2015). “Determination of strain correction factors for bridge weigh-in-motion systems.” *Engineering Structures*, Elsevier, 102, 387–394.